Summer 7-28-2023

# Mid-Gestation Maternofetal Inflammation Impacts Growth, Skeletal Muscle Glucose Metabolism, and Inflammatory Tone in the Ovine Fetus During Late Gestation

Zena Hicks
*University of Nebraska-Lincoln*, zenahicks20@gmail.com

# MID-GESTATION MATERNOFETAL INFLAMMATION IMPACTS GROWTH, SKELETAL MUSCLE GLUCOSE METABOLISM, AND INFLAMMATORY TONE IN THE OVINE FETUS DURING LATE GESTATION

by

Zena Mariah Hicks

A DISSERTATION

Presented to the Faculty of

The Graduate College at the University of Nebraska

In Partial Fulfillment of Requirements

For the Degree of Doctor of Philosophy

Major: Animal Science

(Physiology)

Under the Supervision of Professor Dustin T. Yates

Lincoln, Nebraska

August 2023

# MID-GESTATION MATERNOFETAL INFLAMMATION IMPACTS GROWTH, SKELETAL MUSCLE GLUCOSE METABOLISM, AND INFLAMMATORY TONE IN THE OVINE FETUS DURING LATE GESTATION

Zena Mariah Hicks, Ph.D.

University of Nebraska, 2023

Advisor: Dustin T. Yates

Our 1st and 2nd studies assessed the impact of mid-gestation maternofetal inflammation on growth, skeletal muscle glucose metabolism, and inflammatory tone in the late gestation ovine fetus. The objective was to determine if inducing maternofetal inflammation during peak placental growth would lead to more profound IUGR characteristics in the fetus. MI-IUGR fetuses exhibited reduced body and skeletal muscle weights and hallmark asymmetric growth at late gestations. Fetuses had higher baseline glucose:insulin ratios and reduced glucose-stimulated insulin secretion. Moreover, hindlimb glucose oxidation was impaired independent of glucose uptake. Skeletal muscle specific glucose uptake and oxidation was reduced in MI-IUGR fetuses. MI-IUGR fetuses also had increased circulating cytokines and cytokine receptor content in skeletal muscle. Therefore, targeting inflammation during mid- to late gestation is an area of interest for future IUGR therapeutic treatments.

Our 3rd study examined the differentially expressed genes in neonatal skeletal muscle transcriptome in response to maternofetal inflammation (MI-IUGR) or maternal hyperthermia (PI-IUGR) during gestation. Although PI-IUGR lambs exhibited a more severe IUGR phenotypically, skeletal muscle of MI-IUGR exhibited showed more transcriptomic changes. Regardless of the source of maternal stress, a large percentage of

genes and pathways impacted in the IUGR fetus were related to inflammation. These data further support the role of the inflammatory pathway in IUGR pathologies.

Our final study examined the changes in tissue composition of the sheep hindlimb across different stages of development. We found that 40% of the tissue in the fetal hindlimb is skeletal muscle compared to 65% of the tissue in the juvenile lamb. This was an important gap in the literature not previously addressed, and could help us more accurately interpret the results of *in vivo* metabolic studies.

# DEDICATION

I dedicate this dissertation to the loving memory of my papa, John Roberts, who I know would be beyond thrilled to see me finally finished with school.

# ACKNOWLEDGMENTS

I'd like to begin by first thanking my Lord and Savior Jesus Christ for all of his blessings and mercies, especially the opportunity to complete this degree and the strength to endure through this program. Without him, I am nothing.

I'd like to thank my committee chair, Dr. Dustin Yates for his mentorship throughout this program. Thank you for taking a chance on a PhD student who had little physiology experience, and giving me the opportunity to do things I never imagined were possible. I will always be grateful for my time in this program. I'd also like to thank my committee members, Drs. Jessica Petersen, Ty Schmidt, and Satish Kumar Natarajan, for all of their mentorship, support, and expertise throughout my program. You have taught me so much during my time here. There are many graduate students who I have worked beside throughout my time here who have truly shaped my program into what it was. Thank you for all your support and help throughout my time. They say it takes a village to raise a child, but I think it takes a village to make it through grad school. Although I could not possibly list all the people who have been there for me in the page limits allowed, I'd like to thank Dr. Rachel Gibbs for all of her support and friendship. You made all the hours in the analyzer room more enjoyable. I will miss our game nights, trips to wineries, and overall good times! I could not even think of writing this without thanking my other lab members Pablo Grijalva, Melanie White, Micah Most, Haley Beer, and Taylor Lacey for all of their help throughout my projects. It is impossible in this lab to work alone and I truly could not have done this without you. Your help was always appreciated!

I would be remiss not to acknowledge the friendships that have remained across multiple degrees, state lines, and time zones. With that, I would like to especially thank the best matron of honor Dr. Taylor Barnes Ross, Dr. Ariel Bergeron, Faith Wheelock, and my roomies for life Aubrey Videtich and Brogan Horton for your continued support throughout this journey. I appreciate your visits to see me, messages checking in on things, and just letting my vent about my grad school experience (even when you didn't understand it). I would not be here today without you!! A very special thank you to Dr. Callan Lichtenwalter who has stuck with me through all three degrees and being thousands of miles apart! Your support and daily cat pictures will mean more to me than you can know!

I'd also like to thank Dr. Jason Apple and Dr. Janeal Yancey for taking a timid freshman who only knew animal science as a path to vet school and showing me the many possibilities and opportunities animal science has to offer. I cannot thank you enough for all of the time and knowledge you have poured into me during my years at Arkansas and beyond. Without their mentorship, I would not be where I am today.

I'd like to thank my family for their love and encouragement in all of my endeavors. To my mom, thank you for instilling the love of education and learning. To my dad, thank you for instilling the pursuit of perfection. Thank you to my granny and brothers for their love and support as well (and for giving me two adorable nieces to spoil once grad school is over!). I would also like to thank my second family for their unending support throughout this journey! Thank you for always grounding us and giving us perspective!

Finally, I'd like to thank my husband, Nicolas Herrera, for being a part of my roller coaster ride of grad school. My PhD was much more enjoyable with you being apart of it. Thank you for accompanying me to 8 pm blood draws and always being willing to help during the midnight and 4 am lamb feeding shifts. You have been my strongest supporter, my sounding board, the solver of all my problems (or at least you're always trying to solve them), and a positive spin for every situation. My love for you is immeasurable, and my respect for you is immense. Your hardworking attitude, outgoing and inviting personality, and ability to ask the questions that make people think are just a few of the qualities I admire about you. You inspire me daily, and I could not have done this without you.

## Table of Contents

## Table of Figures

### Chapter 1



### Chapter 2

**Chapter 3**

## Table of Tables

### Chapter 2



### Chapter 3



### Chapter 4

**Chapter 5**

# CHAPTER 1 – Literature Review

Portions of this chapter were published as a review in *Frontiers in Animal Science*, which is a peer-reviewed publication

Hicks, Z.; Yates, D.; Going Up Inflame: Reviewing the Underexplored Role of Inflammatory Programming in Stress-Induced Intrauterine Growth Restricted Livestock: Review article. Front. Anim. Sci. Vol. 2. 2021
https://doi.org/10.3389/fanim.2021.761421

## Abstract

The impact of intrauterine growth restriction (IUGR) in humans is well known. It is the 2nd leading cause of perinatal mortality worldwide, and it is associated with deficits in metabolism and muscle growth that increase lifelong risk for hypertension, obesity, hyperlipidemia, and type 2 diabetes in survivors. Comparatively, the impact of IUGR in food animals is less recognized by the industry. Livestock born with low birthweight due to IUGR are beset with greater early death loss, inefficient growth, and reduced carcass merit. These animals exhibit poor feed-to-gain ratios, less lean mass, and greater fat deposition, which collectively increase production costs and decrease value. Ultimately, this reduces the amount of meat produced by each animal and threatens the economic sustainability of livestock industries. IUGR is most commonly the result of fetal programming responses to placental insufficiency, but the exact mechanisms by which this occurs are not well understood. In uncompromised pregnancies, inflammatory cytokines produced at normal rates by placental and fetal tissues play an important role in fetal development. However, unfavorable intrauterine conditions can cause their activity to be excessive during critical windows of fetal development. Our recent evidence indicates that this impacts developmental programming of muscle growth and

metabolism and contributes to the IUGR phenotype. In this review, we outline the role of inflammatory cytokine activity during normal and IUGR pregnancies. We discuss the fetal origins of inflammatory cytokines and how each may contribute to this phenotype. Finally, we highlight the contributions of sheep and other animal models in identifying mechanisms for IUGR pathologies.

## 1. Introduction

Intrauterine growth restriction (IUGR) frequently results from stress-induced placental insufficiency, which reduces $O_2$ and nutrients available to the fetus and consequently stunts growth of the highly metabolic fetal muscle tissues (Yates et al., 2018; Pendleton et al., 2021). In livestock, low birthweight due to stress-induced IUGR causes substantial economic losses for the industry due to greater neonatal mortality, less metabolic efficiency, and lower carcass quality (Reynolds et al., 2010; Liu and He, 2014; Ji et al., 2017; Yates et al., 2018). Estimates indicate low birthweight-related losses at approximately 8% of the potential annual product for US producers and up to 20% of the global annual product (Wu et al., 2006; Flinn et al., 2020). Thrifty metabolic adaptations associated with IUGR cause offspring to be disadvantaged at birth due to insufficient energy stores and poor thermoregulation, which often results in reduced nursing success and a failure to thrive throughout the early neonatal period (Dwyer et al., 2016; Yates et al., 2018). IUGR-born offspring that survive exhibit reduced feed efficiency, making it cost more to get them to harvest weight (Bérard et al., 2008; Yates et al., 2018; Gibbs et al., 2020). Thrifty programming also manifests as reduced muscle growth capacity and increased fat deposition (Greenwood et al., 2000; D T Yates et al., 2012; Gibbs et al.,

2020), which lowers carcass yield and affects meat quality parameters such as tenderness, muscle pH, meat color, and cooking loss (Liu and He, 2014; Matyba et al., 2021). Similar to livestock, IUGR afflicts human pregnancies as well (Saleem et al., 2011; Marcondes Machado Nardozza et al., 2017). Estimates indicate that upward of 53 million infants worldwide are born IUGR each year (Sedgh et al., 2014). These babies are at increased risk for perinatal morbidity and mortality (Aucott et al., 2004; Alisi et al., 2011; Alisjahbana et al., 2019) as well as life-long health problems such as asthma, type II diabetes, cardiovascular disease, obesity, and neurocognitive disorder that begin in early childhood and reduce life expectancy and quality of life (Briana and Malamitsi-Puchner, 2009; Marcondes Machado Nardozza et al., 2017; Darendeliler, 2019; Xing et al., 2020).

The scientific community recognized by the late 1950s that individuals with metabolic disease often exhibited physiological indicators of predispositions as early as shortly after birth (Neel, 1962). However, it was the work of Hales and Barker in the early 1990s and the subsequent publication of their Thrifty Phenotype hypothesis that popularized the link between fetal developmental programming and lifelong metabolic health (Hales et al., 1991; Hales and Barker, 1992). In the almost three decades since, a number of studies in humans and animal models have confirmed this link and begun to uncover details regarding how stress before birth causes tissue-specific programming of growth and metabolism (Morrison, 2008; Posont et al., 2017; Yates et al., 2018; Posont and Yates, 2019; Pendleton et al., 2021). These nutrient-sparing fetal adaptations help to increase the chances for survival in utero but also create permanent changes that are detrimental to long-term health of the offspring (Sharma et al., 2016a; Kesavan and Devaskar, 2019; Posont and Yates, 2019). Identifying the exact mechanistic facilitators of

these changes has been challenging, but one likely potential mechanism that has recently come to light is inflammatory programming (Cadaret et al., 2018; Posont et al., 2018; Posont et al., 2021). This review highlights the findings that provide insight for how fetal stress leads to programmed changes in the inflammatory pathways that regulate growth and metabolism, with a primary focus on the implications for meat animals.

## 2. Causes and Progression of IUGR

### *2.1 IUGR is the developmental response to maternofetal stress*

Clinical IUGR, alternatively termed fetal growth restriction (FGR; Marcondes Machado Nardozza et al., 2017), is characterized by less intrauterine growth of the fetus or fetal tissues relative to its expected growth potential (Sharma et al., 2016b; Reynolds et al., 2019). It is a pathological condition brought on by fetal nutrient restriction or other maternofetal stress, although genetic abnormalities can increase the risk (Sharma et al., 2017), and it is a leading cause for small-for-gestational age (SGA) offspring (Chu et al., 2020). In the research field of developmental origins of health and disease (DOHaD), IUGR is often used to describe the broader pathological phenotype resulting from chronic fetal stress, which typically but not always includes measurable reductions in placental function and birthweight (Sharma et al., 2016b). A number of different maternal conditions can result in placental stunting when coinciding with critical windows for placental growth and development (Sharma et al., 2016b; Yates et al., 2018). In livestock, common factors include environmental stress, illness or forage toxicity, nutritional imbalances, young age of the dam, uterine trauma from previous pregnancies, twin/triplet pregnancies, and side effects from assisted reproductive technologies (Greenwood and

Bell, 2003; Greenwood and Cafe, 2007). Such stressors often redirect maternal blood flow from the gravid uterus, thus reducing nutritional support for placental hyperplasia and vasculogenesis (Burton and Jauniaux, 2018). Placental functional capacity is determined in large part by the successful establishment of uteroplacental circulation via the rapid development of villous blood vessels beginning toward the end of the first trimester and continuing throughout the second trimester (Regnault et al., 2003; Burton and Jauniaux, 2018). Indeed, it is during this critical window that the placenta is most vulnerable to insults that may lead to reduction in its surface area and production of proteins needed for maternal-fetal nutrient exchange (Regnault et al., 2005; Burton and Jauniaux, 2018). During such insults, placental tissues are typically characterized by unusually high levels of inflammation, oxidative stress, and apoptotic cells (Cotechini and Graham, 2015; Burton and Jauniaux, 2018).

The diminished maternofetal interface associated with placental insufficiency ultimately reduces $O_2$ transfer to the fetus, and reductions in placental glucose and amino acid transporters likewise reduce the availability of these nutrients to the fetus (Brown, 2014a; Yates et al., 2018; Beede et al., 2019). Indeed, fetal hypoxemia and hypoglycemia in heat stress-induced sheep models of placental insufficiency can exceed 50% reductions near term (Macko et al., 2016; Wai et al., 2018; Stremming et al., 2020), creating the need for changes in metabolic processes and growth trajectories (Lackman et al., 2001; Gagnon, 2003). The phenomenon of fetal hypoglycemia can be partially mimicked by sustained maternal undernutrition, which can decrease fetal growth despite little or no impact on the size or vascularity of the placenta (Lemley et al., 2012; Eifert et al., 2015; Edwards et al., 2020). Interestingly, diminished placental transfer of amino acids due to

the downsizing of system A and L transporters does not necessarily manifest in reduced fetal blood concentrations (Pantham et al., 2016; Wai et al., 2018), as the IUGR fetus compensates by slowing its protein utilization and accretion rates (Rozance et al., 2018b; Wai et al., 2018; Stremming et al., 2020).

The hypoxic and hypoglycemic conditions resulting from placental insufficiency cause a robust hormone-driven stress response by the IUGR fetus. Low blood $O_2$ concentration detected by $O_2$-sensitive $K^+$ channels on the chromaffin cells of the adrenal medulla stimulates secretion of the catecholamines, norepinephrine and epinephrine (Adams and McMillen, 2000), inducing the hallmark hypercatecholaminemia that progressively worsens over the 3rd trimester of pregnancy. Catecholamines act as strong inhibitors of insulin secretion, which together with hypoglycemia results in a chronic state of fetal hypoinsulinemia (Chen et al., 2017; Limesand and Rozance, 2017). Fetal hypoxemia also leads to an increase in circulating inflammatory cytokines (Krajewski et al., 2014; Visentin et al., 2014), which will be discussed in detail in later sections. Additional inflammatory components such as chemokine C-C motif ligand 16 (CCL16) and acute phase protein C-reactive protein (CRP) have also been found to be increased in IUGR fetuses (Mäkikallio et al., 2012; Visentin et al., 2014).

### *2.2 IUGR impairs growth capacity and metabolic function*

In most cases, the fetus is able to survive the unfavorable conditions created by placental insufficiency by altering the development of growth and metabolic processes to reduce metabolic demands in several ways (Gagnon, 2003). First, the combined endocrine response to the low fetal blood $O_2$ content causes a redirection of blood flow

away from skeletal muscle and other less vital tissues to maintain support for the brain, liver, adrenals, and pancreas (Gagnon, 2003; Poudel et al., 2014). Indeed, greater vascular resistance in muscle-dense areas such as the hindlimb can reduce blood flow to the area by as much as 45%, which in turn reduces $O_2$ delivery by up to 40% (Rozance et al., 2018b). Secondly, hypoinsulinemia reduces glucose utilization by the insulin-sensitive muscle tissue (Davis et al., 2020). Interestingly, this can lead to transient enhancement of insulin sensitivity in the early neonatal period as a compensatory response (Soto et al., 2003; Ong et al., 2004). However, this wanes relatively quickly (Mericq et al., 2005), exposing underlying impairment of insulin action (Jensen et al., 2002).

*2.2.1 Poor skeletal muscle growth leads to asymmetric body composition*

The intentional reduction in nutrient supply to IUGR fetal skeletal muscle cause it to develop more conservative growth rates that are apparent in late gestation but also persist throughout the lifetime of the animal. Indeed, IUGR fetal sheep and rats were found to have smaller muscle fiber areas near term for all fiber types (Yates et al., 2016; Cadaret et al., 2019a), indicating that less muscle hypertrophy was occurring during gestation. Intrinsic functional deficits in muscle stem cells called myoblasts are a major underlying factor for impaired muscle growth capacity (Yates et al., 2014a; Soto et al., 2017; Posont et al., 2018). In ruminants and humans, muscle hyperplasia is completed early in the 3rd trimester, and subsequent muscle growth is the result of myofiber hypertrophy (Maier et al., 1992; Wilson et al., 1992). Indeed, postnatal muscle growth results from the accumulation of new nuclei within muscle fibers from fusion with myoblasts, which increases capacity for protein synthesis by the fiber (Allen et al., 1979;

Davis and Fiorotto, 2009). Some fetal myoblasts form quiescent populations between the sarcolemma and the basal lamina of muscle fibers. These latent myoblasts are called satellite cells and can later be activated to serve as progenitors for further muscle growth (Davis and Fiorotto, 2009; Yin et al., 2013). Before fusing, myoblasts undergo several cycles of proliferation and then terminal differentiation, which are rate-limiting functional stages for muscle growth (Allen et al., 1979; Allen and Boxhorn, 1989). However, myoblasts from IUGR fetal sheep and rats exhibited reduced proliferation and differentiation capabilities (Yates et al., 2014; Soto et al., 2017; Posont et al., 2018; Cadaret et al., 2019a), leading to reduced muscle mass at birth and throughout postnatal life (Figure 1).

Offspring born with low birthweight due to IUGR initially continue to exhibit slower postnatal growth. For example, lambs born IUGR due to maternal heat stress or maternofetal inflammation remained about 20% smaller at 30 days of age, with comparable reductions in average daily gain (Cadaret et al., 2019b; Yates et al., 2019; Posont et al., 2021). As IUGR-born offspring reach the juvenile stage, many begin to exhibit postnatal catch-up growth, whereby their bodyweights equalize with uncompromised herd mates. Indeed, bodyweights and average daily gain for lambs born IUGR due to maternal heat stress were reduced by only about 12% by 60 days of age (Gibbs et al., 2020), and IUGR-born beef cattle were about 8% lighter at 30 months of age (Greenwood et al., 2005; Greenwood and Cafe, 2007). However, this does not typically equate to recovery of muscle growth, and thus body composition remains impaired; 60-day old IUGR lambs had smaller loin eye areas, reduced muscle protein, and greater fat-to-protein ratios (Gibbs et al., 2020), and 30-month old IUGR beef cattle

had smaller carcass weight, ribeye area, and *longissimus* muscle weight, resulting in less retail yield (Greenwood and Cafe, 2007). Estimates from these cattle indicate that each 1-kg reduction in birthweight equated to a 4.4-kg reduction in slaughter weight (Robinson et al., 2013; Greenwood and Bell, 2019).

### *2.2.3 Thrifty muscle glucose metabolism*

In concert with conservative muscle growth, the IUGR fetus undergoes a glucose-conserving, muscle-centric metabolic shift characterized in by reduced oxidation and greater glycolytic lactate production. When IUGR fetal sheep were made hyperglycemic or hyperinsulinemic near term, whole-body glucose oxidation was decreased even though whole-body glucose utilization remained unchanged (Limesand et al., 2007; Brown et al., 2015). Later studies in sheep confirmed that the reduction in glucose oxidation rates were muscle-specific and persisted after birth (Cadaret et al., 2019b; Yates et al., 2019; Gibbs et al., 2021; Posont et al., 2021). Four-fold greater circulating lactate concentrations together with greater hepatic expression of gluconeogenic genes in the IUGR fetal sheep (Brown et al., 2015) indicate that lactate produced in greater amounts by IUGR skeletal muscle supports hepatic glucose production. This process, called the Cori cycle, seemingly provides a benefit to the nutrient-restricted IUGR fetus by engaging an otherwise inactive source for glucose (Thorn et al., 2009; Davis et al., 2021). However, it is important to note that the reduction in glucose oxidation arises from a programmed change in mitochondrial functional capacity that does not appear to be reversible. Although pyruvate dehydrate functional activity was increased in IUGR fetal sheep muscle (Pendleton et al., 2019), mitochondrial $O_2$ consumption and electron transport

chain Complex 1 activity were impaired (Pendleton et al., 2020). Gene expression for isocitrate dehydrogenase, mitochondrial pyruvate carrier, and other integral components of mitochondrial oxidative metabolism were also reduced in IUGR muscle, whereas gene expression for lactate dehydrogenase B (converts pyruvate to lactate) was increased 2.5-fold (Pendleton et al., 2020). It is worth noting that reduced glucose oxidation rates do not appear to be offset by compensatory amino acid oxidation (Pendleton et al., 2021). In fact, oxidation rates for the representative amino acid, leucine, were slightly reduced in IUGR fetal sheep (Brown et al., 2012; Wai et al., 2018). Moreover, impaired glucose oxidation coincided with reduced proportions of oxidative myofibers in hindlimb muscles of IUGR fetal sheep (Yates et al., 2016).

### *2.2.4 Insulin dysfunction*

Growth and metabolic deficits in IUGR skeletal muscle are at least partially a product of disruptions in insulin signaling through Akt-mediated pathways. Insulin is a primary promotor of muscle growth, as it enhances protein synthesis (Davis and Fiorotto, 2009) and is a well-established stimulator of proliferation and differentiation in adult myoblasts (Allen et al., 1985; Sumitani et al., 2002). More recent studies found that hyperinsulinemia also increases myoblast function in fetal sheep (Brown et al., 2016; Soto et al., 2017). Additionally, skeletal muscle is the primary tissue for insulin-mediated glucose uptake from the blood (Baron et al., 1988; Brown, 2014a). This is facilitated when circulating insulin binds to receptors on the muscle fiber surface and initiates rapid mobilization of sequestered glucose transporter 4 (Glut-4) to the cell membrane, where they facilitate glucose diffusion into the cell (Kubota et al., 2011). In addition to its

effects on glucose uptake, insulin stimulation increased skeletal muscle glucose oxidation rates 1.5 to 4-fold in fetal sheep (Brown et al., 2015; Cadaret et al., 2019) and 2 to 8-fold in growing lambs (Barnes et al., 2019; Cadaret et al., 2019b; Swanson et al., 2020; Posont et al., 2021). However, several studies have indicated that insulin/Akt signaling is impaired in IUGR muscle. Insulin activates Akt by serine463 phosphorylation, but the proportion of phosphorylated Akt was reduced in flexor digitorum superficialis muscle from IUGR fetal and neonatal sheep (Cadaret et al., 2019; Posont et al., 2021). This deficit was observed at both low and high insulin concentrations and did not coincide with any reductions in insulin receptor content (Thorn et al., 2009; Yates et al., 2019). IUGR skeletal muscle also exhibited reduced content of the insulin-sensitive glucose transporter, Glut-4, before and after birth (Limesand et al., 2007; Yates et al., 2019), likely due to epigenetic mechanisms such as DNA methylation at the Glut-4 promoter region or histone modifications (Raychaudhuri et al., 2008; Wang et al., 2016).

### *2.2.5 Dysfunction in non-muscle tissues*

Stress conditions resulting from placental insufficiency induce programming in other tissues that further compounds muscle-centric dysfunction. Chief among these affected tissues are pancreatic islets, which are diminished in both development and functionality (Boehmer et al., 2017). Near term, IUGR fetal sheep islets are reduced in size by 40% (Rozance et al., 2015; Brown et al., 2016), and β cell mass is reduced by 60% due to a 40 to 60% reduction in mitosis (Limesand et al., 2005; Brown et al., 2016). In addition to being smaller, these β cell populations are less productive, as IUGR fetal islets contain only about 20% the amount of insulin found in normal fetal islets

(Limesand et al., 2006). Deficits in islet microanatomy are preceded by insufficient islet vascular formation, which is observable early in the 3rd trimester (Rozance et al., 2015). Islet under-development may be due in part to the less profound HGF paracrine activity originating from islet endothelial cells (Rozance et al., 2015; Brown et al., 2016), which appears particularly necessary for β cell development and performance (Dai et al., 2005; Johansson et al., 2009). Like muscle, IUGR fetal islets are also less capable of glucose oxidation, which is the impetus for glucose-stimulated insulin secretion (Limesand et al., 2006). These programmed deficits persist is offspring, as islets from IUGR-born lambs maintained substantially reduced insulin content and glucose stimulus-secretion coupling (Yates et al., 2019), leading to impairments in glucose-stimulated insulin secretion that are comparable to the fetus (Cadaret et al., 2019b; Yates et al., 2019). Interestingly, α cell mass is reduced in IUGR fetal islets, but not to the same magnitude observed for β cells. Moreover, their capacity to appropriately secrete glucagon appears to be unaffected (Limesand et al., 2005).

## 3 The role of inflammatory cytokines in IUGR outcomes

### *3.1 Cytokines regulate muscle growth and metabolism*

Cytokines are a broad class of peptide chemical messengers produced by a wide array of cell and tissue types, often as a response to the presence of pathogens, toxins, enterotoxins, free radicals, or other sources of stress (Tracey and Cerami, 1993; Reid and Li, 2001). Among their other immune functions, inflammatory cytokines modify metabolic activity in muscle and other tissues in order to reappropriate $O_2$, glucose, and other energy substrates (Li and Reid, 2001; Cadaret et al., 2017). They are also potent

regulators of muscle growth via their complex impact on myoblast function and insulin sensitivity (Otis et al., 2014; Posont et al., 2018). This makes the broad cytokine milieu integral to metabolic homeostasis and, in turn, general metabolic health.

Tumor necrosis factor α (TNFα) is perhaps the most comprehensively studies inflammatory cytokine. It is produced in greatest quantities by circulating monocytes and their tissue counterparts, macrophages, but are produced by glycolytic skeletal muscle fibers and fat cells as well (Tracey and Cerami, 1993; Li and Reid, 2001; Plomgaard et al., 2005; Dyck et al., 2006). Basal circulating TNFα concentrations are typically low but increase rapidly and profoundly when stimulated (Tracey and Cerami, 1993; Li and Reid, 2001). Pathological metabolic states such as excessive fat deposition, insulin resistance, and hyperglycemia are associated with substantially greater production and secretion of TNFα (Saghizadeh et al., 1996; Lo et al., 2007), as is pathological muscle atrophy (Li and Reid, 2001). Most cell types express one or both of two surface TNFα receptor isoforms (TNFR1, TNFR2), and TNFR1 is predominant for muscle (Popa et al., 2007). Once activated by TNFα, the intracellular domain of TNFR1 binds and activates TNF receptor-associated death domain (TRADD) protein (Popa et al., 2007), which in turn activates Fas-associated death domain (FADD) pathways and TNF receptor-associated factor 2 (TRAF2)/NF-κB pathways (Popa et al., 2007). In skeletal muscle, these pathways are most associated with protein catabolism, lipolysis, and metabolic suppression (Cheema et al., 2000; Li and Reid, 2001; Popa et al., 2007). It also decreases synthesis of the myofibril components myosin and actin as well as sarcoplasmic proteins (Cheema et al., 2000; Li and Reid, 2001; Lang et al., 2002) . In differentiating myoblasts, TNFα inhibits MyoD expression, which impedes their progression, and in mature fibers it increases

protein catabolism, which reduces the content of myosin and other integral proteins for muscle function (Li and Reid, 2001). Both of these outcomes appear to be mediated by the canonical nuclear factor-κB (NFκB) pathway (Li and Reid, 2001; Remels et al., 2015). TNFα-activated NFκB pathways also increase the proportion of glucose undergoing glycolytic lactate production in muscle through the activity of hypoxia-inducible factor-1α (HIF-1α), which was concurrent with reduced glycogen synthesis (Boscá and Corredor, 1984; Rhoades et al., 2005; Remels et al., 2015). The effect of TNFα on glucose oxidation rates are more complex, as exposure appears to be stimulatory when acute but inhibitory when sustained (Gao et al., 2012; Cadaret et al., 2017; Cadaret et al., 2019). In addition to the direct effects on muscle growth and metabolism, TNFα also impairs insulin sensitivity. In rats, this diminished the effects of insulin on skeletal muscle glucose uptake by 50% (Youd et al., 2000; Li and Reid, 2001), perhaps by increasing the content of diacylglyceride (DAG) a potent activator of the insulin antagonist protein kinase C (Bruce and Dyck, 2004; Dyck et al., 2006). In pancreatic islet cells, TNFα exposure was shown to reduce glucose metabolism in β cells and, in turn, glucose-stimulated insulin secretion (Oleson et al., 2015).

The interleukin IL-6 is produced by leukocytes and muscle cells, often in response to rising TNFα concentrations (Tracey and Cerami, 1993; Haddad et al., 2005). Consequently, circulating IL-6 concentrations follow similar patterns as TNFα during sub-acute and chronic inflammatory conditions (Wolsk et al., 2010). When bound, the soluble IL-6 receptor (sIL-6R) forms a heterodimer with the downstream messenger gp130 (Wang et al., 2013), which primarily activates the JAK/STAT3 pathway but can also activate the PI3K/Akt/mTOR and Ras/Raf/MEK/ERK pathways (Wang et al., 2013;

Johnson et al., 2018). Elevated IL-6 activity limits hypertrophic muscle growth by interfering with growth hormone and IGF-I activity and also increases muscle protein catabolism, thus contributing to muscle atrophy (Haddad et al., 2005; Bodell et al., 2009). Although it may increase myoblast proliferation at some concentrations, IL-6 also reduced the progression of differentiation in primary fetal sheep myoblasts (Haddad et al., 2005; Posont et al., 2018). The predominant aspects of metabolic regulation by IL-6 are similar to those of TNFα. First, the exact nature of IL-6 effects on skeletal muscle appear to be dependent on the magnitude and duration of exposure, as evidence indicates that sustained exposure is substantially more detrimental. Additionally, IL-6 is associated with pathological metabolic states, presumably due to its propensity to decrease skeletal muscle carbohydrate metabolism in favor of fatty acid oxidation and to disrupt insulin signaling (Bruce and Dyck, 2004; Wolsk et al., 2010; Knudsen et al., 2017). Finally, IL-6 is detrimental to pancreatic islet function, as overexpression of IL-6 in β cells resulted in alterations to islet structure, increased fibrosis, and decreased insulin production (Campbell et al., 1994).

Additional inflammatory cytokines appear to have roles in muscle regulation but have been less extensively studied. For example, IL-1β is involved in collagen degradation, muscle protein catabolism, and branched-chain amino acid metabolism (Nawabi et al., 1990; Dinarello, 2000; Li et al., 2009). Consequently, it is associated with reduced myofiber width, myofibril construction, and actin content (Li et al., 2009). In islets, IL-1β promotes β cell apoptosis, which impairs glucose-stimulated insulin secretion (Harms et al., 2015; Oleson et al., 2015). IL-18, IL-8, and TWEAK appear to have similar roles in regulating muscle growth and metabolism.

### *3.2 Inflammatory tone in the IUGR fetus*

Studies in a multitude of mammalian species show that IUGR fetuses exhibit greater circulating leukocyte and cytokine concentrations, which correlate closely with hypoxemia and can adversely affect tissue development (Romero et al., 2008; Rong Guo et al., 2010; Cadaret et al., 2019; Oh et al., 2019). Increased TNFα, IL-6, and IL-18 were observed in cord blood of IUGR infants at delivery and in blood serum at 24 hours after delivery (Krajewski et al., 2014; Visentin et al., 2014). In fact, high concentrations of inflammatory cytokines in cord blood are considered reliable clinical markers for diagnosing fetal inflammatory response syndrome (FIRS; Kemp, 2014). In IUGR fetal sheep, greater circulating TNFα in the mid-3rd trimester coincided with increased monocytes, granulocytes, and total white blood cells (Cadaret et al., 2019). Similarly, IUGR fetal rodents exhibited elevated blood concentrations of TNFα, IL-6, and IFNγ, as well as greater leukocyte activity (Hudalla et al., 2018; Cadaret et al., 2019a). In addition to circulating concentrations, cytokine expression is elevated in IUGR tissues including lungs, brain, skeletal muscle, and white blood cells (Kemp, 2014; Cadaret et al., 2019a), but not necessarily in pancreatic islets (Kelly et al., 2017).

### *3.3 Enhanced inflammatory sensitivity in IUGR tissues*

Some rodent models of IUGR indicate that greater circulating cytokine concentrations are maintained into adulthood. Indeed, IUGR-born rat and mice offspring exhibited greater circulating TNFα, IL-6, and IL-1β from birth to adulthood (Desai et al., 2009; Riddle et al., 2014; Chisaka et al., 2016; Oliveira et al., 2017). However, recent findings indicate that enhanced cytokine signaling pathways in muscle and other tissues

maintain increased inflammatory tone even when elevated circulating cytokines subside after birth. We have postulated that this enhanced responsiveness to cytokines contributes to the persistent dysregulation of muscle growth and metabolic function observed in IUGR-born offspring (Yates et al., 2018; Posont and Yates, 2019). At term, skeletal muscle from IUGR rat pups exhibited greater gene expression for TNFR1, IL6R, and Fn14 (Cadaret et al., 2019a). Moreover, muscle from IUGR-born mice and rats exhibited greater TNFα and IL-6 gene expression at 2 and 12 months after birth (Sutton et al., 2010; Tarry-Adkins et al., 2016). In sheep, proliferation and differentiation rates of primary IUGR fetal myoblast were reduced when exposed to basal or high TNFα or IL-6 concentrations (Posont et al., 2018). Additional unpublished data from these samples indicate increased gene expression for TNFR1 and IL6R in IUGR myoblasts and semitendinosus muscle, as well as reduced muscle IκBα protein content and increased c-Fos protein content. As neonates, IUGR-born lambs exhibited increased TNFR1 protein content in semitendinosus muscle and greater circulating concentrations of monocytes, granulocytes, and platelets (Posont et al., 2021). Transcriptomics was subsequently performed in muscle samples from these lambs, and preliminary findings indicate that gene expression for numerous components of TNFα, IL-6, IL-1β, and IL-12 pathways are upregulated, as summarized in Table 1. This paralleled similar transcriptomics findings in skeletal muscle from IUGR fetal sheep (Cadaret et al., 2019; Posont and Yates, 2019). Interestingly, these IUGR-born lambs also exhibited greater muscle IκBα protein content and a 50% reduction in circulating TNFα, perhaps as a compensatory mechanism for the enhanced cytokine sensitivity (Posont et al., 2021). Although additional studies are needed to fully understand the magnitude and nature of inflammatory programming in

IUGR skeletal muscle, it is clear that such enhanced activity would help to explain the deficits in myoblast function, muscle growth, body composition, insulin action, and metabolic efficiency described in earlier sections.

### *3.4 Targeting inflammatory adaptations may improve IUGR outcomes*

Inflammatory programming is likely one of several underlying mechanisms for IUGR-associated pathologies, but its ability to be targeted makes it of particular interest. In fact, several studies have provided fundamental evidence that treating IUGR fetuses and IUGR-born offspring with anti-inflammatory nutrients or pharmaceuticals can help to mitigate or improve growth and metabolic deficits. In mice, maternal supplementation of the anti-inflammatory nutraceutical folic acid reduced the frequency and severity of IUGR resulting from maternal inflammation (Zhao et al., 2013). These mice receiving folic acid also exhibited a less severe increase in amniotic concentrations of IL-6 and other cytokines and well as nitric oxide. Although not assessed in muscle, the enhancement of cytokine signaling pathways observed in IUGR placental tissues was mitigated by folic acid (Zhao et al., 2013). In sheep, direct daily infusion of the anti-inflammatory nutraceutical eicosapentaenoic acid (EPA) into the bloodstream of IUGR fetuses during the mid-3rd trimester of gestation for 5 days resulted in less severe fetal hypoxia, hypoglycemic, and hyperlactatemia (Beer et al., 2021). In addition, the greater lactate production observed for IUGR fetuses during hyperglycemia was improved substantially, perhaps indicating a less severe metabolic shift to glycolytic lactate production by muscle (Lacey et al., 2021). This coincided with an improvement in fetal growth and body symmetry. EPA infusion also improved whole hindlimb mass as well as

loin and flexor digitorum superficialis muscle mass in the IUGR fetuses, which is indicative of improved muscle growth during late gestation (Lacey et al., 2021). It is worth noting that growth was not recovered for all muscles, which may have been due to the natural differences in size, insulin sensitivity, and metabolic phenotypes among muscle groups (Kirchofer et al., 2002). After IUGR fetuses had been infused with EPA for 5 days, they exhibited improved basal and glucose-stimulated insulin secretion, indicating partial rescue of pancreatic islet function (Lacey et al., 2021). These fetuses also exhibited improvements in blood pH, HCO+, $Na^{+}$, and $Ca^{++}$ concentrations, which indicate improved fetal health and wellbeing (Lacey et al., 2021). In addition to nutrient compounds, maternal delivery of anti-inflammatory pharmaceuticals may also represent an effective intervention strategy. A recent clinical study showed that high doses of the nonsteroidal anti-inflammatory drug (NSAID) aspirin taken by pregnant women during critical windows of fetal development reduced the frequency of IUGR (Roberge et al., 2017). Of course, the benefits of such drugs must be considered in combination with potential side effects for fetal development. Inflammatory programming can also be targeted in offspring, which is of particular interest in livestock. Dietary supplementation of the anti-inflammatory nutraceutical curcumin to IUGR-born neonatal pigs and mice mitigated the elevated concentrations of blood TNFα, IL-6, and IL-1β, which improved insulin sensitivity, lipid homeostasis, and neonatal growth (Niu et al., 2019a; Niu et al., 2019c; Niu et al., 2019b).

## 4 Implications

The link between maternofetal stress, IUGR-induced low birthweight, and postnatal deficits in metabolic efficiency and growth potential are well established in livestock, but scientific advancements regarding the molecular mechanisms underlying this link have been lacking. However, recent studies provide evidence that systemic fetal inflammation and developmental programming that enhances tissue sensitivity to inflammatory cytokines are contributing factors to growth and metabolic deficits, particularly those that are muscle centric. Although inflammatory programming is likely one of many underlying mechanisms, it is of particular interest to the livestock industry because it is both identifiable and treatable. Indeed, there are a number of currently-marketed nutritional supplements and pharmaceuticals with anti-inflammatory properties, which could provide producers a number of options for mitigation and treatment strategies. Food animals born with low birthweight due to stress-induced IUGR are persistently one of the greatest barriers to US and global livestock production. Moreover, the emergence of climate change will likely increase the incidence of environmental stress on pregnant animals, creating a greater challenge for sustainable livestock production. As the global population continues to increase, recovering growth, efficiency, and meat production in low birthweight animals through practical management strategies represents one of the most realistic options for increasing meat production without greater land and water resource inputs. Although more work is warranted, early evidence indicates that treatment of enhanced inflammatory tone in IUGR-born animals may be an effective approach.

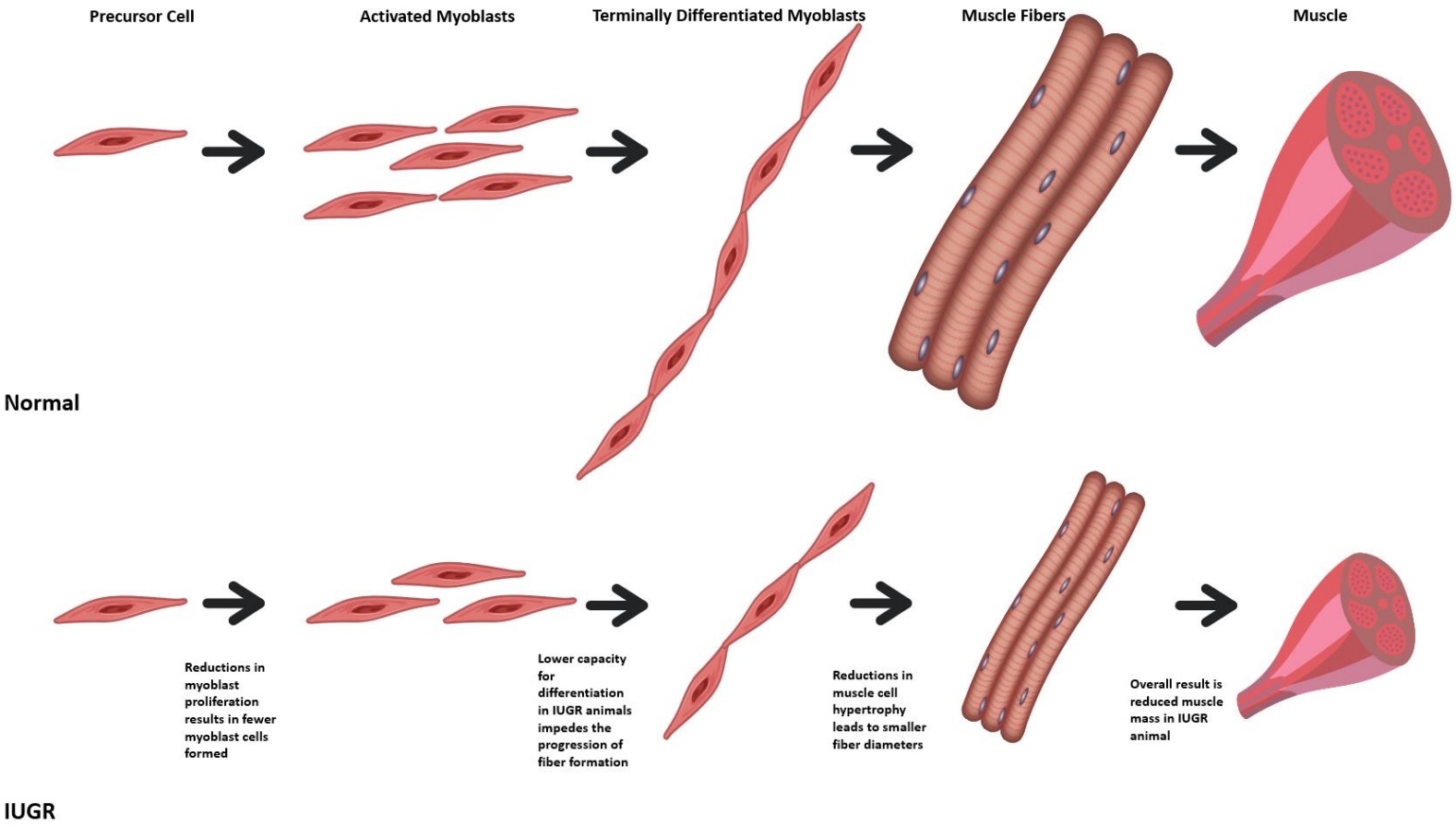


**Figure 1.1**. Functional steps of myoblasts (muscle stem cells) and their facilitation of hypertrophic growth in normal and IUGR skeletal muscle.

| Cytokine | Tissue | | |
|---|---|---|---|
| | **Skeletal muscle** | **Pancreatic islets** | **Other** |
| TNFα | ↓MyoD (Li and Reid, 2001; Alvarez et al., 2020)<br>↓Myoblast differentiation (Alvarez et al., 2020)<br>↓Myosin, actin, and sarcoplasmic proteins (Alvarez et al., 2020)<br>↑Protein catabolism (Cheema et al., 2000; Popa et al., 2007)<br>↑Glycolysis (Boscá and Corredor, 1984; Rhoades et al., 2005; Remels et al., 2015) | ↓Glucose oxidation in β cells (Oleson et al., 2015)<br>↓Glucose-stimulated insulin secretion (Oleson et al., 2015)<br>↓Insulin sensitivity (Youd et al., 2000; Li and Reid, 2001) | ↑Lipolysis in fat deposits (Cheema et al., 2000; Popa et al., 2007) |
| IL-6 | ↓Muscle hypertrophy (Haddad et al., 2005; Bodell et al., 2009)<br>↓Myoblast differentiation (Haddad et al., 2005; Posont et al., 2018)<br>↑Muscle atrophy (Haddad et al., 2005; Bodell et al., 2009) | Altered islet structure (Campbell et al., 1994)<br>↑Fibrosis (Campbell et al., 1994)<br>Impaired insulin signaling (Bruce and Dyck, 2004; Wolsk et al., 2010; Knudsen et al., 2017) | ↓GH and IGF-1 secretion and sensitivity, multiple tissues (Haddad et al., 2005; Bodell et al., 2009) |
| IL-1β | ↑Protein catabolism (Nawabi et al., 1990; Dinarello, 2000; Li et al., 2009)<br>↓Myofiber width (Li et al., 2009)<br>↓Actin content (Li et al., 2009) | ↑β cell apoptosis (Harms et al., 2015; Oleson et al., 2015)<br>↓Glucose-stimulated insulin secretion (Harms et al., 2015; Oleson et al., 2015) | Collagen degradation, multiple tissues (Nawabi et al., 1990; Dinarello, 2000; Li et al., 2009) |

**Figure 1.2**. Summary of major effects that key inflammatory cytokines elicit in tissues affecting growth and efficiency in meat animals.

# CHAPTER 2 – Mid-gestation maternofetal inflammation causes intrauterine growth restriction in part by reducing myoblast function in the late gestation ovine fetus


## Abstract

Maternofetal inflammation occurring in the 3rd trimester causes fetal intrauterine growth restriction (**IUGR**) in part by impairing peak muscle growth. However, the impact of maternofetal inflammation occurring at mid-gestation, which precedes peak muscle growth but coincides with peak placental growth, has not been explored. Therefore, the objective of this study was to examine this impact on fetal growth, body composition, and myoblast function. Pregnant ewes were injected every 3rd day from the 50th to the 65th d of gestational age (**dGA**; term=150 dGA) with saline placebo (control; n=12) or with bacterial lipopolysaccharide endotoxin (0.1 μg/kg) to induce maternofetal inflammation and fetal IUGR (**MI-IUGR**; n=15). Fetuses were surgically catheterized on dGA 118 to collect daily blood samples and necropsied on dGA 125 to assess growth metrics. Cross sections of the *semitendinosus* muscle were fixed for immunohistochemistry. Primary myoblasts were isolated from upper hindlimb muscles. MI-IUGR fetuses had reduced ($P < 0.05$) partial pressure of $O_2$ and increased ($P < 0.05$) TNFα and IL-6 compared to controls. At necropsy, bodyweights were 23% lighter ($P < 0.05$), hindlimbs were 25% smaller ($P < 0.05$), and cannon bones were 6% shorter ($P < 0.05$) for MI-IUGR fetuses compared to controls. MI-IUGR fetuses also had lighter ($P < 0.05$) *semitendinosus, flexor digitorum superficialis,* and *longissimus dorsi* muscles compared to controls. Heart, liver,

and brain mass did not differ between control and MI-IUGR fetuses, but brain/bodyweight and heart/bodyweight were greater ($P < 0.05$) for MI-IUGR fetuses. MI-IUGR fetuses tended to have 14% fewer ($P = 0.06$) proliferating myoblasts and had 32% fewer ($P < 0.05$) differentiating myoblasts in the *semitendinosus*, independent of total myoblasts present. Furthermore, *semitendinosus* muscle fibers were 13% smaller ($P < 0.05$) for MI-IUGR fetuses than controls. *Ex vivo* proliferation rates were increased ($P < 0.05$) and differentiation rates were reduced ($P < 0.05$) for myoblasts isolated from MI-IUGR fetuses compared to controls. We conclude that sustained maternofetal inflammation during peak placental development reduced myoblast functional capacity by impairing normal differentiation, which in turn contributed to reduced skeletal muscle mass and asymmetrical body composition near term. This reflects the growth phenotype in models of placental insufficiency-induced IUGR and implicates inflammation as a major factor in the adaptive growth restriction of skeletal muscle in IUGR fetuses.

## Introduction

Intrauterine growth restriction (**IUGR**) is a worldwide health problem that impacts up to 53 million babies each year (Wu et al., 2006; Sedgh et al., 2014; Flinn et al., 2020). The same condition in animals causes a 20% reduction in the global annual product from livestock species (Wu et al., 2006). IUGR-born offspring exhibit reduced feed efficiency, increased proportional fat deposition, and reduced muscle growth, which increase the cost to produce the animal and decrease the value of the carcass (Greenwood et al., 2000; Bérard et al., 2008; Yates et al., 2012; Yates et al., 2018; Gibbs et al., 2020).

In humans, IUGR-born individuals are at increased risk for metabolic dysfunction as a result of adaptive fetal programming, which leads to reduced quality of life and life expectancy (Briana and Malamitsi-Puchner, 2009; Marcondes Machado Nardozza et al., 2017; Darendeliler, 2019; Xing et al., 2020). Sustained fetal inflammation is a common underlying state across IUGR animal models (Hicks and Yates, 2021). Elevated circulating inflammatory cytokines in particular have been observed in IUGR fetuses of several species and from several maternal-stress causes (Kemp, 2014; Krajewski et al., 2014; Visentin et al., 2014; Hudalla et al., 2018; Cadaret et al., 2019; Hicks and Yates, 2021). These cytokines, including TNFα and IL-6, impair myoblast differentiation, reduce accretion of skeletal muscle protein, and increase the rates of protein catabolism and muscle atrophy (Cheema et al., 2000; Dinarello, 2000; Haddad et al., 2005; Popa et al., 2007; Bodell et al., 2009; Posont et al., 2018; Alvarez et al., 2020; Hicks and Yates, 2021).

Studies by us and others have shown that the heightened inflammatory regulation of IUGR fetal and neonatal tissues occurs on multiple levels, as detailed in our recent review (Hicks and Yates, 2021). Indeed, studies in a multitude of species demonstrate increased circulating monocytes and other white blood cells as well as circulating inflammatory cytokines in IUGR fetuses (Romero et al., 2008; Rong Guo et al., 2010; Caitlin N. Cadaret et al., 2019; Oh et al., 2019; Hicks and Yates, 2021). Additionally, studies have identified increases in cytokines within IUGR tissues, including the lungs, brain, skeletal muscle, and white blood cells (Kemp, 2014; Cadaret et al., 2019a).s Furthermore, transcriptomic analyses show that IUGR skeletal muscle exhibits enhanced cytokine signaling pathways, even when circulating cytokines are no longer elevated

postnatal (Hicks and Yates, 2021). Thus, stress-induced programming of inflammatory pathways appears to be a chief mechanism for IUGR muscle growth dysregulation when it occurs in late gestation when muscle growth is at its peak. However, it is unclear whether inflammation occurring prior to peak muscle growth but during peak placental growth and development affects subsequent fetal and fetal muscle growth. Therefore, the objective for our study was to determine the impact of mid-gestation maternofetal inflammation on the growth, body composition, and myoblast function of fetuses during late gestation. We hypothesized that inducing maternofetal inflammation earlier in gestation would induce more profound placental stunting, which would in turn lead to larger growth deficits in the MI-IUGR fetus during late gestation.

## Materials and Methods

### *Animals and Experimental Design*

This study was approved by the Institutional Animal Care and Use Committee at the University of Nebraska-Lincoln (**UNL**). Animal studies were performed at the UNL Animal Science Complex, which is accredited by AAALAC International. Polypay cross ewes were purchased from a single commercial source and were time-mated to a single sire. Twenty-seven pregnant ewes were identified via blood pregnancy tests at 30 d gestational age (**dGA**) and were randomly assigned to the control group or MI-IUGR group. All ewes were individually housed under thermoneutral conditions and maintained on a diet of commercial alfalfa pellets. Ewes were given *ad libitum* access to water and

mineral supplements. MI-IUGR fetuses were produced as previously described by Cadaret et al. (2019), with minor modifications. Briefly, ewes were injected IV with bacterial lipopolysaccharide (**LPS**) endotoxin (100 ng/kg bodyweight in 1 ml saline; *Escherichia coli* O55:B5; MilliporeSigma, St. Louis, MO) every 72 h from the $50^{th}$ to the $65^{th}$ dGA. Ewes carrying control fetuses were injected every 72 h with 1 ml saline carrier only. Maternal body (rectal) temperatures and blood samples (jugular venipuncture) were collected at 0, 3, 6, 12, 24, 48, and 72 h after each injection to assess maternal responses to LPS administration. Blood was collected into heparinized and EDTA syringes. Glucose, lactate, pH, partial pressure of $CO_2$ (**$pCO_2$**), partial pressure of $O_2$ (**$pO_2$**), $HCO_3^-$, oxyhemoglobin, carboxyhemoglobin, $Na^+$, $K^+$, $Cl^-$, and $Ca^{2+}$ were measured in heparinized whole blood with an ABL90 FLEX blood gas analyzer (Radiometer, Brea, CA). Total and differential white blood cells (**WBC**), hematocrit, mean corpuscular volume, red blood cell distribution width, hemoglobin, mean corpuscular hemoglobin concentration, red blood cells, platelets, and mean platelet volume were measured in EDTA-treated whole blood with a HemaTrue Veterinary Hematology Analyzer (Heska Corp, Loveland, CO). Plasma was separated from EDTA-treated whole blood via centrifuge (14,000 x *g*, 2 min) and stored at -80°C. Fetal hindlimb catheterization surgeries were performed at 118 ± 2 dGA. Maternal venous and fetal arterial blood samples were collected twice daily at 800 (fasted) and 1400 (unfasted) from dGA 119 to 125. Ewes were euthanized by double barbiturate overdose and fetuses were necropsied at 125 ± 2 dGA. Fetal bodyweights were recorded at necropsy, as were the weights of the hindlimb, heart, lungs, brain, liver, kidneys, and the *biceps femoris, semitendinosus, flexor digitorum superficialis, soleus, longissimus dorsi* skeletal muscles. Rear cannon

bone length was also measured. Cross-sectional samples from the mid-region of the fetal *semitendinosus* were collected for immunohistochemistry and upper hindlimb muscle was used to isolate myoblasts.

### *Fetal Surgical Hindlimb Preparation*

A partial caesarian was performed to place fetal femoral arterial and venous catheters as previously described (Cadaret et al., 2019). Briefly, ewes were fasted overnight, induced by IV injection of ketamine (10 mg/kg bodyweight) and midazolam (0.11 mg/kg bodyweight), intubated, and maintained under anesthesia by inhalation of 1% to 5% isoflurane gas in $O_2$. Fetal hindlimbs were exteriorized and indwelling catheters (Tygon ND-100-80 Flexible Plastic Tubing; outer diameter, 1.4 mm, inner diameter, 0.9 mm; US Plastics, Lima, OH) were were placed with the tip advanced into the external iliac artery via the femoral artery and into the common iliac vein via the femoral vein. Catheters were filled with heparinized saline (30 U/ml, 0.9% NaCl, Nova-Tech, Inc., Grand Island, NE) and were tunneled through the abdominal-facing wall of the uterus and subcutaneously to the flank. They were exteriorized through a skin incision and kept in a plastic mesh pouch sutured to the skin. Ewes were administered 6,600 U/kg penicillin G procaine, 10 mg/kg phenylbutazone, and 4 mg/kg atropine at the time of surgery. Postoperative phenylbutazone was continued for a minimum of 3 d following surgery, and ewes were allowed to recover for 1 d before performing studies. Catheters were flushed twice daily with heparinized saline. Fetal arterial blood was collected via catheters into EDTA-treated syringes (~1.0 ml) and heparinized syringes (~0.4 ml). Blood plasma was isolated from the EDTA-treated whole blood by centrifugation at

14,000 × *g* for 2 min. Plasma was utilized to assess circulating TNFα and IL-6 concentrations using commercial ELISA kits (Sheep TNFα ELISA, Fine Biotech, Ltd., Wuhan, China; Sheep High Sensitivity Interleukin 6 [HSIL6] ELISA Kit, MyBioSource.com, San Diego, CA, respectively). Whole blood partial pressures of oxygen (**$pO_2$**) were determined via ABL90 FLEX blood gas analyzed (Radiometer, Brea, CA) from 90-µl aliquots of filtered whole blood collected into heparinized syringes.

***Immunohistochemistry***

The cross-sectional fetal *semitendinosus* sample collected at necropsy was fixed in 4% paraformaldehyde (MilliporeSigma) in phosphate-buffer saline (**PBS**), embedded in OTC Compound (Fisher Scientific, Waltham, MA), and frozen at -80°C as previously described (Yates et al., 2016). Ten-µm cross sections prepared via cryostat were mounted on Fisherbrand Superfrost Plus microscope slides (Fischer Scientific). Slides were dried at 37°C for 2 h, washed in PBS, and steamed/cooled with 10 mM citric acid (pH 6; MilliporeSigma) for antigen retrieval. Nonspecific binding was blocked with 0.5% NEN blocking buffer (Perkin-Elmer, Waltham, MA). Primary antiserum diluted in PBS + 1% bovine serum albumin was applied overnight at 4°C. Primary antiserum was excluded for negative controls. Muscle sections were stained with mouse antiserum raised against pax7 (1:10; Developmental Studies Hybridoma Bank (**DSHB**), Iowa City, IA) to identify myoblasts and counterstained with rabbit antiserum raised against Ki67 (1:400; Cell Signaling Technologies, Danvers, MA) to identify proliferating myoblasts. Additional sections were stained with mouse antiserum raised against myogenin (1:5; DSHB) to identify differentiated myoblasts and with rabbit antiserum raised against dystrophin

(1:100; Cell Signaling Technologies, Danvers, MA) to assess muscle fiber area. Immunocomplexes were detected with affinity-purified immunoglobulin antiserum conjugated to AlexaFluor 488, AlexaFluor 555, or AlexaFluor 594 (1:1000; Cell Signaling Technologies, Danvers, MA). Immunofluorescent images were visualized on an Olympus IX73 and digitally captured with a DP80 microscope camera (Olympus Corp., Center Valley, PA). Images were analyzed with Olympus cellsSens Dimension software to determine myoblast population profiles and muscle fiber area. Animal identifications and experimental designations were de-identified prior to analyses. Myoblast populations within each muscle were assessed from a minimum of 800 nuclei across 3 non-overlapping fields of view. Average fiber area for each muscle was determined from a minimum of 100 muscle fibers across 3 non-overlapping fields of view.

### *Myoblast Isolation*

Primary fetal myoblasts were isolated from fetal hindlimb muscle collected at necropsy as previously described by Posont et al. (2022). Briefly, ~50 g of muscle from the biceps femoris and semitendinosus from each fetus were trimmed of adipose and connective tissue and washed in cold PBS containing 1% antibiotic-antimycotic (AbAm; Gibco Life Technologies, Grand Island, NY) and 0.5% gentamicin (Gibco). Muscle was finely minced and divided into 50-ml conical tubes (5 g/tube). Minced muscle was then washed in fresh PBS, resuspended in PBS containing 1.25 mg/ml protease type XIV from Streptomyces griseus (MilliporeSigma), and digested at 37°C for 1 h to liberate myoblasts. After digestion, samples were serial-centrifuged (500 × g for 10, 8, and 1 min)

at room temperature. After each centrifugation, the supernatant containing the liberated myoblasts was collected into a separate tube by aspiration. The supernatant was then centrifuged (1500 × g, 5 min) to pellet the isolated myoblasts. Pellets were re-suspended in commercial DMEM (Gibco Life Technologies, Grand Island, NY) containing 10% fetal bovine serum (FBS; Atlas Biologicals, Ft. Collins, CO) and incubated for 2 h (37°C; 95% $O_2$, 5% $CO_2$) to remove fibroblasts. Purified myoblasts were then grown in complete growth media (DMEM containing 20% FBS, 1% AbAm, 0.5% gentamycin, and 0.4% fungizone) on fibronectin-coated culture plates (10 µg/ml; MilliporeSigma) for 24 h. Myoblasts were expanded for 24 h, lifted from plates with Accutase (MilliporeSigma), and pre-plated in DMEM + 10% FBS (3 x 2 h) to increase purity. They were then resuspended in complete growth media containing 10% dimethyl sulfoxide (DMSO; MilliporeSigma), slowly frozen to -80°C, and stored in liquid nitrogen.

***Myoblast Functional Studies***

To determine myoblast purity, myoblasts were quickly thawed at 37°C, plated in DMEM containing 10% FBS for 2 h (37°C; 95% $O_2$, 5% $CO_2$), and then collected into tubes. A subsample of 5,000 cells was stained in suspension for the myoblast marker pax7 as previously described (Cadaret et al., 2017). Isolates from all fetuses were determined to be ≥85% myoblasts before use in studies.

Proliferative capacity was estimated as previously described by Posont et al., (2022). Briefly, 5,000 myoblasts were seeded into each well of fibronectin-coated 6-well tissue culture plates, grown in complete growth media for 3 d, and then incubated in complete growth media containing 1% bovine serum albumen (**BSA**; MilliporeSigma)

and either 0 (i.e., basal) or 5 mU/ml insulin (Humulin R; Lilly, Indianapolis, IN). Myoblasts were then pulse-labelled for 2 h with EdU (10 nM; Thermo Fischer), which is incorporated into the DNA of replicating cells during DNA synthesis. Myoblasts were then lifted from plates with Accutase and fixed in suspension with 4% PFA for 10 min. Proliferation rates were calculated as the percentage of myoblasts incorporating EdU (i.e., undergoing DNA synthesis) during the 2-h pulse period. These cells were identified by staining for EdU in suspension using the ClickIT EdU Alexa Fluor 555 Cell Proliferation Assay Kit (Thermo Fisher) according to the manufacturer's recommendations. Fixed cells were incubated in 200 µl of a permeabilization/blocking buffer consisting of PBS containing 1% BSA, 2% FBS, and 0.5% Triton X-100 (MilliporeSigma) for 10 min at 4°C. Cells were then pelleted by centrifugation (400 × *g*, 5 min) and resuspended in 200 µl of ClickIT reaction cocktail prepared according to manufacturer's recommendation. After incubating at room temperature for 30 min, cells were pelleted, washed twice, and resuspended in MoxiCyte Reagent (ORFLO Technologies, Ketchum, ID) for analysis.

Differentiation capacity was estimated as previously described by Posont et al., (2022). Briefly, 20,000 cells per well were seeded in fibronectin-coated 6-well tissue culture plates, grown overnight, and incubated for 96 h in differentiation media (DMEM containing 2% FBS, 1% AbAm, and 0.5% gentamycin) that contained 1% BSA and 0 (i.e., basal) or 5 mU/ml insulin. Media were replaced daily. At the end of the differentiation period, cells were lifted from plates using Accutase and fixed in 4% PFA. Differentiated myoblasts were identified by staining with antiserum raised in the mouse against myogenin (F5B; 1:50; Pharmingen) and desmin (DE-U-10; 1:250; GeneTex). Primary antibodies were diluted in permeabilization/blocking buffer and applied in

suspension for 1 h at room temperature. Afterward, myoblasts were pelleted, washed, and incubated for 1 h at room temperature with a secondary affinity-purified anti-mouse IgG PE-Conjugate antibody (1:250; Cell Signaling). Cells were then washed twice and resuspended in MoxiCyte Reagent. All samples analyzed for purity, proliferation, and differentiation were analyzed on a zEPI flow cytometer (ORFLO Technologies), with gates set from negative controls produced by incubating a subset of cells from each fetus in permeabilization/blocking buffer containing no primary antibody.

### *Statistical Analysis*

Immunohistochemistry and other data collected at necropsy were analyzed by ANOVA using the mixed procedure of SAS 9.4 (SAS Institute, Cary, NC) for the fixed effects of experimental group, sex, and the number of fetuses/pregnancy. Interactions among these effects were not included due to insufficient power. However, all sex and fetal number categories were represented in both groups. Fetus was considered the random variable. Fisher's LSD test was used for mean separation. Fetal blood components assessed over time were analyzed using the mixed procedure with repeated measures to analyze the effects of experimental group, day, time of day, and the interactions, as well as sex and fetal number. Best-fit statistics were used to select appropriate covariance structures. Fetus was considered the experimental unit. Maternal data were analyzed with the mixed procedure to determine effects of experimental group (saline vs. LPS-injected), with ewe as the experimental unit. Significant differences for all analyses were identified by $P$-values of $\leq 0.05$, and tendencies toward differences

were indicated by *P*-values of ≤ 0.10. All data are presented as least-squares means ± standard error of the mean.

## Results

### *Maternal Inflammatory Response to LPS Injections*

There were experimental group x time interactions observed ($P < 0.05$) for maternal total WBC, lymphocytes, monocytes, granulocytes, and rectal body temperatures during the LPS challenge. Maternal total WBC were decreased ($P < 0.05$) in LPS-injected ewes compared to control ewes when measured at 3 h after each injection and did not differ between groups prior to the 1st injection and at 6 h after all but the 2nd injection (**Figure 2.1**). However, WBC were increased ($P < 0.05$) in LPS-injected ewes compared to control ewes at all other time points assessed. Maternal lymphocyte concentrations were decreased ($P < 0.05$) in LPS-injected ewes at 3 h after the 2nd and 3rd injection and at 3 and 6 h after the 6th injection (**Figure 2.2**). Lymphocytes did not differ between groups at 0, 3, and 6 after the 1st injection, at 6 h after the 2nd and 3rd injection, and at 3 and 6 h after the 4th and 5th injections, and they were increased ($P < 0.05$) at all other timepoints. Maternal monocyte concentrations were reduced ($P < 0.05$) in LPS-injected ewes at 3 h after the 1st through 4th injections, did not differ at 6 h after the 1st through 4th injections or at 3 or 6 h after the 5th and 6th injections, and were increased ($P < 0.05$) in LPS-injected ewes at all other timepoints (**Figure 2.3**). Maternal granulocytes were reduced ($P < 0.05$) in LPS-injected ewes at 3 h after all injections and at 6 h after the 2nd injection (**Figure 2.4**). Granulocytes did not differ between groups at 6 h after all but the 2nd injection and were increased ($P < 0.05$) in LPS-injected ewes at all other

timepoints. Rectal body temperatures were increased ($P < 0.05$) in LPS-injected ewes compared to controls at 3 h after all injections and at 6 h after the 1st, 2nd, 3rd, and 5th injections, but they did not differ between groups at any other timepoints (**Figure 2.5**). Maternal plasma TNFα concentrations did not differ between groups prior to the 3rd injection but were increased ($P < 0.05$) in LPS-injected ewes at all timepoints after the 3rd injection (**Figure 2.6**). Hematocrit, hemoglobin, red blood cells, and platelets were greater ($P < 0.05$) and mean corpuscular hemoglobin concentration was reduced ($P < 0.05$) in LPS-injected ewes compared to control ewes, regardless of timepoint (**Table 2.1**). Mean corpuscular volume, red cell distribution width, and mean platelet volume did not differ between groups during the LPS injections.

There were experimental group x time interactions observed ($P < 0.05$) for maternal blood glucose, pH, $pCO_2$, $HCO_3^-$, base excess, $O_2$-bound hemoglobin, $K^+$, $Cl^-$, and $pO_2$ during the LPS challenge. Maternal blood glucose concentration was reduced ($P < 0.05$) in LPS-injected ewes at 6, 12, 24, and 48 h after the 1st injection, at 6 and 12 h after the 2nd injection, and at 3, 6, and 12 h after the 3rd, 4th, and 5th injections, but glucose did not differ between groups at any other timepoints (**Figure 2.7**). Maternal blood pH was elevated ($P < 0.05$) in LPS-injected ewes at 12 and 24 h after the 1st injection, at 6 and 12 h after the 2nd injection, at 6, 12, and 24 h after the 3rd injection, at 12 h after the 4th injection, and at 6 and 12 h after the 5th injection, but pH did not differ between groups at any other time point (**Figure 2.8**). Maternal blood $pCO_2$ was reduced ($P < 0.05$) in LPS-injected ewes at 6 h after the 1st and 3rd injection but elevated ($P < 0.05$) at 48 and 72 h after the 1st, 2nd, 3rd, 5th, and 6th injections and at 12 and 24 h after the 4th injection (**Figure 2.9**). Blood $pCO_2$ did not differ between groups at any other timepoints.

Maternal blood $HCO_3^-$ concentration was reduced ($P < 0.05$) in LPS-injected ewes at 6 h after the 1st injection and elevated ($P < 0.05$) at 24 and 72 h after the 1st injection, at 12 and 24 h after the 2nd and 3rd injections, at 6, 12, and 24 h after the 4th injection, at 12 and 72 h after the 5th injection, and at 24 h after the 6th injection (**Figure 2.10**). Blood $HCO_3^-$ did not differ between groups at any other timepoint. Maternal blood base excess was reduced ($P < 0.05$) in LPS-injected ewes at 6 h after the 1st injection but elevated ($P < 0.05$) at 24 h after the 1st injection, at 12 and 24 h after the 2nd and 3rd injections, at 6, 12, and 24 h after the 4th injection, at 12 h after the 5th injection, and at 12 and 24 h after the 6th injection (**Figure 2.11**). Maternal base excess did not differ between groups at any other timepoints. Maternal oxyhemoglobin was elevated ($P < 0.05$) in LPS-injected ewes at 6 and 24 h after the 1st injection and at 6 h after the 2nd and 3rd injections and was decreased ($P < 0.05$) at 72 h after the 2nd injection, 48 and 72 h after the 3rd injection, 3 h after the 5th injection, and 3, 24, and 72 h after the 6th injection (**Figure 2.12**). Maternal blood $K^+$ concentration was elevated ($P < 0.05$) in LPS-injected ewes 12 h after the 1st injection but reduced ($P < 0.05$) at 3 h after all injections, at 12 h after the 3rd injection, and at 48 h after the 6th injection (**Figure 2.13**). Maternal blood $Cl^-$ concentration was elevated ($P < 0.05$) in LPS-injected ewes at 0 h but was reduced ($P < 0.05$) at 12 h after the 2nd injection, at 12 and 48 h after the 3rd injection, at 12 and 24 h after the 4th injection, at 6 h after the 5th injection, and at 12 h after the 6th injection (**Figure 2.14**). Maternal $pO_2$ was elevated ($P < 0.05$) in LPS-injected ewes at 6 h after the 2nd and 3rd injections and reduced ($P < 0.05$) at 48 and 72 h after the 2nd injection, at 24, 48, and 72 h after the 3rd injection, and at 24 and 72 h after the 6th injection (**Figure 2.15**). Maternal blood lactate concentrations, hemoglobin concentrations, and hematocrit were elevated

($P < 0.05$) and carboxyhemoglobin and blood $Ca^{2+}$ concentration were reduced ($P < 0.05$) in LPS-injected ewes compared to control ewes, regardless of timepoint (**Table 2.2**). Blood $Na^{+}$ concentrations did not differ between groups.

***Fetal Blood $pO_2$ and Inflammatory Cytokines***

Daily fetal blood $pO_2$ was reduced ($P < 0.05$; **Figure 2.16**) and fetal plasma TNFα and IL-6 concentrations were increased ($P < 0.05$; **Figures 2.17A** and **B**) for MI-IUGR fetuses compared to control fetuses.

***Fetal Metrics***

At necropsy, fetal bodyweights and hindlimb weights were less ($P < 0.05$) for MI-IUGR fetuses compared to controls (**Figures 2.18 and 2.19A**). Hindlimb weight/bodyweight tended to be less ($P = 0.08$) for MI-IUGR fetuses compared to controls (**Figure 2.19B**). *Semitendinosus*, *flexor digitorum superficialis*, and *longissimus dorsi* were lighter ($P < 0.05$) for MI-IUGR fetuses compared to controls, but *biceps femoris* and *soleus* did not differ in weight between experimental groups (**Figure 2.20A-E**). The average total mass of the muscles assessed in this study was lighter ($P < 0.05$) for MI-IUGR fetuses compared to controls (**Figure 2.20F**). No differences in heart, liver, kidney, or brain weights were observed between experimental groups (**Figure 2.21**). However, heart/bodyweight, liver/bodyweight, kidney/bodyweight, and brain/bodyweight were greater ($P < 0.05$) for MI-IUGR fetuses compared to controls (**Figure 2.22**). Lung weights were lighter ($P < 0.05$) for MI-IUGR fetuses compared to controls, but no differences in lung/bodyweight was observed between experimental groups (**Figure 2.23**). Rear cannon bones were shorter ($P < 0.05$) for MI-IUGR fetuses compared to

controls (**Figure 2.24**). Hindlimb/bodyweight tended to be greater ($P = 0.08$) for females compared to males, regardless of experimental group. Furthermore, heart/bodyweight was greater ($P < 0.05$) and rear cannon bones were longer ($P < 0.05$) for males compared to females (**Table 2.3**).

***Myoblast Profiles***

Total myoblasts (i.e., % pax7$^+$ nuclei) present in the *semitendinosus* did not differ between control and MI-IUGR fetuses (**Figure 2.25**). However, the percentages of proliferating myoblasts (i.e., Ki-67$^+$/pax7$^+$ nuclei) tended to be less ($P = 0.06$) and differentiated myoblasts (i.e., % myogenin$^+$ nuclei) in the *semitendinosus* were less ($P < 0.05$) for MI-IUGR fetuses compared to controls (**Figures 2.26** and **2.27**). Furthermore, average *semitendinosus* myofiber cross-sectional areas were smaller ($P < 0.05$) for MI-IUGR fetuses compared to controls (**Figure 2.28**). Average primary myoblast purity (i.e., % pax7$^+$ myoblasts) for all isolates was 86.3% ± 1.6% (data not shown). Myoblast proliferation rates (i.e., % EdU$^+$ myoblasts/2 h) were increased ($P < 0.05$) in MI-IUGR fetuses compared to controls (**Figure 2.29A**). Regardless of group, myoblast proliferation rates were reduced ($P < 0.05$) in insulin-spiked media compared to basal media (**Figure 2.29B**). The percentage of differentiated nuclei expressing myogenin (i.e., % myogenin$^+$) and the percentage expressing desmin (i.e., % desmin$^+$) were reduced ($P \leq 0.05$) in MI-IUGR myoblasts compared to controls (**Figure 2.30A-B**).

**Discussion**

In this study, we showed that sustained maternofetal inflammation occurring at mid-gestation produced asymmetric fetal growth restriction near term. Lighter fetal bodyweights for our MI-IUGR fetal sheep coincided with only mild reductions in heart, liver, kidney, and brain weights and in bone growth but with more severe decreases in hindlimb and skeletal muscle weights. In concert with disproportional muscle growth restriction, myoblast differentiation capacity appeared to be deficient in MI-IUGR fetuses, despite normal relative numbers of myoblasts in the muscle. The reduction in this rate-limiting function of myoblasts almost certainly contributes to the smaller average myofiber size observed in MI-IUGR fetuses and helps to explain the disproportionate deficit in muscle mass. Moreover, poor function persisted when isolated MI-IUGR fetal myoblasts were studied in culture, which demonstrates that the deficits are intrinsically programmed. Together, these findings show that maternofetal inflammation at mid-gestation produces the stereotypical IUGR growth phenotype reported for clinical IUGR cases in humans and observed in other IUGR animal models. Moreover, the study demonstrates a primary role for heightened fetal inflammation in the disproportionate reduction of skeletal muscle growth in the IUGR fetus.

Pregnant ewes mounted a robust inflammatory response to serial LPS administration that did not appear to wane in intensity for the later injections. The pattern of circulating leukocytes and other indicators observed at mid-gestation in the present study was similar to patterns observed when serial LPS injections were administered to ewes at the start of the 3$^{rd}$ trimester of gestation (Cadaret et al., 2019). In hallmark fashion, circulating lymphocytes, monocytes, and granulocytes concentrations transiently

dropped in the hours immediately following each LPS injection before spiking to peak elevated concentrations 12 to 24 hours later and then gradually decreasing toward baseline near the 72-hour mark. These patterns reflect the abrupt migration of white blood cells out of circulation and into tissues upon exposure to the endotoxin, followed by the increased mobilization of stored white blood cells into the bloodstream from bone marrow (Yates et al., 2011; Cadaret et al., 2019; Dickson et al., 2019). Additionally, the magnitude of the observed response was generally maintained for all six LPS injections in the series, which comparable to when the same injection regimen was performed in pregnant ewes much later in pregnancy (Cadaret et al. 2019a), This indicated that the ewes did not develop any particular desensitization to the repeated doses of the endotoxin, unlike pregnant rats in a previous study (Cadaret et al., 2019a). Interestingly, the initial injection of LPS did not elevate circulating TNFα levels, which was somewhat unexpected considering the marked febrile response. However, circulating TNFα rose after the 2$^{nd}$ LPS injection and remained elevated throughout the rest of the administration period.

Maternofetal inflammation disproportionately restricted skeletal muscle growth relative to overall growth, which is a mechanism by which MI-IUGR fetuses conserve nutrients for vital organ and tissue growth. To illustrate, MI-IUGR fetuses were 20% lighter than normal, but their lungs were only 12% lighter, and the other vital organs, the heart, liver, kidney, and brain were not reduced in size compared to uncompromised fetuses. Moreover, these organs comprised as much as 22% more of the MI-IUGR fetuses' total bodyweight. Conversely, MI-IUGR fetal hindlimbs, which are comprised of about 40% skeletal muscle (Hicks and Yates, 2021), were 25% smaller than normal and

comprised 4% less of the total fetal bodyweight for MI-IUGR fetuses than uncompromised fetuses. Although effects differed among individual muscle groups, the skeletal muscles assessed in this study comprised an average of 14% less of the total bodyweight for MI-IUGR fetuses. Skeletal growth was also preserved, as cannon bone length was reduced by a meager 5% in MI-IUGR fetuses. Nutrient repartitioning to prioritize the most vital tissues is one of the chief hallmarks presented by fetuses where IUGR results from placental insufficiency (Gagnon, 2003). Thus, our observation of asymmetrical fetal growth restriction in these fetuses likely indicates the occurrence of placental stunting. Indeed, daily fetal blood draws demonstrated a chronic state of hypoxemia in these MI-IUGR fetuses, which is a primary pathology associated with placental insufficiency. Placental stunting was not an unexpected outcome considering the maternal response to endotoxin injections. Specifically, elevated maternal circulating concentrations of inflammatory cytokines were sustained over a time that coincided with peak placental development. Previous studies have shown that cytokines such as TNFα, IL-6, and IL-1β disrupt tissue growth and increase degradation of collagen and other cellular proteins (Nawabi et al., 1990; Dinarello, 2000; Li et al., 2009). This supports our postulation that even when inflammation is transient, placental vasculature, surface area, and transporter content are irreparably compromised, thus causing placental insufficiency in late gestation (Hicks and Yates, 2021).

The hypoxemic state of the MI-IUGR fetuses in late gestation almost certainly contributed to their heightened systemic inflammation. Low-$O_2$ conditions have been shown to induce whole-body and tissue-specific inflammatory responses (Eltzschig and Carmeliet, 2011; Watts and Walmsley, 2019). In adult humans, for example, high

altitude-induced hypoxemia resulted in increased serum concentrations of IL-6, C-reactive protein, and other inflammation mediators (Hartmann et al., 2000; Eltzschig and Carmeliet, 2011). In guinea pig fetuses, chronic hypoxemia increased circulating IL-6 and TNFα as well as mRNA expression of these cytokines in fetal brain and heart (Dong et al., 2009). Human placental tissues exposed to hypoxia *in vitro* released more damage associated molecular patterns (**DAMP**) molecules and inflammatory cytokines including TNFα, IL-6, and IL-1β (Baker et al., 2021). Hypoxemic conditions cause translocation of the α and β subunits of hypoxia-inducible factor (**HIF**), which bind to the hypoxia response promoter element (**HRE**) to promote transcription of genes involved in inflammation including nuclear factor κB (**NF-κB**) and toll-like receptors (**TLR**; Eltzschig and Carmeliet, 2011). Of course, other factors in addition to hypoxemia could have contributed to elevated fetal cytokines. Although it appears that most bacterial LPS does not cross the placenta in sheep (Gomez-Lopez et al., 2018), it almost certainly increases placental production of inflammatory cytokines. Previous studies in pregnant mice and in human placental extravillous trophoblast cells have shown that exposure to LPS increased the production of IL-1β, IL-6, IL-8, and TNF-α (Anton et al., 2012; Fricke et al., 2018), some of which may presumably be entering fetal circulation. Furthermore, LPS transiently increases circulating cortisol in ewes (Yates et al., 2011), which can cross the placenta and suppress fetal inflammation during maternal inflammation (Dixon et al., 1970). Such sustained fetal exposure to higher concentrations of cortisol would likely reduce cortisol sensitivity in the MI-IUGR fetus, which would in turn result in compensatory overproduction of fetal cytokines later in gestation (Brooks et al., 1992; Katsu and Baker, 2021).

Systemic inflammation observed in MI-IUGR fetuses during late gestation was associated with reductions in fetal skeletal muscle growth. Previous studies have shown that heightened exposure to inflammatory cytokines promotes skeletal muscle atrophy by reducing protein accretion and causing myoblast dysfunction (Cheema et al., 2000; Haddad et al., 2005; Popa et al., 2007; Li et al., 2009; Posont et al., 2018). Indeed, the disproportional decreases in many (although not all) muscles observed in MI-IUGR fetuses in the present study appeared to have been due in large part to rate-limiting disruption of myoblast function. This was characterized by the 14% reduction in myoblasts exhibiting proliferation and the 32% reduction in differentiated myoblasts in the *semitendinosus* at the time of necropsy, which coincided with a 13% reduction in average muscle fiber size. Interestingly, *ex vivo* myoblast proliferation was increased 13% in MI-IUGR fetuses, which is consistent with enhanced inflammatory responsiveness (Posont et al., 2022) and indicates that poor myoblast proliferation *in vivo* was not an intrinsic deficit. Rather, myoblast proliferation was presumably dampened *in vivo* by circulating hormones or other factors that were not present *ex vivo*. Previous studies of cultured myoblasts have shown that incubation of control or IUGR fetal myoblasts with serum from IUGR fetal sheep reduced proliferation rates and myoD mRNA expression (Yates et al., 2014a). This previous study did not identify the bioactive component in IUGR fetal serum. However, it is possible that circulating cytokines concentrations in MI-IUGR fetuses were elevated enough to inhibit proliferation *in vivo*, as very high concentrations has been shown to be inhibitory (Steyn et al., 2019). Conversely, the amount of cytokines in culture would be limited to what is produced by the myoblasts themselves. Alternatively, the chronically-hypoxemic MI-IUGR fetuses

could have been affected by heightened *in vivo* activation of the hypoxia-inducible factor-1 (**HIF-1**) pathway, which is a negative regulator of myoblast proliferation (Li et al., 2007). In myoblast cultures, $O_2$ saturation is maintained at normal atmospheric conditions, which presumably do not increase HIF-1 activation. Unlike proliferation, primary myoblast differentiation rates were reduced across *ex vivo* conditions, as the percentage of myogenin$^+$ MI-IUGR myoblasts after 96-h differentiation was reduced by 55%, and the percentage of desmin$^+$ MI-IUGR myoblasts was reduced by 24%. This is strong evidence that myoblast differentiation in MI-IUGR myoblasts was impaired by programmed intrinsic factors, as differentiation rates were not recovered *ex vivo*. Myoblast function is rate-limiting for muscle hypertrophy in late gestation and beyond, and thus their proliferation and differentiation rates are major determinants of skeletal muscle mass near term and after birth (Yates et al., 2014a; Posont et al., 2018). Overexposure to inflammatory cytokines is known to reduce myoblast functionality. Specifically, TNFα and IL-6 at high concentrations or for sustained periods decrease myoblast differentiation (Li and Reid, 2001; Haddad et al., 2005; Posont et al., 2018; Alvarez et al., 2020), and IL-1β has been linked to decreased myofiber diameter (Li et al., 2009). Disrupted myoblast function and the consequent decrease in muscle fiber hypertrophy has been documented pre- and postnatal (Haddad et al., 2005; Bodell et al., 2009). We interpret the outcomes from this study as conclusive evidence for the role of systemic fetal inflammation in the hallmark growth deficits of IUGR skeletal muscle.

Together, our findings indicate that mid-gestation maternofetal inflammation creates unfavorable intrauterine conditions that subsequently result in fetal growth restriction, skeletal muscle deficits, and myoblast dysfunction later in gestation. These

poor outcomes appeared to be driven in large part by the increased systemic inflammation of the MI-IUGR fetus, although other stress conditions such as moderate hypoxemia were also presumable contributors. The increase in circulating fetal inflammatory cytokines, regardless of their origin, persisted in late gestation, which was comparable to fetal conditions from known causes of placental insufficiency and IUGR such as heat stress. This further establishes the underlying role of systemic fetal inflammation in the development of hallmark IUGR pathologies (Romero et al., 2008; Rong Guo et al., 2010; Krajewski et al., 2014; Visentin et al., 2014; Caitlin N. Cadaret et al., 2019; Oh et al., 2019). Interestingly, inducing maternofetal inflammation at mid-gestation to coincide with peak placental growth and development produced outcomes that were only minimally dissimilar to those observed with late-gestation induction of maternofetal inflammation. Nevertheless, increased proportional weights of vital organs together with decreased skeletal muscle mass were consistent with the hallmark asymmetric fetal growth restriction known to result from placental insufficiency. This study provides the basis for future work aimed at leveraging fetal inflammation as a target for therapeutic interventions and treatments to prevent or improve IUGR deficits.

**Tables and Figures**

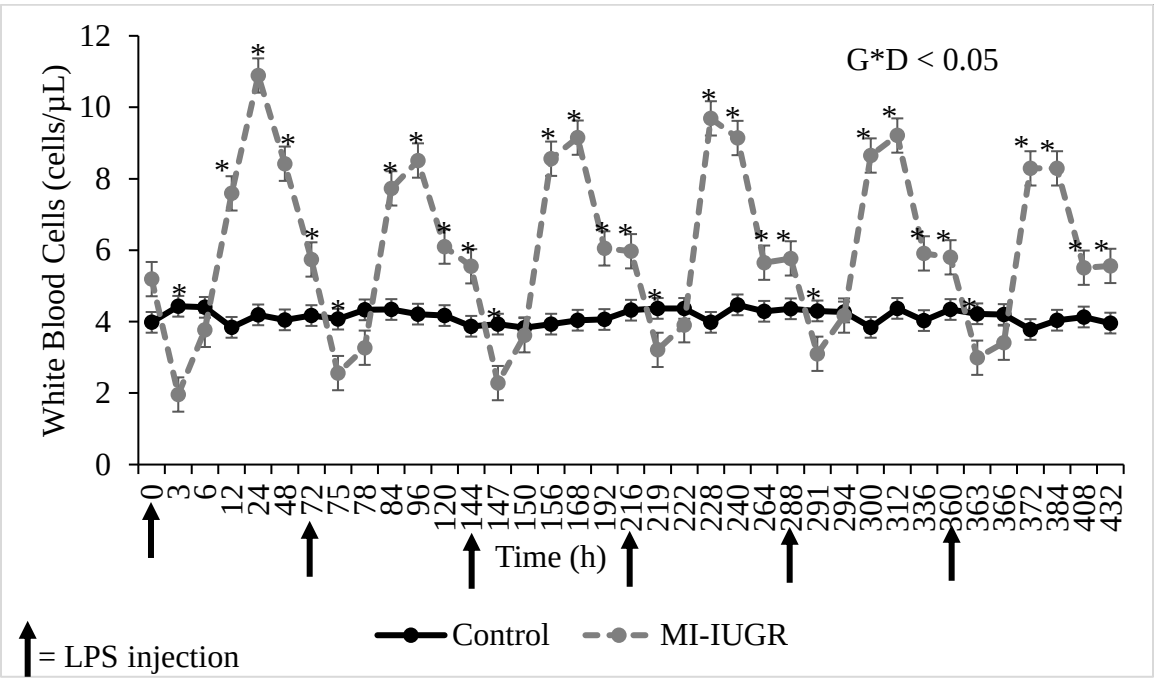


**Figure 2.1**. Maternal responses to serial administration of LPS during the early 2nd trimester of pregnancy. Ewes were injected I.V. with *E. coli* O55:B5 LPS (MI-IUGR; n=18) or saline controls (n=11) every 72 h from dGA 50 to 65. Data are shown for whole blood concentrations of white blood cells. Effect of maternal injections (GRP), time of blood draw relative to initiating injections (DRAW), and the interaction (G*D) are noted when significant. Arrows denote when injections were administered. Time points that are significant are denoted (*$P < 0.05$).

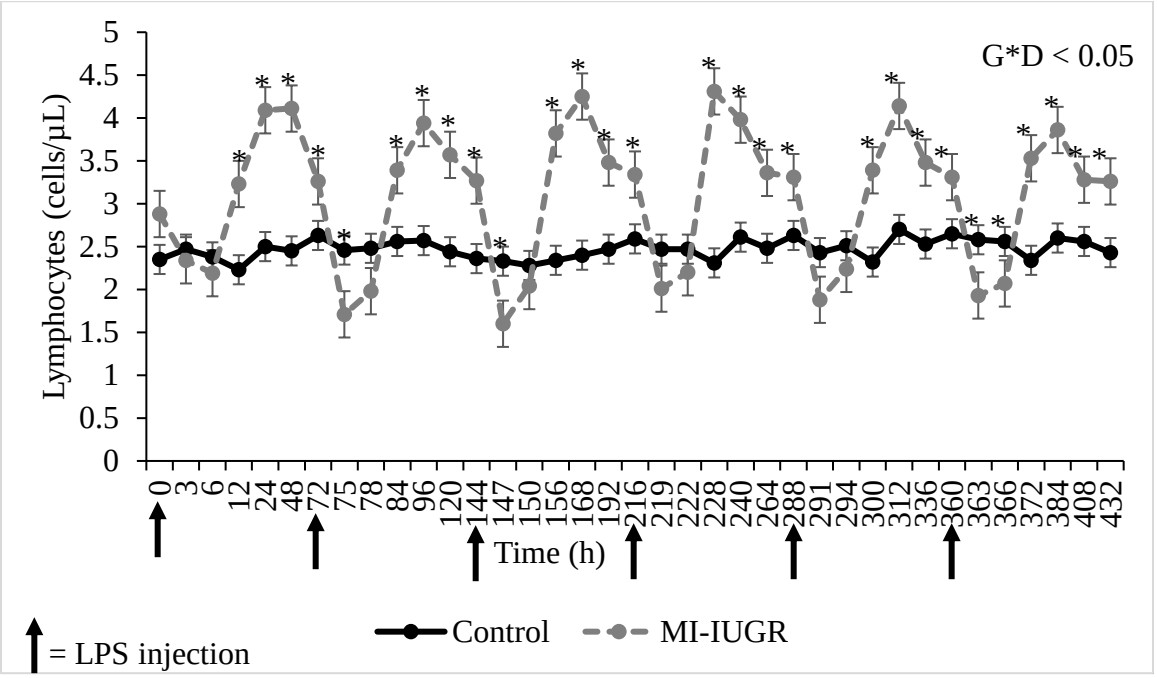


**Figure 2.2** Maternal responses to serial administration of LPS during the early 2nd trimester of pregnancy. Ewes were injected I.V. with *E. coli* O55:B5 LPS (MI-IUGR; n=18) or saline controls (n=11) every 72 h from dGA 50 to 65. Data are shown for whole blood concentrations of lymphocytes. Effect of maternal injections (GRP), time of blood draw relative to initiating injections (DRAW), and the interaction (G*D) are noted when significant. Arrows denote when injections were administered. Time points that are significant are denoted (*$P < 0.05$).

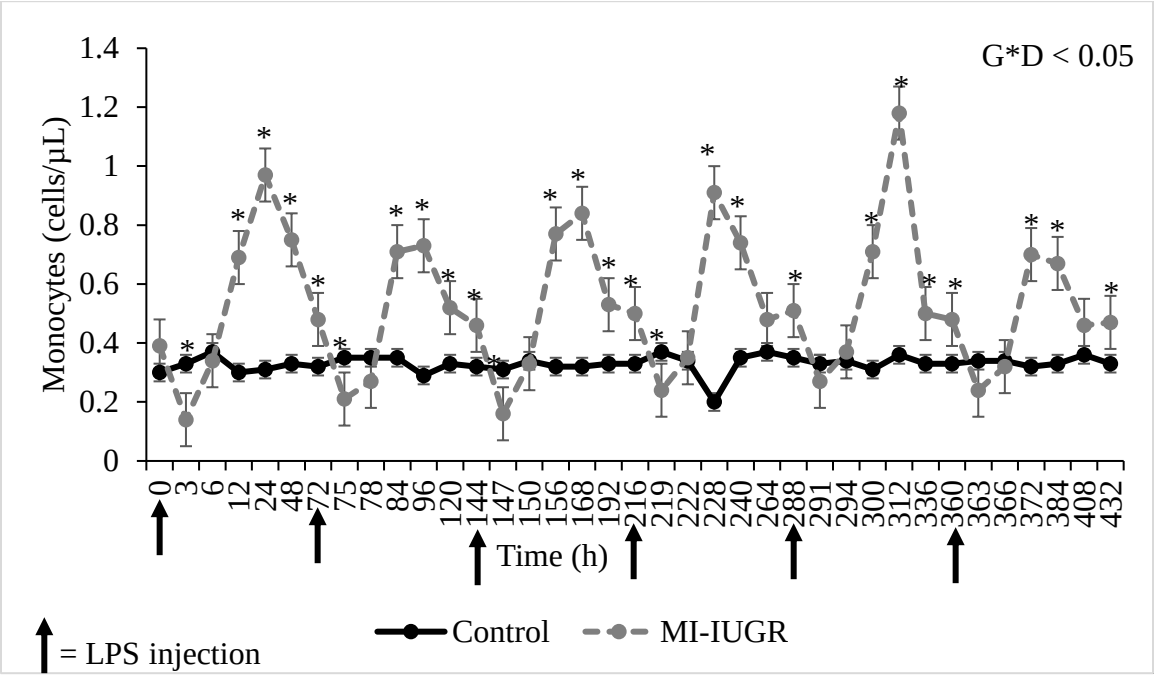


**Figure 2.3** Maternal responses to serial administration of LPS during the early 2nd trimester of pregnancy. Ewes were injected I.V. with *E. coli* O55:B5 LPS (MI-IUGR; n=18) or saline controls (n=11) every 72 h from dGA 50 to 65. Data are shown for whole blood concentrations of monocytes. Effect of maternal injections (GRP), time of blood draw relative to initiating injections (DRAW), and the interaction (G*D) are noted when significant. Arrows denote when injections were administered. Time points that are significant are denoted (*$P < 0.05$).

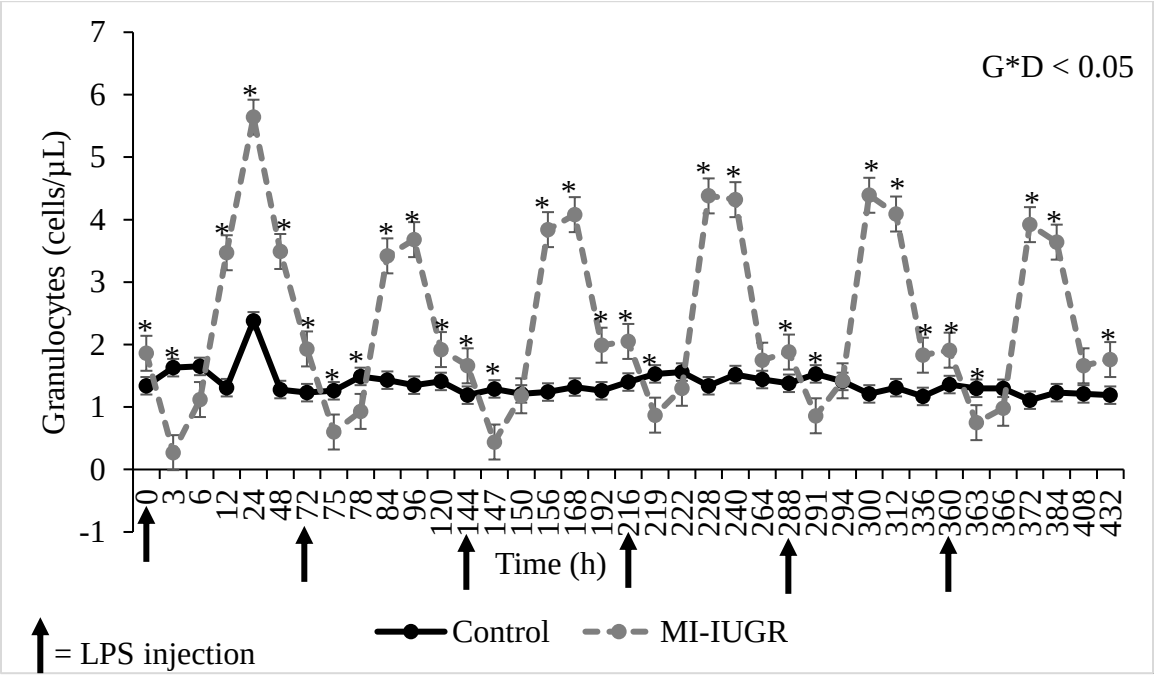


**Figure 2.4** Maternal responses to serial administration of LPS during the early 2nd trimester of pregnancy. Ewes were injected I.V. with *E. coli* O55:B5 LPS (MI-IUGR; n=18) or saline controls (n=11) every 72 h from dGA 50 to 65. Data are shown for whole blood concentrations of granulocytes. Effect of maternal injections (GRP), time of blood draw relative to initiating injections (DRAW), and the interaction (G*D) are noted when significant. Arrows denote when injections were administered. Time points that are significant are denoted (*$P < 0.05$).

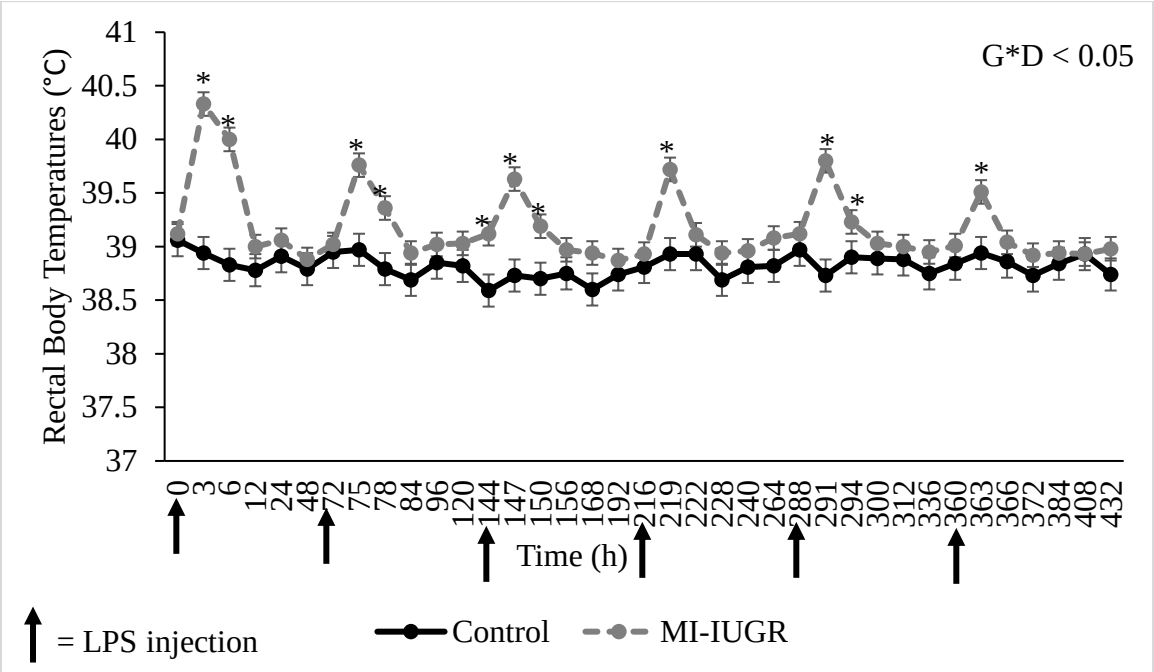


**Figure 2.5** Maternal responses to serial administration of LPS during the early 2nd trimester of pregnancy. Ewes were injected I.V. with *E. coli* O55:B5 LPS (MI-IUGR; n=18) or saline controls (n=11) every 72 h from dGA 50 to 65. Data are shown for rectal body temperatures. Effect of maternal injections (GRP), time of blood draw relative to initiating injections (DRAW), and the interaction (G*D) are noted when significant. Arrows denote when injections were administered. Time points that are significant are denoted (*$P < 0.05$).

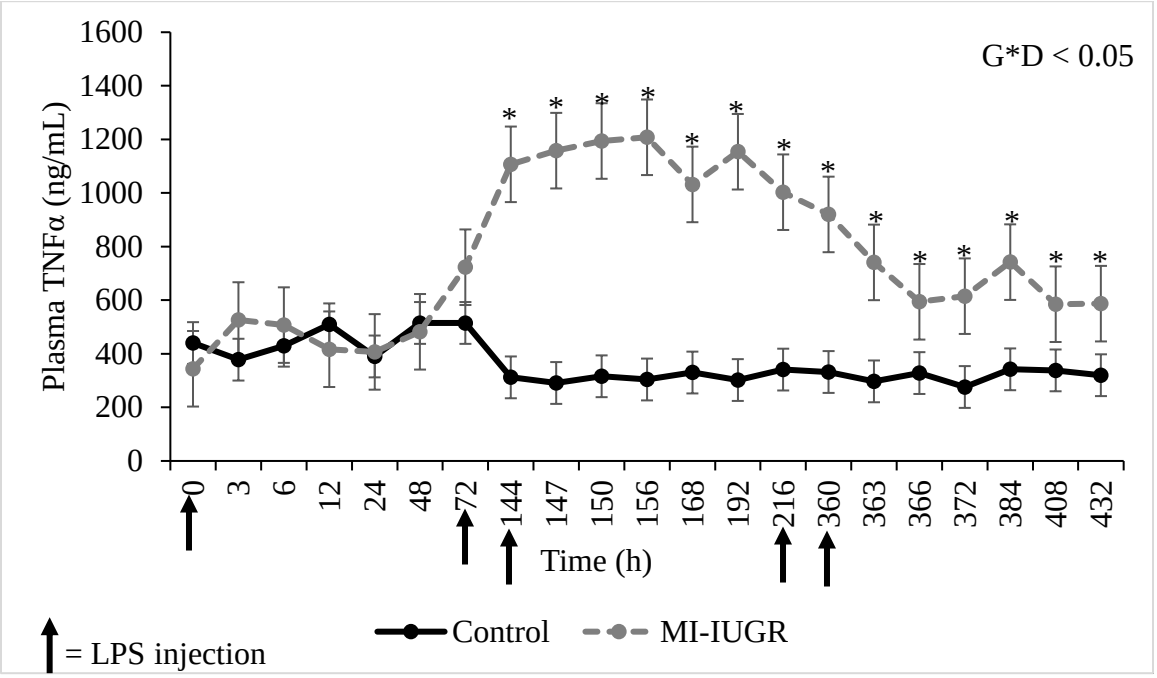


**Figure 2.6** Maternal responses to serial administration of LPS during the early 2nd trimester of pregnancy. Ewes were injected I.V. with *E. coli* O55:B5 LPS (MI-IUGR; n=18) or saline controls (n=11) every 72 h from dGA 50 to 65. Data are shown for plasma TNF-α concentrations. Effect of maternal injections (GRP), time of blood draw relative to initiating injections (DRAW), and the interaction (G*D) are noted when significant. Arrows denote when injections were administered. Time points that are significant are denoted (*$P < 0.05$).

**Table 2.1.** The main effect of group on maternal whole blood counts assessed during the induction of maternofetal inflammation. Ewes were injected I.V. with E. coli O55:B5 LPS (MI-IUGR) or saline controls every 72 h from dGA 50 to 65.

| | Control (n=11) | MI-IUGR (n=18) | *P*-value |
|---|---|---|---|
| Hematocrit | 28.45±0.26 | 30.51±0.12 | <0.001 |
| Mean Corpuscular Volume | 32.03±0.13 | 32.07±0.07 | NS |
| Red Cell Distribution Width | 20.56±0.10 | 20.56±0.05 | NS |
| Hemoglobin | 10.75±0.10 | 11.46±0.05 | <0.001 |
| Mean Corpuscular Hemoglobin Concentration | 38.02±0.06 | 37.65±0.06 | <0.001 |
| Red Blood Cells | 8.91±0.08 | 9.53±0.04 | <0.001 |
| Platelets | 152±2 | 165±2 | <0.001 |
| Mean Platelet Volume | 5.19±0.01 | 5.17±0.01 | NS |

NS = not significant ($P > 0.05$)

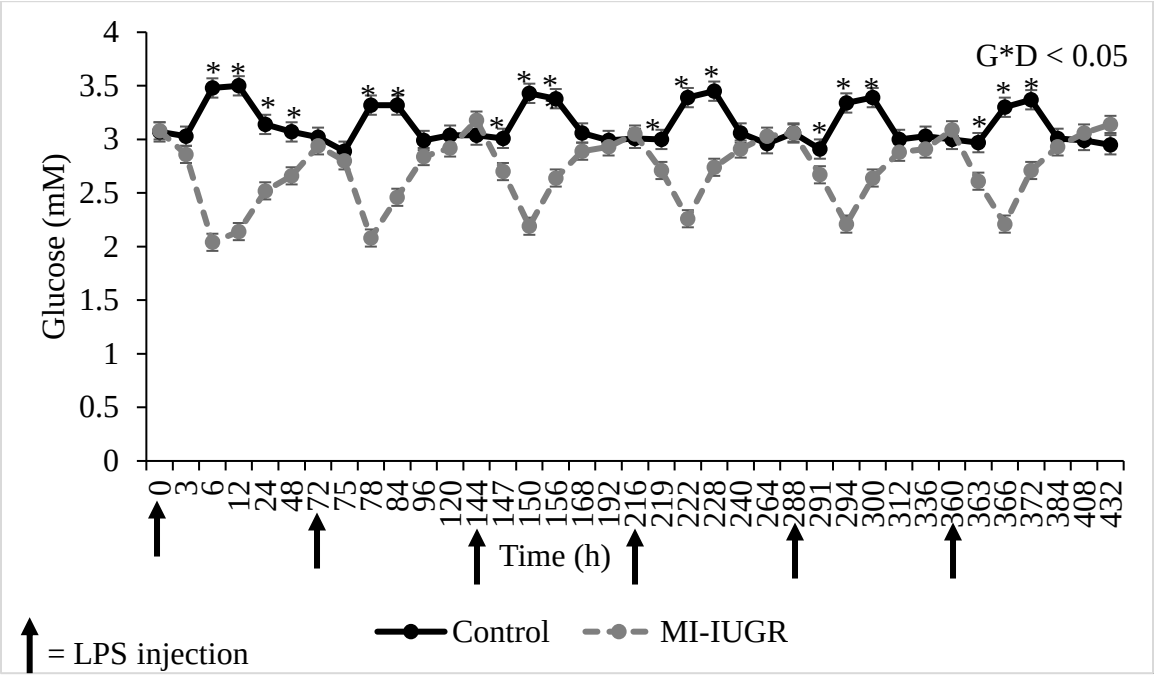


**Figure 2.7** Maternal responses to serial administration of LPS during the early 2nd trimester of pregnancy. Ewes were injected I.V. with *E. coli* O55:B5 LPS (MI-IUGR; n=18) or saline controls (n=11) every 72 h from dGA 50 to 65. Data are shown for maternal blood glucose. Effect of maternal injections (GRP), time of blood draw relative to initiating injections (DRAW), and the interaction (G*D) are noted when significant. Arrows denote when injections were administered. Time points that are significant are denoted (*$P < 0.05$).

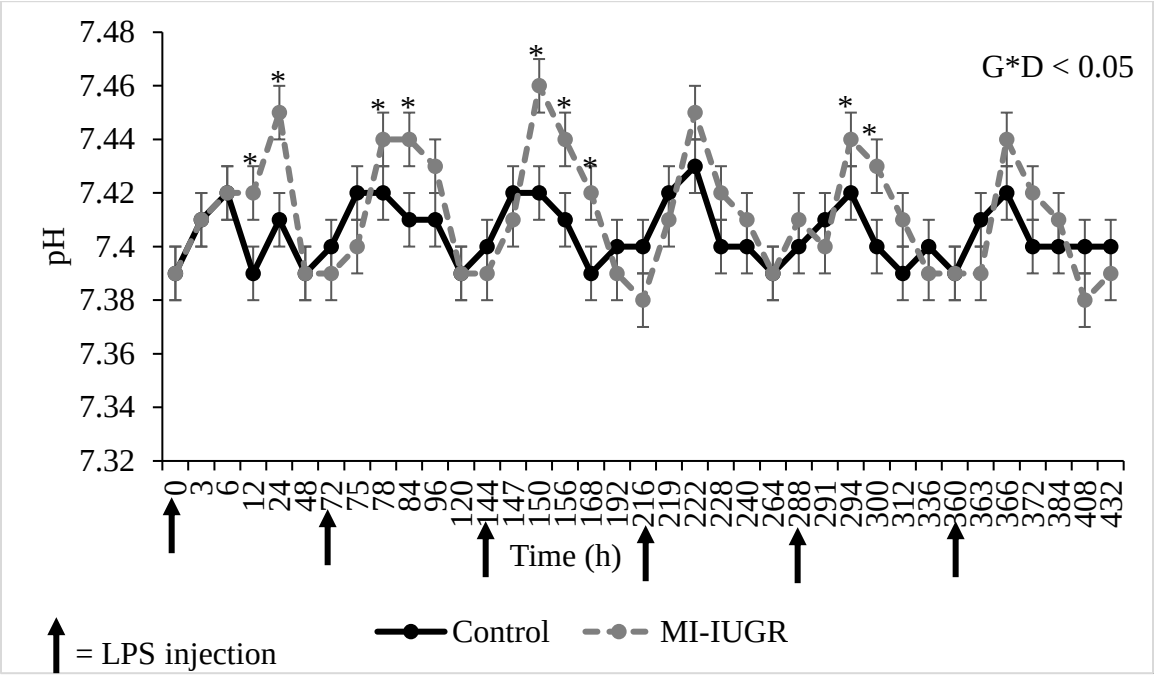


**Figure 2.8** Maternal responses to serial administration of LPS during the early 2nd trimester of pregnancy. Ewes were injected I.V. with *E. coli* O55:B5 LPS (MI-IUGR; n=18) or saline controls (n=11) every 72 h from dGA 50 to 65. Data are shown for maternal blood pH. Effect of maternal injections (GRP), time of blood draw relative to initiating injections (DRAW), and the interaction (G*D) are noted when significant. Arrows denote when injections were administered. Time points that are significant are denoted (*$P < 0.05$).

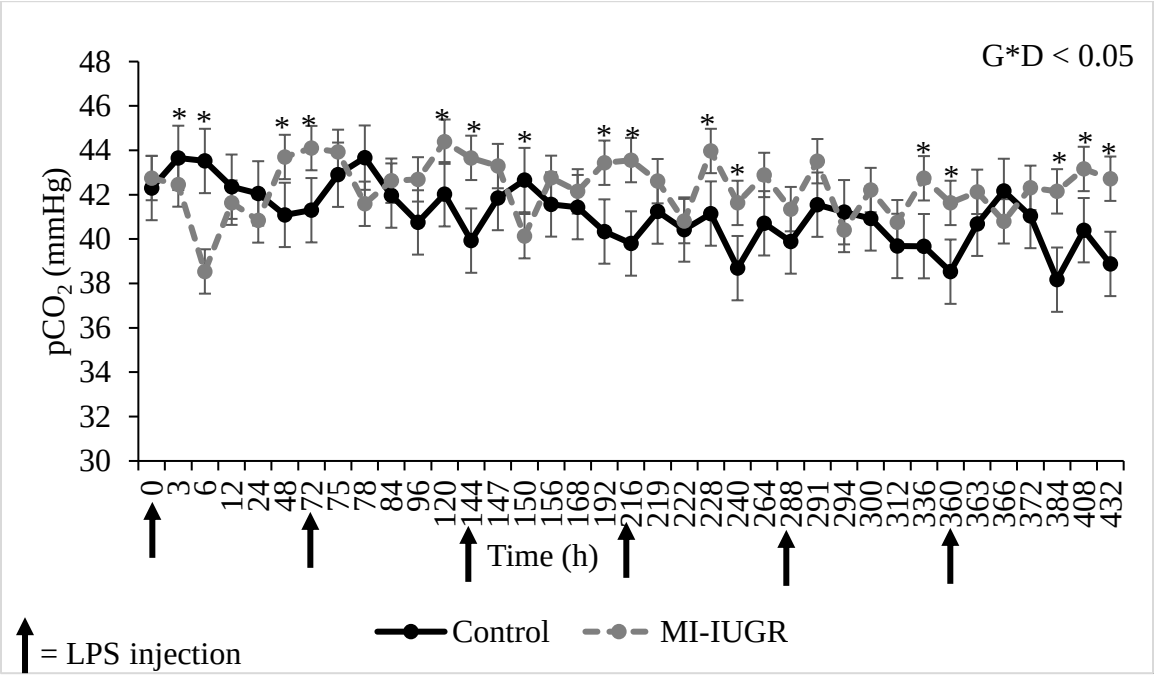


**Figure 2.9** Maternal responses to serial administration of LPS during the early 2nd trimester of pregnancy. Ewes were injected I.V. with *E. coli* O55:B5 LPS (MI-IUGR; n=18) or saline controls (n=11) every 72 h from dGA 50 to 65. Data are shown for maternal blood partial pressure of $CO_2$. Effect of maternal injections (GRP), time of blood draw relative to initiating injections (DRAW), and the interaction (G*D) are noted when significant. Arrows denote when injections were administered. Time points that are significant are denoted (*$P < 0.05$).

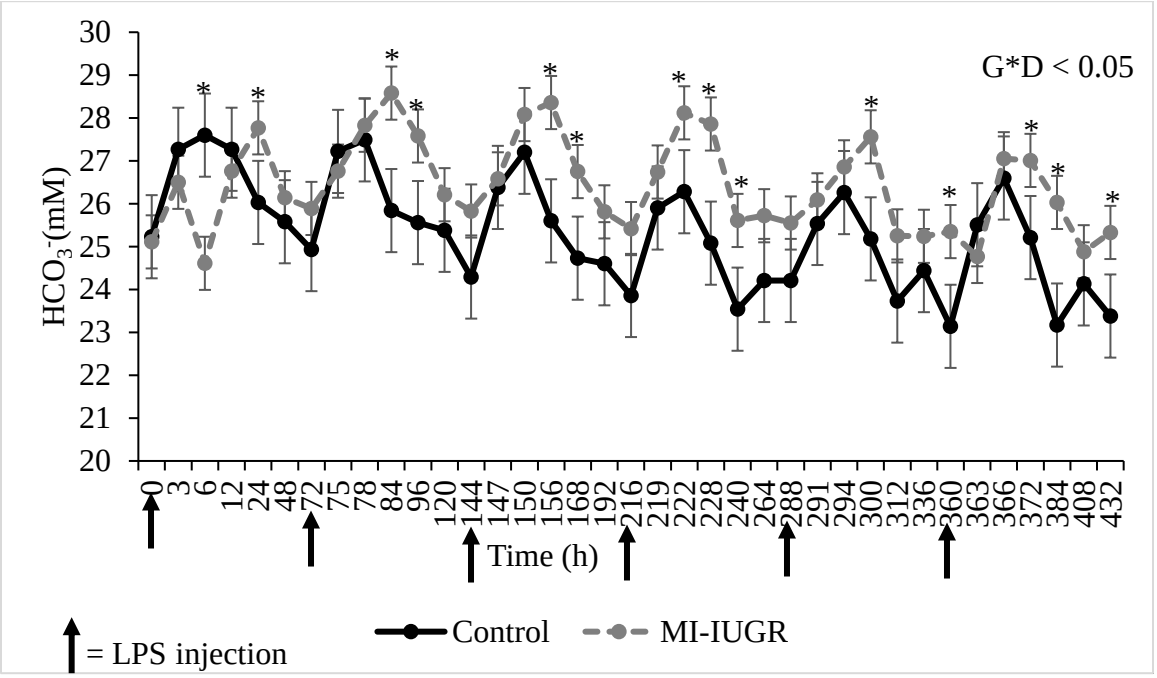


**Figure 2.10** Maternal responses to serial administration of LPS during the early 2nd trimester of pregnancy. Ewes were injected I.V. with *E. coli* O55:B5 LPS (MI-IUGR; n=18) or saline controls (n=11) every 72 h from dGA 50 to 65. Data are shown for maternal blood $HCO_3^-$. Effect of maternal injections (GRP), time of blood draw relative to initiating injections (DRAW), and the interaction (G*D) are noted when significant. Arrows denote when injections were administered. Time points that are significant are denoted (*$P < 0.05$).

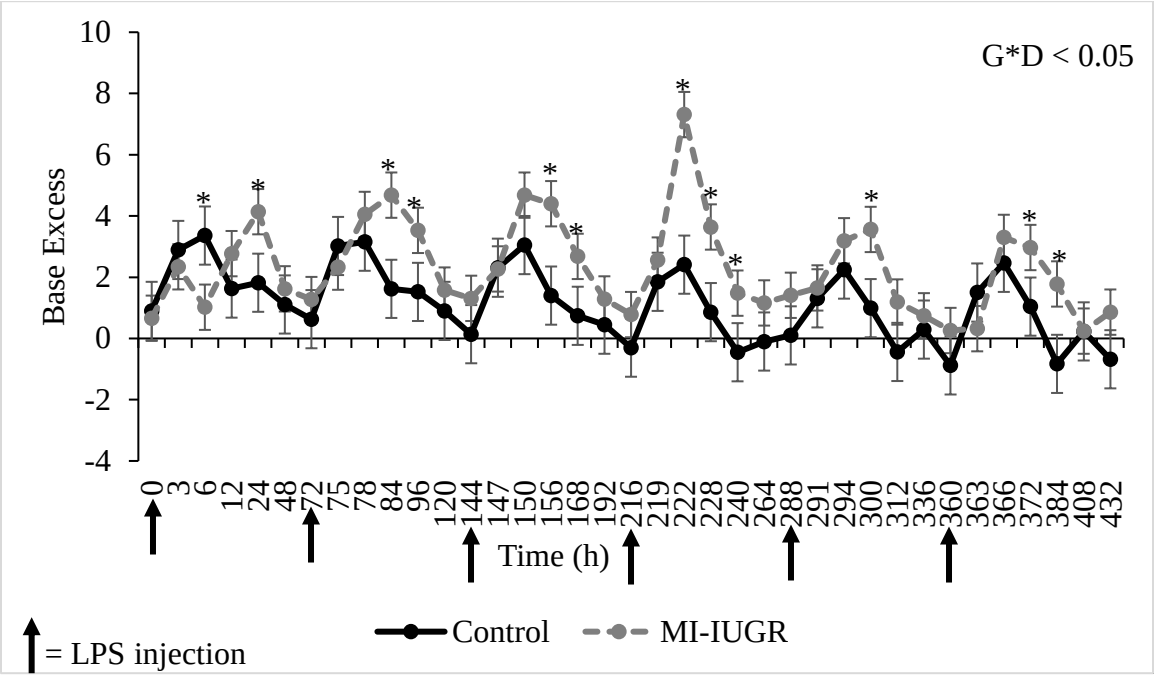


**Figure 2.11** Maternal responses to serial administration of LPS during the early 2nd trimester of pregnancy. Ewes were injected I.V. with *E. coli* O55:B5 LPS (MI-IUGR; n=18) or saline controls (n=11) every 72 h from dGA 50 to 65. Data are shown for maternal blood base excess. Effect of maternal injections (GRP), time of blood draw relative to initiating injections (DRAW), and the interaction (G*D) are noted when significant. Arrows denote when injections were administered. Time points that are significant are denoted (*$P < 0.05$).

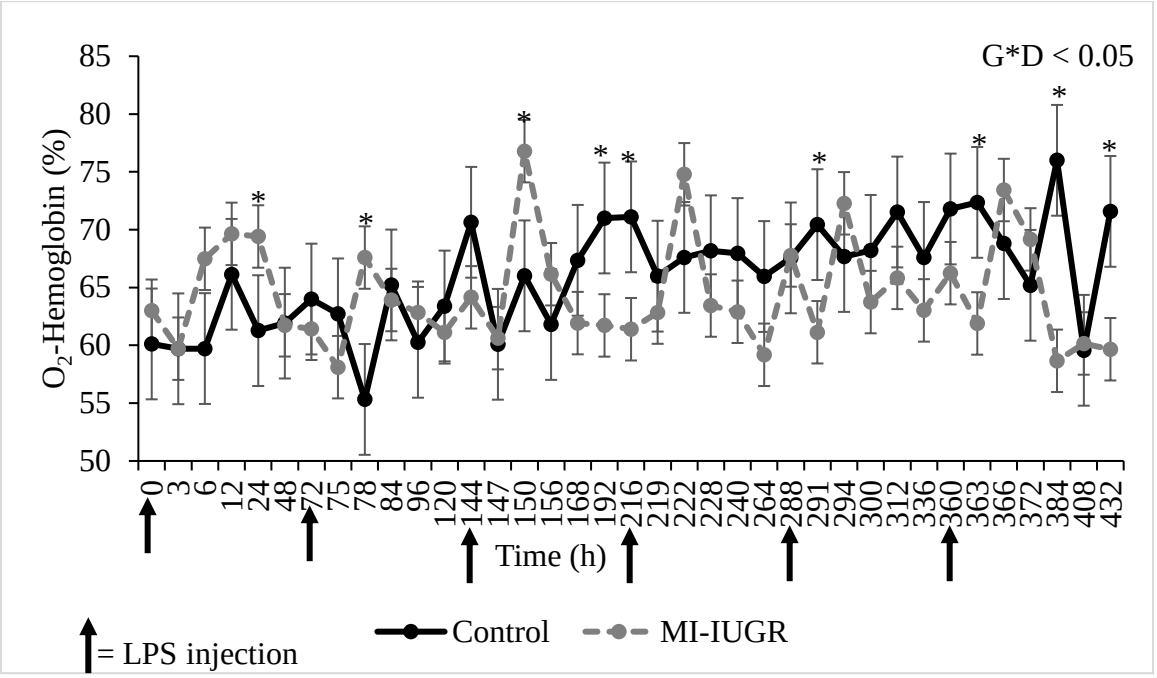


**Figure 2.12.** Maternal responses to serial administration of LPS during the early 2nd trimester of pregnancy. Ewes were injected I.V. with *E. coli* O55:B5 LPS (MI-IUGR; n=18) or saline controls (n=11) every 72 h from dGA 50 to 65. Data are shown for maternal blood oxyhemoglobin percentage. Effect of maternal injections (GRP), time of blood draw relative to initiating injections (DRAW), and the interaction (G*D) are noted when significant. Arrows denote when injections were administered. Time points that are significant are denoted (*$P < 0.05$).

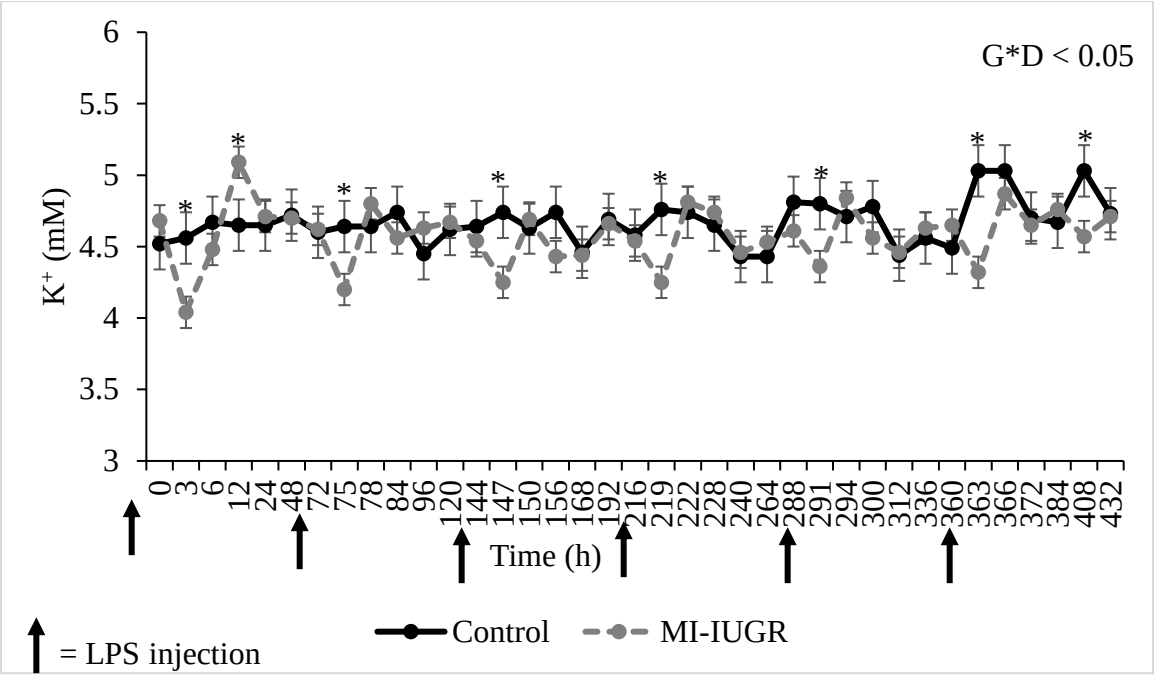


**Figure 2.13**. Maternal responses to serial administration of LPS during the early 2nd trimester of pregnancy. Ewes were injected I.V. with *E. coli* O55:B5 LPS (MI-IUGR; n=18) or saline controls (n=11) every 72 h from dGA 50 to 65. Data are shown for maternal blood $K^+$ concentration. Effect of maternal injections (GRP), time of blood draw relative to initiating injections (DRAW), and the interaction (G*D) are noted when significant. Arrows denote when injections were administered. Time points that are significant are denoted (*$P < 0.05$).

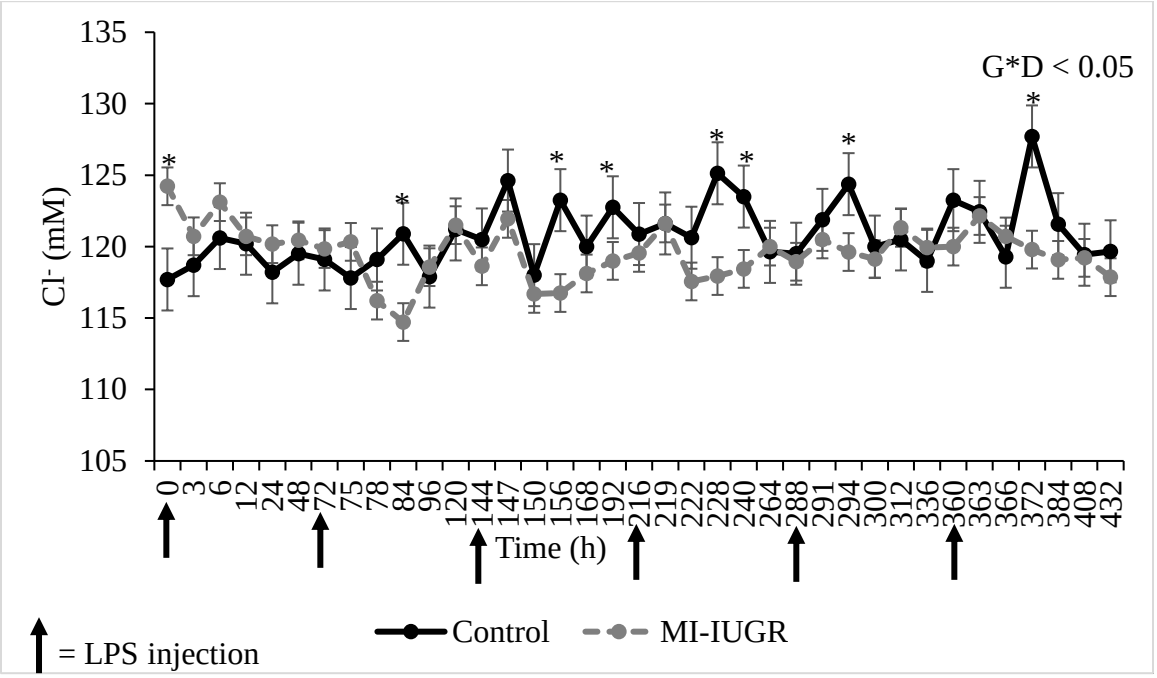


**Figure 2.14**. Maternal responses to serial administration of LPS during the early 2nd trimester of pregnancy. Ewes were injected I.V. with *E. coli* O55:B5 LPS (MI-IUGR; n=18) or saline controls (n=11) every 72 h from dGA 50 to 65. Data are shown for maternal blood $Cl^-$ concentration. Effect of maternal injections (GRP), time of blood draw relative to initiating injections (DRAW), and the interaction (G*D) are noted when significant. Arrows denote when injections were administered. Time points that are significant are denoted (*$P < 0.05$).

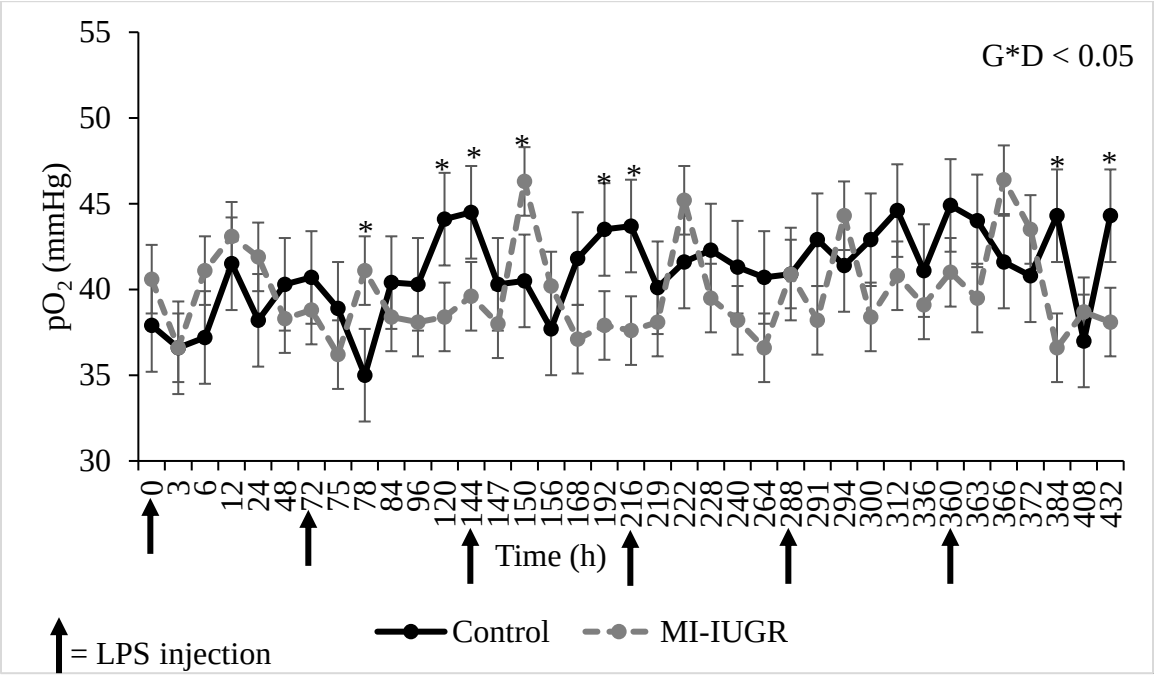


**Figure 2.15**. Maternal responses to serial administration of LPS during the early 2nd trimester of pregnancy. Ewes were injected I.V. with *E. coli* O55:B5 LPS (MI-IUGR; n=18) or saline controls (n=11) every 72 h from dGA 50 to 65. Data are shown for maternal blood $O_2$ partial pressures. Effect of maternal injections (GRP), time of blood draw relative to initiating injections (DRAW), and the interaction (G*D) are noted when significant. Arrows denote when injections were administered. Time points that are significant are denoted (*$P < 0.05$).

**Table 2.2.** The main effect of group on maternal blood gases and metabolites assessed during the induction of maternofetal inflammation. Ewes were injected I.V. with E. coli O55:B5 LPS (MI-IUGR) or saline controls every 72 h from dGA 50 to 65.

| | Control (n=11) | MI-IUGR (n=18) | *P*-value |
|---|---|---|---|
| Lactate | 0.77±0.04 | 1.03±0.03 | <0.001 |
| Hemoglobin | 10.91±0.11 | 11.84±0.05 | <0.001 |
| Hematocrit | 33.43±0.34 | 36.24±0.17 | <0.001 |
| CO-Hb | 1.71±0.05 | 1.43±0.02 | <0.001 |
| $Na^+$ | 156.8±0.3 | 156.9±0.2 | NS |
| $Ca^{2+}$ | 1.19±0.00 | 1.15±0.00 | <0.001 |

NS = not significant ($P > 0.05$)

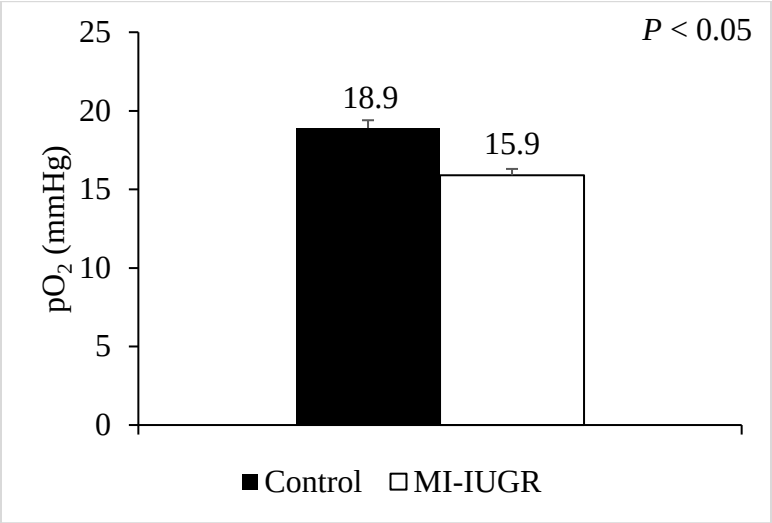


**Figure 2.16** Daily partial pressure $O_2$ in arterial blood collected from control (n=12) or MI-IUGR fetuses (n=13) from 120 dGA to 125 dGA. There was no interaction between group and day (P > 0.05).

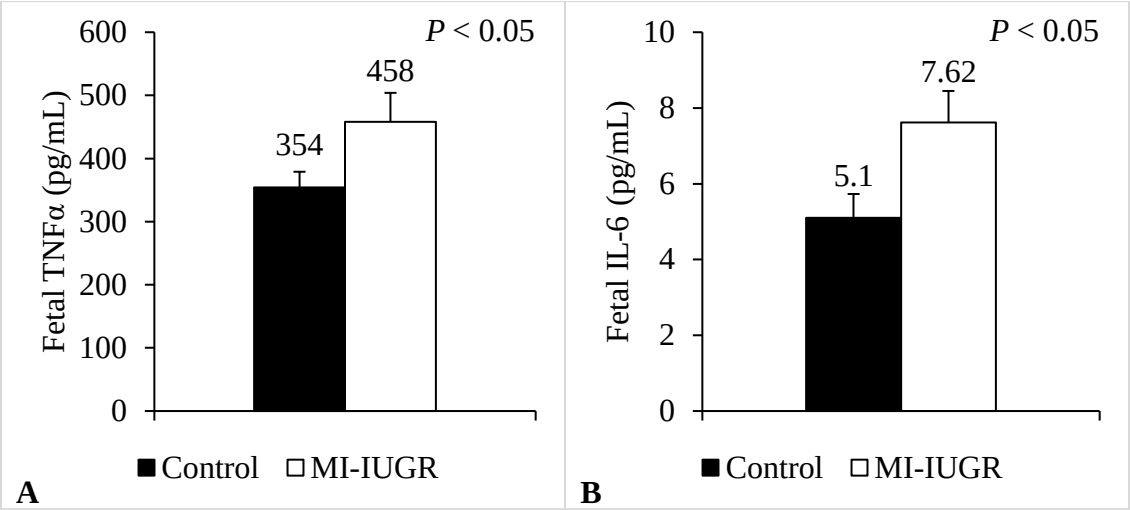


**Figure 2.17** Fetal plasma (**A)** TNFα and **(B)** IL-6 concentrations assessed from 120 dGA to 125 dGA in control (n=11) and MI-IUGR (n=13) fetuses. There was no significant interaction between group and day (P > 0.05).

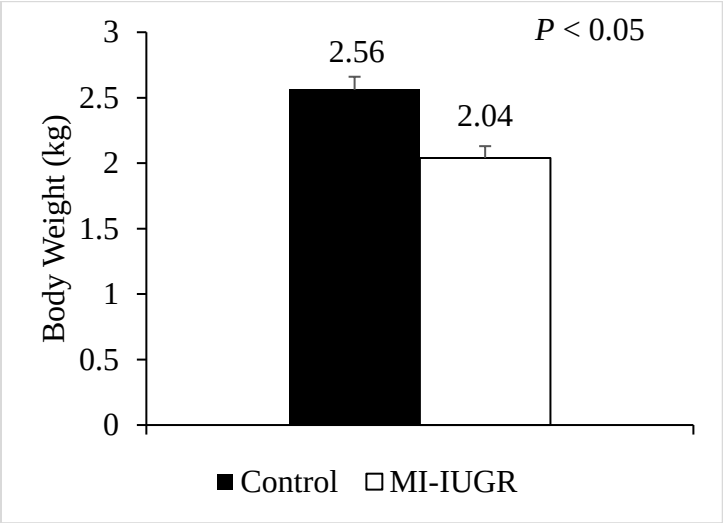


**Figure 2.18.** Whole body weight of fetuses exposed to mid-gestation maternofetal inflammation (MI-IUGR; n=15) or controls (n=12) assessed at dGA 125 ($P < 0.05$)

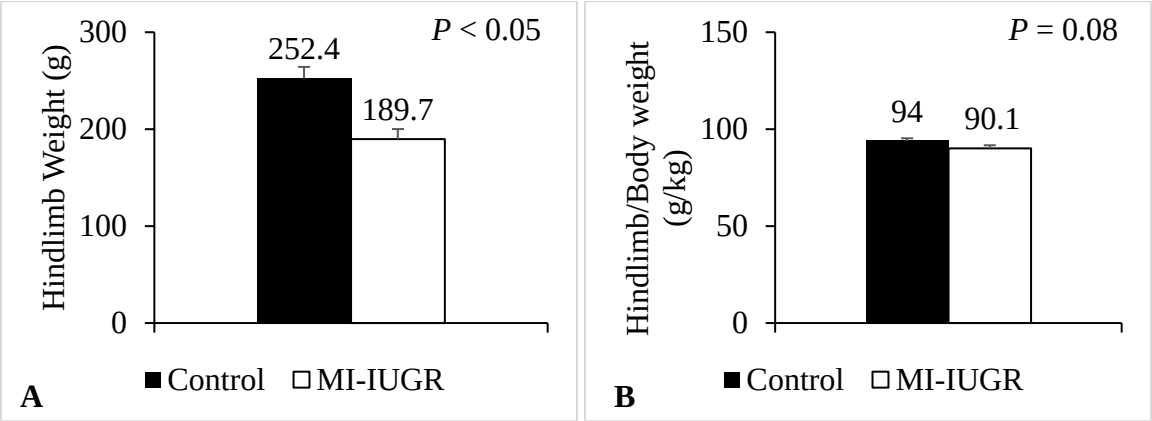


**Figure 2.19. (A)** Hindlimb weights and **(B)** proportional hindlimb weights of fetuses exposed to mid-gestation maternofetal inflammation (MI-IUGR; n=15) or controls (n=12) assessed at dGA 125.

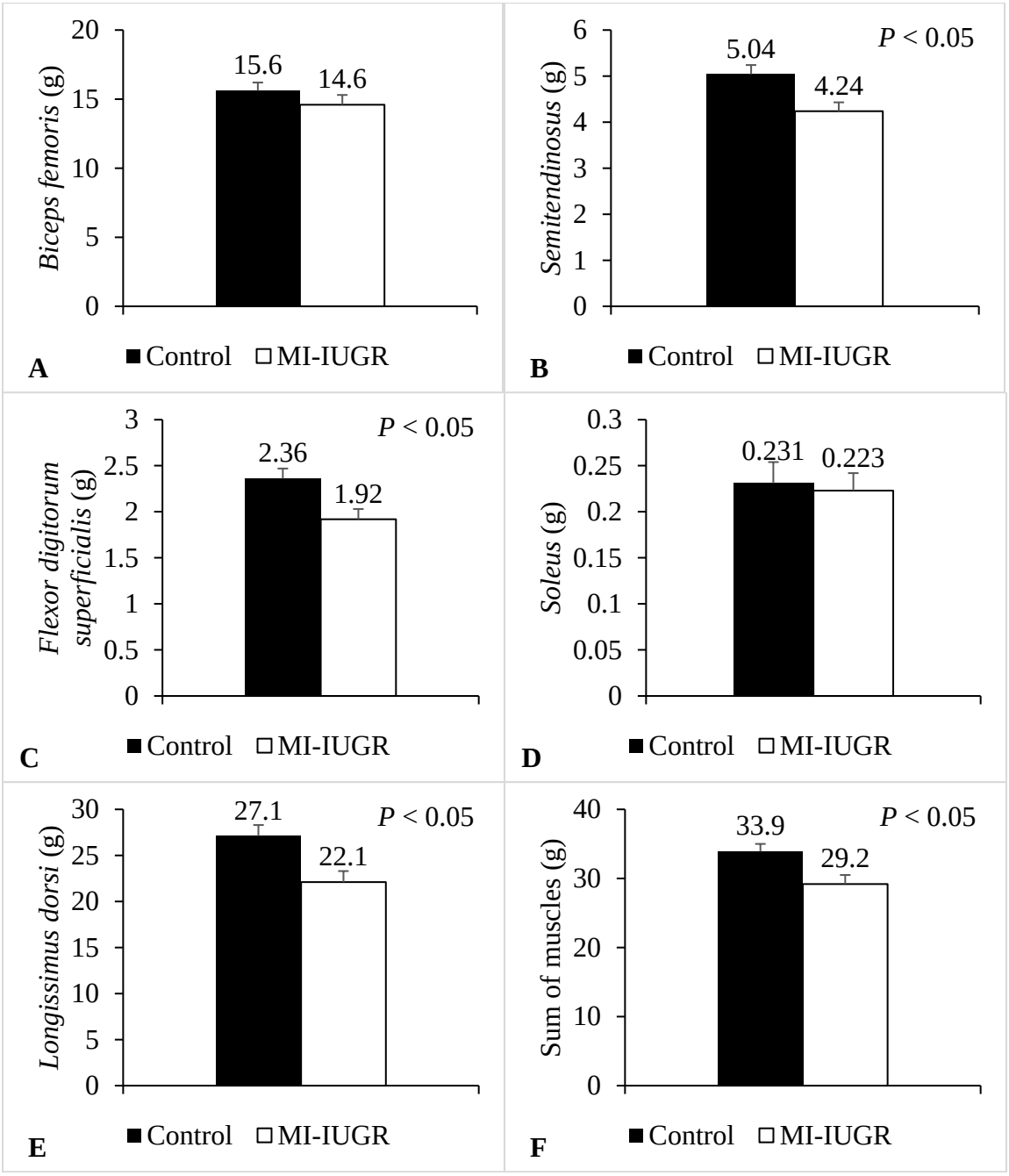


**Figure 2.20** Weight of **(A)** Biceps femoris, **(B)** Semitendinosus, **(C)** Flexor digitorum superficialis, **(D)** Soleus, **(E)** Longissimus dorsi, and **(F)** total muscle collected in fetuses exposed to mid-gestation maternofetal inflammation (MI-IUGR; n=15) or controls (n=12) assessed at dGA 125.

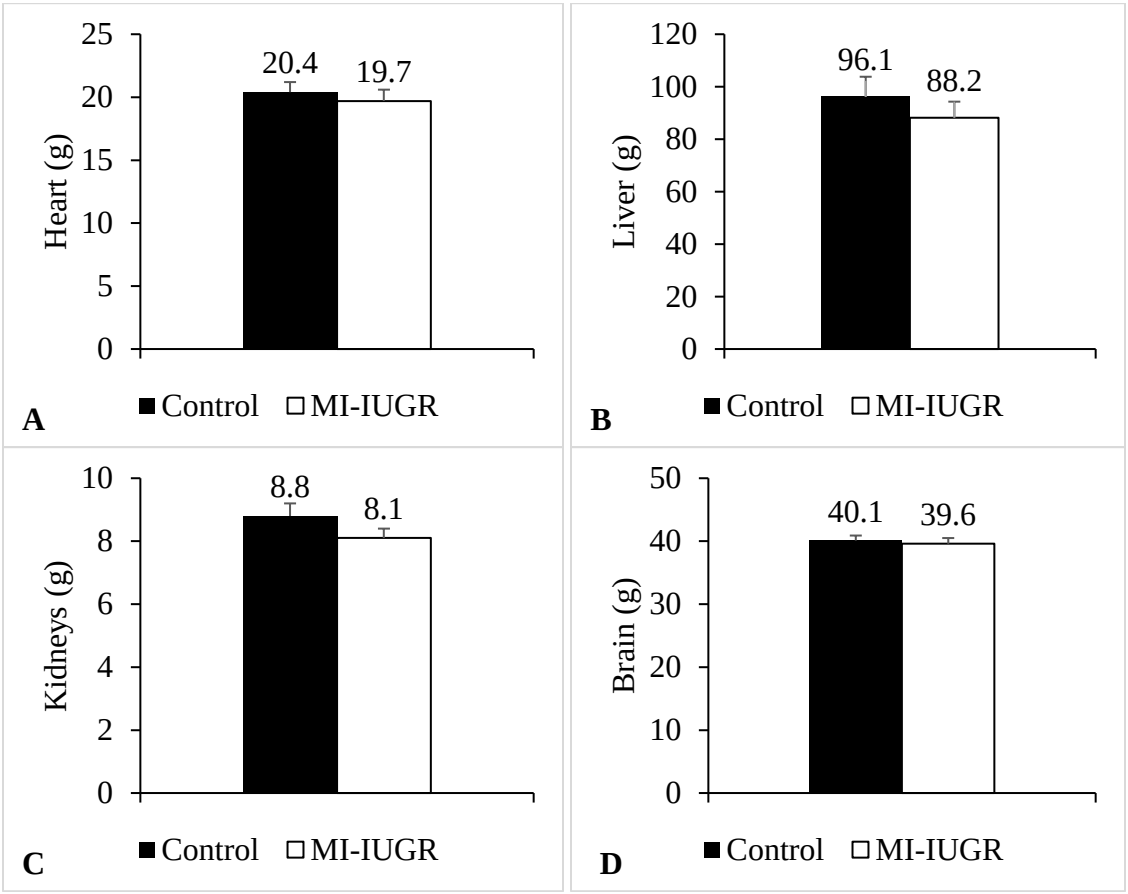


**Figure 2.21** Weight of fetal **(A)** heart, **(B)** liver, **(C)** kidneys, and **(D)** brain in fetuses exposed to mid-gestation maternofetal inflammation (MI-IUGR; n=15) or controls (n=12) assessed at dGA 125.

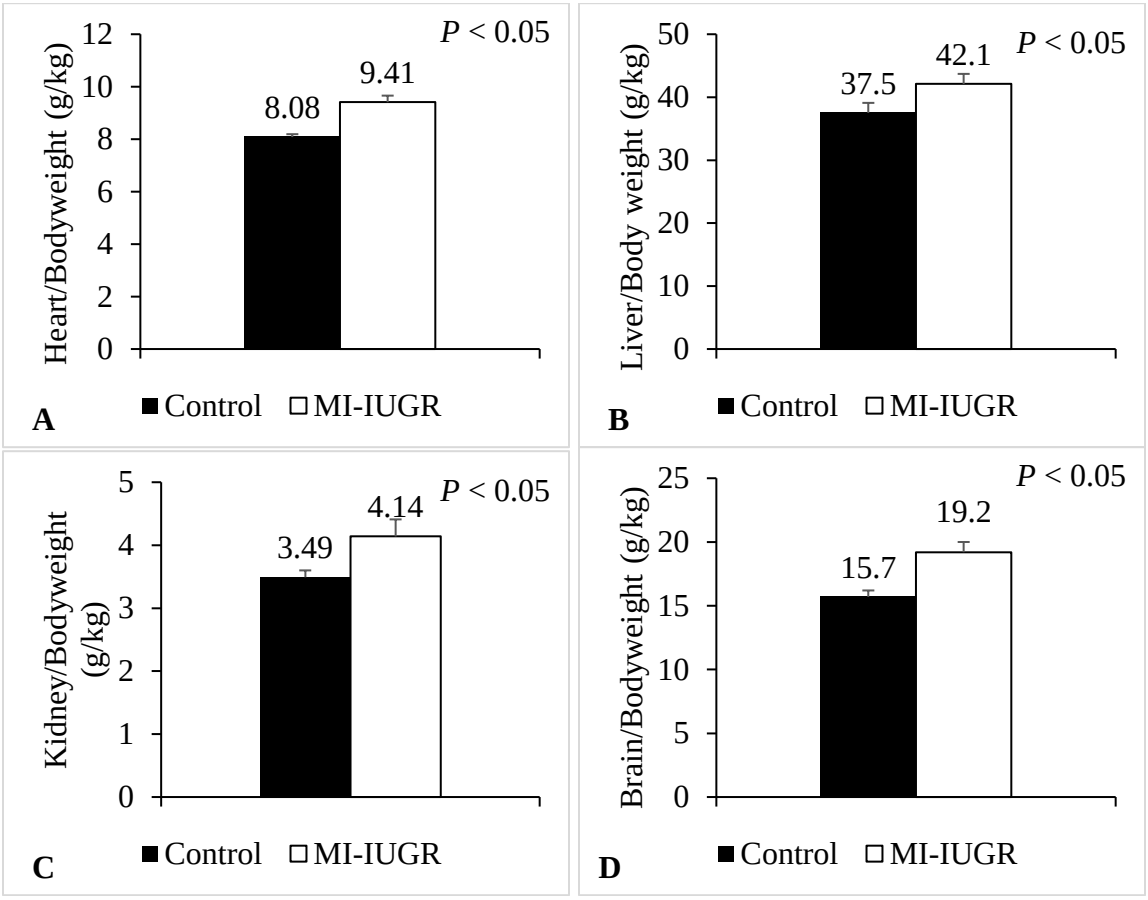


**Figure 2.22** The proportional weight of the **(A)** heart/bodyweight, **(B)** liver/bodyweight, **(C)** kidneys/bodyweight, and **(D)** brain/bodyweight in fetuses exposed to mid-gestation maternofetal inflammation (MI-IUGR; n=15) or controls (n=12) assessed at dGA 125.

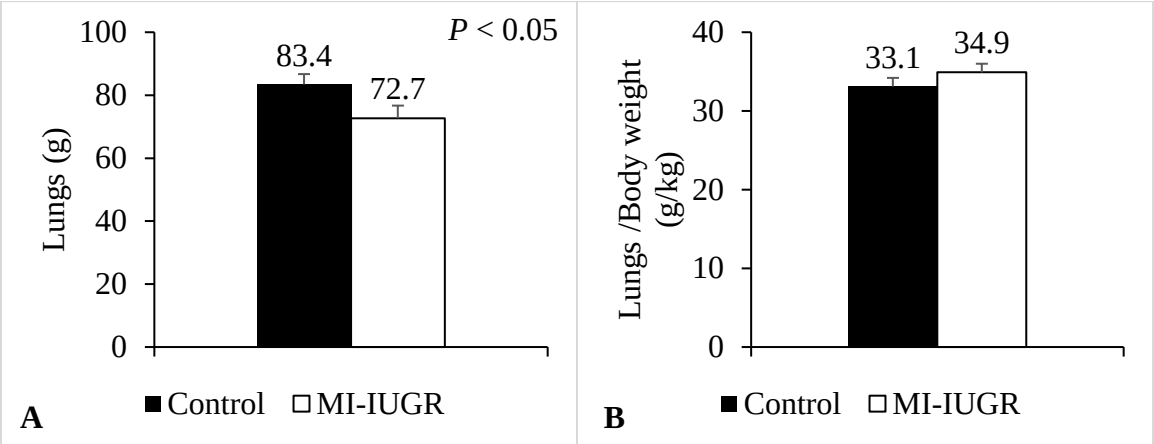


**Figure 2.23** The weight of **(A)** lungs and proportional weight of **(B)** lungs/bodyweight in fetuses exposed to mid-gestation maternofetal inflammation (MI-IUGR; n=15) or controls (n=12) assessed at dGA 125.

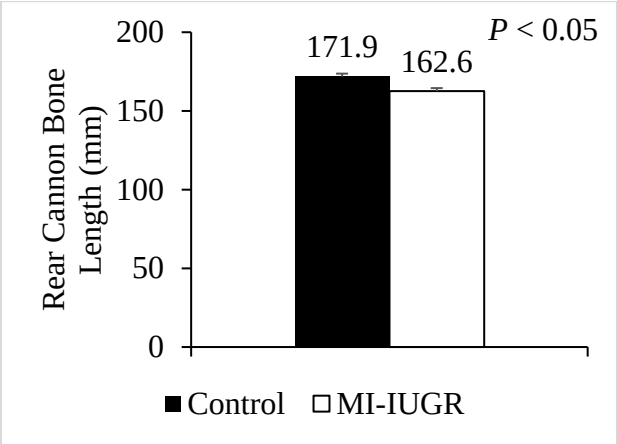


**Figure 2.24** Rear cannon bone length in fetuses exposed to mid-gestation maternofetal inflammation (MI-IUGR; n=15) or controls (n=12) assessed at dGA 125.

**Table 2.3**. The main effect of fetal sex on morphometric data collected from control fetuses (n=12) or fetuses exposed to mid-gestation maternofetal inflammation (n=15) collected at dGA 125.

| Variable | Female (n=15) | Male (n=12) | *P*-value |
|---|---|---|---|
| **Absolute Mass** | | | |
| Cannon Bone Length (mm) | 163.9±2 | 170.6±2 | 0.02 |
| **Proportional Mass (g tissue/kg bodyweight)** | | | |
| Hindlimb | 94.1±1.5 | 90.2±1.5 | 0.08 |
| Heart | 8.47±0.16 | 9.01±0.16 | 0.02 |

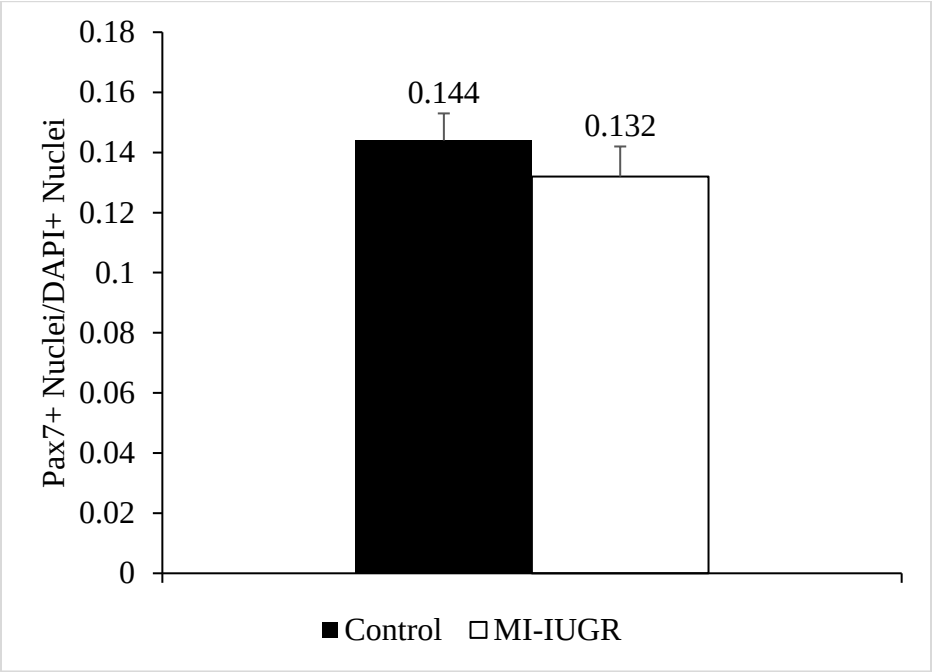


**Figure 2.25** Myoblast profiles and skeletal muscle fiber size in mid-gestation MI-IUGR fetuses. Cross-sectional samples of semitendinosus muscle were collected at dGA 125 from control (n=11) or MI-IUGR (n=11) fetuses. Data are presented for the percentage of cells expressing Pax7.

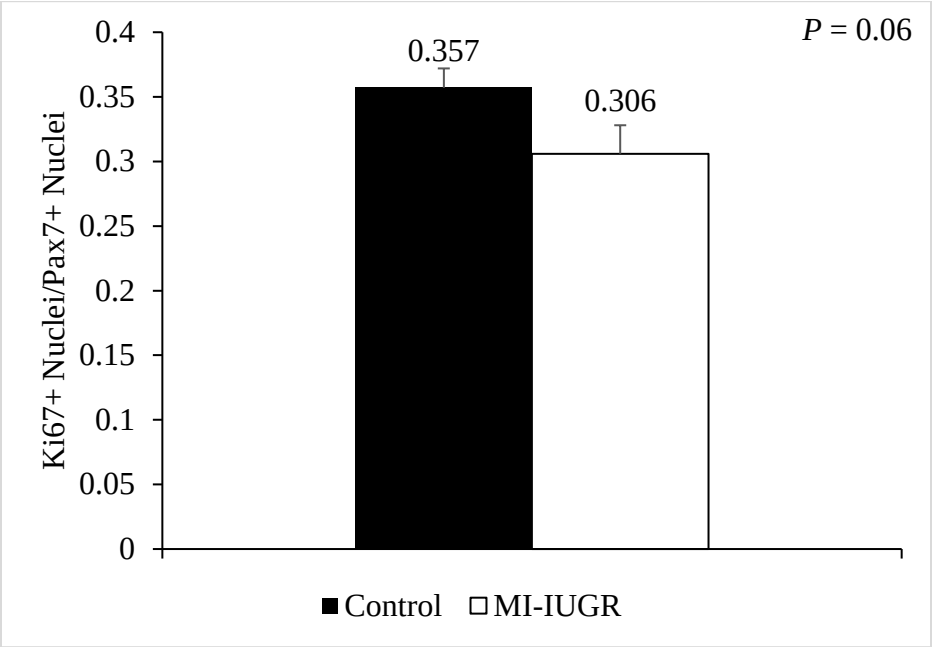


**Figure 2.26** Myoblast profiles and skeletal muscle fiber size in mid-gestation MI-IUGR fetuses. Cross-sectional samples of semitendinosus muscle were collected at dGA 125 from control (n=11) or MI-IUGR (n=11) fetuses. Data are presented for the percentage of $Pax7^{+}$ myoblasts expressing Ki67.

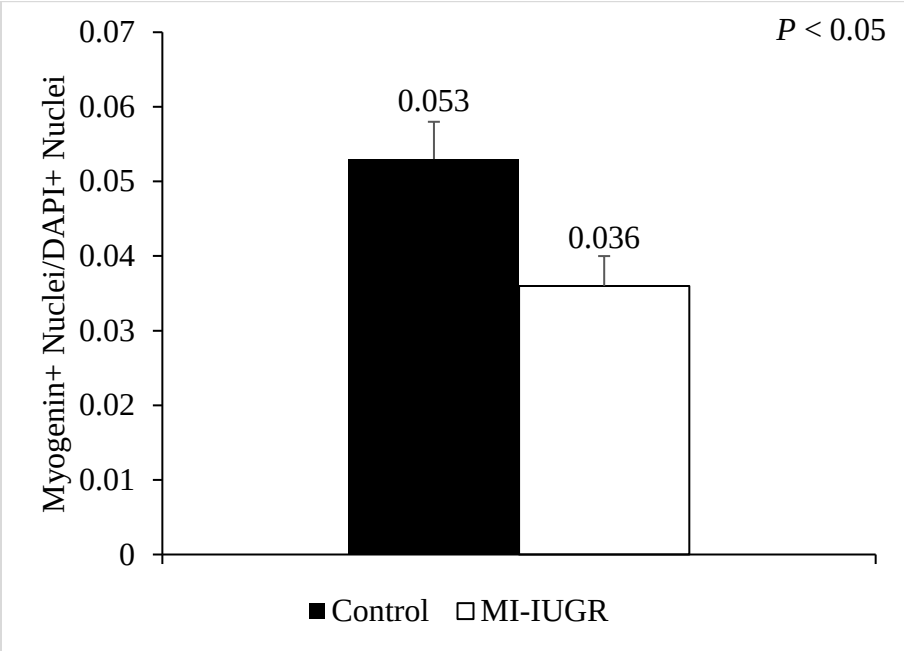


**Figure 2.27** Myoblast profiles and skeletal muscle fiber size in mid-gestation MI-IUGR fetuses. Cross-sectional samples of semitendinosus muscle were collected at dGA 125 from control (n=11) or MI-IUGR (n=11) fetuses. Data are presented for the percentage of myoblasts expressing myogenin.

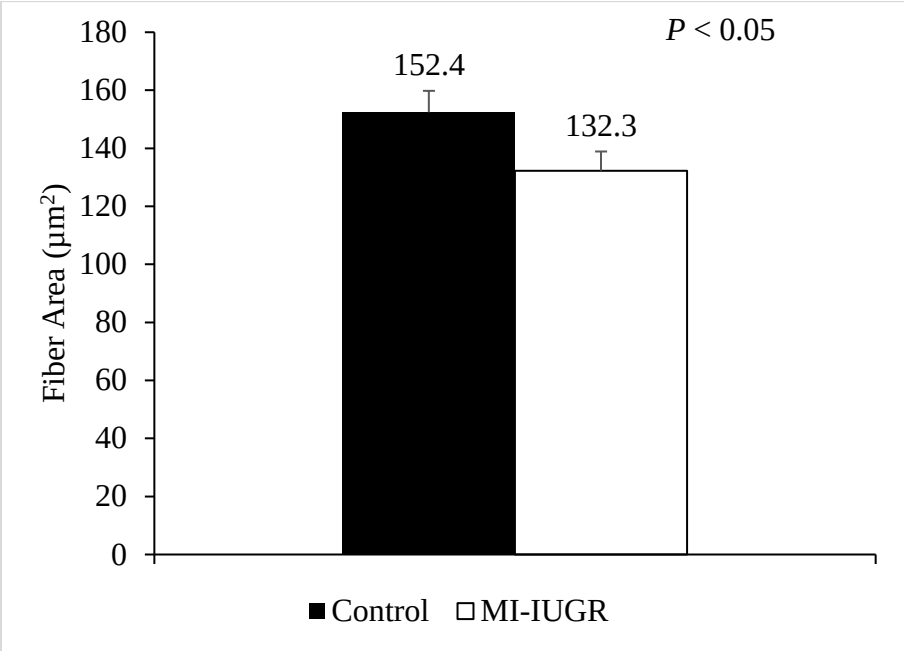


**Figure 2.28** Myoblast profiles and skeletal muscle fiber size in mid-gestation MI-IUGR fetuses. Cross-sectional samples of semitendinosus muscle were collected at dGA 125 from control (n=11) or MI-IUGR (n=11) fetuses. Data are presented for the muscle fiber area.

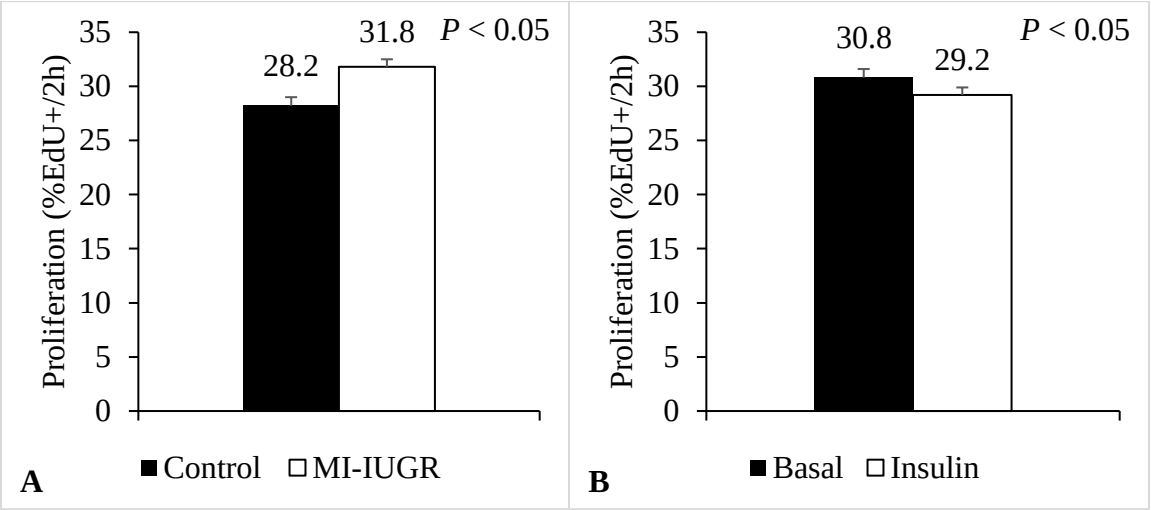


**Figure 2.29** Proliferation and differentiation rates for MI-IUGR fetal myoblasts. Primary myoblasts were isolated from upper hindlimb muscles collected from control (n=5) or MI-IUGR fetuses (n=5) at dGA 125. Proliferation was determined by 2h EdU pulse after 24h incubation in complete growth media with no additive (basal) or 5 mU/mL insulin. There were no interactive effects between experiment group and media ($P > 0.05$). The main effects of (**A**) group and (**B**) media are presented above.

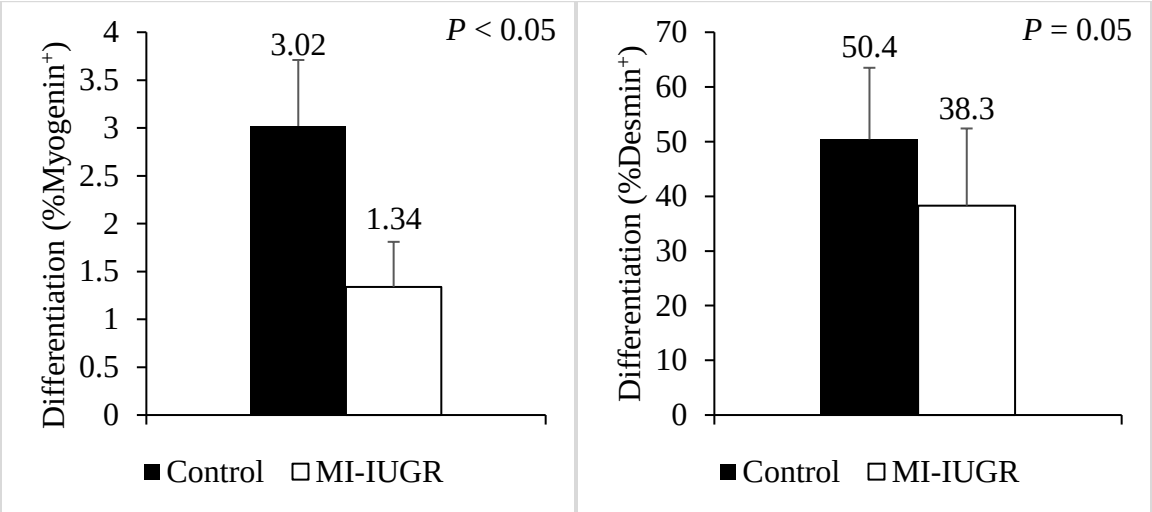


**Figure 2.30** Proliferation and differentiation rates for MI-IUGR fetal myoblasts. Primary myoblasts were isolated from upper hindlimb muscles collected from control (n=5) or MI-IUGR fetuses (n=5) at dGA 125. Differentiation was assessed by the percentages of myoblasts expressing (**A**) myogenin or (**B**) desmin after a 96h incubation in differentiation media containing no additive (basal) or 5 mU/mL insulin. There were no interactive effects between experiment group and media ($P > 0.05$). The group main effect is presented above.

**CHAPTER 3 – Maternofetal inflammation at mid-gestation effects subsequent fetal glucose-stimulated insulin secretion, skeletal muscle glucose metabolism, and inflammatory tone during late gestation**

## Abstract

Maternofetal inflammation occurring in the 3rd trimester of pregnancy causes fetal intrauterine growth restriction (**IUGR**) in part by disproportionately restricting muscle growth. However, the impact of maternofetal inflammation occurring at mid-gestation, which precedes peak muscle growth and development but coincides with peak placental growth, has not been explored. Therefore, the objective of this study was to examine the impact of sustained inflammation at mid-gestation on fetal inflammatory status, insulin secretion, and metabolism. Pregnant ewes were injected every 3rd day from the 50th to the 65th d of gestational age (**dGA**; term=150 dGA) with saline placebo (control; n=12) or with bacterial lipopolysaccharide endotoxin (0.1 μg/kg) to induce maternofetal inflammation and fetal IUGR (**MI-IUGR**; n=15). Fetuses were surgically catheterized on dGA 118 to collect daily blood samples and conduct metabolic studies. Glucose-stimulated insulin secretion (**GSIS**) and hindlimb hyperinsulinemic-euglycemic clamp (**HEC**) studies were performed at dGA 122 and 123, respectively. At 125 dGA, fetuses were necropsied, *ex vivo* HEC studies were performed on primary muscle, and *ex vivo* fatty acid mobilization was measured in primary abdominal adipose tissue. Circulating white blood cells, lymphocytes, and red blood cells were reduced ($P < 0.05$) and granulocytes and platelets were increased ($P < 0.05$) in MI-IUGR fetuses compared to controls. Blood lactate and methemoglobin were increased ($P < 0.05$) and $HCO_3^-$, hematocrit, hemoglobin, oxyhemoglobin, carboxyhemoglobin, $K^+$, and partial pressure of

$O_2$ (**$pO_2$**) were decreased ($P < 0.05$) in MI-IUGR fetuses. Maternofetal gradients for blood glucose were reduced ($P < 0.05$) but gradients for blood lactate, $Na^+$, $Cl^-$, $pO_2$, and $K^+$ were increased ($P < 0.05$) in MI-IUGR pregnancies compared to controls. Fetal plasma TNFα and IL-6 were increased ($P < 0.05$) in MI-IUGR fetuses. Additionally, MI-IUGR fetal skeletal muscle had increased ($P < 0.05$) protein content for TNFR1 and IL6R and tended to have increased ($P = 0.06$) TLR4 protein content. Adrβ2 skeletal muscle protein content was similar between groups. Basal plasma insulin did not differ between groups, but glucose-stimulated insulin secretion was reduced ($P < 0.05$) in MI-IUGR fetuses. *In vivo* hindlimb glucose uptake was similar between groups, but hindlimb glucose oxidation was reduced ($P < 0.05$) in MI-IUGR fetuses. Basal glucose: insulin ratio was increased ($P < 0.05$) in MI-IUGR fetuses. *Ex vivo* glucose uptake, glucose oxidation, and phospho-Akt were reduced ($P < 0.05$) in MI-IUGR muscle, and *ex vivo* fatty acid mobilization was decreased ($P < 0.05$) in MI-IUGR adipose tissue. Skeletal muscle glycogen content tended to be increased ($P = 0.06$) in MI-IUGR fetuses. We conclude that sustained maternofetal inflammation during peak placental development reduced fetal glucose-stimulated insulin secretion and impaired capacity for skeletal muscle glucose oxidation and fat mobilization. This reflects the thrifty metabolic phenotype observed following placental insufficiency-induced IUGR and implicates inflammation as a major factor in the adaptive metabolism of skeletal muscle and adipose tissue in IUGR individuals.

## Introduction

Intrauterine growth restriction (**IUGR**) is a health problem that impacts as many as 1 in 5 babies each year worldwide (Wu et al., 2006; Sedgh et al., 2014; Flinn et al., 2020). Adaptive fetal programming in IUGR-born individuals makes them at increased risk for lifelong metabolic dysfunction, which leads to reduced quality of life and a shorter life expectancy (Briana and Malamitsi-Puchner, 2009; Marcondes Machado Nardozza et al., 2017; Darendeliler, 2019; Xing et al., 2020) This same perinatal condition in livestock species creates as much as a 20% loss in yearly global annual product (Wu et al., 2006). IUGR-born livestock have increased input costs to get the animal through the production system due to their reduced feed efficiency, and they produce lower-value carcasses due to increased fat deposition and reduced muscle growth (Greenwood et al., 2005; Greenwood and Cafe, 2007; Robinson et al., 2013; Greenwood and Bell, 2019). Despite varying etiologies, IUGR fetuses typically have a common underlying state of sustained systemic inflammation (Hicks and Yates, 2021). Indeed, IUGR fetuses across various species and methods of inducing maternal stress have been found to exhibit elevated circulating inflammatory cytokines (Kemp, 2014; Krajewski et al., 2014; Visentin et al., 2014; Hudalla et al., 2018; Cadaret et al., 2019; Cadaret et al., 2019a; Hicks and Yates, 2021). These cytokines, including TNFα and IL-6, create a shift in skeletal muscle metabolism by reducing oxidative metabolism by as much as 50% and proportionally increasing glycolytic lactate production (Boscá and Corredor, 1984; Rhoades et al., 2005; Remels et al., 2015; Hicks and Yates, 2021). Likewise, cytokines decrease glucose oxidation in pancreatic β cells (the impetus for insulin stimulus-secretion coupling), thus impairing glucose stimulated-insulin secretion (Youd et al.,

2000; Reid and Li, 2001; Harms et al., 2015; Oleson et al., 2015; Hicks and Yates, 2021). Our recent review details the multiple levels of heightened inflammatory regulation and responsiveness in IUGR fetal and neonatal tissues observed in our studies and others (Hicks and Yates, 2021). For example, studies in a multitude of mammalian species have demonstrated an increase in circulating monocytes and other white blood cells occurring in concert with heightened circulating inflammatory cytokines in IUGR fetuses (Romero et al., 2008; Rong Guo et al., 2010; Cadaret et al., 2019; Oh et al., 2019; Hicks and Yates, 2021). Additional studies have shown that IUGR lung, brain, skeletal muscle, and white blood cells have elevated cytokine production and content (Kemp, 2014; Cadaret et al., 2019a). Further transcriptomic analyses have elucidated enhanced programming of cytokine signaling pathways in IUGR skeletal muscle that persists even when circulating cytokines are no longer elevated postnatally (Hicks and Yates, 2021). Thus, systemic inflammation-induced programming of inflammatory signaling pathways appears to be a mediator for IUGR metabolic dysfunction when the inflammation is sustained in late gestation. However, it is unclear whether inflammation occurring at mid-gestation prior to peak muscle growth but during peak placental growth and development would affect the subsequent metabolic characteristics of the fetus and offspring. Thus, the objective of this study was to determine the impact of mid-gestation maternofetal inflammation on fetal inflammatory tone, β cell function, and skeletal muscle-specific glucose metabolism during late gestation. We hypothesized that inducing maternofetal inflammation at this stage in gestation would result in profound placental stunting, which in turn would lead to larger metabolic deficits in the maternofetal inflammation-induce IUGR (**MI-IUGR**) fetus during late gestation.

## Materials and Methods

### *Animals and Experimental Design*

This study was approved by the Institutional Animal Care and Use Committee at the University of Nebraska-Lincoln (**UNL**). All animal studies were performed at the University of Nebraska-Lincoln Animal Science Complex, which is accredited by AAALAC International. Polypay-cross ewes were purchased from a single commercial source and were time-mated to a single sire. Twenty-four pregnant ewes were identified via blood pregnancy tests at 30 d of gestational age (**dGA**) and were randomly assigned to the control or MI-IUGR groups described below. All ewes were individually housed at ambient temperatures and fed a diet consisting of alfalfa pellets. Ewes were given *ad libitum* access to water and mineral supplements. The MI-IUGR fetuses (n = 15) were produced by injecting ewes with IV bacterial lipopolysaccharide (**LPS**) endotoxin (100 ng/kg bodyweight suspended in 1 ml saline; *Escherichia coli* O55:B5; Sigma Aldrich, St. Louis, MO) every 72 h from the $50^{th}$ to the $65^{th}$ dGA. Ewes carrying control fetuses (n = 12) were injected every 72 h with 1 ml saline only. Fetal hindlimb catheterization surgeries were performed on dGA 118 ± 2. Twice-daily maternal and fetal blood samples were collected from dGA 119 to 125 at 800 and 1400. Each set of simultaneous maternal venous (jugular venipuncture) and fetal arterial blood samples were collected into EDTA syringes (~1.5 ml/sample) and heparinized syringes (~0.4 ml/sample). Fetal metabolic studies were performed on dGA 122 and 123, respectively. Ewes were euthanized by double barbiturate overdose and fetuses were necropsied on dGA 125 ± 2.

### *Fetal Surgical Hindlimb Preparation*

Fetal femoral arterial and venous catheters were surgically placed as previously described (Cadaret et al., 2018). Briefly, ewes were fasted overnight, induced by IV injection of ketamine (10 mg/kg bodyweight) and midazolam (0.11 mg/kg bodyweight), intubated, and maintained under anesthesia by inhalation of 1% to 5% isoflurane gas in $O_2$. The fetal hindlimbs were exteriorized by partial cesarean, and indwelling catheters (Tygon ND-100-80 Flexible Plastic Tubing; outer diameter, 1.4 mm, inner diameter, 0.9 mm; US Plastics, Lima, OH) were surgically placed in the descending aorta and inferior vena cava via the femoral artery and vein of each hindlimb. Catheters were filled with heparinized saline (30 U/ml, 0.9% NaCl, Nova-Tech, Inc., Grand Island, NE) and were tunneled subcutaneously to the flank, exteriorized through a skin incision, and kept in a plastic mesh pouch sutured to the skin. Ewes were administered 6,600 U/kg penicillin G procaine, 10 mg/kg phenylbutazone, and 4 mg/kg atropine at the time of surgery. Postoperative phenylbutazone was continued for 3 d following surgery, and ewes were allowed to recover for 1 d before performing studies. Catheters were flushed twice daily with heparinized saline.

### *In Vivo Metabolic Studies*

#### *Glucose-Stimulated Insulin Secretion*

A square-wave hyperglycemic clamp was performed at 122 dGA to measure basal (i.e., resting) and 2$^{nd}$-phase glucose-stimulated insulin secretion as previously described (Posont et al., 2021; Cadaret et al., 2022; Gibbs, 2023). Briefly, a series of three arterial blood samples were collected in 5-min intervals to measure basal blood glucose and

plasma insulin concentrations. Afterward, an intravenous bolus of 33% dextrose (Vet One; Boise, ID) in saline was administered to deliver 250 mg/kg glucose. The bolus was followed immediately by the initiation of a continuous, variable-rate 33% dextrose infusion until the targeted steady-state hyperglycemic condition (2.5-fold basal glucose concentration ± 15%) was achieved. At a minimum of 20 min from the dextrose bolus, another three arterial blood samples were collected during steady-state hyperglycemia in 5-min intervals. Due to catheter failures and loss of some fetuses, hyperglycemic clamp studies were performed on 11 controls and 11 MI-IUGR fetuses.

*Hindlimb Glucose Metabolic Flux*

A hyperinsulinemic-euglycemic clamp (**HEC**) was performed at dGA 123 to assess hindlimb-specific glucose metabolism under basal and insulin-stimulated conditions as previously described (Cadaret et al., 2019; Posont et al., 2021; Cadaret et al., 2022; Gibbs, 2023). Briefly, fetuses were infused with [$^{14}$C(U)-D-glucose (37.2 μCi/ml; PerkinElmer Life Sciences, Boston, MA) suspended in saline at 1 ml/h following a 1-ml bolus. After 40 min, basal arterial and venous blood samples were simultaneously collected in 5-min intervals (4 paired samples total). Hyperinsulinemia was then induced by a 2-ml bolus of insulin (250 mU/kg; HumulinR; Lilly, Indianapolis, IN) followed by a constant infusion at 4 mU/min/kg. Fetal euglycemia was concurrently maintained with a 33% dextrose infusion that was adjusted in response to arterial plasma glucose concentration measured every 5 to 10 min until fetal glycemic conditions were at steady state. Beginning at least 1 h after hyperinsulinemia/euglycemia was initiated, 4 additional sets of simultaneous arterial and venous blood samples were collected at 5-min intervals.

Hindlimb-specific glucose utilization and oxidation rates were estimated by the Fick Principle as previously described (Rozance et al., 2018a). Glucose utilization was estimated using the arteriovenous differences in glucose concentration from paired samples. Differences were normalized to hindlimb weight at necropsy. Glucose oxidation rates were determined using 3 technical replicates of whole blood from each arterial and venous sample. Blood from each sample was added to microcentrifuge tubes, each containing 2 M HCl and suspended inside a sealed 20-ml scintillation vial over a pool of 1 M NaOH. The HCl allowed $CO_2$ to be released from the blood and captured by the NaOH at the bottom of the scintillation vial. After 24-h incubation at room temperature, the centrifuge tube was removed and UltimaGold scintillation fluid (PerkinElmer Inc, Waltham, MA) was added to the scintillation vial. Concentrations of $^{14}CO_2$ captured from each sample were determined using a Beckman-Coulter 1900 TA LC counter (Beckman Coulter, Fullerton, CA). Glucose oxidation rates were estimated from the difference between venous and arterial $^{14}C$-specific activities. The amount of glucose oxidized in nmol was calculated by normalizing blood $^{14}C$ values to the $^{14}C$-specific activity of the infusate. The calculated amount of glucose oxidized was then normalized to the hindlimb weight determined at necropsy. Due to loss of catheters or fetuses, hindlimb glucose metabolism was measured in 10 controls and 11 MI-IUGR fetuses.

***Blood Component Analyses***

Concentrations of total white blood cells, lymphocytes, monocytes, granulocytes, red blood cells, hematocrit, hemoglobin, and platelets were determined from 125 µl of EDTA-treated whole blood via a HemaTrue Veterinary Hematology Analyzer (Heska,

Loveland, CO) using the manufacturer-recommended ovine software specifications, as previously described (Cadaret et al., 2019). Blood glucose, lactate, pH, partial pressure of $CO_2$ (**$pCO_2$**), partial pressure of $O_2$ (**$pO_2$**), $HCO_3^-$, base excess, oxyhemoglobin, carboxyhemoglobin, $Na^+$, $K^+$, $Cl^-$, and $Ca^{2+}$ were measured from 90 µl of filtered heparinized whole blood with an ABL90 FLEX blood gas analyzer (Radiometer, Brea, CA). Plasma was separated from EDTA-treated whole blood via centrifuge (14,000 × *g*, 5 min). Plasma insulin (Bovine Insulin; Alpco, Windham, NE), TNFα (Sheep TNFα ELISA; Fine Biotech, Ltd., Wuhan, China; CAT#ESH0025), IL-6 (Sheep High Sensitivity Interleukin-6 ELISA Kit; MyBioSource.com, San Diego, CA ;CAT#MBS9362722), and non-esterified fatty acids (**NEFA**; NEFA-HR(2); Fujifilm, Richard, VA) concentrations were determined in duplicate by commercial ELISA kits as previously described (Cadaret et al., 2019; Gibbs, 2023). Intra-assay coefficients of variance were less than 15% for insulin and less than 20% for all others. Inter-assay coefficients of variance were less than 15% for all assays.

***Ex Vivo Skeletal Muscle Glucose Metabolism***

At necropsy, the *flexor digitorum superficialis* (**FDS**) muscles were collected and used to assess *ex vivo* glucose metabolism as previously described (Cadaret et al., 2019; Posont et al., 2021; Cadaret et al., 2022; Gibbs, 2023). Briefly, muscles were split into longitudinal strips (33.4 ± 1.05 mg). Strips were pre-incubated for 1 h at 37.5°C and 5% $CO_2$ in Krebs-Henseleit Buffer (**KHB**; Sigma-Aldrich, St. Louis, MO) with 5 mM glucose (Sigma-Aldrich), 0.1% bovine serum albumin (**BSA**; Sigma-Aldrich) and either no additional stimulant (basal), 5 mU/ml insulin (HumulinR), or 10 ng/ml TNFα (Sigma-

Aldrich). Following pre-incubation, muscle strips were washed in glucose-free KHB with the respective additive for 20 min. To measure glucose oxidation, muscle strips were placed in sealed dual-well chambers and incubated in KHB media containing the respective additive and 5 mM [$^{14}$C-U]-D-glucose (0.25 µCi/mmol) that was gassed with 95% $O_2$ for 2 h. The adjacent well of each chamber contained 1 M NaOH (Sigma-Aldrich). After the incubation, chambers were cooled on ice and the wells containing KHB were injected with 2M HCl (Sigma-Aldrich) and allowed to incubate at 4°C for an additional 1 h. This allowed $^{14}CO_2$ to be released from the media and captured by the NaOH in the adjacent well. The NaOH was collected into a 20-ml scintillation vial and combined with UltimaGold. The $^{14}$C specific activity was determined using liquid scintillation, and $^{14}$C specific activity of the media used to calculate the $^{14}CO_2$ content. To measure glucose uptake, muscle strips were incubated in KHB media containing the respective additives and 1 mM [$^{3}$H]2-deoxyglucose (300 µCi/mmol) and 39 mM $^{14}$C-mannose (1.25 µCi/mmol) for 20 min. After incubation, muscle strips were cooled on ice, washed in cold PBS, placed in a 20-ml scintillation vial, and lysed in 2M NaOH. UltimaGold was then added to the scintillation vials and $^{3}$H specific activity was determined by liquid scintillation. The concentration of intracellular [$^{3}$H]2-deoxyglucose was estimated from the $^{3}$H specific activity of the media. The volume of extracellular fluid in the muscle lysate was calculated using the $^{14}$C specific activity. The contribution of the extracellular fluid to the $^{3}$H specific activity was subtracted from the total $^{3}$H specific activity to create a lysate total. *Ex vivo* glucose uptake and oxidation rates were normalized to incubation time and muscle strip mass.

***Akt Western Immunoblots***

Insulin-signaling responsiveness in FDS muscle was estimated from proportions of phosphorylated Akt to total Akt protein as previously described (Cadaret et al., 2022). In parallel with glucose uptake incubations, additional muscle strips were incubated in basal or insulin-spiked KHB media for 20 min at 37.5°C and 5% $CO_2$ and then snap frozen. These muscle strips were homogenized in muscle lysis buffer (**MLB**) comprised of 20 mM TRIS, 1 mM EDTA, 0.1% SDS, 1% Triton-X 100, and 10% glycerol and containing manufacturer-recommended concentrations of protease and phosphatase inhibitors (2.5%; ThermoFisher). Homogenates were sonicated for 30 sec and centrifuged (14,000 × *g*, 5 min, 4°C). Total protein concentrations were determined from the supernatant using a Pierce BCA Protein Assay Kit (ThermoFisher). Protein (35 µg) was combined with BioRad 4X Laemmli Sample Buffer to make a 1X solution, heated for 5 min at 95°C, and separated by SDS-PAGE. Gels were transferred to polyvinylidene fluoride low-fluorescent membranes (**PVDF**; BioRad Laboratories, Hercules, CA), incubated in Odyssey blocking buffer (LI-COR Biosciences, Lincoln, NE) for 1 h at room temperature, and washed with 1X TBS-T (20 mM Tris-HCl + 150 mM NaCl + 0.01% Tween 20). Membranes were then incubated with rabbit antiserum raised against Akt (1:1,000; Cell Signaling Technologies, Danvers, MA; CAT#9272) and $Ser^{473}$ phosphorylated Akt (1:2,000; Cell Signaling Technologies; CAT#4060) at 4°C overnight as previously described (Posont et al., 2021; Cadaret et al., 2022). Finally, membranes were incubated with goat anti-rabbit IR800 IgG secondary antiserum (1:10,000; LI-COR) at room temperature for 1 h, scanned with the Odyssey Infrared Imaging System, and analyzed with Image Studio Lite Software Ver 5.2 (LI-COR).

### *Ex Vivo Fatty Acid Mobilization*

Fatty acid mobilization was determined as previously described (Beard, 2020) using a protocol adapted from Raclot and Groscolas (1993). At necropsy, visceral adipose tissue (~15 g) was collected and immediately placed in modified Krebs Ringer buffer (15 mM $NaHCO_3$, 3.32 mM $CaCal_2$, and 4% fatty acid-free bovine serum albumin; Sigma-Aldrich) that had been warmed to 37°C. Tissue was minced with scissors and filtered to remove excess buffer, and 400 mg was transferred to a 50-ml conical tube containing 5 ml fresh buffer warmed to 37°C and spiked with 0 to 10 µM epinephrine (Sigma-Aldrich). Tubes were incubated for 2 h at 37°C in a shaking water bath. After incubation, the contents were filtered with a glass microfiber filter (VWR, West Chester, PA; CAT#28297-978). Filtrate was allocated into 1.5-ml Eppendorf tubes and stored at -80°C. The amount of fatty acid mobilized during the incubation period was estimated from the concentration in the buffer, which was determined using a commercial assay kit (Free Fatty Acid Quantification Kit, Sigma-Aldrich; CAT#MAK044-1KT).

### *Skeletal Muscle Glycogen Content*

Intramuscular glycogen content was quantified from snap-frozen *semitendinosus* muscle collected at necropsy as previously described (Yates et al., 2019; Gibbs, 2023). Briefly, 10 mg of muscle was homogenized in double-distilled water via sonification for 30 sec, heated at 95°C for 5 min, and centrifuged (14,000 × *g*, 5 min, 4°C). Glycogen content was quantified in duplicate from 50-µl aliquots of supernatant with a commercial

assay kit (Glycogen Assay Kit, Sigma-Aldrich; CAT#MAK016). Intra-assay coefficient of variance was less than 15%.

### *Skeletal Muscle Protein Expression*

Total protein was isolated from *semitendinosus* muscle that was snap-frozen in liquid nitrogen at necropsy and used to determine relative myosin heavy chain (**MyHC**) content as previously described (Yates et al., 2016; Gibbs, 2023). Briefly, muscle samples were homogenized via sonification (3 × 30 sec) in MLB containing manufacturer-recommended concentrations of protease and phosphatase inhibitors and then centrifuged (14,000 × *g*, 5 min, 4°C). Total protein concentration was quantified from the supernatant utilizing a Pierce BCA Assay Kit (ThermoFisher). To estimate MyHC proportions, 40 µg of protein was combined with Bio-Rad 4X Laemmli sample buffer to create a 1X sample, which was heated at 70°C for 10 min. Proteins were separated via electrophoresis, with an upper running buffer comprised of 100 mM Tris, 150 mM glycine, 0.1% SDS, and 0.07% β-mercaptoethanol in distilled water and a lower running buffer comprised of 50 mM Tris, 75 mM glycine, and 0.05% SDS in distilled water. Electrophoresis was performed at room temperature for 3 h at a constant voltage of 110 V. Gels were stained overnight with Gel-Code Blue (ThermoFisher) at room temperature, washed in double-distilled water, and imaged using an Odyssey infrared imaging system (LI-COR Biosciences). Quantification of bands for MyHC-1, MyHC-2a, and MyHC-2x was completed by densitometry (Image Studio Lite Ver 5.2; LI-COR) to estimate fiber type ratios.

For western immunoblots, snap-frozen *semitendinosus* samples collected at necropsy were extracted in MLB buffer containing manufacturer-recommended concentrations of protease and phosphatase inhibitors (ThermoFisher) as previously described (Yates et al., 2019; Cadaret et al., 2022; Gibbs, 2023). Homogenates were sonicated for 30 sec and centrifuged (14,000 × *g*, 5 min, 4°C). Total protein concentrations were determined from the supernatant using a Pierce BCA Protein Assay Kit (ThermoFisher). Protein aliquots (40 to 50 µg) were combined with BioRad 4X Laemmli Sample Buffer to make a 1X solution, heated for 5 min at 95°C, cooled to room temperature, and separated by SDS-PAGE as described above. Gels were transferred to PVDF or nitrocellulose membranes (BioRad Laboratories), incubated in Odyssey blocking buffer (LI-COR Biosciences) for 1 h at room temperature, and washed with 1X TBS-T (20 mM Tris-HCl + 150 mM NaCl + 0.01% Tween 20). Membranes were then incubated with rabbit antiserum raised against the β2 adrenoceptor (**Adrβ2**; 1:500; Cohesion Biosciences, London, UK; CAT#CPA3116), TNFα receptor 1 (**TNFR1**; 1:250; Cell Signaling Technologies; CAT#3736S), toll-like receptor 4 (**TLR4**; 1:500; ProteinTech, Rosemont, IL; CAT#19811-1-AP), or IL-6 receptor (**IL6R**; 1:1000; Abcam, Boston, MA; CAT#ab271042) at 4°C overnight as previously described (Posont et al., 2021; Cadaret et al., 2022). Membranes were then incubated with goat anti-rabbit IR800 IgG secondary antiserum (1:10,000; LI-COR; CAT#926-32211) at room temperature for 1 h, scanned with the Odyssey Infrared Imaging System, and analyzed with Image Studio Lite Software Ver 5.2 (LI-COR).

### *Statistical Analysis*

All data were analyzed by analysis of variance (**ANOVA**) using the mixed procedure of SAS 9.4 (SAS Institute, Cary, NC) to determine the effect of the experimental group, sex, and the number of fetuses/pregnancy. Interactions among these effects were not included in the model due to insufficient power. However, all sex and fetal number categories were represented in both groups. Fetus was considered the random variable. Fisher's LSD test was used for mean separation. Daily maternal and fetal blood samples were analyzed for the effects of the experimental group, day of sample, time of sample, and their interactions, as well as for sex and fetal number with repeated measures. Best-fit statistics were used to select appropriate covariance structures. Fetus was considered the experimental group. Data from *in vivo* metabolic studies and *ex vivo* metabolic studies were likewise analyzed using the mixed procedure, with study period and incubation condition as the respective repeated measures. For each period of the *in vivo* metabolic studies, the samples were averaged, and the mean is reported. Similarly, the technical reps/incubation condition in the *ex vivo* metabolic studies were averaged, and the mean is reported. Significance was reported at $P \leq 0.05$ and tendencies were declared at $P \leq 0.1$. All data are presented as the mean ± the standard error of the mean (**SEM**).

## Results

### *Daily Fetal Physiological Parameters and Maternofetal Gradients*

There was a group × draw time interaction observed ($P < 0.05$) for daily fetal $pCO_2$, but there were no interactions observed for any other fetal blood parameters or

maternofetal gradients. Regardless of day of gestational age or time of day, MI-IUGR fetuses had lower ($P < 0.05$) concentrations of white blood cells, lymphocytes, and red blood cells but greater ($P < 0.05$) granulocyte concentrations compared to controls **(Figure 3.1A-D)**. MI-IUGR fetuses also tended to have lower ($P < 0.1$) platelet concentrations than controls (**Figure 3.1E**). Monocytes, hematocrit, mean corpuscular volume (**MCV**), red cell distribution width (**RDWa**), hemoglobin, mean corpuscular hemoglobin concentration (**MCHC**), and mean platelet volume (**MPV**) did not differ between groups (**Table 3.1**). Regardless of day, MI-IUGR fetuses had lower ($P < 0.05$) $pCO_2$ than controls, however, the magnitude of this difference was more profound at 0800 than at 1400. MI-IUGR fetuses had greater ($P < 0.05$) blood lactate concentrations and methemoglobin but lower ($P < 0.05$) $HCO_3^-$, hematocrit, hemoglobin, oxyhemoglobin, carboxyhemoglobin, $K^+$, and $pO_2$ compared to control fetuses (**Figures 3.3 and 3.4**). Blood glucose, pH, base excess, $Na^+$, $Cl^-$, and $Ca^{2+}$ concentrations did not differ between groups (**Table 3.2**).

MI-IUGR pregnancies had smaller ($P < 0.05$) maternofetal gradients for blood glucose, but there was no difference in maternofetal glucose ratios compared to controls (**Figure 3.5**). MI-IUGR pregnancies had larger ($P < 0.05$) maternofetal gradients and ratios for lactate, $Na^+$, $Cl^-$, and $pO_2$ (**Figures 3.6, 3.7, 3.8, and 3.9**). MI-IUGR pregnancies also had larger ($P < 0.05$) maternofetal $K^+$ proportion, but similar maternofetal $K^+$ gradients (**Figure 3.10**). All other maternofetal gradients and ratios were similar between groups.

### *Fetal Inflammatory Tone*

MI-IUGR fetuses had greater ($P < 0.05$) circulating plasma TNFα and IL-6 compared to controls (**Figure 3.11**) as well as greater ($P \leq 0.05$) expression of TNFR1 and IL6R in *semitendinosus* muscle and a tendency ($P = 0.06$) for greater TLR4 expression (**Figure 3.12A-C).** β2 adrenoceptor protein content in *semitendinosus* did not differ between groups (**Figure 3.12D**).

### *In vivo Metabolic Studies*

#### *Fetal Glucose-Stimulated Insulin Secretion*

During the square-wave hyperglycemic clamp, there were group × period interactions observed ($P < 0.05$) for plasma insulin, blood carboxyhemoglobin, and blood $K^+$ but not for any other components. Plasma insulin concentrations during the basal period did not differ between groups but were less ($P < 0.05$) for MI-IUGR fetuses than for controls during hyperglycemia (**Figure 3.13**). Blood glucose did not differ between groups and was by design greater ($P < 0.05$) at hyperglycemia compared to basal (**Figure 3.14**). Lactate was also greater ($P < 0.05$) at hyperglycemia compared to basal, regardless of experimental group (**Figure 3.15**). Blood $pO_2$ was less ($P < 0.05$) for MI-IUGR fetuses than controls regardless of period (**Figure 3.16**). Blood $K^+$ was less ($P < 0.05$) for MI-IUGR fetuses than controls by 8.2% under basal conditions and by 6.8% at hyperglycemia (**Figure 3.17**). Carboxyhemoglobin was less ($P < 0.05$) for MI-IUGR fetuses than controls by 38% under basal conditions and by 35% at hyperglycemia (**Figure 3.18**). Regardless of period, MI-IUGR fetuses had lower ($P < 0.05$) blood concentrations of $HCO_3^-$, hemoglobin, and hematocrit compared to controls (**Table 3.3**).

Blood pH, $pCO_2$, oxyhemoglobin, methemoglobin, $Na^+$. $Cl^-$, and $Ca^{2+}$ did not differ between groups. Regardless of experimental group, blood pH, $pCO_2$, $HCO_3^-$, methemoglobin, and $Cl^-$ were less ($P < 0.05$) and hemoglobin, hematocrit, and oxyhemoglobin were greater ($P < 0.05$) under basal conditions compared to hyperglycemia, and blood $Na^+$ and $Ca^{2+}$ concentrations did not differ between periods (**Table 3.4**).

*Fetal Hindlimb Glucose Metabolism*

During the HEC, there was a group × period interaction observed ($P < 0.05$) for arterial glucose: insulin ratio and a tendency for an interaction observed ($P = 0.07$) for hindlimb glucose oxidation, but no interactions were observed for any other output. Hindlimb glucose uptake rates did not differ between groups and were greater ($P < 0.05$) at hyperinsulinemia compared to the basal period (**Figure 3.19**). Regardless of period, hindlimb glucose oxidation rates were reduced ($P < 0.05$) for MI-IUGR fetuses compared to control fetuses (**Figure 3.20**). By design, circulating plasma insulin was greater ($P < 0.05$) during hyperinsulinemia compared to the basal period, regardless of experimental group (**Figure 3.21**). Likewise, blood glucose was by design not different between groups or period (**Figure 3.22**). Glucose: insulin ratios were greater ($P < 0.05$) for MI-IUGR fetuses compared to controls at basal conditions but did not differ during hyperinsulinemia (**Figure 3.23**). Arterial blood lactate was greater ($P < 0.05$) at hyperinsulinemia compared to the basal period and tended to be less ($P = 0.06$) for MI-IUGR fetuses compared to controls (**Figure 3.24**). Blood $pO_2$ was less ($P < 0.05$) for MI-IUGR fetuses compared to controls, regardless of period, and was lower ($P < 0.05$) at

hyperinsulinemia compared to basal conditions, regardless of group (**Figure 3.25**). Venous blood glucose did not differ between groups and tended to be greater ($P = 0.08$) during hyperinsulinemia than the basal period (**Figure 3.26**). Venous blood lactate was reduced ($P = 0.05$) for MI-IUGR fetuses compared to controls and was greater ($P = 0.05$) during hyperinsulinemia compared to the basal period (**Figure 3.27**). Venous $pO_2$ was reduced ($P < 0.05$) for MI-IUGR fetuses compared to controls and was less ($P < 0.05$) at hyperinsulinemia than basal conditions (**Figure 3.28**).

Blood pH, $HCO_3^-$, oxyhemoglobin, and $K^+$ was reduced ($P < 0.05$) for MI-IUGR fetuses in both arterial and venous blood samples (**Table 3.5**). Carboxyhemoglobin was greater ($P < 0.05$) for MI-IUGR fetuses in arterial blood samples but not venous blood samples compared to controls. Methemoglobin was greater ($P < 0.05$) for MI-IUGR fetuses than controls in arterial and venous samples. Blood $pCO_2$, hemoglobin, hematocrit, $Na^+$, $Cl^-$, and $Ca^{2+}$ did not differ between groups in arterial or venous samples (**Table 3.5**). Regardless of group, blood $pCO_2$, methemoglobin, $Na^+$, $Cl^-$, and $Ca^{2+}$ were greater ($P < 0.05$) and pH, $HCO_3^-$, hemoglobin, and oxyhemoglobin were lower ($P < 0.05$) at hyperinsulinemia compared to basal conditions. Arterial hematocrit and venous carboxyhemoglobin were less ($P < 0.05$) at hyperinsulinemia (**Table 3.6**).

***Ex vivo Metabolic Studies***

There was a group × media interaction observed ($P < 0.05$) for fatty acid mobilization but not for any other *ex vivo* output. *Ex vivo* glucose uptake was reduced ($P < 0.05$) for primary muscle from MI-IUGR fetuses compared to controls, regardless of media (**Figure 3.29A**). Glucose uptake was greatest ($P < 0.05$) for muscle incubated in

insulin-treated media, lowest ($P < 0.05$) for muscle incubated in TNFα-treated media, and intermediate for muscle incubated in basal media, regardless of group (**Figure 3.29B**). *Ex vivo* glucose oxidation was reduced ($P < 0.05$) for muscle from MI-IUGR fetuses compared to controls, regardless of media (**Figure 3.30A**). Moreover, glucose oxidation was greatest ($P < 0.05$) for muscle incubated in insulin-treated media, least ($P < 0.05$) for muscle incubated in basal media, and intermediate for muscle incubated in TNFα-treated media, regardless of group (**Figure 3.30B**). Phospho-Akt/total Akt protein content was less ($P < 0.05$) for muscle from MI-IUGR fetuses compared to controls, regardless of media, and was increased ($P < 0.05$) for muscle incubated in insulin-treated media compared to basal media (**Figure 3.32A** and **B**). Fatty acid mobilization was less ($P < 0.05$) for adipose tissue from MI-IUGR fetuses than controls by 30% in basal media, by 52% in media containing 100 mM epinephrine, and by 42% in media containing 1 µM epinephrine (**Figure 3.33**). Fatty acid mobilization did not differ between groups when incubated in media containing 10 µM epinephrine.

***Skeletal Muscle Metabolic Phenotype***

Proportional content of MyHC-1, MyHC-2a, and MyHC-2x in fetal *semitendinosus* muscles was similar across experimental groups (**Figure 3.34**). However, glycogen content of the *semitendinosus* tended to be greater ($P = 0.06$) in MI-IUGR fetuses compared to controls (**Figure 3.35**).

**Discussion**

In this study, we showed that sustained maternofetal inflammation occurring during the early 2nd trimester of pregnancy resulted in the subsequent impairment of fetal glucose metabolism and metabolic homeostasis in late gestation. The disruption in glucose metabolism was in large part skeletal muscle-specific, as MI-IUGR fetuses exhibited a 27% reduction in hindlimb glucose oxidation, which was independent of glucose uptake and was recapitulated in primary muscle incubations. Deficient glucose oxidation was compounded by poor responsiveness of muscle to insulin, as MI-IUGR hindlimb glucose oxidation was normal under resting insulinemic conditions. The 32.5% greater basal glucose: insulin ratios further indicate insulin resistance in MI-IUGR fetuses, as does the diminished phospho-activation of the insulin signaling hub, Akt, in MI-IUGR primary muscle. However, defects in insulin responsiveness were not solely responsible for poor metabolism, as glucose uptake and oxidation rates in primary muscle from MI-IUGR fetuses were comparably impaired whether incubated under basal, insulin-stimulated, or TNFα-stimulated conditions. Additionally, MI-IUGR fetuses exhibited poor β cell function that reduced the circulating insulin available to drive glucose clearance, as glucose-stimulated insulin secretion was reduced 23% in MI-IUGR fetuses. Mechanistically, MI-IUGR fetuses showed strong evidence of increased inflammatory tone that persisted long after experimental maternofetal inflammation had subsided, which helps to explain many of the observed metabolic deficits. The sustained systemic fetal inflammation was comparable to that previously observed in ovine fetuses where sustained maternofetal inflammation had been induced early in the 3rd trimester (Cadaret et al., 2019). We postulate that in both studies, fetal inflammation near term was

due in part to placental stunting and placental-mediated inflammation, as LPS bacterial endotoxins and maternal cytokines are typically unable to permeate the ovine placenta (Aaltonen et al., 2005; Gomez-Lopez et al., 2018). Although MI-IUGR fetuses were not hypoglycemic, their moderate hypoxemia and larger maternofetal gradients for $O_2$, lactate, $Na^+$, $K^+$, and $Cl^-$ were consistent with placental deficiency (Rozance et al., 2018a; Yates et al., 2018; Caitlin N. Cadaret et al., 2019). Together, these findings demonstrate that maternofetal inflammation induced early in the 2$^{nd}$ trimester by serial LPS injections resulted in the same hallmark fetal metabolic phenotype observed in IUGR human pregnancies and in other IUGR animal models (Limesand et al., 2007; Brown et al., 2015; Cadaret et al., 2019). The persistently-heightened fetal inflammatory tone exhibited by these fetuses illustrates the underlying inflammation that occurs during placental insufficiency-induced IUGR and provides a potential mechanistic target for treating or preventing IUGR-related metabolic deficits.

Pancreatic islet dysfunction in near-term MI-IUGR fetuses following maternofetal inflammation at mid-gestation was characterized by impaired insulin stimulus-secretion coupling. This deficit resulted in normal circulating insulin concentrations under resting glycemic conditions but marked impairment of the normal spike in circulating insulin when fetuses were made hyperglycemic. Previous studies found that pancreas from severely IUGR fetal sheep had smaller islets (Rozance et al., 2015; Brown et al., 2016) with fewer β cells (Limesand et al., 2005; Brown et al., 2016) and poorer insulin secretion (Limesand et al., 2006; Boehmer et al., 2017). Additionally, IUGR fetal pancreatic islets had impaired glucose oxidative capacity, which directly mediated less glucose-stimulated insulin secretion (Limesand et al., 2006; Hicks and Yates, 2021).

Hypoxemia impairs β cell function both directly and by increasing circulating catecholamines that inhibit glucose-stimulated insulin secretion through α2 adrenergic signaling pathways (Yates et al., 2012; Macko et al., 2016; Boehmer et al., 2017). Likewise, hypoxemia can chronically increase circulating inflammatory cytokines, which are also detrimental to pancreatic islets (Hicks and Yates, 2021). Culture studies show that TNFα reduces β cell glucose oxidation, glucose-stimulated insulin secretion, and insulin sensitivity (Youd et al., 2000; Li and Reid, 2001; Oleson et al., 2015). Thus, the combination of hypoxemia and the consequent increase in adrenergic and inflammatory tone likely resulted in the reduction of pancreatic function in MI-IUGR fetuses. When maternal hyperthermia was used to induce placental insufficiency and fetal IUGR (**PI-IUGR**), fetuses exhibited reductions in both basal and glucose-stimulated insulin secretion during late gestation (Limesand et al., 2006; Limesand et al., 2013; Boehmer et al., 2017). Fetal hypoxemia and inflammation appear to be common pathologies between PI-IUGR and MI-IUGR fetuses (Yates et al., 2012; Macko et al., 2016; Boehmer et al., 2017; Cadaret et al., 2019; Hicks and Yates, 2021; Posont et al., 2022). However, PI-IUGR fetuses also experience chronic hypoglycemia (Limesand et al., 2013), which was not present in MI-IUGR fetuses in our present or previous study (Cadaret et al., 2019). Because basal glucose concentrations were reduced by as much as 50% in PI-IUGR fetuses, basal insulin concentrations also fell in response (Limesand et al., 2006; Limesand et al., 2013). Additionally, hypoglycemia in PI-IUGR fetuses can also increase adrenal cortisol and norepinephrine secretion, which would further inhibit glucose-stimulated insulin secretion (Morrison, 2008; Yates et al., 2012; Macko et al., 2016).

MI-IUGR fetal sheep exhibited a hallmark reduction in skeletal muscle glucose oxidation that was consistent with thrifty metabolic fetal programming. When normalized to the weight of the fetal hindlimb, which is about 40% skeletal muscle (Hicks et al., 2021), reduced glucose oxidation rates in MI-IUGR fetuses occurred independently of hindlimb glucose uptake rates. Thus, MI-IUGR fetal muscle appeared to have lost about ¼ of its capacity for glucose oxidation despite normal utilization rates and normal glucose availability in circulation. Rather, the reduction in glucose oxidation could have been precipitated by reduced $O_2$ availability, as MI-IUGR fetuses consistently had 12 to 16% less blood $O_2$ than normal. Evidence indicates that hypoxemic fetuses readily reappropriate $O_2$ from skeletal muscle in favor of more vital brain, heart, and endocrine tissues (Yates et al., 2012; Jones et al., 2019). Thus, less glucose utilized by MI-IUGR fetal muscle undergoes oxidative metabolism and is instead redirected to one of two likely fates: anaerobic glycolytic metabolism or storage as glycogen. Glucose undergoing anaerobic glycolytic metabolism will ultimately be converted into lactate (Rogatzki et al., 2015), and indeed circulating lactate was increased by ~14% in our MI-IUGR fetuses. Previous studies in IUGR fetal sheep found increased hepatic glucose production, which utilizes muscle-derived lactate through the Cori cycle (Limesand et al., 2007). This allows the fetus to utilize the lactate produced from glycolytic glucose metabolism to produce more glucose, as glucose itself cannot be secreted by muscle (Limesand et al., 2007; Thorn et al., 2009). This also prevents the IUGR fetus from experiencing dangerous hyperlactatemia (Limesand et al., 2007; Yates et al., 2012). Glucose that is taken up by skeletal muscle but not immediately utilized for metabolism is converted into glycogen for storage (Blanco and Blanco, 2017). In addition to increased apparent lactate

production, our MI-IUGR fetal *semitendinosus* muscles exhibited about 63% grater glycogen content.

In primary muscle experiments, glucose uptake and oxidation rates were reduced in MI-IUGR skeletal muscle regardless of the inclusion of insulin or TNFα in incubation media. This illustrates that MI-IUGR skeletal muscle has inherent metabolic deficits that are not necessarily dependent upon stimulation. This may be due in part to impaired signaling pathways for insulin and other growth factors, as inflammatory cytokines can interfere with IRS-PI3K-Akt pathways independent of their degree of ligand-driven activation (Wei et al., 2008). Indeed, the ratio of phospho-activated Akt in MI-IUGR fetal muscle was reduced comparably when incubated at basal and high insulin concentrations. Furthermore, inclusion of inflammatory cytokines in incubations did not further reduce glucose uptake or oxidation in MI-IUGR muscle, which we postulate reflects an already dampened glucose metabolism due to enriched inflammatory signaling that is not further inhibited by greater presence of inflammatory cytokines. This is similar to recent findings in IUGR fetal myoblast function (Posont et al., 2022) and further indicates that targeting enhanced inflammatory pathways in MI-IUGR fetuses could improve deleterious metabolic outcomes. Interestingly, a reduction in glucose uptake was observed in MI-IUGR skeletal muscle in culture that was not seen *in vivo*, perhaps because the hindlimb is comprised of adipose tissue and connective tissues in addition to skeletal muscle (Hicks et al., 2021). Local regulation of hindlimb glucose utilization by products secreted from these other tissues, particularly adipocytes, may have masked muscle-specific deficits in glucose uptake capacity (Gastaldelli et al., 2017). Indeed, IUGR-born animals

ultimately develop increased adiposity (Posont and Yates, 2019; Gibbs, 2023), which illustrates a lack of programmed growth restriction for fat tissues (Sarr et al., 2012).

The loss of glucose oxidation capacity occurred without changes in skeletal muscle metabolic phenotype, as myosin heavy chain ratios indicated no changes in fiber type composition. Although this differs from previous observations of aberrant fiber type ratios in PI-IUGR fetuses (Yates et al., 2016), normal fiber type ratios have been reported for MI-IUGR fetal rats (Cadaret et al., 2019a) and sheep (Cadaret et al., 2019) following maternofetal inflammation in late gestation. It is important to remember that fiber type is determined by the content of oxidative enzymes, which does not necessarily reflect the enzymes' functional rates (Schiaffino and Reggiani, 2011).s Nevertheless, cytokines have been shown to reduce glucose oxidative metabolism and increase anaerobic glycolysis and glycogen synthesis (Boscá and Corredor, 1984; Rhoades et al., 2005; Al-Khalili et al., 2006; Remels et al., 2015; C N Cadaret et al., 2017; Hicks and Yates, 2021).

Fetal growth restriction observed in this study appeared to be the result of placental stunting, as MI-IUGR fetuses were hypoxemic and had larger maternofetal gradients for $O_2$ and other blood components. In fact, the maternofetal gradients observed for these MI-IUGR fetuses were reasonably similar to those recently observed for PI-IUGR fetal sheep (Beer, 2022). One noteworthy exception was the maternofetal gradient for glucose, which was greater for PI-IUGR pregnancies in the previous study but was actually smaller for our MI-IUGR pregnancies. This unexpected observation was not consistent with gradients for $O_2$ and other indicators of placental insufficiency, but it does help to explain why MI-IUGR fetuses were normoglycemic. Glucose is transported across the placenta by glucose transporters (**GLUT**) (Stanirowski et al., 2018), and

different stressors may reduce placental GLUT expression to differing magnitudes (Sandovici et al., 2012).

In addition to systemic inflammation, MI-IUGR fetuses exhibited evidence of enriched inflammatory sensitivity in muscle tissue, as protein content for TNFR1, IL6R, and TLR4 were elevated in the *semitendinosus*. Importantly, elevated circulating cytokines and skeletal muscle signaling components were observed well after the experimental maternofetal inflammation had been lifted. The greater fetal inflammatory tone was unlikely to have been derived from placental transfer of maternal cytokines or LPS endotoxin, as neither readily cross the ovine placenta (Zaretsky et al., 2004; Aaltonen et al., 2005; Gomez-Lopez et al., 2018). However, it is almost certain that LPS exposure would have stimulated cytokine production by the placenta, which may have been released into fetal circulation. Previous studies of pregnant mice and primary placental extravillous trophoblast cells from humans found that administration of LPS increased placental production of inflammatory cytokines (Anton et al., 2012; Fricke et al., 2018). Additionally, human placental tissues exposed to hypoxia *in vitro* released more inflammatory cytokines (Baker et al., 2021). Most likely, however, fetal cytokine production itself was increased as a result of the stressful intrauterine conditions brought on by placental stunting. Regardless of the model, IUGR fetuses experience a hypoxemic state, which is a powerful stimulant of whole-body and tissue-specific inflammatory responses (Hartmann et al., 2000; Dong et al., 2009; Eltzschig and Carmeliet, 2011; Watts and Walmsley, 2019). Activation of hypoxia-inducible factors (**HIF**) cause them to bind to hypoxia response promoter elements (**HRE**), which promote the transcription of genes involved in inflammation such as cytokines and nuclear factor κB (**NF-κB;**

Eltzschig and Carmeliet, 2011). As a result, fetal plasma TNFα and IL-6 were increased by 29% and 49%, respectively, in our MI-IUGR fetuses. Moreover, TNFR1 and IL6R content in MI-IUGR fetal skeletal muscle was increased by 2.40-fold and 1.51-fold, respectively. The combined increases in circulating cytokines and tissue receptor content create an enhanced inflammatory tone in the IUGR fetus. Furthermore, MI-IUGR fetuses had increased circulating white blood cells and platelets, but decreased red blood cells. During the formation of blood cells (hematopoiesis), common myeloid progenitor cells give rise to granulocytes, macrophages, megakaryocytes (i.e., cells that produce platelets), and erythrocytes in regulated proportions (Akashi et al., 2000). Extracellular signals from myriad different pathways, including TNFα/NF-κB and interferons/JAK-STAT dictate differentiation into the different blood cell types (Dzierzak and Bigas, 2018). Exact mechanisms that drive differentiation into each of these cell types has not fully been elucidated, but several studies have identified inflammatory cytokines as factors in the production and differentiation of myeloid progenitor cells (Hume and MacDonald, 2012; Maltby et al., 2014; Behrens and Alexander, 2018; Su et al., 2020). We postulate that increased differentiation of these progenitor cells into white blood cells results in less erythrocytes in response to increased inflammatory status.

Experimental induction of maternofetal inflammation at mid-gestation produced similar indicators of fetal inflammation near term as previously observed when maternofetal inflammation was induced later in gestation, as maternofetal inflammation in the 3$^{rd}$ trimester elevated white blood cells, monocytes, granulocytes, and circulating TNFα (Cadaret et al., 2019). However, inflammatory tone begins to shift postnatal, as granulocytes, monocytes, and platelets were elevated in MI-IUGR neonatal lambs but

circulating TNFα was reduced by 50% (Posont et al., 2021). This shift was likely a compensatory response to the high prenatal cytokine exposure demonstrated in the present study. Importantly, however, TNFR1 protein content was still elevated in MI-IUGR neonatal skeletal muscle, which is evidence that enhanced cytokine sensitivity is programmed in IUGR muscle (Posont et al., 2021). Our study corroborates this by demonstrating that increased fetal inflammatory tone persisted months after LPS injections were discontinued.

From this study, we conclude that maternofetal inflammation during the critical window for peak placental development results in fetal inflammation throughout the rest of gestation. Moreover, these findings show that the enhanced skeletal muscle inflammatory sensitivity previously observed in IUGR-born neonates develops before birth as a developmental programming response to fetal conditions and not as a postnatal compensatory response. Furthermore, placental insufficiency and the resulting fetal hypoxemia appeared to be a primary impetus for fetal inflammation, although other sources cannot be completely ruled out. Regardless, this study provides substantial evidence that fetal inflammation could be a promising prenatal target to prevent inflammatory programming and improve metabolic outcomes of IUGR.

**Tables and Figures**

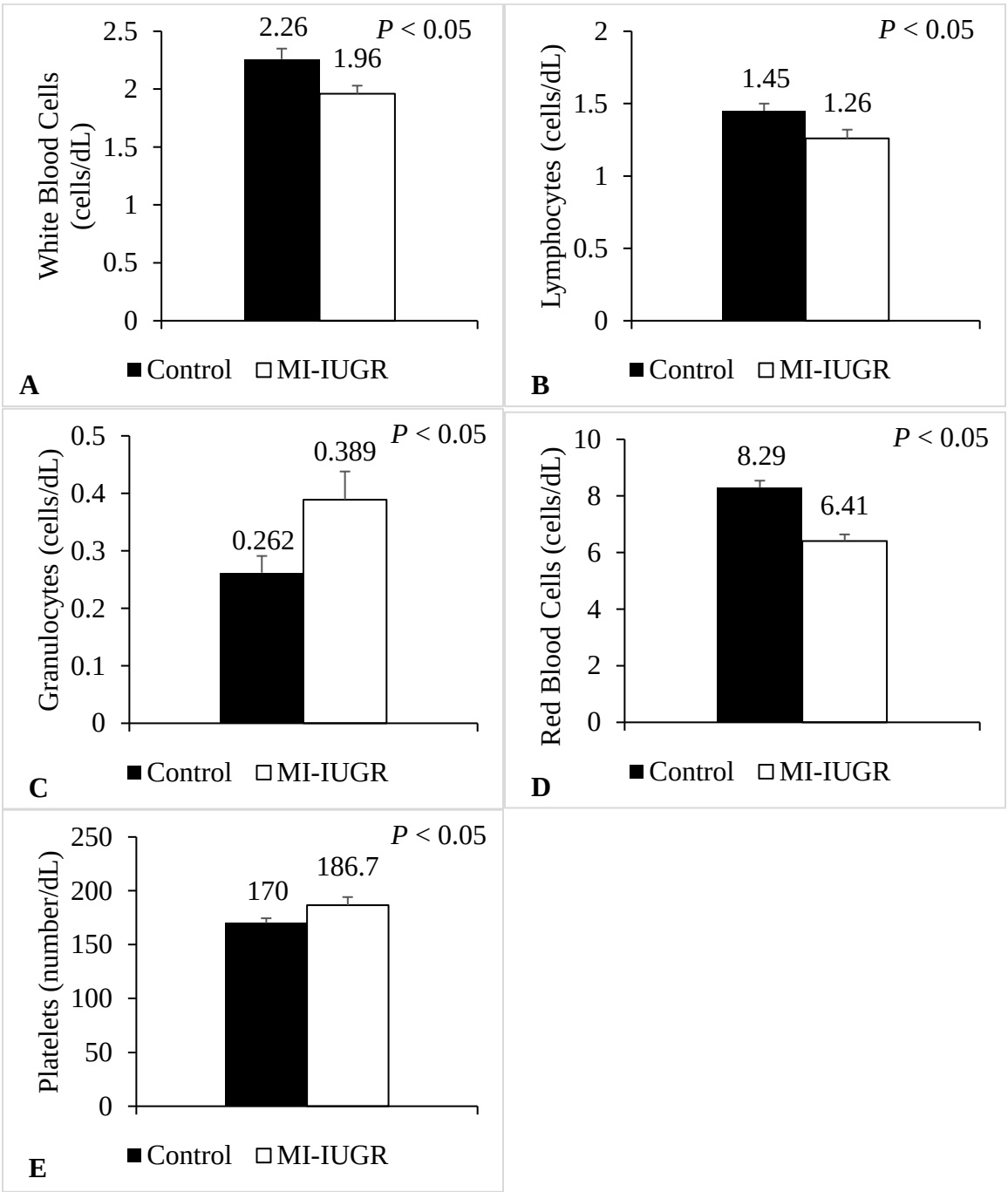


**Figure 3.1** Daily **(A)** white blood cell, **(B)** lymphocyte, **(C)** granulocyte, **(D)** red blood cell, and **(E)** platelet concentration in arterial blood collected from control (n=12) or MI-IUGR fetuses (n=13) from 120dGA to 125 dGA. There was no interaction between group and day ($P > 0.05$).

**Table 3.1** Daily fetal arterial complete blood cell counts for control and MI-IUGR fetuses from 120 dGA to 125 dGA.

| | Control (n=12) | MI-IUGR (n=13) | *P*-value |
|---|---|---|---|
| Monocytes | 0.205 ± 0.009 | 0.205 ± 0.011 | NS |
| Hematocrit | 28.7 ± 0.7 | 27.3 ± 0.9 | NS |
| MCV | 46.93 ± 0.33 | 47.82 ± 0.48 | NS |
| RDWa | 31.9 ± 0.4 | 31.2 ± 0.5 | NS |
| Hemoglobin | 9.66 ± 0.21 | 9.19 ± 0.29 | NS |
| MCHC | 33.9 ± 0.1 | 33.8 ± 0.2 | NS |
| MPV | 5.43 ± 0.04 | 5.48 ± 0.03 | NS |

NS = not significant ($P > 0.05$)

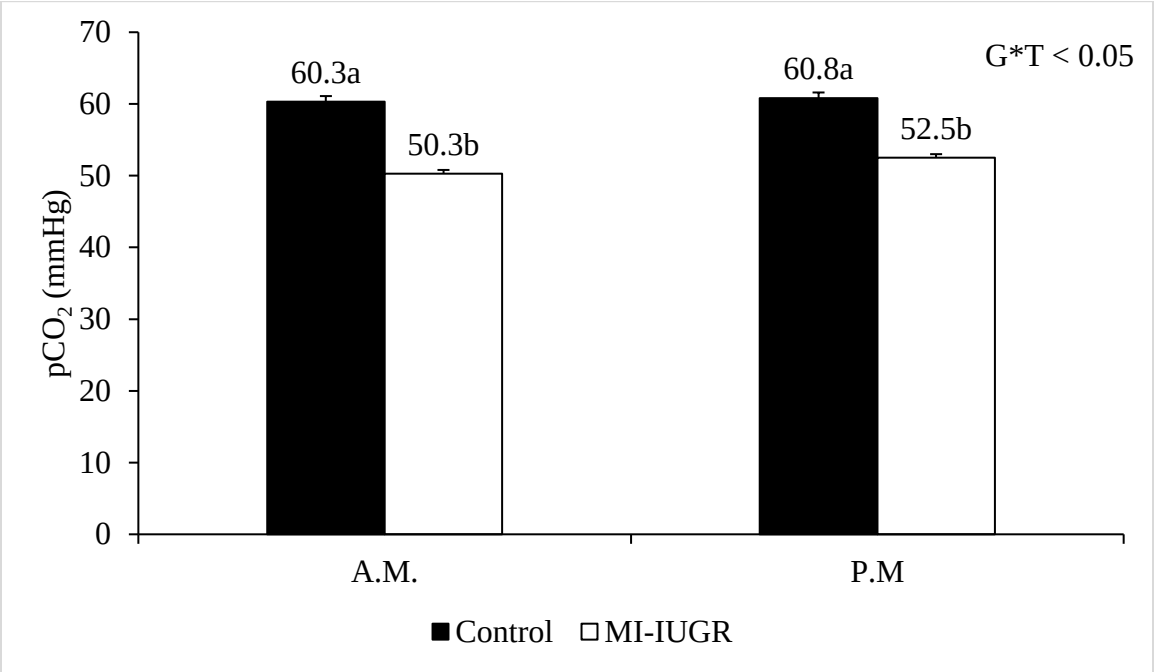


**Figure 3.2** Daily partial pressure of carbon dioxide in arterial blood collected from control (n=12) or MI-IUGR fetuses (n=13) from 120 dGA to 125 dGA at 0800 (A.M.) and 1400 (P.M.). There was a significant interaction between group and time of draw (G*T $P < 0.05$).

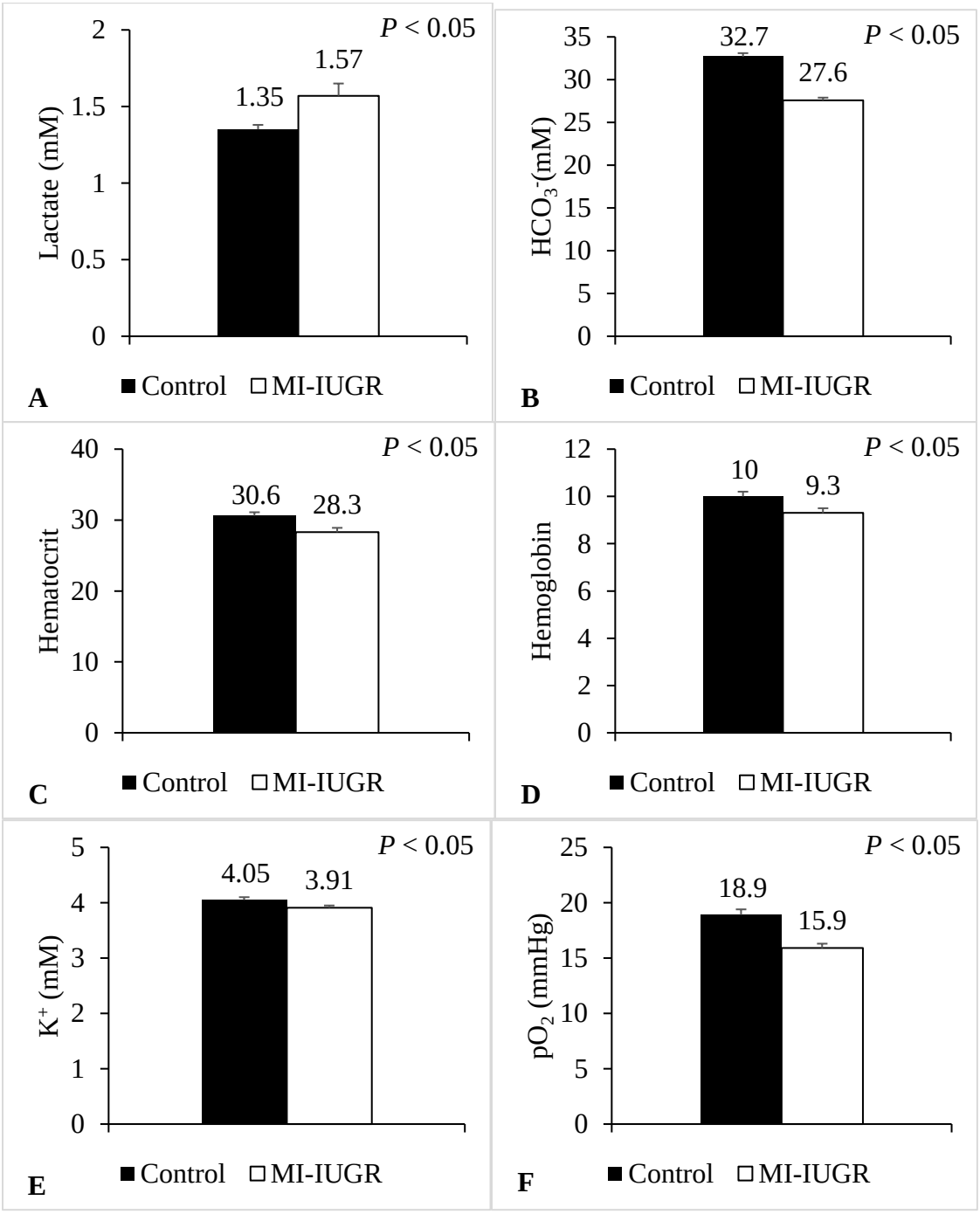


**Figure 3.3** Daily **(A)** lactate, **(B)** bicarbonate, **(C)** hematocrit, **(D)** hemoglobin, **(E)** potassium ion, and **(F)** partial pressure $O_2$ in arterial blood collected from control (n=12) or MI-IUGR fetuses (n=13) from 120dGA to 125 dGA. There was no interaction between group and day ($P > 0.05$).

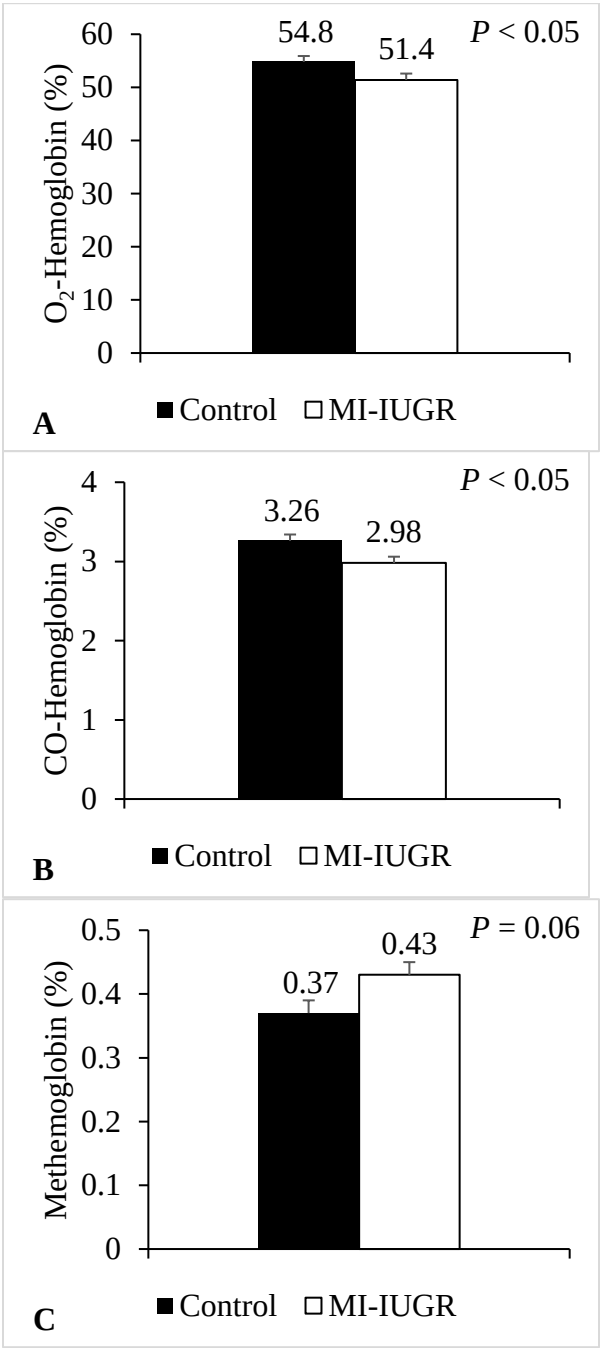


**Figure 3.4** Daily percentages of **(A)** oxyhemoglobin **(B)** carboxyhemoglobin and **(C)** methemoglobin in arterial blood collected from control (n=12) or MI-IUGR fetuses (n=13) from 120dGA to 125 dGA. There was no interaction between group and day ($P > 0.05$).

**Table 3.2** Daily blood gas and metabolite values in control or MI-IUGR fetuses from 120 dGA to 125 dGA

| | Control (n=12) | MI-IUGR (n=13) | *P*-value |
|---|---|---|---|
| Glucose | 1.00 ± 0.03 | 0.95 ± 0.02 | NS |
| pH | 7.365 ± 0.002 | 7.360 ± 0.005 | NS |
| Base Excreted | 3.1 ± 0.3 | 3.1 ± 0.3 | NS |
| $Na^+$ | 148.4 ± 0.8 | 149.2 ± 0.7 | NS |
| $Cl^-$ | 110.4 ± 0.8 | 111.1 ± 0.7 | NS |
| $Ca^{2+}$ | 1.384 ± 0.009 | 1.372 ± 0.012 | NS |

NS = not significant ($P > 0.05$)

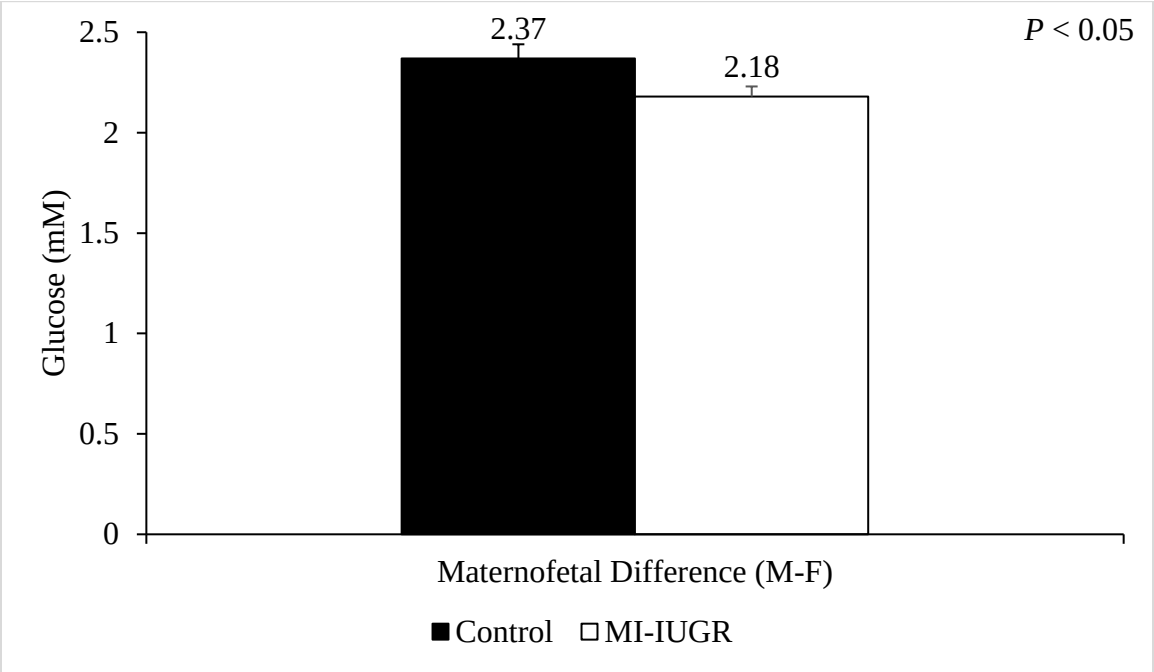


**Figure 3.5** Difference ($P < 0.05$) between blood glucose concentration in maternal venous blood and fetal arterial blood collected from control (n=12) or MI-IUGR fetuses (n=13) from 120dGA to 125 dGA. There was not a significant interaction between group and time of draw ($P > 0.05$).

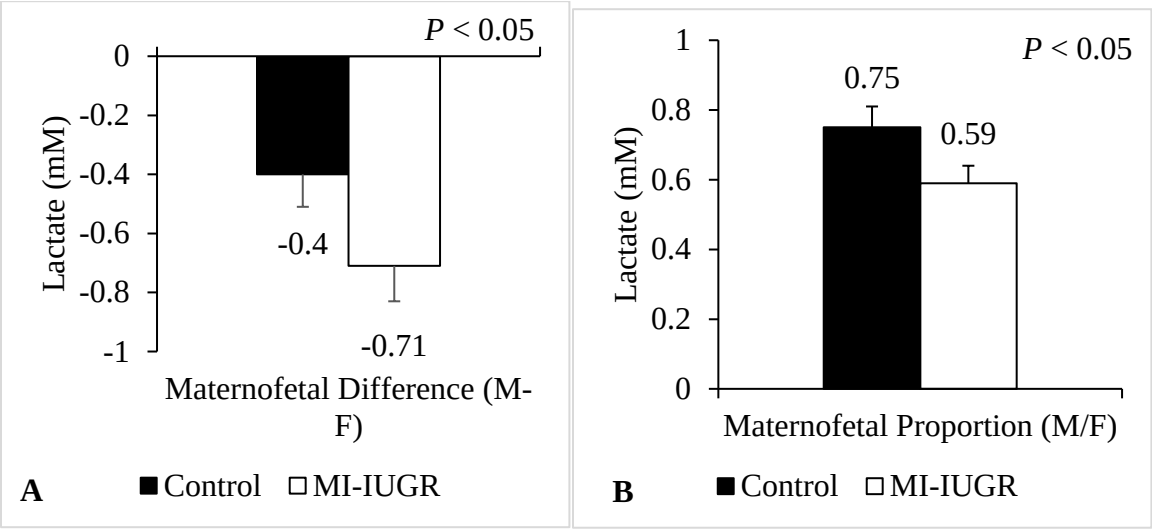


**Figure 3.6** (**A**) Difference ($P < 0.05$) between blood lactate concentration in maternal venous and fetal arterial blood and (**B**) proportion *(*$P < 0.05$) of blood lactate in maternal venous and fetal arterial blood collected from control (n=12) or MI-IUGR fetuses (n=13) from 120dGA to 125 dGA. There was not a significant interaction between group and time of draw ($P > 0.05$).

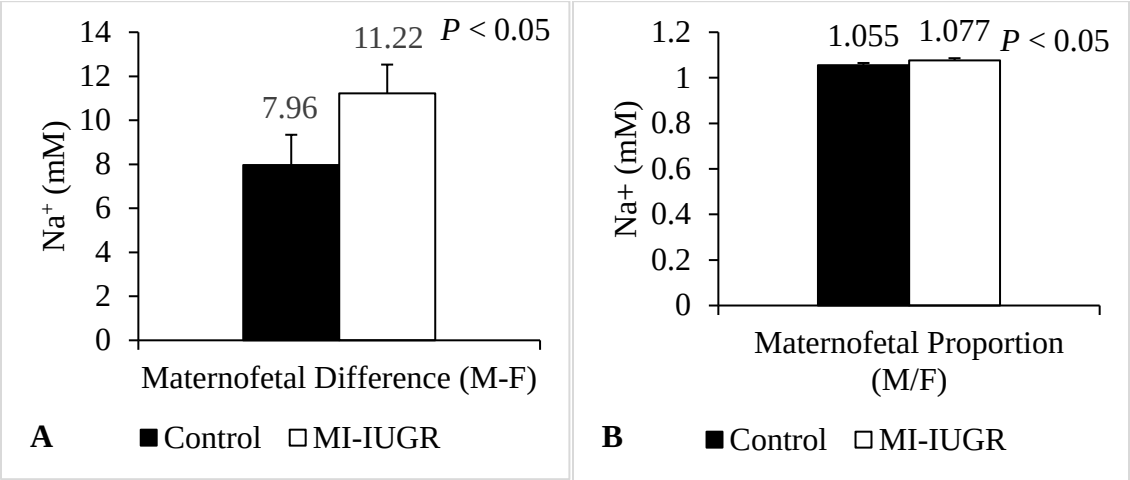


**Figure 3.7** (**A**) Difference ($P < 0.05$) between sodium ion concentration in maternal venous and fetal arterial blood and (**B**) proportion ($P < 0.05$) of sodium ions in maternal venous and fetal arterial blood collected from control (n=12) or MI-IUGR fetuses (n=13) from 120dGA to 125 dGA. There was not a significant interaction between group and time of draw ($P > 0.05$).

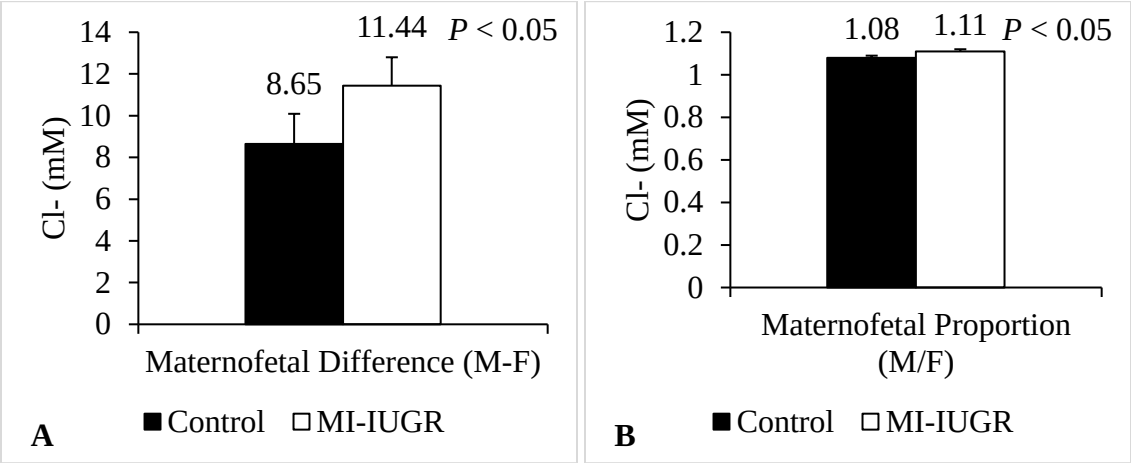


**Figure 3.8** (**A**) Difference ($P < 0.05$) between chloride ion concentration in maternal venous and fetal arterial blood and (**B**) proportion ($P < 0.05$) of chloride ions in maternal venous and fetal arterial blood collected from control (n=12) or MI-IUGR fetuses (n=13) from 120dGA to 125 dGA. There was not a significant interaction between group and time of draw ($P > 0.05$).

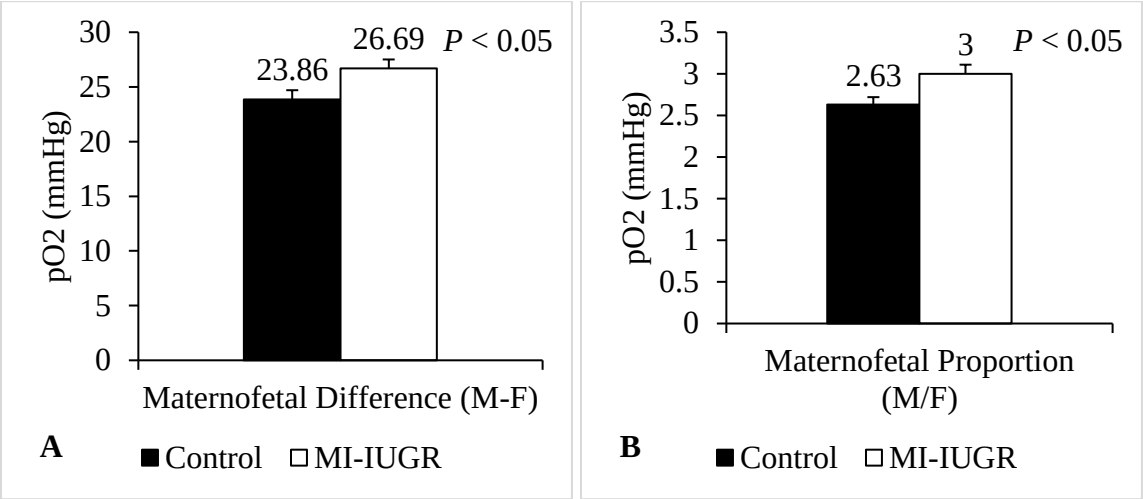


**Figure 3.9** (**A**) Difference ($P < 0.05$) between partial pressure of oxygen in maternal venous and fetal arterial blood and (**B**) proportion ($P < 0.05$) of oxygen in maternal venous and fetal arterial blood collected from control (n=12) or MI-IUGR fetuses (n=13) from 120dGA to 125 dGA. There was not a significant interaction between group and time of draw ($P > 0.05$).

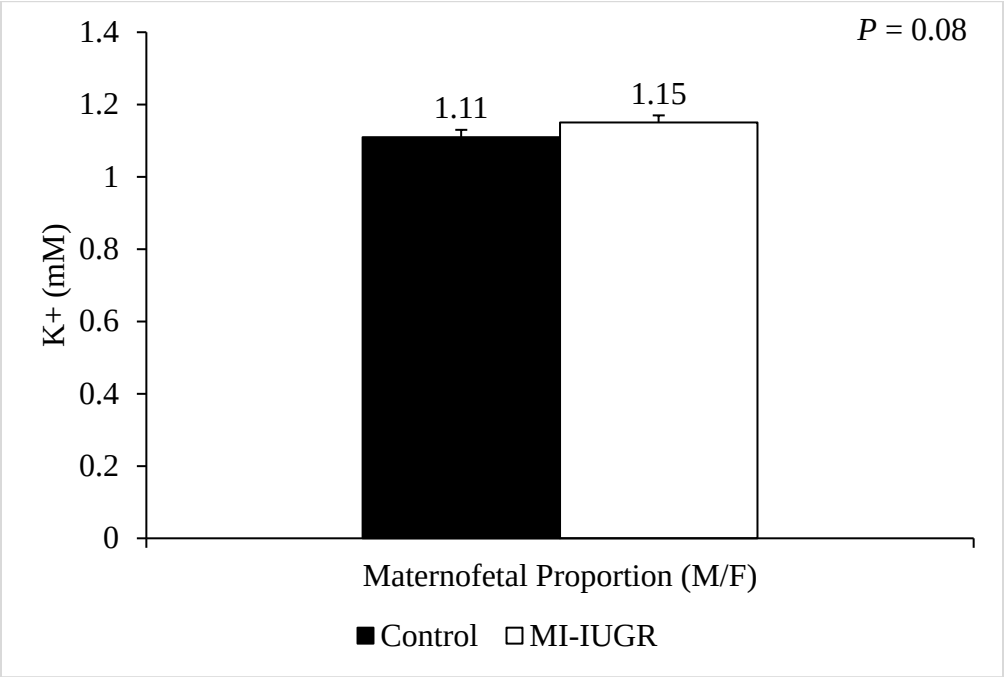


**Figure 3.10** The proportion of potassium ions present in maternal venous blood and glucose concentrations in arterial blood collected from control (n=12) or MI-IUGR fetuses (n=13) from 120dGA to 125 dGA. There was not a significant interaction between group and time of draw ($P > 0.05$).

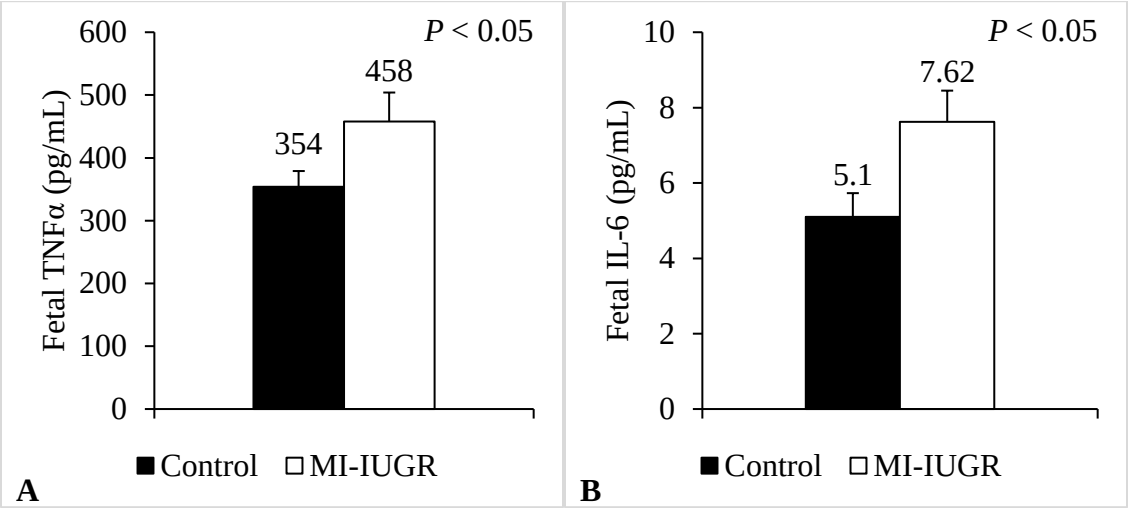


**Figure 3.11** Fetal plasma (**A)** TNFα and **(B)** IL-6 concentrations assessed from 120 dGA to 125 dGA in control (n=11) and MI-IUGR (n=13) fetuses. There was no significant interaction between group and day ($P > 0.05$).

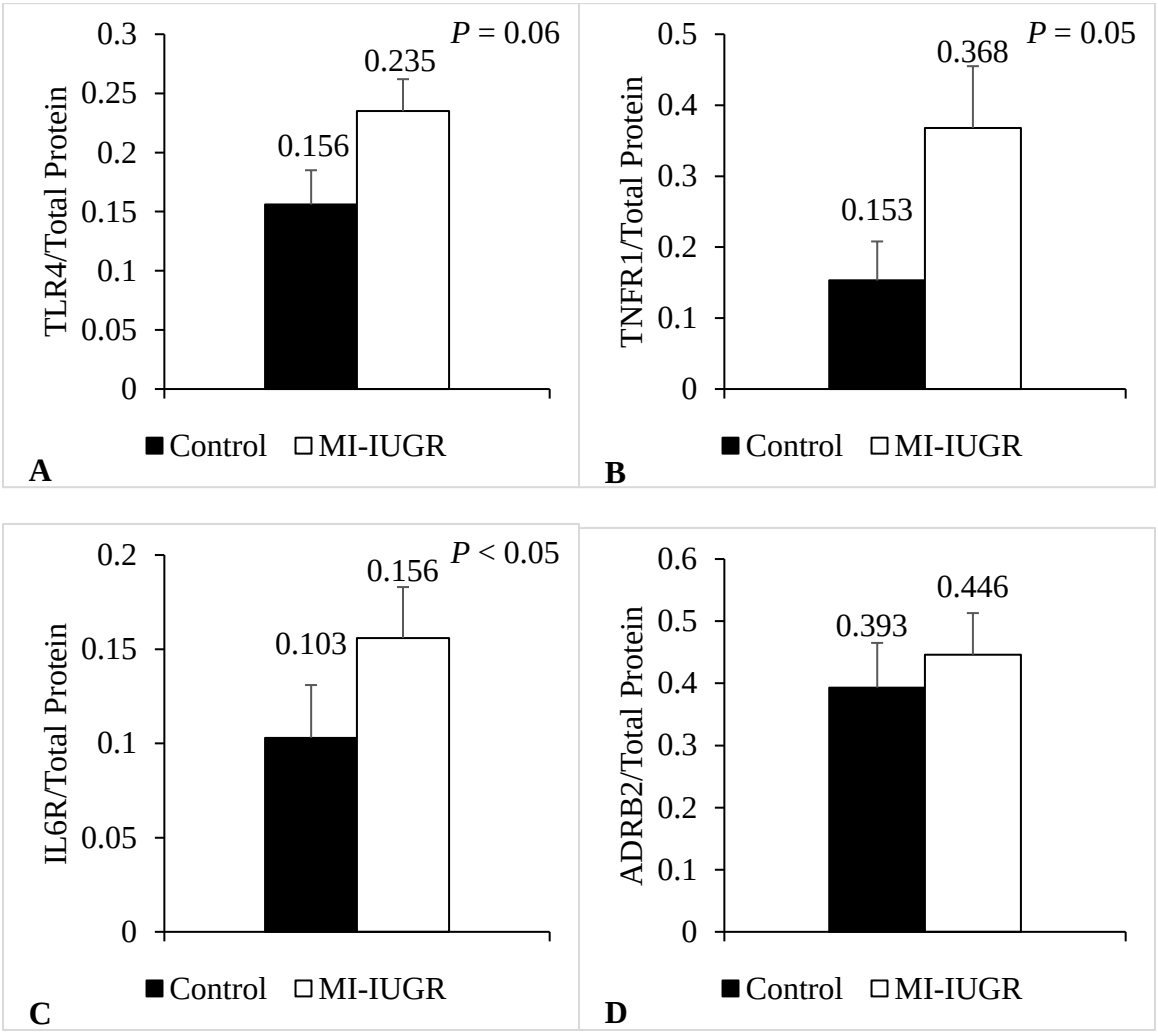


**Figure 3.12** The protein levels of **(A)** toll-like receptor 4 (TLR4), **(B)** tumor necrosis factor receptor 1 (TNFR1), **(C)** interleukin-6 receptor (IL6R), and **(D)** adrenergic receptor β2 (ADRB2),) in the semitendinosus muscle of control (n=11) or MI-IUGR (n=11) fetuses at 125 dGA.

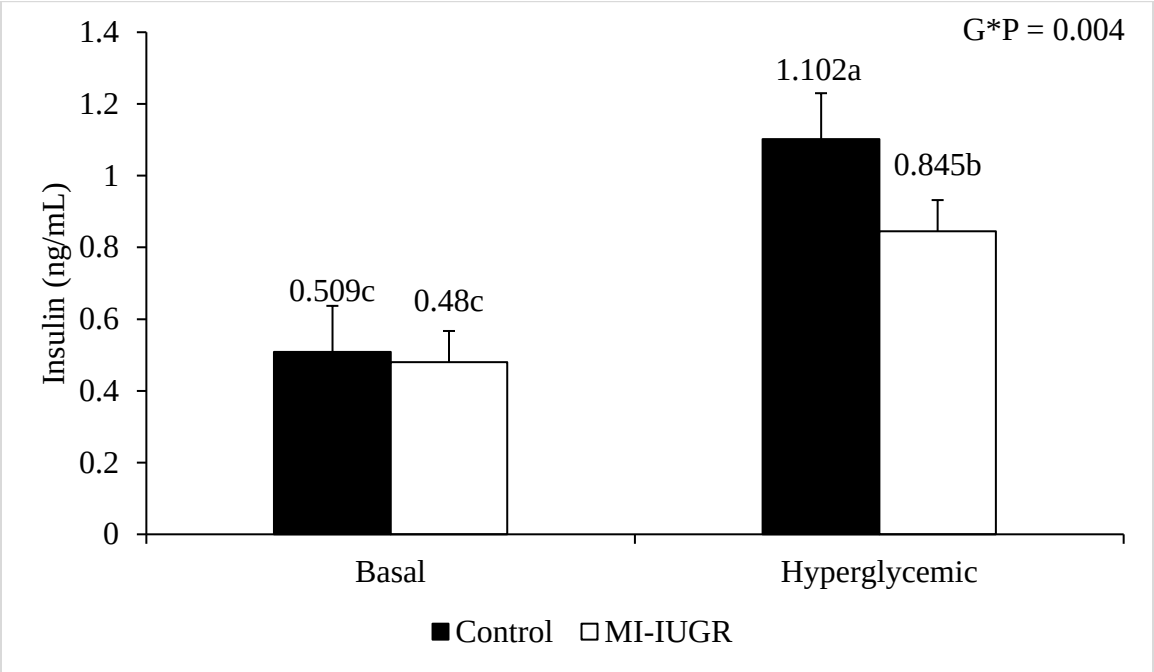


**Figure 3.13** The circulating arterial plasma insulin concentration of control (n=11) or MI-IUGR fetuses (n=11) in response to basal or hyperglycemic conditions (PER) during the fetal glucose-stimulated insulin secretion study completed at 122 dGA.

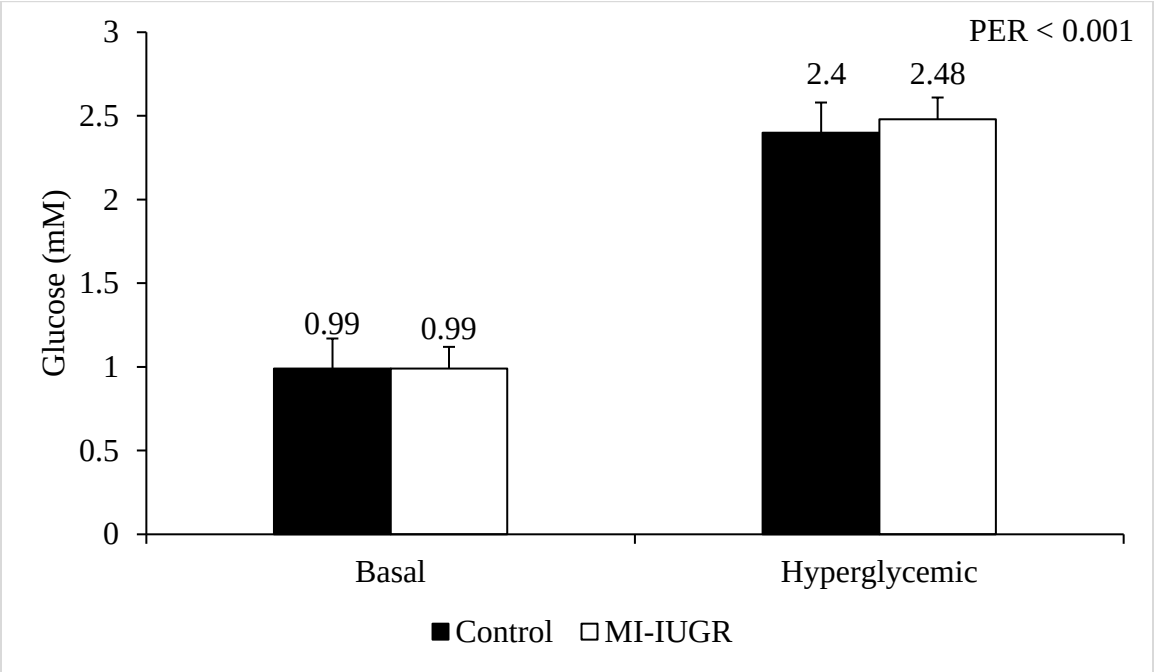


**Figure 3.14** The arterial blood glucose concentration of control (n=11) or MI-IUGR fetuses (n=11) in response to basal or hyperglycemic conditions (PER) during the fetal glucose-stimulated insulin secretion study completed at 122 dGA.

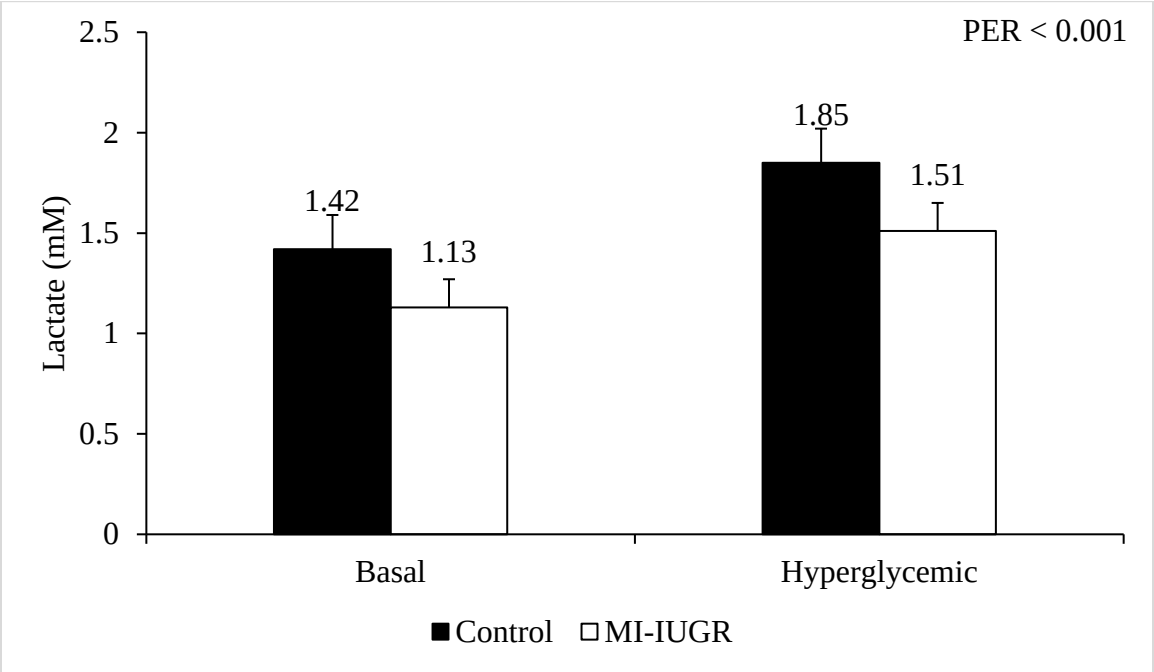


**Figure 3.15** The arterial blood lactate concentration of control (n=11) or MI-IUGR fetuses (n=11) in response to basal or hyperglycemic conditions (PER) during the fetal glucose-stimulated insulin secretion study completed at 122 dGA.

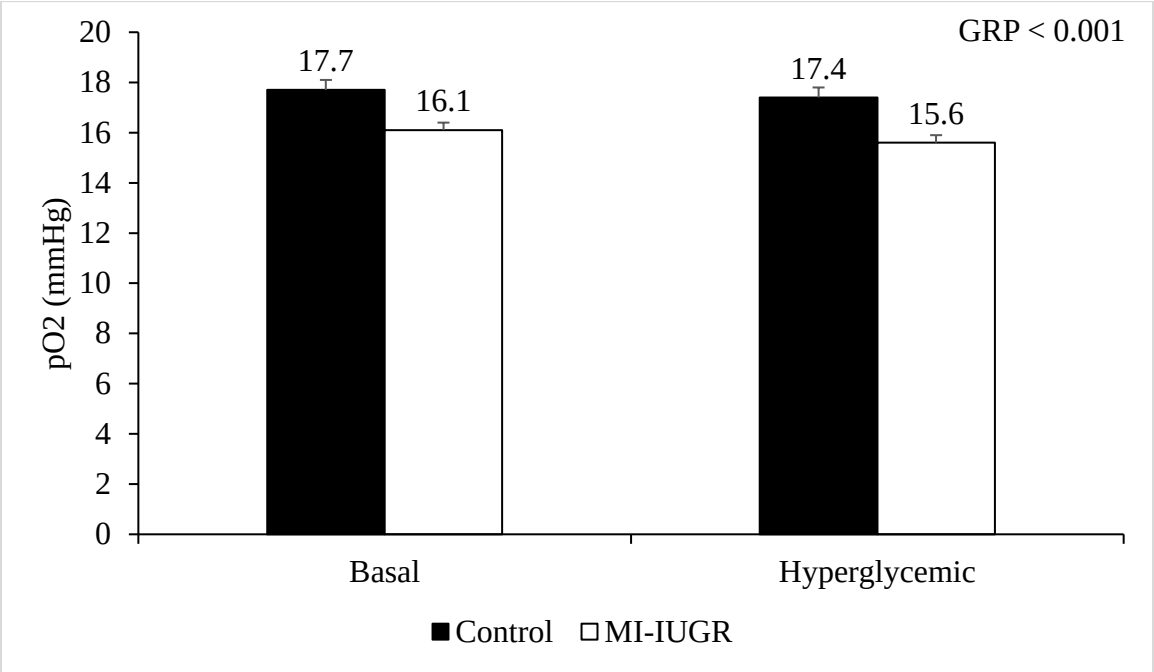


**Figure 3.16** The arterial oxygen partial pressure of control (n=11) or MI-IUGR fetuses (n=11) in response to basal or hyperglycemic conditions (PER) during the fetal glucose-stimulated insulin secretion study completed at 122 dGA.

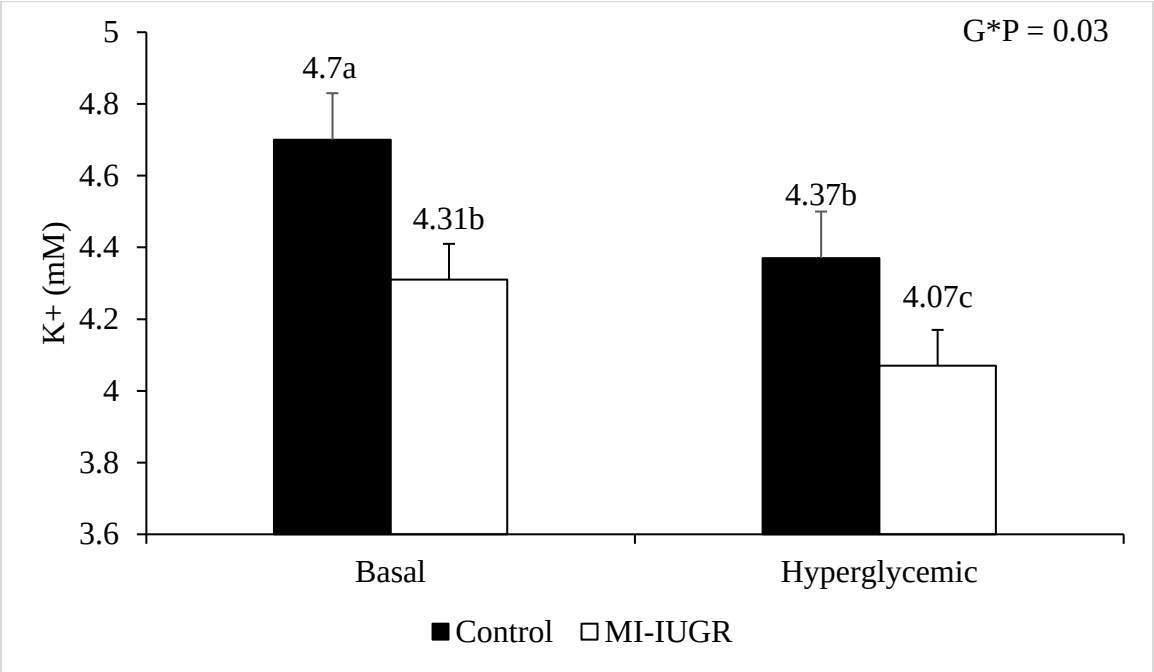


**Figure 3.17** The arterial potassium ion concentration of control (n=11) or MI-IUGR fetuses (n=11) in response to basal or hyperglycemic conditions (PER) during the fetal glucose-stimulated insulin secretion study completed at 122 dGA.

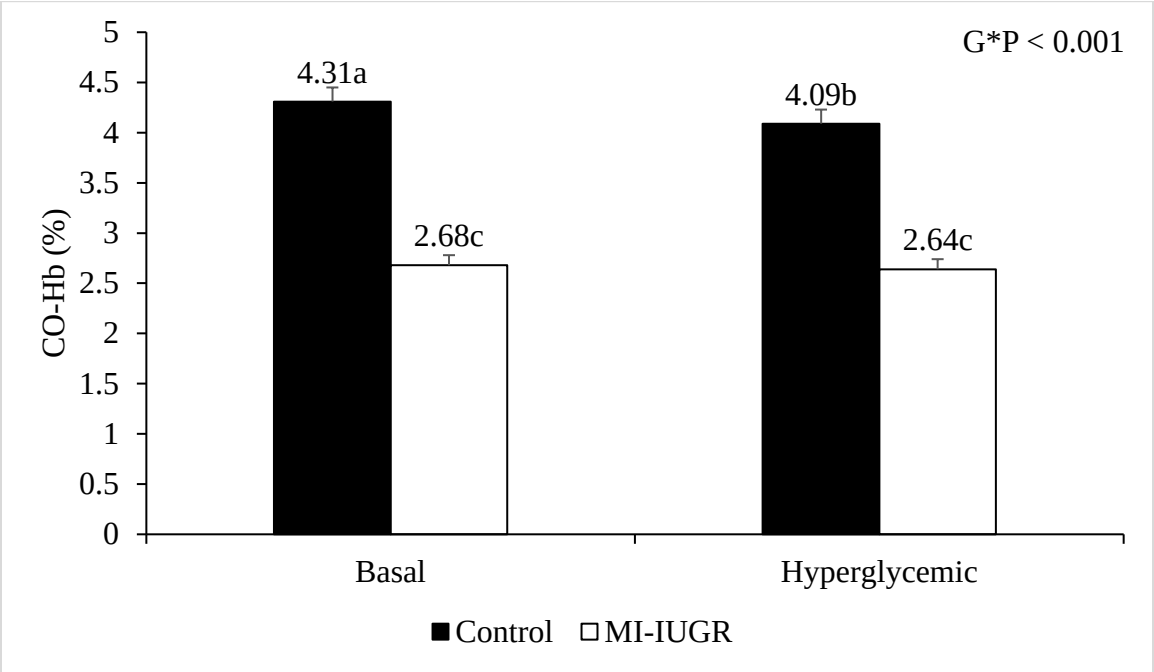


**Figure 3.18** The arterial percentage of carbon monoxide-bound hemoglobin of control (n=11) or MI-IUGR fetuses (n=11) in response to basal or hyperglycemic conditions (PER) during the fetal glucose-stimulated insulin secretion study completed at 122 dGA.

**Table 3.3** Arterial blood gas and metabolite concentrations of control and MI-IUGR fetuses during the glucose-stimulated insulin secretion studies.

| | Control (n=11) | MI-IUGR (n=11) | *P*-value |
|---|---|---|---|
| pH | 7.357 ± 0.009 | 7.356 ± 0.004 | NS |
| $pCO_2$ | 49.00 ± 0.70 | 49.65 ± 0.39 | NS |
| $HCO_3^-$ | 27.73 ± 0.53 | 26.26 ± 0.33 | 0.03 |
| Hemoglobin | 11.30 ± 0.32 | 9.01 ± 0.52 | <0.001 |
| Hematocrit | 34.98 ± 0.97 | 27.10 ± 1.72 | <0.001 |
| $O_2$-Hb | 61.47 ± 2.14 | 60.78 ± 2.26 | NS |
| MetHb | 0.42 ± 0.03 | 0.31 ± 0.06 | NS |
| $Na^+$ | 138.4 ± 0.84 | 137.87 ± 0.52 | NS |
| $Cl^-$ | 101.73 ± 0.77 | 100.33 ± 0.89 | NS |
| $Ca^{2+}$ | 1.52 ± 0.02 | 1.53 ± 0.02 | NS |

NS = not significant ($P > 0.05$)

**Table 3.4** Arterial blood gas and metabolite concentrations of control and MI-IUGR fetuses during the glucose-stimulated insulin secretion studies at either basal or hyperglycemic conditions.

| | Basal | Hyperglycemic | *P*-value |
|---|---|---|---|
| pH | 7.373 ± 0.005 | 7.340 ± 0.005 | <0.001 |
| $pCO_2$ | 48.31 ± 0.43 | 50.34 ± 0.40 | <0.001 |
| $HCO_3^-$ | 27.38 ± 0.31 | 26.61 ± 0.31 | <0.001 |
| Hemoglobin | 10.28 ± 0.31 | 10.03 ± 0.30 | <0.001 |
| Hematocrit | 31.42 ± 1.00 | 30.67 ± 0.98 | <0.001 |
| $O_2$-Hb | 62.45 ± 1.46 | 59.79 ± 1.72 | <0.001 |
| MetHb | 0.33 ± 0.03 | 0.40 ± 0.04 | 0.01 |
| $Na^+$ | 138.03 ± 0.50 | 138.25 ± 0.56 | NS |
| $Cl^-$ | 100.38 ± 0.63 | 101.68 ± 0.59 | 0.001 |
| $Ca^{2+}$ | 1.52 ± 0.01 | 1.53 ± 0.01 | NS |

NS = not significant ($P > 0.05$)

**Table 3.5.** Arterial and venous blood gas concentrations of control and MI-IUGR fetuses during the hyperinsulinemic-euglycemic clamp study.

| | **Arterial** | | | **Venous** | | |
|---|---|---|---|---|---|---|
| | Control (n=10) | MI-IUGR (n=11) | *P*-value | Control (n=10) | MI-IUGR (n=11) | *P*-value |
| pH | 7.365±0.002 | 7.359 ± 0.002 | 0.02 | 7.336±0.002 | 7.329±0.002 | 0.03 |
| $pCO_2$ | 50.4±0.3 | 50.6±0.2 | NS | 55.0±0.3 | 55.3±0.3 | NS |
| $HCO_3^-$ | 28.37±0.20 | 27.81±0.07 | 0.01 | 28.9±0.2 | 28.3±0.1 | 0.01 |
| Hemoglobin | 8.99±0.22 | 8.88±0.05 | NS | 9.00±0.22 | 8.94±0.05 | NS |
| Hematocrit | 27.56±0.68 | 27.25±0.15 | NS | 28.02±0.50 | 28.81±2.37 | NS |
| $O_2$-Hb | 50.13±1.08 | 46.77±0.69 | 0.01 | 32.88±0.92 | 29.29±0.71 | 0.006 |
| CO-Hb | 3.35±0.05 | 3.53±0.07 | 0.05 | 2.92±0.05 | 2.88±0.06 | NS |
| MetHb | 0.584±0.026 | 0.739±0.024 | <0.001 | 0.803±0.020 | 0.933±0.024 | <0.001 |
| $Na^+$ | 147.8±0.5 | 147.2±0.6 | NS | 152.4±0.8 | 150.8±0.7 | NS |
| K+ | 3.60±0.04 | 3.43±0.03 | 0.005 | 3.56±0.04 | 3.41±0.03 | 0.009 |
| $Cl^-$ | 109.5±0.7 | 109.2±0.4 | NS | 112.4±0.8 | 112.0±0.7 | NS |
| $Ca^{2+}$ | 1.425±0.006 | 1.422±0.009 | NS | 1.385±0.008 | 1.396±0.009 | NS |

NS = not significant ($P > 0.05$)

**Table 3.6**. Arterial and venous blood gas concentrations of control and MI-IUGR fetuses at either basal or hyperinsulinemic-euglycemic conditions during the hyperinsulinemic-euglycemic clamp study.

| | **Arterial** | | | **Venous** | | |
|---|---|---|---|---|---|---|
| | Basal | HEC | *P*-value | Basal | HEC | *P*-value |
| pH | 7.376±0.002 | 7.348±0.002 | <0.001 | 7.348±0.002 | 7.317±0.002 | <0.001 |
| $pCO_2$ | 49.6±0.2 | 51.4±0.2 | <0.001 | 54.0±0.3 | 56.3±0.3 | <0.001 |
| $HCO_3^-$ | 28.46±0.15 | 27.71±0.15 | 0.001 | 29.0±0.1 | 28.2±0.1 | <0.001 |
| Hemoglobin | 9.21±0.16 | 8.66±0.16 | 0.02 | 9.25±0.16 | 8.70±0.16 | 0.02 |
| Hematocrit | 28.23±0.49 | 26.58±0.49 | 0.02 | 30.34±1.71 | 26.49±1.71 | NS |
| $O_2$-Hb | 51.37±0.89 | 45.52±0.89 | <0.001 | 34.56±0.8 | 27.61±0.8 | <0.001 |
| CO-Hb | 3.46±0.06 | 3.41±0.06 | NS | 3.02±0.06 | 2.78±0.06 | 0.005 |
| MetHb | 0.596±0.025 | 0.728±0.025 | <0.001 | 0.804±0.022 | 0.931±0.022 | <0.001 |
| $Na^+$ | 146.7±0.6 | 148.4±0.6 | 0.04 | 150.1±0.7 | 153.1±0.7 | 0.007 |
| K+ | 3.94±0.04 | 3.08±0.04 | <0.001 | 3.92±0.04 | 3.05±0.04 | <0.001 |
| $Cl^-$ | 108.4±0.6 | 110.3±0.6 | 0.03 | 110.6±0.7 | 113.8±0.7 | 0.004 |
| $Ca^{2+}$ | 1.397±0.008 | 1.451±0.008 | <0.001 | 1.370±0.009 | 1.411±0.009 | 0.002 |

NS = not significant ($P > 0.05$)

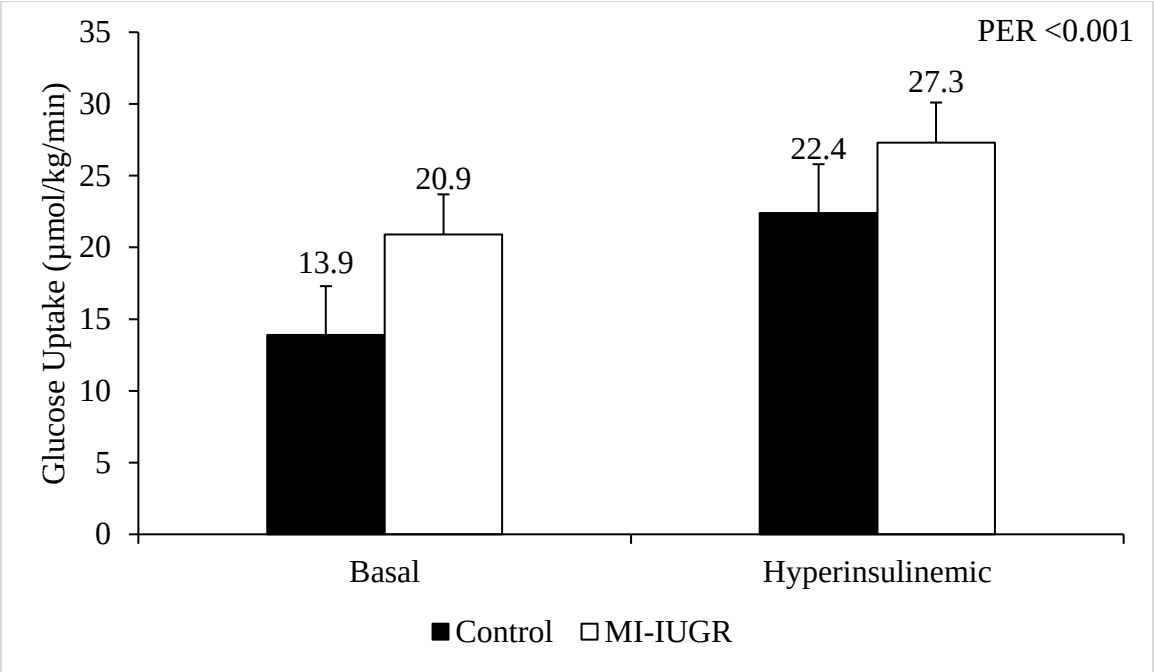


**Figure 3.19** Hindlimb specific glucose uptake of control (n=10) or MI-IUGR fetuses (n=11) in response to basal or hyperinsulinemic conditions.

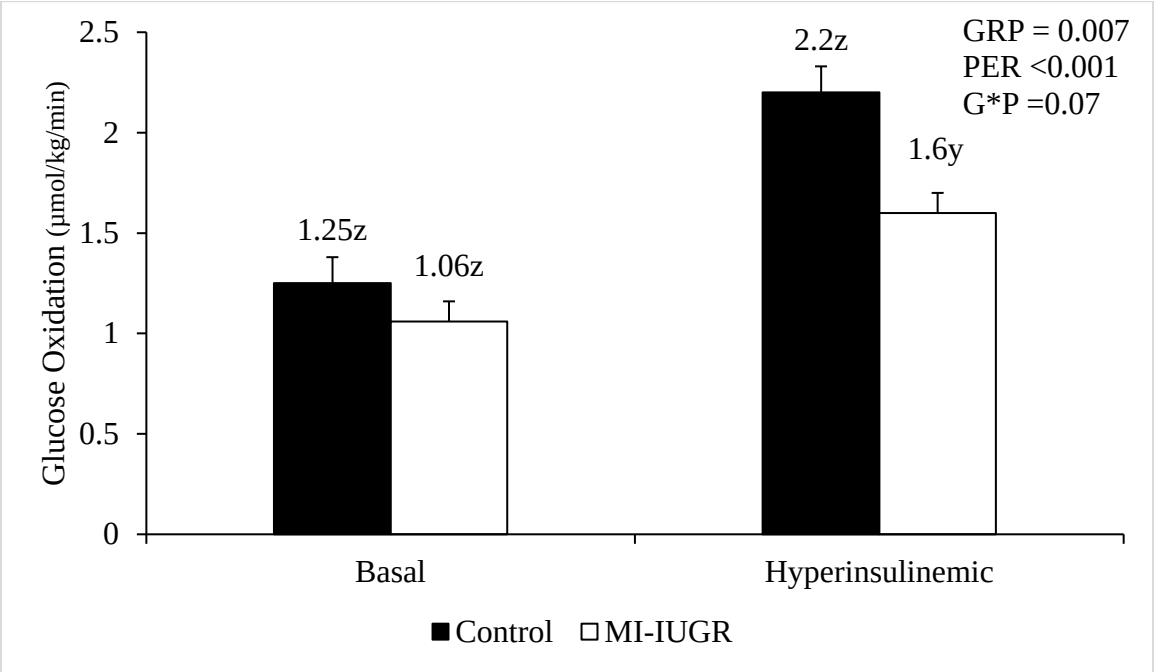


**Figure 3.20** Hindlimb specific glucose oxidation of control (n=10) or MI-IUGR fetuses (n=11; GRP) in response to basal or hyperinsulinemic conditions (PER).

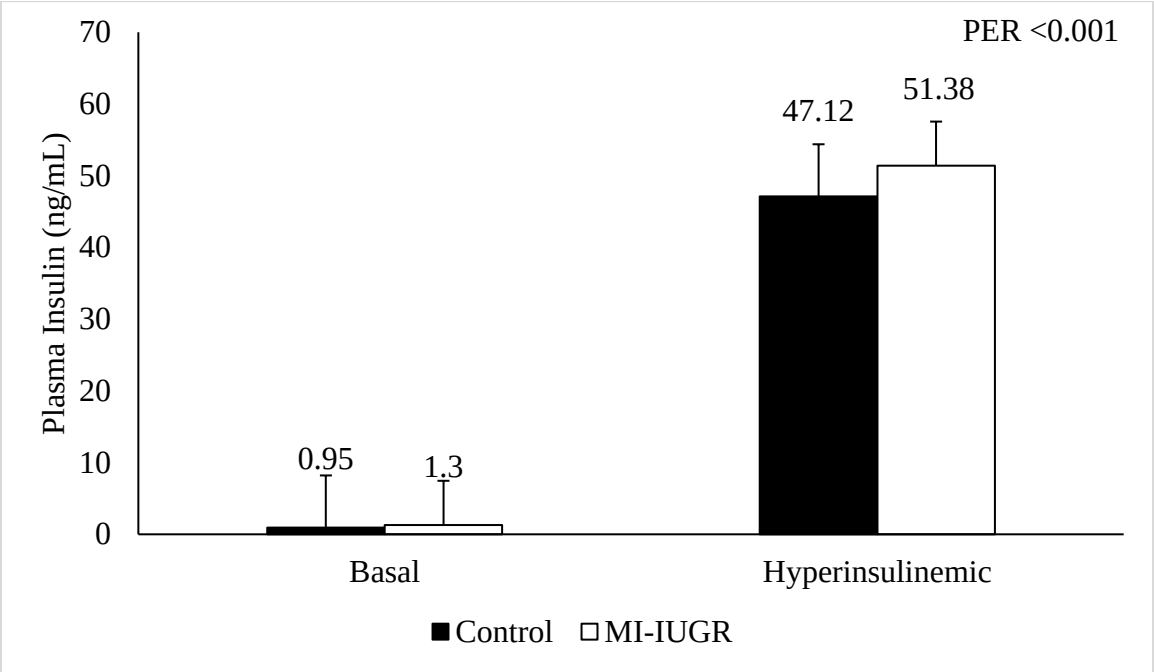


**Figure 3.21** Circulating plasma insulin concentration of control (n=10) or MI-IUGR fetuses (n=11) in response to basal or hyperinsulinemic conditions (PER).

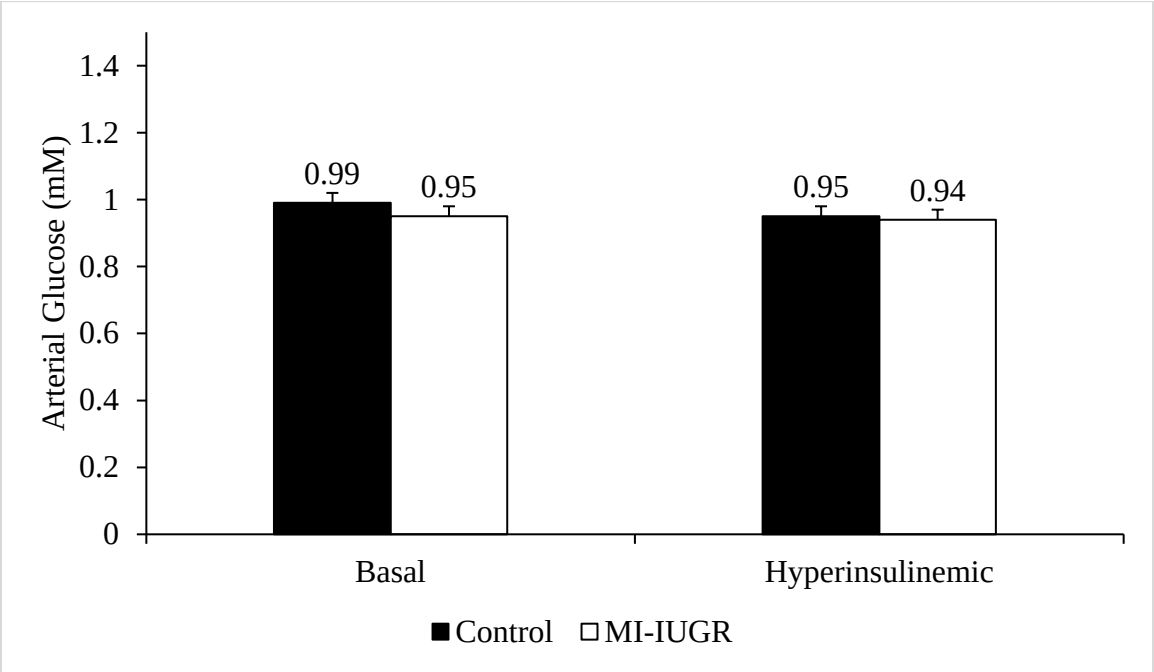


**Figure 3.22** Arterial blood glucose concentration of control (n=10) or MI-IUGR fetuses (n=11) in response to basal or hyperinsulinemic conditions.

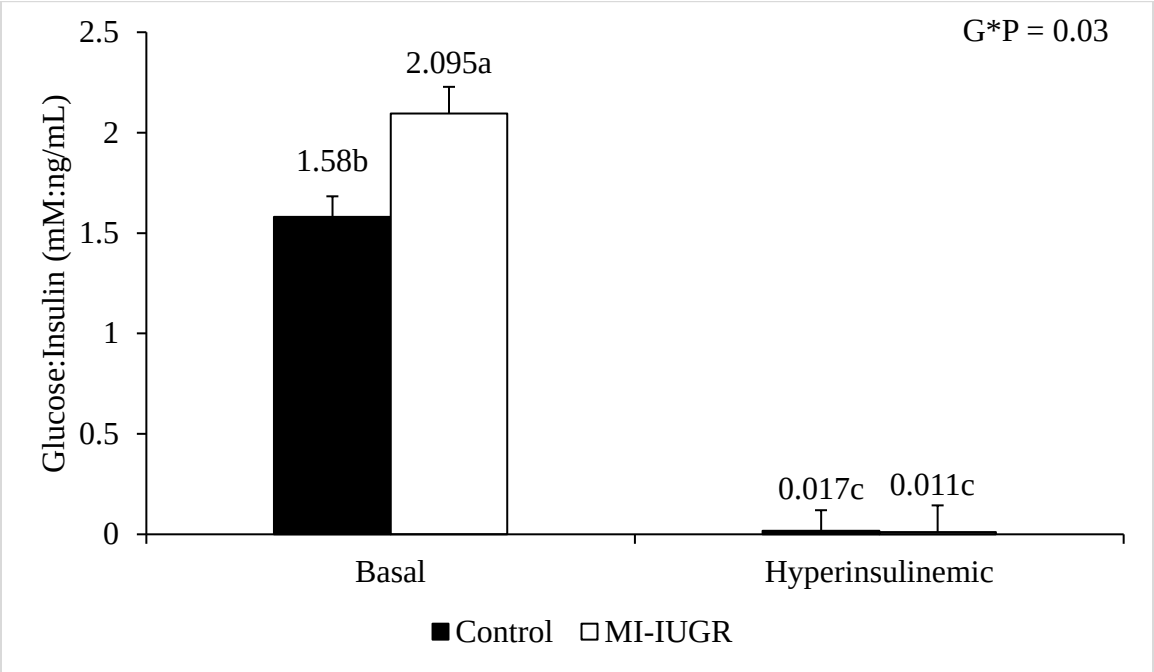


**Figure 3.23** The ratio of arterial blood glucose and insulin concentration of control (n=10) or MI-IUGR fetuses (n=11; GRP) in response to basal or hyperinsulinemic conditions (PER).

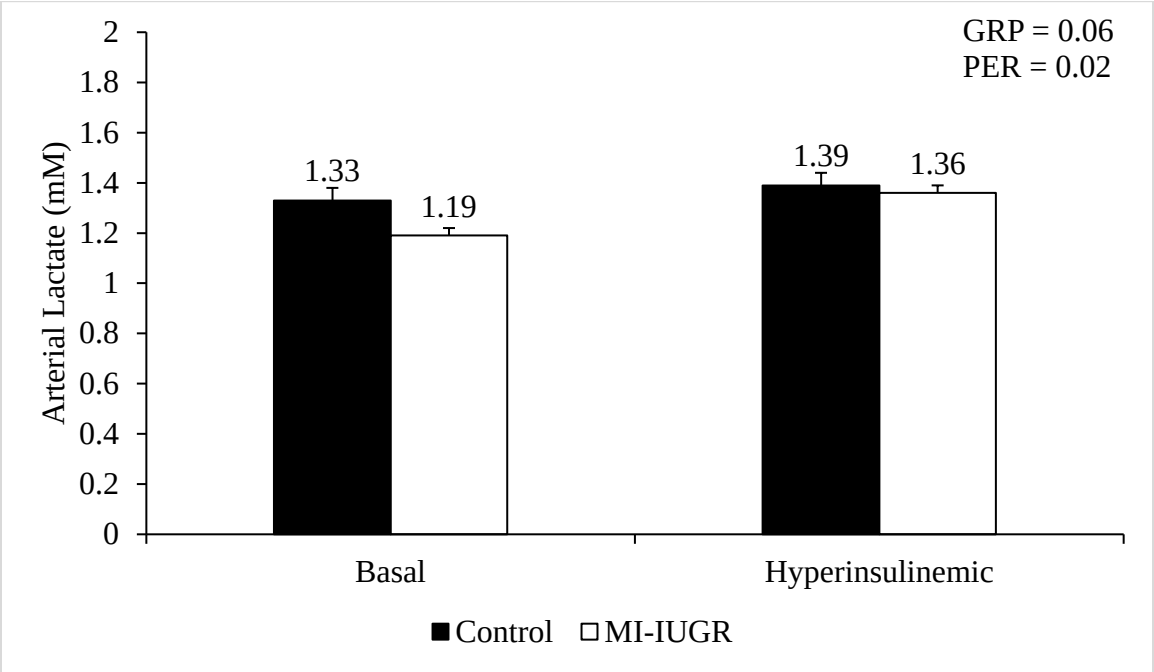


**Figure 3.24** Arterial lactate concentration of control (n=10) or MI-IUGR fetuses (n=11; GRP) in response to basal or hyperinsulinemic conditions (PER).

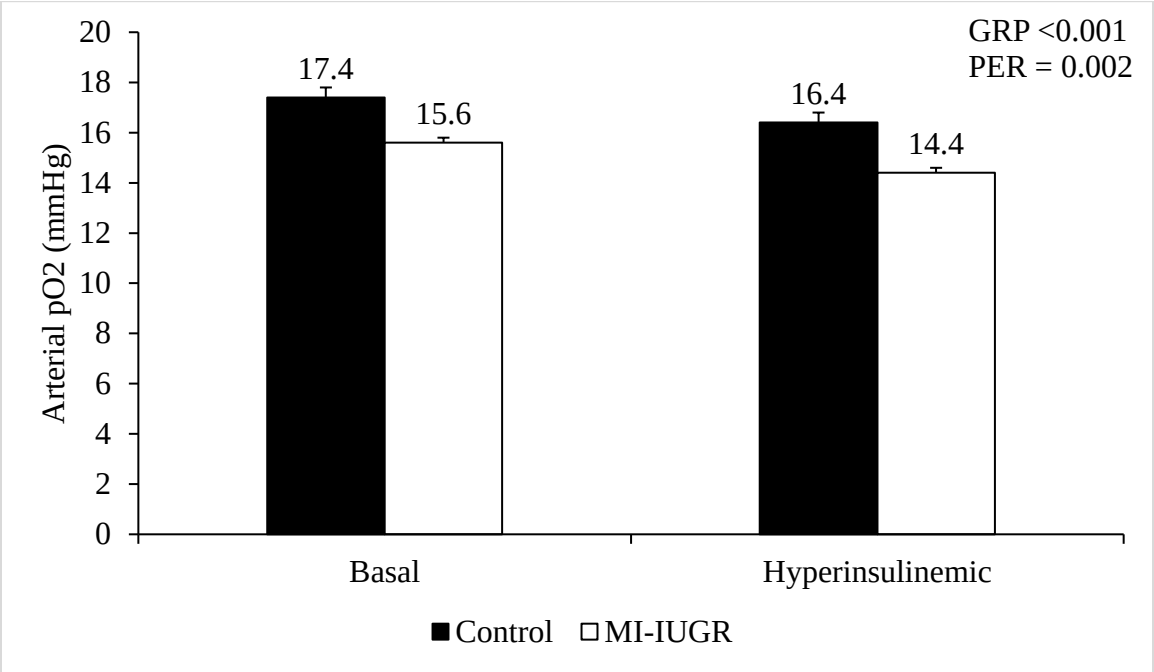


**Figure 3.25.** Arterial partial pressure of oxygen of control (n=10) or MI-IUGR fetuses (n=11; GRP) in response to basal or hyperinsulinemic conditions (PER).

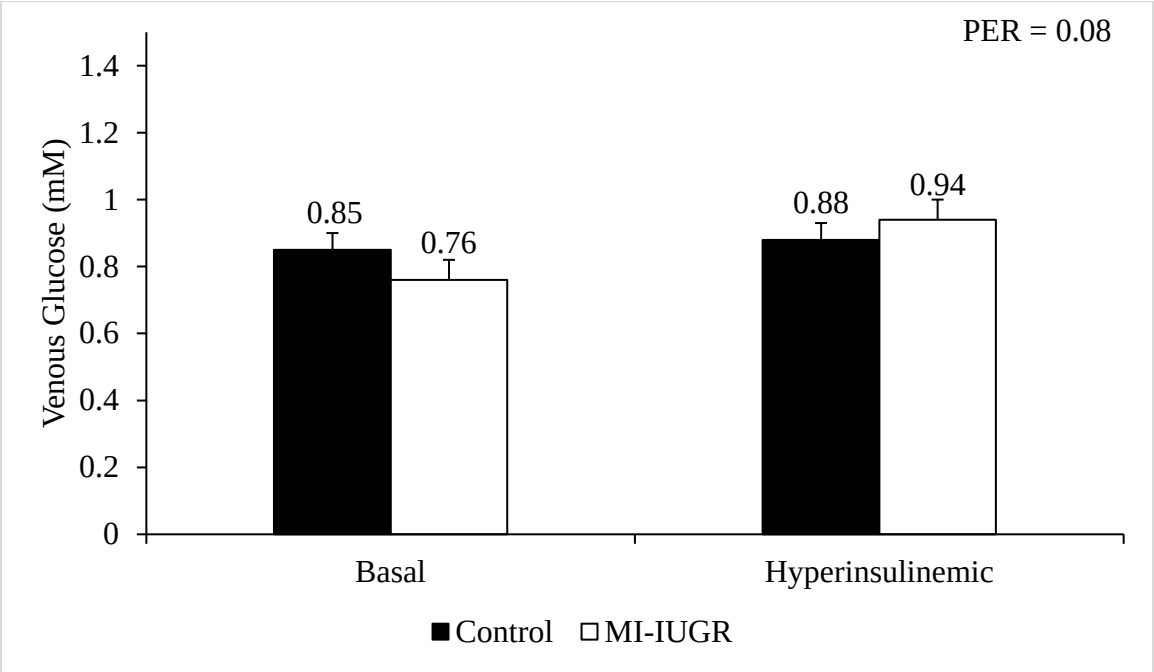


**Figure 3.26.** Venous glucose concentration of control (n=10) or MI-IUGR fetuses (n=11; GRP) in response to basal or hyperinsulinemic conditions.

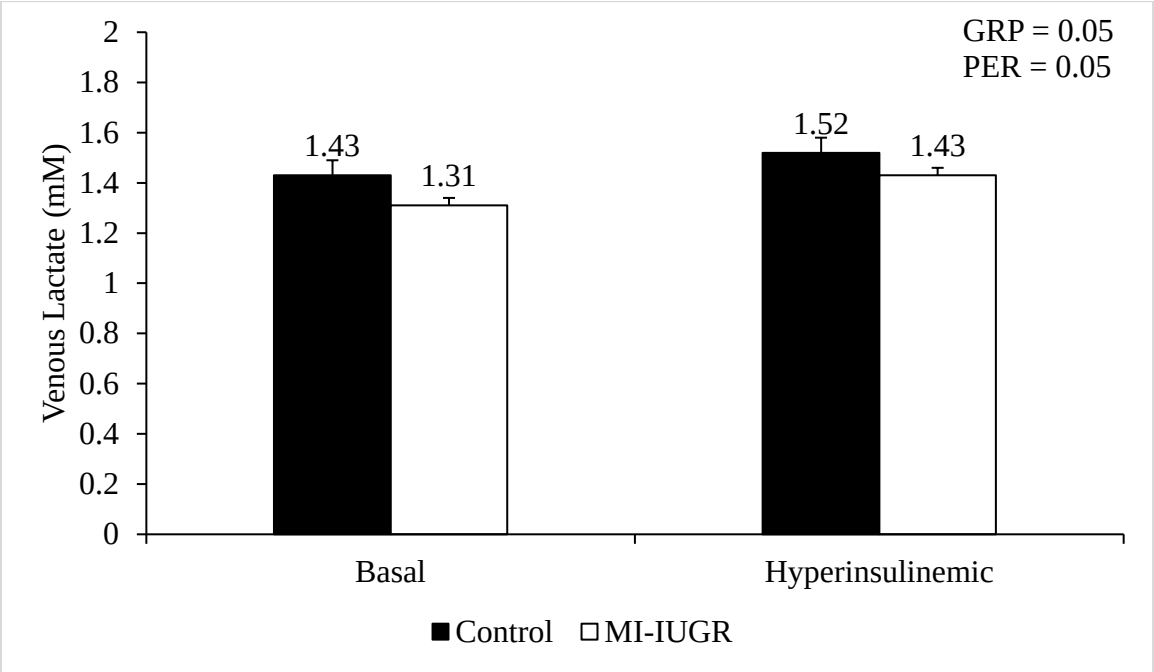


**Figure 3.27.** Venous lactate concentration of control (n=10) or MI-IUGR fetuses (n=11; GRP) in response to basal or hyperinsulinemic conditions (PER).

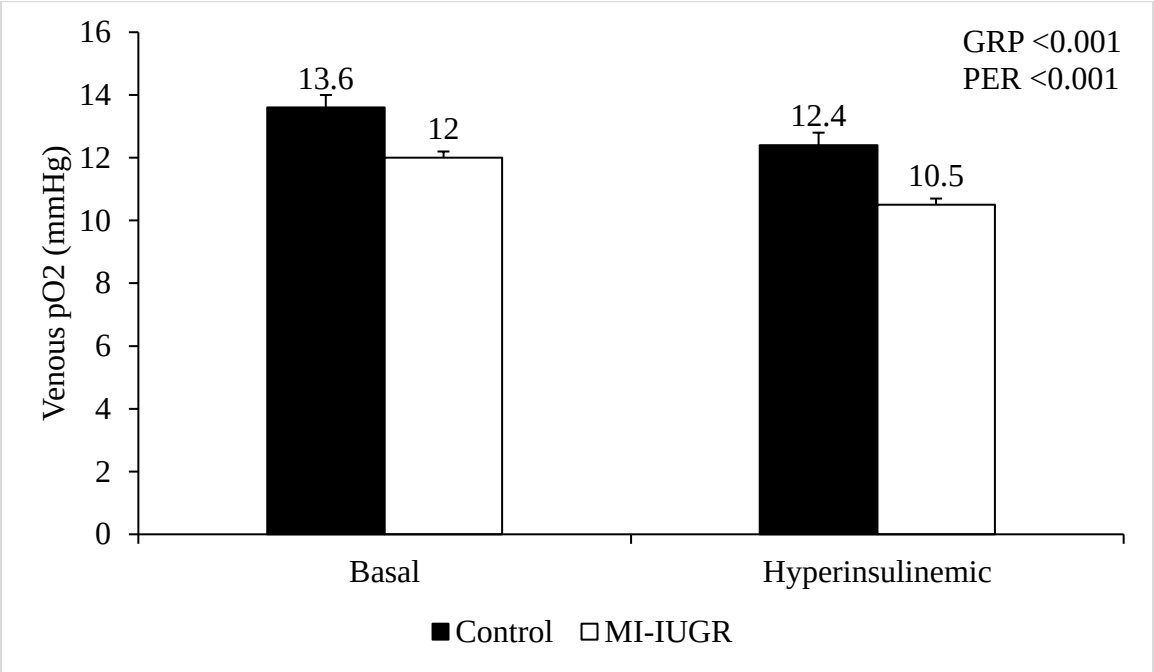


**Figure 3.28.** Venous partial pressure of oxygen of control (n=10) or MI-IUGR fetuses (n=11; GRP) in response to basal or hyperinsulinemic conditions (PER).

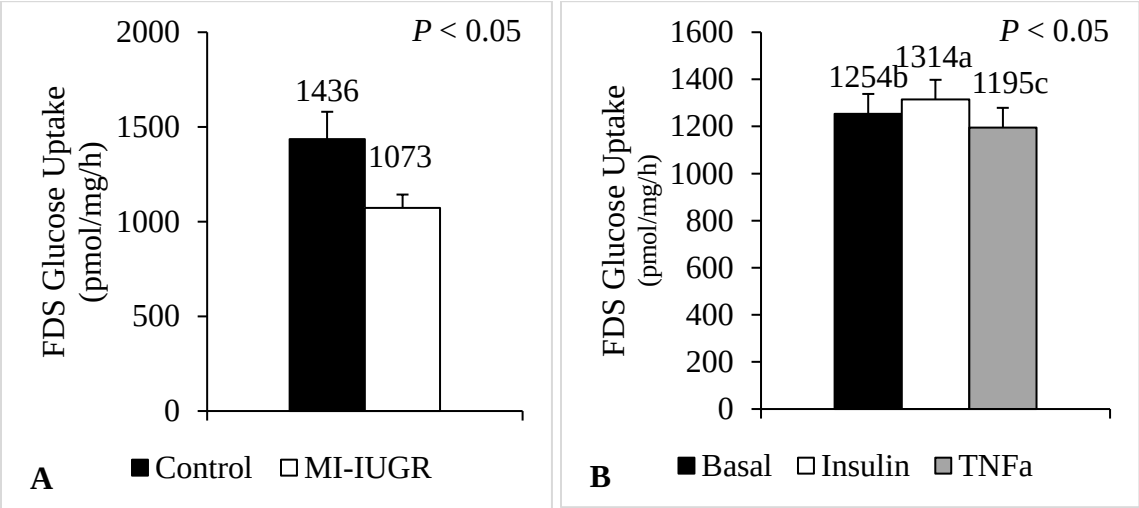


**Figure 3.29.** *Ex vivo* glucose uptake of fetal flexor digitorum superficialis muscle after isolation on dGA 125 and incubation in media without (basal) or with 5 mU/mL insulin (insulin) or with 10 ng/mL TNFα (TNFα). There was no interaction between incubation media and group ($P > 0.05$); **(A)** Main effect of group ($P < 0.05$) or **(B)** main effect of media ($P < 0.05$).

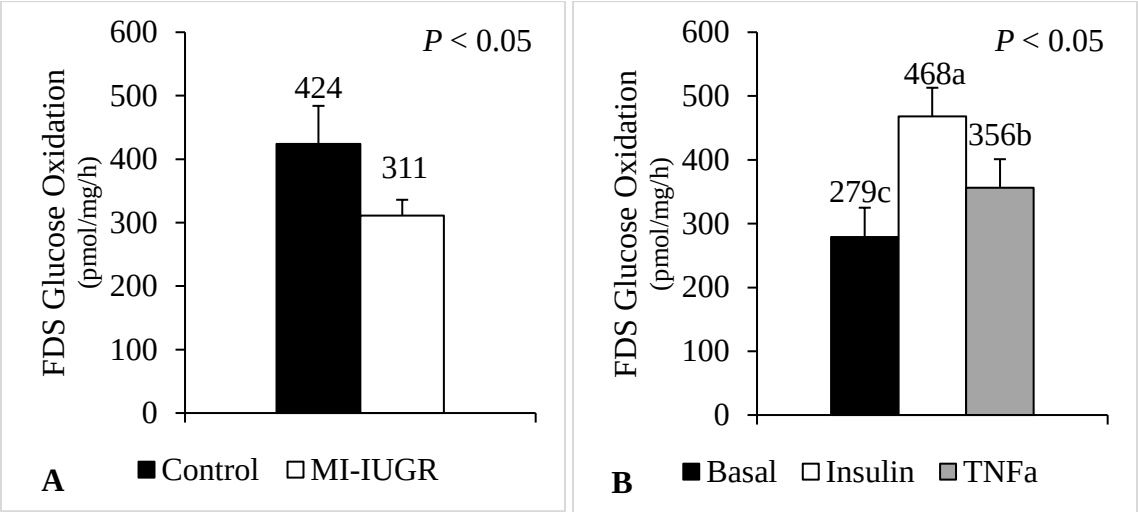


**Figure 3.30.** *Ex vivo* glucose oxidation of fetal flexor digitorum superficialis muscle after isolation on dGA 125 and incubation in media without (basal) or with 5 mU/mL insulin (insulin) or with 10 ng/mL TNFα (TNFα). There was no interaction between incubation media and group ($P > 0.05$); **(A)** Main effect of group ($P < 0.05$) or **(B)** main effect of media ($P < 0.05$).

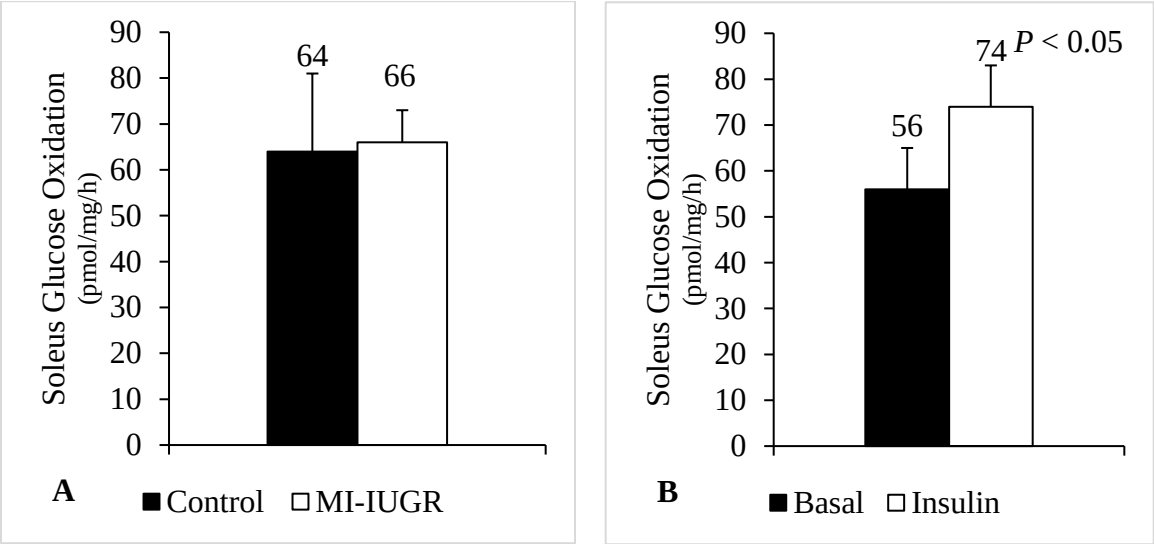


**Figure 3.31.** *Ex vivo* glucose oxidation of fetal soleus muscle after isolation on dGA 125 and incubation in media without (basal) or with 5 mU/mL insulin (insulin). There was no interaction between incubation media and group ($P > 0.05$); **(A)** Main effect of group ($P > 0.05$) or **(B)** main effect of media ($P < 0.05$).

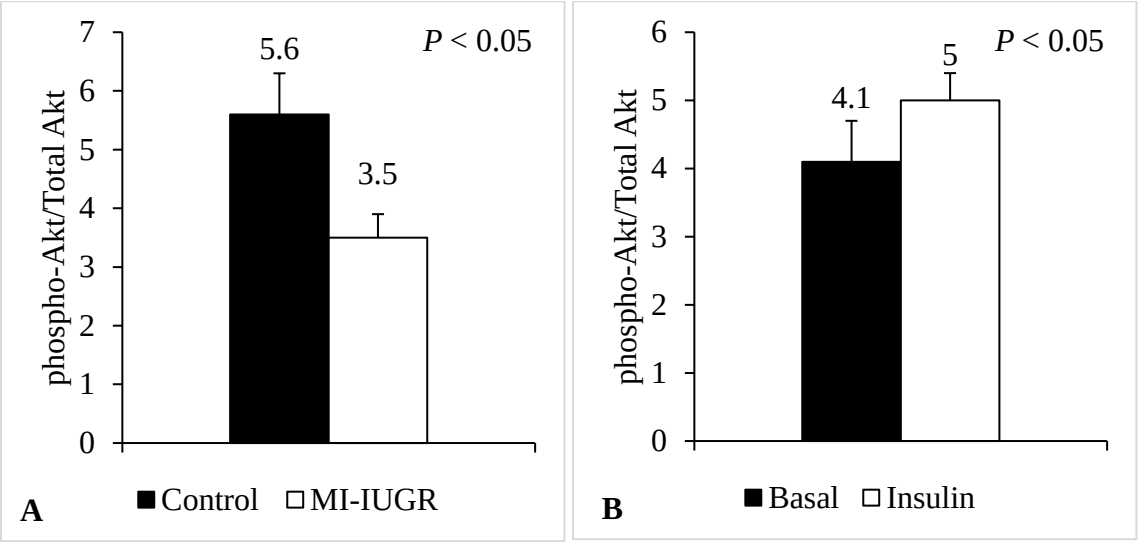


**Figure 3.32.** *Ex vivo* Akt phosphorylation of fetal flexor digitorum superficialis muscle after isolation on dGA 125 and incubation in media without (basal) or with 5 mU/mL insulin. There was no interaction between incubation media and group ($P > 0.05$); **(A)** Main effect of group ($P < 0.05$) or **(B)** main effect of media ($P < 0.05$).

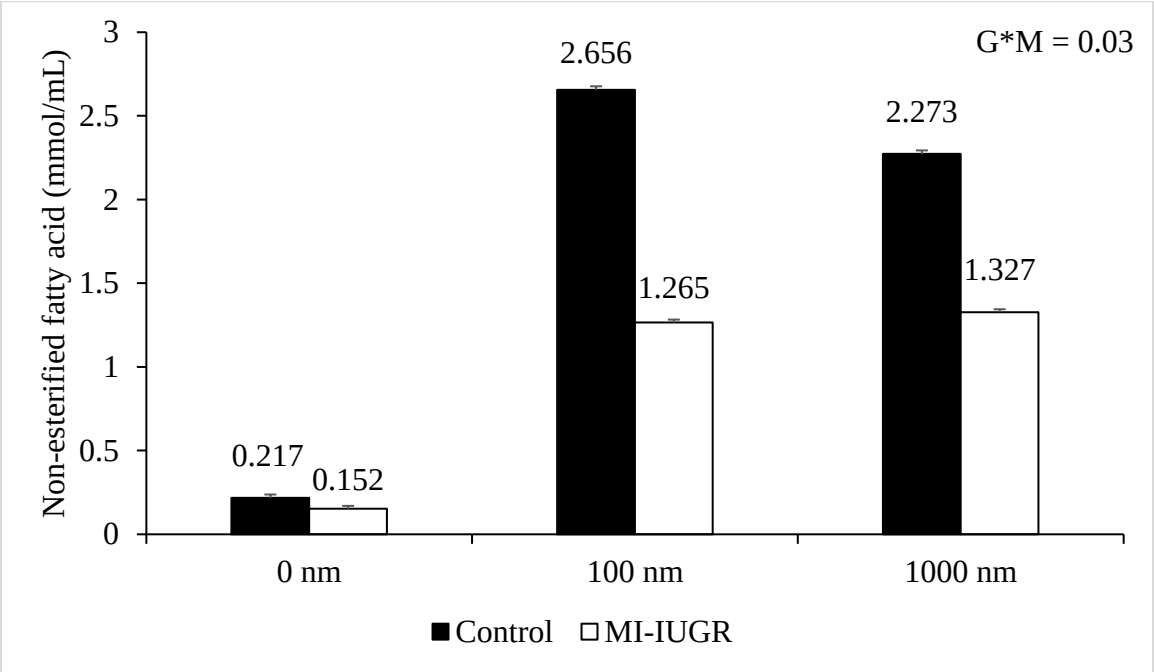


**Figure 3.33.** The concentration of ex vivo non-esterified fatty acids (NEFAs) mobilized from perirenal adipose tissue collected at 125 dGA and treated with 0 nM, 100 nM, or 1000 nM epinephrine (MEDIA) from control (n=11) or MI-IUGR (n=11) fetuses (GRP).

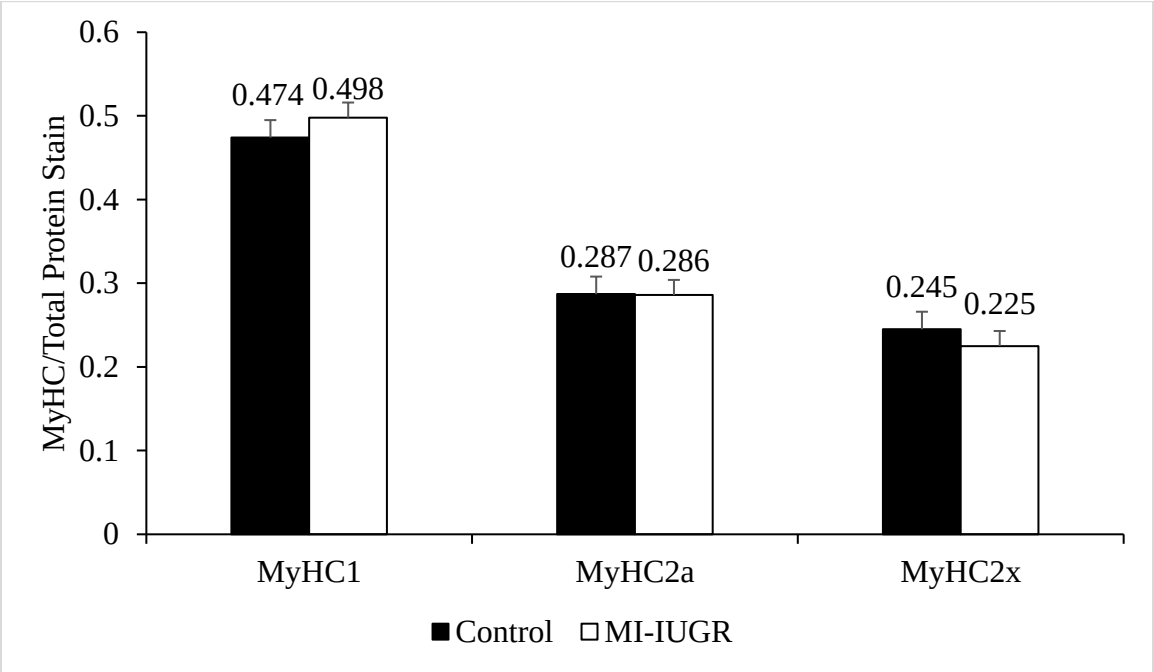


**Figure 3.34.** The proportion of myosin heavy chain 1 (MyHC1), myosin heavy chain 2a (MyHC2a) and myosin heavy chain 2x (MyHC2x) present in the semitendinosus muscle of control (n=11) and MI-IUGR fetuses (n=11) at 125 dGA.

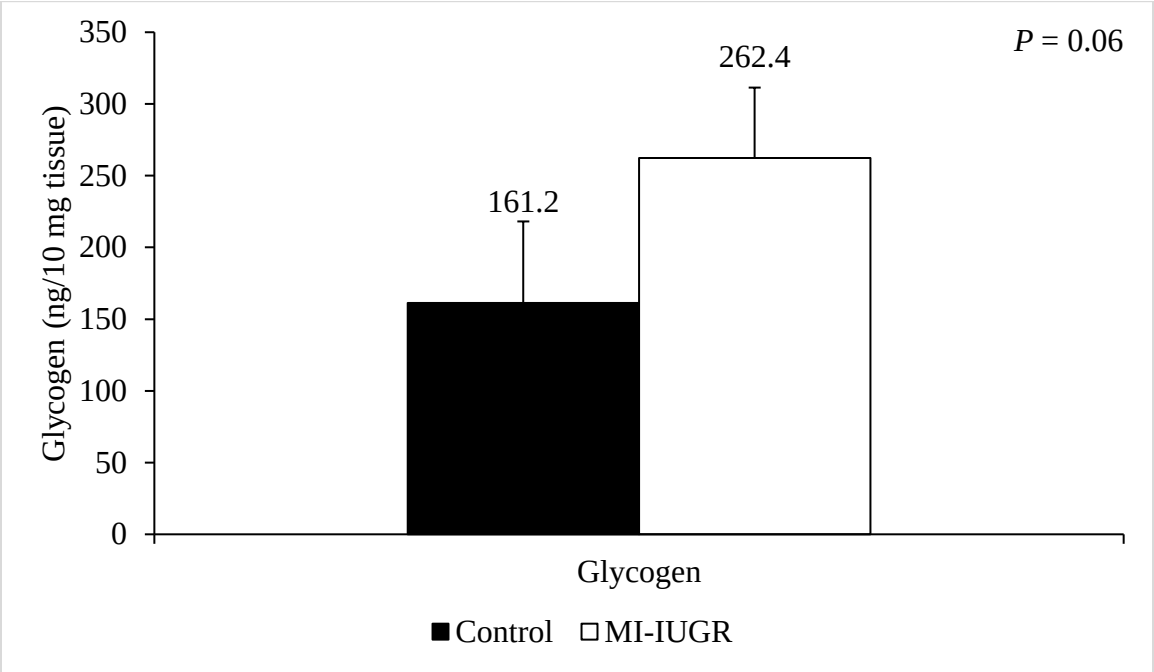


**Figure 3.35.** The amount of glycogen present in the semitendinosus muscle of control (n=11) and MI-IUGR fetuses (n=11) at 125 dGA.

# CHAPTER 4 – Maternofetal inflammation and maternal hyperthermia during gestation alter the transcriptome of the *semitendinosus* muscle in neonatal lambs


## Abstract

The phenotypic changes in IUGR-born animals are well-documented, but the underlying changes in tissue-specific gene expression have not been elucidated. Therefore, the objective of our study was to identify differentially expressed loci and their potential effects on biological pathways in skeletal muscle from IUGR-born lambs following maternofetal inflammation or maternal hyperthermia. *Semitendinosus* muscle was collected from 30-d old lambs following no experimental prenatal insult (controls; n = 9) or following IUGR induced by maternal hyperthermia and placental insufficiency (**PI-IUGR**, n = 4) or maternofetal inflammation during late gestation (**MI-IUGR**, n = 5). Total RNA was isolated and sequenced. Transcript counts were statistically analyzed with DESeq2 and pathway analysis was conducted using genes that were differentially expressed at an adjusted *P*-value (***P*adj**) of ≤ 0.10. This allowed elucidation of molecular pathway changes via the database for annotation, visualization, and integrated discovery (i.e., DAVID) Knowledgebase version v2023q1. For MI-IUGR lambs, 37 potential skeletal muscle pathways were impacted ($P < 0.10$) compared to controls. These included pathways associated with inflammation, metabolism, and growth. Only 1 gene was upregulated (*P*adj < 0.10) in MI-IUGR muscle, but 12 genes were downregulated (*P*adj < 0.10) compared to controls. These included *IFI6*, *ISG15*, *ENO3*, which are associated with inflammation, and *RAMP1*, which is associated with muscle growth. For PI-IUGR lambs, the insulin resistance pathway was predicted to be impacted ($P < 0.10$) compared

to controls. Additionally, expression for the *PGAM1* and *LOC121816987* genes was upregulated (*P*adj < 0.10) in PI-IUGR muscle compared to controls. Only one skeletal muscle gene, the growth-associated *S100A2*, was differentially expressed in both IUGR models. These findings identify several specific genes involved in inflammatory signaling, glucose metabolism, and skeletal muscle growth that were altered in their expression patterns by IUGR. Understanding the identity of these genes and the associated pathways helps to explain the mechanistic causes for IUGR pathologies and provides potential therapeutic targets for improving IUGR outcomes.

## Introduction

Maternal stress during pregnancy induces permanent fetal adaptations that impair skeletal muscle growth capacity, dysregulate oxidative metabolism, and yield changes in body composition throughout the life of the offspring (Yates et al., 2018). These permanent adaptations, which are characterized by fetal intrauterine growth restriction (**IUGR**) and low birthweight, put afflicted humans at risk for metabolic diseases such as obesity and type II diabetes and reduce feed efficiency, carcass merit, and value in livestock (Powell and Aberle, 1980; Barker et al., 1993; Greenwood et al., 2000; Gondret et al., 2005; Gatford et al., 2010; Yates et al., 2018). Skeletal muscle is the most abundant tissue in the body and is responsible for utilizing around 65% of the body's total glucose supply (Defronzo et al., 1981; Merz and Thurmond, 2020). Muscle is also the main tissue responsible for clearing glucose from circulation, as it accounts for 85% of insulin-driven glucose uptake (Brown, 2014b). Thus, it is the chief tissue involved in the development of insulin resistance (Merz and Thurmond, 2020). Dysregulation and disruption of the insulin signaling pathway in skeletal muscle leads to insulin resistance and, ultimately, type II diabetes (Merz and Thurmond, 2020). Animal studies have shown that IUGR-born offspring have deficits in skeletal muscle insulin responsiveness, growth, and oxidative metabolism following intrauterine stress (reviewed in detail by Yates et al. (2018)). Several techniques for inducing maternal stress have been utilized to create animal-based IUGR models (Beede et al., 2019). Maternal heat stress in pregnant ewes is perhaps the most popular and best characterized large-animal IUGR model, as it effectively and naturally induces predictable degrees of placental stunting and fetal IUGR (Yates et al., 2018). However, our lab has recently shown that maternofetal inflammation in pregnant

ewes reliably produces a comparable IUGR phenotype (Cadaret et al., 2019; Posont et al., 2021). Although the phenotypic outcomes of IUGR have been well documented, the mechanisms by which these deficits occur are still largely unknown. Transcriptomic studies allow the identification of shifts in gene expression that can help elucidate the specific biological mechanisms impacted by IUGR. Therefore, the objective of this study was to investigate the skeletal muscle transcriptome of IUGR-born neonatal sheep that were produced by experimental maternofetal inflammation during late gestation or hyperthermia-induced placental insufficiency and to identify the specific pathways and genes affected.

## Materials and Methods

### *Animals and Experimental Design*

All animal studies were approved by the Institutional Animal Care and Use Committee at the University of Nebraska-Lincoln, which is accredited by AAALAC International. Portions of the *semitendinosus* muscle were collected from a total of 20 lambs necropsied at 30 ± 1 d of age. Lambs were produced from two previous IUGR studies that resulted in 4 experimental groups: controls (n = 10; Posont et al., 2021; Cadaret et al., 2022), maternofetal inflammation-induced IUGR (**MI-IUGR**; n = 5; Posont et al., 2021), and placental insufficiency-induced IUGR (**PI-IUGR**; n = 6; Cadaret et al., 2022; **Table 1**). *Semitendinosus* portions were collected, flash frozen in liquid nitrogen, and stored at -80°C.

### *RNA Extraction*

RNA extraction was completed as previously described (Beer, 2022). Briefly, total RNA was extracted using TRIzol reagent (Sigma-Aldrich, St. Louis, MO) following the protocol from a RNeasy Plus Mini Kit. Per manufacturer's instructions, RNA was washed and eluted on columns with DNase I treatment (Direct-zol RNA MiniPrep Plus, Zymo, Irvine, CA). RNA integrity and concentrations were determined via Agilent Bioanalyzer (Agilent, Santa Clara, CA). Illumina TruSeq stranded, Poly-A selected libraries were prepared and 100 bp paired-end sequencing was performed to a targeted depth of 20 million reads/sample at the Oklahoma Medical Research Foundation Clinical Genomics Center (Oklahoma City, OK). Raw reads for all samples were trimmed using TrimGalore (Barbraham Bioinformatics – Trim Galore!) and counts were estimated as

transcripts per million with STAR (Dobin et al., 2013) based on the following parameters: minimum 20 read quality and 35 bp minimum output read.

### *Data Processing and Analysis*

Transcript counts were statistically analyzed with DESeq2 (Love et al., 2014). Samples that had counts of 50 or above were analyzed. In addition to the assessment of gene expression of pairwise combinations via heatmap, where the cutoff of an average correlation of 0.75 or lower was utilized, a variance-stabilizing transformation was applied to the normalized count matrix to aid in identifying outliers. The matrix was then rlog transformed and inserted into the rrcov R package PcaGrid, thereby detecting outliers via robust principal component analysis (Todorov and Filzmoser, 2009). Outliers or any sample with an orthogonal distance or score distance outside of default parameter cutoff values were removed. Differentially expressed genes were defined as those genes with an adjusted-*P*-value (***P*adj**) $\leq 0.1$. Differentially expressed loci with a raw *P*-value $\leq 0.01$ and were used to elucidate molecular pathway changes via the database for annotation, visualization, and integrated discover (DAVID) Knowledgebase version v2023q1 (Huang et al., 2009a; Huang et al., 2009b).

**Results**

For these analyses, the average read depth across all experimental groups was 14,298,220.5 reads per sample, with 86.6% uniquely mapped reads included in analyses. The *semitendinosus* of MI-IUGR neonates had a mean RNA integrity number (**RIN**) of 9.46. There were no outliers removed from the MI-IUGR group. PI-IUGR neonates had a mean RIN of 9.32. There were 2 outliers removed from the PI-IUGR group as they were highly correlated with each other ($R^2 \geq 0.9$) but lowly correlated with the rest of the samples ($R^2 \leq 0.75$). Control neonates had a mean RIN of 9.5. There was 1 outlier removed from the control group as it was lowly correlated with the rest of the samples ($R^2 \leq 0.75$).

A total of 40 molecular pathways within the *semitendinosus* were predicted to be altered ($P < 0.1$) among the three experimental groups: 37 pathways differed ($P < 0.1$) between MI-IUGR and controls and 3 pathways differed ($P < 0.1$) between PI-IUGR and controls (**Table 2**). A total of 6 loci were differentially expressed ($P$adj < 0.05) (**Table 3)**. These included 4 genes that differed ($P$adj < 0.05) between MI-IUGR and controls and 2 genes that differed ($P$adj < 0.05) between PI-IUGR and controls. An additional 9 loci tended to be differentially expressed ($P$adj < 0.1), which included 8 genes that differed between MI-IUGR and controls and 1 gene that differed between PI-IUGR and controls (**Table 3**). All 4 differentially-expressed genes in MI-IUGR muscle (*Beta 2 microglobulin, 60S ribosomal L37a, S100A2,* and *LOC114109685*) were downregulated ($P$adj < 0.05) compared to controls. Seven of the genes that tended to be differentially expressed in MI-IUGR muscle (*IFI6, ENO3, ISG15, LOC101120797, LOC105607887, RAMP1*, and *GCNT1*) were downregulated ($P$adj < 0.1) and 1 gene (*CSTL1*) was

upregulated (*P*adj < 0.1). For PI-IUGR neonates, both genes that were differentially expressed (*NADH-ubiquinone oxidoreductase chain 5-like* and *PGAM1*) were upregulated (*P*adj < 0.05) compared to controls, and the gene that tended be differentially expressed (*S100A2*) was downregulated (*P*adj < 0.1).

**Discussion**

In this study, we found gene expression patterns by IUGR neonatal skeletal muscle that help to explain the growth and metabolic deficits that follow prenatal stress. The specific genes and biological pathways affected were not identical between IUGR lambs produced by maternal hyperthermia and those produced by maternal inflammation. For both models, however, the greatest number of changes occurred for genes and pathways associated with inflammatory responses and metabolism. Interestingly, lambs made IUGR by maternofetal inflammation *in utero* exhibited notably more differentially-expressed genes than did those made IUGR by maternal hyperthermia, despite the latter having the more severe growth-restricted phenotype (Posont et al., 2021; Cadaret et al., 2022). Nevertheless, pathway analyses indicated extensive modification of inflammation-oriented pathways in both models of IUGR. Indeed, 67.5% of the pathways impacted in MI-IUGR and nearly 67% of pathways impacted in PI-IUGR lambs were relating to inflammation, such as the HIF-1 signaling pathway, antigen processing and presentation, and a host of autoimmune and infectious disease pathways. Of the remaining pathways impacted, the majority (20% of MI-IUGR pathways and 33% of PI-IUGR pathways) were related to metabolism or metabolic dysfunction. This helps to confirm the underlying role of muscle-centric inflammatory programming in the hallmark growth and metabolic deficits of IUGR-born offspring.

The *semitendinosus* transcriptome of MI-IUGR neonatal lambs revealed that little upregulation of genes occurred as part of the programming response to maternofetal inflammation in late gestation. Indeed, the only gene found to be upregulated was *CSTL1*, which codes for cystatin-like 1, a member of the superfamily of cysteine protease

inhibitors (RefSeq - CSTL1, 2023). Some CSTL are nonfunctional pseudogenes and is important to note that the functionality of cystatin-like 1 has not yet been established, but other members of the superfamily have been linked to cellular apoptosis and inflammation (Magister and Kos, 2013). Thus, the upregulation of *CSTL1* in MI-IUGR neonates could reflect the known heightened inflammatory state of these animals (Posont et al., 2018).

Several of the genes that were downregulated in MI-IUGR skeletal muscle were associated with immune function and inflammatory responses, presumably as compensatory responses to heightened prenatal inflammation and enhanced cytokine signaling pathways (Cadaret et al., 2019; Hicks and Yates, 2021; Posont et al., 2021). *LOC114108604* is predicted to code for β2-microglobulin (RefSeq - LOC114108604, 2022), which is a ubiquitously-expressed component of the major histocompatibility complex (**MHC**) class I molecule (Tarrant, 2017). Presence of the MHC Class I molecule on the surface of the animal's own cells allows immune cells to distinguish them from foreign cells (Becar and Kasi, 2023). However, MHC-I expression can be disrupted by the canonical inflammatory cytokine signaling hub, NF-κB, which binds to the MHC-I gene promoter region (Cadaret et al., 2018; Taylor and Balko, 2022). Another downregulated gene, *LOC114109685*, codes for the protein proteasome maturation protein-like, as it is 97.7% analogous with the proteasome maturation protein (**POMP**; RefSeq - LOC114109685). Little has been documented about the function of proteasome maturation protein-like and whether it differs from POMP. However, POMP functions as a chaperone for the assembly of proteasome 20S, the proteasome responsible for

degrading antigenic proteins into peptides that can be displayed on the MHC Class I molecule (Sijts and Kloetzel, 2011).

*IFI6*, also downregulated in MI-IUGR muscle, is a well-studied gene of interest in many different cancers, autoimmune diseases such as lupus, and microbial infections, with 272 papers since 1992 that investigate the loci or protein cross-referenced in PubMed. *IFI6* codes for interferon alpha-inducible protein 6 (RefSeq - IFI6, 2023), which is an interferon-stimulated gene (**ISG**) that regulates cellular apoptosis by preventing the release of mitochondrial cytochrome c (Cheriyath et al., 2007; Villamayor et al., 2023). More recent studies have shown that IFI6 negatively regulates retinoic acid-inducible gene-1 (**RIG-1**) activation, which would limit the activation of inflammatory pathways including IFN regulatory factors 3 and 7 (**IRF-3** and **IRF-7**) and NF-κB (Villamayor et al., 2023). Likewise, the ubiquitin-like modifier interferon-stimulated gene 15, coded by the downregulated *ISG15* gene (RefSeq - ISG15, 2023), is another ISG that plays a role in stabilizing proteins, intracellular trafficking, cell cycle control, and immune modulation (Perng and Lenschow, 2018). It also promotes cell signaling (Zhang et al., 2015) and neutrophil chemotaxis (Owhashi et al., 2003; Perng and Lenschow, 2018). The function of ISG15 has been robustly explored, with 2,425 publications listed in PubMed on this gene/protein since 1982. ISG15 is among the earliest and most abundant genes upregulated in response to infections (Munnur et al., 2022), lipopolysaccharides (**LPS**), and other pathogenic stimuli (Perng and Lenschow, 2018). Extracellular ISG15 also acts as a cytokine by inducing natural killer cell production and dendritic cell maturation and by stimulating the production of IFN-γ (D'Cunha et al., 1996; Padovan et al., 2002; Owhashi et al., 2003; Perng and Lenschow, 2018). Similar to IFI6, ISG15 typically

inhibits the production of inflammatory cytokines, particularly during viral infections (Perng and Lenschow, 2018).

The downregulated gene *LOC101120797,* which codes for the protein caspase-14 (RefSeq - LOC101120797, 2021) has been identified in inflammatory dysfunction (Markiewicz et al., 2021). Although the caspase protein family is mostly comprised of proteins that promote cellular apoptosis, caspase-14 is involved in preventing cellular apoptosis (Markiewicz et al., 2021). Because caspase-14 was originally identified in mammalian skin, many studies have examined its role in skin-related disorders (Mikolajczyk et al., 2004; Nenci et al., 2006; Jung et al., 2014; Markiewicz et al., 2021). For many of these, decreased caspse-14 expression was associated with unhealthy lesions or tissues (Mikolajczyk et al., 2004; Nicotera and Melino, 2007; Jung et al., 2014; Markiewicz et al., 2021). The down regulated *RAMP1* codes for receptor activity modifying protein-1 (RefSeq - RAMP1, 2023), which has been shown in multiple tissues to prohibit the release of inflammatory cytokines such as TNFα, particularly in response to LPS (Tsujikawa et al., 2007; Inoue et al., 2018; Tsuru et al., 2020). Interestingly, both mRNA and protein expression of *RAMP1* was downregulated in omental arteries of fetal rats when pregnancies were complicated by IUGR (Chauhan et al., 2016).

Together, the downregulated genes in MI-IUGR neonates further shows dysregulated immune function in general and inflammation in particular that is exhibited in IUGR animals (Cadaret et al., 2018; Hicks and Yates, 2021; Posont et al., 2021). Indeed, Posont et al. (2018) demonstrated that primary myoblast cells from MI-IUGR fetal lambs had heightened sensitivity to cytokines, as they were stimulated by much lower cytokine concentrations in culture. Moreover, the downregulation of both

inflammatory and anti-inflammatory genes in the MI-IUGR neonate suggests a compensatory response to high inflammatory conditions during gestation.

MI-IUGR neonatal lambs exhibited downregulation of genes related to skeletal muscle growth and metabolic pathways. For example, *LOC101121371* is predicted to code for the 60S ribosomal protein L37a (RefSeq - LOC101121371, 2021). Although *LOC101121371* is underexplored in mammals, in yeasts this ribosomal protein is required for a recruitment step involved in forming the 60S subunit of ribosomes (Gamalinda et al., 2013). Another study that examined lower expression of 44 other ribosomal proteins in the 60S subunit have found that their absence in knockdown mice resulted in dysfunctional cell cycle regulation, cellular metabolism, cellular signal transduction, and ultimately cellular apoptosis or senescence (Luan et al., 2022). If L37a function is similar in mammals, its downregulation could contribute to the deficits in skeletal muscle growth exhibited in IUGR animals (Cadaret et al., 2019b; Posont et al., 2021). The downregulated *ENO3* condes for Enolase 3, an isoenzyme related to skeletal muscle development and regeneration (RefSeq - ENO3, 2022). Furthermore, mutations in this gene have been associated with glycogen storage disorders (Tarnopolsky, 2018), and it was downregulated in satellite cells derived from mice with metabolic myopathies (Ganassi and Zammit, 2022). This clear role in muscle growth means that downregulation of enolase 3 may contribute to skeletal muscle growth restriction and metabolic dysfunction present in IUGR animals (Yates et al., 2018). Little is known about the function of *LOC105607887*, the downregulated gene that codes for phytanoyl-CoA dioxygenase, peroxisomal-like (RefSeq - LOC105607887). However, the peroxisomal phytanoyl-CoA dioxygenase enzyme itself plays a role in the α-oxidative metabolism of

fatty acids (Gould, 2013). The downregulated *GCNT1* gene codes for glucosaminyl (N-acetyl) transferase 1, an enzyme responsible for post-translational modifications essential for the formation of Gal beta 1-3 (GlcNAc beta 1-6) structures and the core 2-O-glycan branch (RefSeq - GCNT1, 2023). The O-GlcNac glycosylation for nuclear proteins has been shown to substantially alter transcription of proteins linked with metabolic diseases such as type 2 diabetes (Cejas et al., 2019). Interestingly, a study in fast and slow-growing poultry lines found that fast-growing chickens had lower expression of *GCNT1* in the *pectoralis major* muscle at hatching and that this correlated with greater intramuscular fat deposition in these birds (Liu et al., 2017). Thus, downregulation of the *GCNT1* gene could be a potential therapeutic target, as IUGR-born animals develop increased fat deposition as they age (Posont et al., 2021; Gibbs, 2023). Collectively, the downregulated genes observed in skeletal muscle from MI-IUGR lambs help to explain how the phenotypic dysfunction in oxidative metabolism and increased fat deposition arise mechanistically in IUGR animals (Yates et al., 2018).

Only a single gene, *S100A2*, was altered in IUGR lambs produced from maternal heat stress and those produced by maternofetal inflammation. This gene, which was downregulated in both groups of IUGR lambs, codes for S100 Calcium Binding Protein A2. This ubiquitously expressed protein plays a role in calcium sensing and modulation and thus influences diverse physiological processes including cell cycle progression and cellular differentiation (RefSeq - S100A2, 2023). Since 1996, almost 300 papers have been published on the functional significance of the S100A2 gene/protein, per PubMed. Many describe its involvement in inflammatory diseases such as psoriasis and cancers, and its degree of heightened expression appears to correlate with the degree of

inflammation present (Sugino and Sawada, 2022). The S100A2 protein has been shown to interact with S100A4, which in turn increases production of NF-κB, TNFα, and other inflammatory products (Sugino and Sawada, 2022). Another study found that S100A2 overexpression increased anaerobic glycolysis (i.e., Warburg effect) and proliferation rates in colorectal cancer cells (Li et al., 2020). Interestingly, this gene was upregulated in fetal MI-IUGR adipose tissue (Beer, 2022), which could indicate how inflammatory pathways are impacted differently across tissues with different functionalities.

Two genes were found to be upregulated in skeletal muscle from PI-IUGR neonatal lambs. One of these, *LOC121816987*, is a pseudogene for NADH-ubiquinone oxidoreductase chain 5-like protein (RefSeq - LOC121816987, 2021). As a pseudogene, it does not code for a protein but could have a role in regulating the expression of other related proteins (Pink et al., 2011). Indeed, because *LOC121816987* codes for a protein similar to NADH-ubiquinone oxidoreductase chain 5, a protein which is involved in the electron transport chain (RefSeq - MT-ND5, 2023), its ability to regulate such proteins could be linked to deficits in oxidative metabolism observed in skeletal muscle of IUGR-born neonates (Cadaret et al., 2019b; Posont et al., 2021). The other upregulated gene, *PGAM1*, codes for phosphoglycerate mutase 1 (RefSeq - PGAM1, 2023), which is an enzyme involved in the glycolytic metabolism pathway (Li and Liu, 2020). Studies in sheep Sertoli cells found that overexpression of *PGAM1* increased cellular proliferation and expression of glycolytic genes in these cells but also increased expression of apoptotic genes (An et al., 2021). Furthermore, *PGAM1* knockout mice exhibited less inflammatory response, apoptosis, and fibrosis in response to myocardial ischemia-reperfusion procedures, further illustrating the role *PGAM1* has in tissue inflammatory

responses (Wu et al., 2021). Based on this literature, we can presume that the greater expression of *PGAM1* in PI-IUGR neonatal skeletal muscle is a factor in the previously-observed deficits in myoblast proliferation (Yates et al., 2014b; Posont et al., 2022).

From our findings, we can conclude that skeletal muscle of IUGR-born neonatal lambs exhibited robust transcriptomic evidence of inflammatory programming, which helps to explain the mechanisms underlying poor growth and metabolism. These data show specific molecular mechanisms that represent biomarkers to improve our understanding of the programmed impacts of IUGR and may even help to identify biological targets for improving outcomes in IUGR-born humans and animals. Because IUGR pathologies progressively worsen as the afflicted individual ages, future studies exploring how transcriptomic changes may differ between fetal, neonatal, and adult stages appear to be warranted. In addition, examining other tissue types may help to better understand the nuances of IUGR pathologies on the more general outcomes of growth and metabolic health.

## Tables and Figures

**Table 4.1** Number of animals in each experimental group collected and the number of samples analyzed after outliers were removed.

| Group | Samples Collected | Outliers Removed | Samples Analyzed |
|---|---|---|---|
| Control | 10 | 1 | 9 |
| MI-IUGR | 5 | 0 | 5 |
| PI-IUGR | 6 | 2 | 4 |

**Table 4.2** Predicted altered pathways in the semitendinosus muscle of MI-IUGR and PI-IUGR neonatal lambs relative to uncompromised control lambs.

| Group | KEGG Pathway | Percentage of Loci | *P*-value |
|---|---|---|---|
| MI-IUGR | Metabolic Pathways | 14.3 | 0.000294 |
| | Chemical carcinogenesis – ROS | 4 | 0.0018 |
| | Influenza A | 3.3 | 0.0033 |
| | Epstein-Barr virus infection | 3.7 | 0.004 |
| | Antigen processing and presentation | 2.2 | 0.0063 |
| | Asthma | 1.5 | 0.0075 |
| | Glycolysis/Gluconeogenesis | 1.8 | 0.014 |
| | Biosynthesis of amino acids | 4 | 0.017 |
| | Coronavirus disease – COVID-19 | 1.5 | 0.017 |
| | Folate biosynthesis | 3.3 | 0.019 |
| | Thermogenesis | 1.8 | 0.025 |
| | Leishmaniasis | 2.6 | 0.025 |
| | Non-alcoholic fatty liver disease | 3.7 | 0.026 |
| | Huntington disease | 1.5 | 0.03 |
| | Intestinal immune network for IgA production | 1.8 | 0.031 |
| | Staphylococcus aureus infection | 1.5 | 0.035 |
| | Allograft rejection | 3.3 | 0.038 |
| | Parkinson disease | 2.9 | 0.043 |
| | Human T-cell leukemia virus 1 infection | 2.9 | 0.045 |
| | Ribosome | 1.5 | 0.045 |
| | Type I diabetes mellitus | 2.2 | 0.048 |
| | Systemic lupus erythematosus | 2.2 | 0.046 |
| | Graft-versus-host disease | 1.5 | 0.046 |
| | Oxidative phosphorylation | 2.2 | 0.046 |
| | Ovarian steroidogenesis | 1.5 | 0.046 |
| | Herpes simplex virus 1 infection | 4 | 0.046 |
| | Inflammatory bowel disease | 1.5 | 0.046 |
| | Autoimmune thyroid disease | 1.5 | 0.046 |
| | Drug metabolism-cytochrome P450 | 1.5 | 0.046 |
| | HIF-1 signaling pathway | 1.8 | 0.046 |
| | Pathways of neurodegeneration | 4.4 | 0.046 |
| | Viral myocarditis | 1.5 | 0.048 |
| | Diabetic cardiomyopathy | 2.6 | 0.048 |
| | Amyotrophic lateral sclerosis | 3.7 | 0.049 |
| | Carbon metabolism | 1.8 | 0.052 |
| | Alzheimer disease | 3.7 | 0.054 |
| | Drug metabolism – other enzymes | 1.5 | 0.054 |
| PI-IUGR | Viral carcinogenesis | 3.5 | 0.093 |
| | Insulin resistance | 2.7 | 0.098 |
| | Epstein-Barr virus infection | 3.5 | 0.098 |

**Table 4.3** Differentially expressed gene loci in the semitendinosus muscle of MI-IUGR and PI-IUGR neonatal lambs relative to uncompromised control lambs.

| Group | Gene ID | Log Fold Change | *P*adj |
|---|---|---|---|
| MI-IUGR | *β2-microglobulin* | -1.33 | 0.015 |
| | *60S ribosomal protein L37a* | -2.31 | 0.015 |
| | *S100A2* | -1.38 | 0.021 |
| | *Proteasome maturation protein-like* | -1.78 | 0.043 |
| | *IFI6* | -2.02 | 0.071 |
| | *ENO3* | -0.63 | 0.071 |
| | *ISG15* | -1.99 | 0.071 |
| | *Caspase-14* | -1.31 | 0.071 |
| | *Phytanoyl-CoA dioxygenase, peroxisomal-like* | -4.28 | 0.073 |
| | *RAMP1* | -1.03 | 0.075 |
| | *CSTL1* | 3.69 | 0.075 |
| | *GCNT1* | -1.14 | 0.098 |
| PI-IUGR | *NADH-ubiquinone oxidoreductase chain 5-like protein* | 3.40 | 0.003 |
| | *PGAM1* | 0.80 | 0.030 |
| | *S100A2* | -1.42 | 0.081 |

# CHAPTER 5 – Hindlimb tissue composition shifts between the fetal and juvenile stages in the lamb

This chapter was published in *Translational Animal Science,* which is a peer-reviewed publication as part of the Western Section Proceedings.

Zena M Hicks and others, Hindlimb tissue composition shifts between the fetal and juvenile stages in the lamb, *Translational Animal Science*, Volume 5, Issue Supplement_S1, December 2021, Pages S38–S40, https://doi.org/10.1093/tas/txab164

## Abstract

Knowing the composition of the hindlimb in lambs is important for understanding their growth progression and for studying hindlimb-specific metabolic rates, but there is currently no literature that reports the tissue composition of the hindlimb of the or juvenile lamb, which we postulate changes substantially between these stages. Therefore, our objective was to determine the percentages of skin, bone, connective tissue, fat, and muscle in the hindlimb of fetal and juvenile lambs. To accomplish this, fetal (130 d of gestational age) and juvenile (60 d of age) lambs were necropsied, and hindlimbs were separated at the acetabulum joint and weighed. Hindlimbs were then dissected into skin, bone, connective tissue, fat, and muscle components. The mass of each component was measured, and its percentage of the hindlimb was calculated. Percentage of muscle was less ($P < 0.05$) for fetal hindlimbs (40.4% ± 0.7%) than for juvenile hindlimbs (63.9% ± 1.0%). Likewise, percentage of fat was less ($P < 0.05$) for fetal hindlimbs (0.08% ± 0.02%) than for juvenile hindlimbs (5.2% ± 0.7%). The percentage of connective tissue was greater ($P < 0.05$) for fetal hindlimbs (7.0% ± 0.7%) than for juvenile hindlimbs (4.8% ± 0.5%). The percentages of skin and bone did not differ between fetal and juvenile hindlimbs. These findings demonstrate that the composition of the hindlimb is

changes substantially as the animal grows and ages. Understanding these differences in composition help to explain differences in hindlimb metabolic rates in fetal and juvenile lambs, which is a major component of whole-body glucose and lipid homeostasis.

**Introduction**

The hindlimb plays an important role in glucose and lipid homeostasis and metabolic health of humans and animals (Bonen et al., 1994). Moreover, its advantageous location and structure make it useful for studying glucose metabolism under pathogenic conditions (Gardner et al., 2003; Rozance et al., 2018a; Caitlin N. Cadaret et al., 2019; Yates et al., 2019). Although an important driver of insulin sensitive metabolism due to its muscle mass, the hindlimb also contains substantial non-muscle tissues. However, exact composition of tissues in the hindlimb of lambs has not been studied at any stage of development despite the popularity of sheep as a biomedical model for growth and metabolism (Beede et al., 2019; Hamernik, 2019). In fact, only recently has the tissue composition of the beef hindlimb been reported (PAPER DR. YATES WAS TALKING ABOUT). Skeletal muscle is markedly more insulin-sensitive than most other tissues, and thus not knowing the tissue composition of the hindlimb is a barrier to understanding its role in metabolic homeostasis (Brown, 2014b; Deshmukh, 2016).

When comparing fetal and juvenile animals, there are clear differences in both size and body composition. Fetal lambs have limited nutrient uptake that is reliant on maternal nutrient availability and placental functionality (Brett et al., 2014). Comparatively, juvenile lambs typically have *ad libitum* nutrient-dense diets, whether from milk while nursing or from calorie-dense grain diets. Adequate or even excess

calories from these diets can cause accumulation of triacylglycerides in the adipocyte (Dashty, 2013), and thus increased fat deposition. Additionally, hindlimb muscle is minimally utilized *in utero*, whereas juvenile lambs persistently utilize hindlimbs for locomotion causing the muscle to undergo hypertrophic growth (McGlory and Phillips, 2015). Therefore, the objective of this project was to determine the tissue composition of the hindlimb from fetal and juvenile lambs and to compare their differences. Our hypothesis was that the composition of tissues in the hindlimbs will reflect greater muscle hypertrophy and fat deposition in the juvenile stage due to the different environment and nutritional opportunities.

**Materials and Methods**

These studies were approved by the Institutional Animal Care and Use Committee at the University of Nebraska-Lincoln, which is accredited by AAALAC International. Fetal (n = 10) and juvenile (n = 10) hindlimbs were collected at necropsy, exsanguinated, and dissected into skin, bone, connective tissue, fat, and muscle components. Briefly, whole-body weights were recorded for the fetuses at 130 days of gestational age and lambs at 60 days of age, and the hindlimb was then removed at the acetabulum joint. Hindlimbs were then hung to remove the remaining blood. Each hindlimb was then dissected by hand into its component parts, which were then weighed. The percentage of each component was calculated by dividing its weight by the weight of the hindlimb. Data were analyzed as an ANOVA using the PROC MIXED function of SAS version 9.4 (SAS Institute, Inc., Cary, NC) to identify the effects of age. Lamb was the experimental

unit, and all data are presented as mean ± standard error. Differences between means were identified by *P*-values ≤ 0.05.

**Results**

Hindlimb mass was greater ($P < 0.05$) for juvenile lambs than for fetuses (**Table 5.1**). Hindlimb mass/body mass was less ($P < 0.05$) for juvenile lambs than for fetuses. Hindlimb skin mass was greater ($P < 0.05$) for juvenile lambs than for fetuses, but skin mass/hindlimb mass did not differ between juvenile lambs and fetuses. The percentage of skin in the hindlimb did not differ between juvenile lambs and fetuses. Bone mass was greater ($P < 0.05$) for juvenile lambs than for fetuses, but bone mass/hindlimb mass did not differ between juvenile lambs and fetuses. Connective tissue mass was greater ($P < 0.01$) for juvenile lambs than for fetuses, however, connective tissue mass/hindlimb mass was less ($P < 0.05$) for juvenile lambs than for fetuses. Fat mass was greater ($P < 0.05$) for juvenile lambs than for fetuses, and the fat mass/hindlimb mass was also greater ($P < 0.05$) for juvenile lambs than for fetuses. Muscle mass was greater ($P < 0.05$) for juvenile lambs than for fetuses, and muscle mass/hindlimb mass was also greater ($P < 0.05$) for juvenile lambs than for fetuses.

**Discussion**

In this study, we show that hindlimbs from lambs contain a higher percentage of muscle and fat at the juvenile stage compared to their fetal stage. Conversely, fetal hindlimbs contain a higher percentage of connective tissue than juvenile lambs. Moreover, the percentage of skin and bone in the hindlimbs did not change as the lambs

grew from fetuses to juveniles. Together these finding demonstrate that composition of the hindlimb changes substantially as the lamb ages.

By the time the lambs reach the juvenile stage, their hindlimb has developed markedly more muscle than was present in utero. On average, juvenile hindlimbs contained well over 800 g more muscle, which was equivalent to an 8.6-fold increase. Because the hindlimb itself grew only 5.3-fold, this represents a nearly 60% increase in hindlimb muscle percentage between the fetal and juvenile stage. We speculate that this is due to the differences in locomotion and the associated structural development in juvenile lambs compared to fetuses. Indeed, fetal lambs contract their hindlimb muscles at only a fraction of rate of offspring and therefore do not require as much metabolically-expensive skeletal muscle. However, juvenile lambs increasingly utilize their hindlimb muscles, which fosters muscle hypertrophy (Bamman et al., 2018).

In addition to muscle, juvenile lambs had developed a substantially greater percentage of hindlimb fat compared to fetal lambs. The additional 80 g of fat contained in the juvenile hindlimb equates to a 6,400% increase in fat percentage compared to fetuses, which were largely devoid of fat. We postulate that this is likely the result of increased nutrient availability for the juvenile lamb compared to the fetus. Fetal lambs typically only receive a certain level of nutrients from maternal circulation via that placenta and thus have a finite supply of energy. Juvenile lambs, however are often privy to a calorie-dense diet that may exceed their requirements for growth. Excess postnatal nutrient consumption presumably leads to greater fat deposition.

As hindlimb proportions of muscle and fat increased with age, the proportion of connective tissue fell. Indeed, the 3.3-fold increase in hindlimb connective tissue mass

between the fetal and juvenile stage compared to the 5.3-fold increase in hindlimb mass equates to a 45% reduction in connective tissue proportion of the hindlimb. This rather striking reduction is likely due more to faster relative expansion of muscle and fat rather than slower connective tissue expansion.

As expected, the hindlimbs of juvenile lambs contained more skin and bone mass than fetuses, but the percentage of bone and skin that composed the hindlimb did not change between the fetal to juvenile stages. This shows that hindlimb bone and skin continue to grow proportionally to the growth of the hindlimb itself, and thus; increased movement and nutrient intake do not necessarily affect how these nutrients are partitioned to skin and bone growth.

**Implications**

Numerous studies have focused on insulin-sensitive glucose metabolism in the hindlimb of lambs at several different stages of life without understanding the hindlimb tissue composition and how it changes with age. Thus, the present study is the first to demonstrate the changing composition of the hindlimb as lambs progress from the fetal stage to the juvenile stage. Identifying hindlimb composition will increase the accuracy of interpreting results when studying hindlimb-specific or even whole-body glucose metabolism. Moreover, documenting the changes in composition increases our understanding of the changes in metabolism between fetuses and offspring. Specifically, knowing the composition of skeletal muscle and fat, which are both insulin-sensitive tissues involved in glucose uptake, and how they vary between the fetal and juvenile hindlimb help explain previously observed differences in glucose metabolism.

**Tables and Figures**

**Table 5.1** Composition of hindlimb tissues in fetal and juvenile lambs.

| | Fetal | Juvenile | *P*-value[1] |
|---|---|---|---|
| Mass (g) | | | |
| Hindlimb | 281 ± 27 | 1512 ± 57 | <0.01 |
| Skin | 64.9 ± 3.5 | 383.6 ± 40.1 | <0.01 |
| Bone | 68.4 ± 11.6 | 336.3 ± 14.5 | <0.01 |
| Connective Tissue | 21.8 ± 3.4 | 73.0 ± 7.9 | <0.01 |
| Fat | 0.3 ± 0.2 | 80.5 ± 10.8 | <0.01 |
| Muscle | 110 ± 12.0 | 951 ± 45 | <0.01 |
| Percentage (%) | | | |
| Hindlimb/BW | 9.2 ± 0.2 | 7.1 ± 0.2 | <0.01 |
| Skin/HL | 23.4 ± 1.1 | 25.5 ± 1.7 | NS |
| Bone/HL | 23.7 ± 2.2 | 22.3 ± 0.8 | NS |
| Connective Tissue/HL | 7.0 ± 0.7 | 4.8 ± 0.5 | 0.02 |
| Fat/HL | 0.1 ± 0.02 | 5.2 ± 0.70 | <0.01 |
| Muscle/HL | 40.4 ± 0.7 | 63.9 ± 1.0 | <0.01 |

[1]NS = not significant ($P > 0.05$)

# CHAPTER 6 – Future Implications

From these studies, we were able to further elucidate the role of maternofetal inflammation in the origin of growth and metabolic deficits experienced in the IUGR fetus. This underlying inflammation creates deficits in placental oxygen transfer, which creates a hypoxic environment for the growing fetus. This study helped solidify the role of hypoxemia in the developmental programming in the IUGR fetus. Thus, future research could look to mitigate the effects of maternofetal inflammation by supplementing pregnant ewes before, during, or after stress with a nutraceutical anti-inflammatory compound to reduce the deleterious effects of inflammation. Potential compounds of interest could include ω-3 polyunsaturated fatty acids, niacin, zinc, Vitamin D, which could target the NF-κB pathway and mitigate inflammation.

Another potential pathway to target in this model could be a nutraceutical compounds that could help increase blood flow. Although this may not mitigate the impact of lesser vasculature developed in the IUGR placenta, supplementing ewes with a supplement like beet juice that is high in nitric oxide could work as a vasodilator and potentially increase the blood flow to the placenta. If this is given earlier in gestation either during or shortly after LPS exposure, the increased blood flow to the uterus and placenta could improve vasculature during critical placenta development. If it is supplemented in late gestation after the stress has occurred, increasing the blood flow could help reduce the oxygen gradient to the stressed fetus, potentially lessening the effects of hypoxemia. Other potential compounds of interest include anthocyanin, curcumin, or capsaicin.

Additional research into the transcriptomic changes across different tissues for this study is also warranted. This data set would allow a greater number of samples and allow us to look at the molecular changes that could be occurring with exposure to maternofetal inflammation earlier in gestation. Looking into more tissues including the skeletal muscle, liver, and pancreatic tissues could help provide a better understanding into both growth and metabolic changes that could be occurring and elucidate a clearer pathway to target to help mitigate the effects of mid-gestation maternofetal inflammation.

Finally, completing further analyses into the placenta and cotyledons collected from this study including analyses focusing on the vasculature development, structural changes, metabolic parameters, cytokine and cytokine receptor content, and transporter expression in the placenta and/or cotyledons could help bolster our understanding of how the placenta itself is impacted by mid-gestation maternofetal inflammation. Transcriptomic data from the placenta may also highlight pathways by which the placenta in impacted to provide a target for therapeutic compounds to try to prevent IUGR from occurring.

## LITERATURE CITED

Aaltonen, R., T. Heikkinen, K. Hakala, K. Laine, and A. Alanen. 2005. Transfer of proinflammatory cytokines across term placenta. Obstet. Gynecol. 106:802–807. doi:10.1097/01.AOG.0000178750.84837.ed.

Adams, M. B., and I. C. McMillen. 2000. Actions of hypoxia on catecholamine synthetic enzyme mRNA expression before and after development of adrenal innervation in the sheep fetus. J. Physiol. 529:519–532. doi:10.1111/j.1469-7793.2000.00519.x. Available from: https://pubmed.ncbi.nlm.nih.gov/11118487

Akashi, K., D. Traver, T. Miyamoto, and I. L. Weissman. 2000. A clonogenic common myeloid progenitor that gives rise to all myeloid lineages. Nature. 404:193–197. doi:10.1038/35004599.

Al-Khalili, L., K. Bouzakri, S. Glund, F. Lönnqvist, H. A. Koistinen, and A. Krook. 2006. Signaling specificity of interleukin-6 action on glucose and lipid metabolism in skeletal muscle. Mol. Endocrinol. 20:3364–3375. doi:10.1210/me.2005-0490.

Alisi, A., N. Panera, C. Agostoni, and V. Nobili. 2011. Intrauterine Growth Retardation and Nonalcoholic Fatty Liver Disease in Children. D. Jezova, editor. Int. J. Endocrinol. 2011:1–8. doi:10.1155/2011/269853. Available from: https://doi.org/10.1155/2011/269853

Alisjahbana, B., D. S. Rivami, L. Octavia, N. Susilawati, M. Pangaribuan, A. Alisjahbana, and A. Diana. 2019. Intrauterine growth retardation (IUGR) as determinant and environment as modulator of infant mortality and morbidity: The Tanjungsari Cohort Study in Indonesia. Asia Pac. J. Clin. Nutr. 28:S17–S31. Available from: https://search.informit.org/doi/10.3316/ielapa.194086733441998

Allen, R. E., and L. K. Boxhorn. 1989. Regulation of skeletal muscle satellite cell proliferation and differentiation by transforming growth factor-beta, insulin-like growth factor I, and fibroblast growth factor. J. Cell. Physiol. 138:311–315. doi:10.1002/jcp.1041380213. Available from: https://onlinelibrary.wiley.com/doi/10.1002/jcp.1041380213

Allen, R. E., L. S. Luiten, and M. V Dodson. 1985. Effect of Insulin and Linoleic Acid on Satellite Cell Differentiation. J. Anim. Sci. 60:1571–1579. doi:10.2527/jas1985.6061571x. Available from: https://doi.org/10.2527/jas1985.6061571x

Allen, R. E., R. A. Merkel, and R. B. Young. 1979. Cellular aspects of muscle growth: myogenic cell proliferation. J. Anim. Sci. 49:115–127.

doi:10.2527/jas1979.491115x.

Alvarez, A. M., C. DeOcesano-Pereira, C. Teixeira, and V. Moreira. 2020. IL-1β and TNF-α Modulation of Proliferated and Committed Myoblasts: IL-6 and COX-2-Derived Prostaglandins as Key Actors in the Mechanisms Involved. Cells. 9:2005. doi:10.3390/cells9092005. Available from: https://www.mdpi.com/2073-4409/9/9/2005

An, X., T. Li, N. Chen, H. Wang, X. Wang, and Y. Ma. 2021. PGAM1 regulates the glycolytic metabolism of SCs in tibetan sheep and its influence on the development of SCs. Gene. 804:145897. doi:10.1016/j.gene.2021.145897.

Anton, L., A. G. Brown, S. Parry, and M. A. Elovitz. 2012. Lipopolysaccharide induces cytokine production and decreases extravillous trophoblast invasion through a mitogen-activated protein kinase-mediated pathway: possible mechanisms of first trimester placental dysfunction. Hum. Reprod. 27:61–72. doi:10.1093/humrep/der362. Available from: https://doi.org/10.1093/humrep/der362

Aucott, S. W., P. K. Donohue, and F. J. Northington. 2004. Increased Morbidity in Severe Early Intrauterine Growth Restriction. J. Perinatol. 24:435–440. doi:10.1038/sj.jp.7211116. Available from: https://doi.org/10.1038/sj.jp.7211116

Baker, B. C., A. E. P. Heazell, C. Sibley, R. Wright, H. Bischof, F. Beards, T. Guevara, S. Girard, and R. L. Jones. 2021. Hypoxia and oxidative stress induce sterile placental inflammation in vitro. Sci. Rep. 11:7281. doi:10.1038/s41598-021-86268-1. Available from: http://www.ncbi.nlm.nih.gov/pubmed/33790316

Bamman, M. M., B. M. Roberts, and G. R. Adams. 2018. Molecular regulation of exercise-induced muscle fiber hypertrophy. Cold Spring Harb. Perspect. Med. 8:1–15. doi:10.1101/cshperspect.a029751.

Barker, D. J., C. N. Hales, C. H. Fall, C. Osmond, K. Phipps, and P. M. Clark. 1993. Type 2 (non-insulin-dependent) diabetes mellitus, hypertension and hyperlipidaemia (syndrome X): relation to reduced fetal growth. Diabetologia. 36:62–67. doi:10.1007/BF00399095.

Barnes, T. L., C. N. Cadaret, K. A. Beede, T. B. Schmidt, J. L. Petersen, and D. T. Yates. 2019. Hypertrophic muscle growth and metabolic efficiency were impaired by chronic heat stress, improved by zilpaterol supplementation, and not affected by ractopamine supplementation in feedlot lambs1. J. Anim. Sci. 97:4101–4113. doi:10.1093/jas/skz271. Available from: https://academic.oup.com/jas/article/97/10/4101/5549707

Baron, A. D., G. Brechtel, P. Wallace, and S. V Edelman. 1988. Rates and tissue sites of

non-insulin- and insulin-mediated glucose uptake in humans. Am. J. Physiol. Metab. 255:E769–E774. doi:10.1152/ajpendo.1988.255.6.E769. Available from: https://doi.org/10.1152/ajpendo.1988.255.6.E769

Beard, J. K. 2020. Quantifying Metabolic Flexibility in Cow-Calf Systems. University of Nebraska.

Becar, M., and A. Kasi. 2023. Physiology, MHC Class I. StatPearls. Available from: https://www.ncbi.nlm.nih.gov/books/NBK556022/

Beede, K. A., S. W. Limesand, J. L. Petersen, and D. T. Yates. 2019. Real supermodels wear wool: Summarizing the impact of the pregnant sheep as an animal model for adaptive fetal programming. Anim. Front. 9:34–43. doi:10.1093/af/vfz018.

Beer, H. N. 2022. Continuous Video Monitoring of Zoo Cheetahs Demonstrates Differential Engagement Patterns for Six Different Types of Environmental Enrichment; Placental Insufficiency Indicators Improve in Intrauterine Growth-Restricted Fetal Sheep Receiving Daily ω-3 Pol. ProQuest Dissertations Publishing.

Beer, H. N., T. A. Lacey, R. L. Gibbs, M. S. Most, Z. M. Hicks, P. C. Grijalva, J. L. Petersen, and D. T. Yates. 2021. Placental insufficiency improves when intrauterine growth-restricted fetal sheep are administered daily ω-3 polyunsaturated fatty acid infusions. Transl. Anim. Sci. 5:S6–S10. doi:10.1093/tas/txab166.

Behrens, K., and W. S. Alexander. 2018. Cytokine control of megakaryopoiesis. Growth Factors. 36:89–103. doi:10.1080/08977194.2018.1498487.

Bérard, J., M. Kreuzer, and G. Bee. 2008. Effect of litter size and birth weight on growth, carcass and pork quality, and their relationship to postmortem proteolysis1. J. Anim. Sci. 86:2357–2368. doi:10.2527/jas.2008-0893. Available from: https://doi.org/10.2527/jas.2008-0893

Blanco, A., and G. Blanco. 2017. Chapter 14 - Carbohydrate Metabolism. In: A. Blanco and G. B. T.-M. B. Blanco, editors. Academic Press. p. 283–323. Available from: https://www.sciencedirect.com/science/article/pii/B9780128035504000148

Bodell, P. W., E. Kodesh, F. Haddad, F. P. Zaldivar, D. M. Cooper, and G. R. Adams. 2009. Skeletal muscle growth in young rats is inhibited by chronic exposure to IL-6 but preserved by concurrent voluntary endurance exercise. J. Appl. Physiol. 106:443–453. doi:10.1152/japplphysiol.90831.2008. Available from: https://doi.org/10.1152/japplphysiol.90831.2008

Boehmer, B. H., S. W. Limesand, and P. J. Rozance. 2017. The impact of IUGR on

pancreatic islet development and β-cell function. J. Endocrinol. 235:R63–R76. doi:10.1530/JOE-17-0076. Available from: https://joe.bioscientifica.com/view/journals/joe/235/2/JOE-17-0076.xml

Bonen, A., M. G. Clark, and E. J. Henriksen. 1994. Experimental approaches in muscle metabolism: Hindlimb perfusion and isolated muscle incubations. Am. J. Physiol. - Endocrinol. Metab. 266. doi:10.1152/ajpendo.1994.266.1.e1.

Boscá, L., and C. Corredor. 1984. Is phosphofructokinase the rate-limiting step of glycolysis? Trends Biochem. Sci. 9:372–373. doi:10.1016/0968-0004(84)90214-7. Available from: https://www.sciencedirect.com/science/article/pii/0968000484902147

Brett, K. E., Z. M. Ferraro, J. Yockell-Lelievre, A. Gruslin, and K. B. Adamo. 2014. Maternal–Fetal nutrient transport in pregnancy pathologies: The role of the placenta. Int. J. Mol. Sci. 15:16153–16185. doi:10.3390/ijms150916153.

Briana, D. D., and A. Malamitsi-Puchner. 2009. Intrauterine growth restriction and adult disease: the role of adipocytokines. Eur. J. Endocrinol. 160:337–347. doi:10.1530/EJE-08-0621. Available from: https://eje.bioscientifica.com/view/journals/eje/160/3/337.xml

Brooks, A. N., I. S. Currie, F. Gibson, and G. B. Thomas. 1992. Neuroendocrine regulation of sheep fetuses. J. Reprod. Fertil. Suppl. 45:69–84. Available from: http://europepmc.org/abstract/MED/1338958

Brown, L. D. 2014a. Endocrine regulation of fetal skeletal muscle growth: impact on future metabolic health. J. Endocrinol. 221:R13–R29. doi:10.1530/JOE-13-0567. Available from: https://pubmed.ncbi.nlm.nih.gov/24532817

Brown, L. D. 2014b. Future Metabolic Health. J Endocrinol. 221:1–27. doi:10.1530/JOE-13-0567.Endocrine.

Brown, Laura D., M. Davis, S. Wai, S. R. Wesolowski, W. W. Hay, S. W. Limesand, and P. J. Rozance. 2016. Chronically Increased Amino Acids Improve Insulin Secretion, Pancreatic Vascularity, and Islet Size in Growth-Restricted Fetal Sheep. Endocrinology. 157:3788–3799. doi:10.1210/en.2016-1328. Available from: https://academic.oup.com/endo/article-lookup/doi/10.1210/en.2016-1328

Brown, L. D., P. J. Rozance, J. L. Bruce, J. E. Friedman, W. W. Hay, and S. R. Wesolowski. 2015. Limited capacity for glucose oxidation in fetal sheep with intrauterine growth restriction. Am. J. Physiol. Integr. Comp. Physiol. 309:R920–R928. doi:10.1152/ajpregu.00197.2015. Available from: https://doi.org/10.1152/ajpregu.00197.2015

Brown, L. D., P. J. Rozance, S. R. Thorn, J. E. Friedman, and W. W. Hay. 2012. Acute supplementation of amino acids increases net protein accretion in IUGR fetal sheep. Am. J. Physiol. Metab. 303:E352–E364. doi:10.1152/ajpendo.00059.2012. Available from: https://www.physiology.org/doi/10.1152/ajpendo.00059.2012

Brown, Laura D, S. R. Wesolowski, J. Kailey, S. Bourque, A. Wilson, S. E. Andrews, W. W. Hay, and P. J. Rozance. 2016. Chronic Hyperinsulinemia Increases Myoblast Proliferation in Fetal Sheep Skeletal Muscle. Endocrinology. 157:2447–2460. doi:10.1210/en.2015-1744. Available from: https://doi.org/10.1210/en.2015-1744

Bruce, C. R., and D. J. Dyck. 2004. Cytokine regulation of skeletal muscle fatty acid metabolism: effect of interleukin-6 and tumor necrosis factor-α. Am. J. Physiol. Metab. 287:E616–E621. doi:10.1152/ajpendo.00150.2004. Available from: https://doi.org/10.1152/ajpendo.00150.2004

Burton, G. J., and E. Jauniaux. 2018. Pathophysiology of placental-derived fetal growth restriction. Am. J. Obstet. Gynecol. 218:S745–S761. doi:https://doi.org/10.1016/j.ajog.2017.11.577. Available from: https://www.sciencedirect.com/science/article/pii/S000293781732344X

Cadaret, C N, K. A. Beede, E. M. Merrick, T. L. Barnes, J. D. Loy, and D. T. Yates. 2017. Maternal inflammation at mid-gestation in pregnant rats impairs fetal muscle growth and development at term. Transl. Anim. Sci. 1:202–206.

Cadaret, Caitlin N., K. A. Beede, H. E. Riley, and D. T. Yates. 2017. Acute exposure of primary rat soleus muscle to zilpaterol HCl (β2 adrenergic agonist), TNFα, or IL-6 in culture increases glucose oxidation rates independent of the impact on insulin signaling or glucose uptake. Cytokine. 96:107–113. doi:10.1016/j.cyto.2017.03.014. Available from: https://www.sciencedirect.com/science/article/pii/S1043466617300777

Cadaret, C. N., E. M. Merrick, T. L. Barnes, K. A. Beede, R. J. Posont, J. L. Petersen, and D. T. Yates. 2018. Sustained maternal inflammation during the early third trimester yields fetal adaptations that impair subsequent skeletal muscle growth and glucose metabolism in sheep1. Transl. Anim. Sci. 2:S14–S18. doi:10.1093/tas/txy047. Available from: https://doi.org/10.1093/tas/txy047

Cadaret, Caitlin N., E. M. Merrick, T. L. Barnes, K. A. Beede, R. J. Posont, J. L. Petersen, and D. T. Yates. 2019. Sustained maternal inflammation during the early third-trimester yields intrauterine growth restriction, impaired skeletal muscle glucose metabolism, and diminished β-cell function in fetal sheep. J. Anim. Sci. 97:4822–4833. doi:10.1093/jas/skz321.

Cadaret, Caitlin N, R. J. Posont, K. A. Beede, H. E. Riley, J. D. Loy, and D. T. Yates. 2019a. Maternal inflammation at midgestation impairs subsequent fetal myoblast

function and skeletal muscle growth in rats, resulting in intrauterine growth restriction at term1. Transl. Anim. Sci. 3:867–876. doi:10.1093/tas/txz037. Available from: https://doi.org/10.1093/tas/txz037

Cadaret, Caitlin N, R. J. Posont, R. M. Swanson, J. K. Beard, T. L. Barnes, K. A. Beede, J. L. Petersen, and D. T. Yates. 2019b. Intermittent maternofetal O2 supplementation during late gestation rescues placental insufficiency-induced intrauterine growth restriction and metabolic pathologies in the neonatal lamb. Transl. Anim. Sci. 3:1696–1700. doi:10.1093/tas/txz060. Available from: https://doi.org/10.1093/tas/txz060

Cadaret, C. N., R. J. Posont, R. M. Swanson, J. K. Beard, R. L. Gibbs, T. L. Barnes, E. S. Marks-Nelson, J. L. Petersen, and D. T. Yates. 2022. Intermittent maternofetal oxygenation during late gestation improved birthweight, neonatal growth, body symmetry, and muscle metabolism in intrauterine growth-restricted lambs. J. Anim. Sci. 100:skab358. doi:10.1093/jas/skab358. Available from: https://doi.org/10.1093/jas/skab358

Campbell, I. L., M. V Hobbs, J. Dockter, M. B. Oldstone, and J. Allison. 1994. Islet inflammation and hyperplasia induced by the pancreatic islet-specific overexpression of interleukin-6 in transgenic mice. Am. J. Pathol. 145:157–166. Available from: https://pubmed.ncbi.nlm.nih.gov/8030746

Cejas, R. B., V. Lorenz, Y. C. Garay, and F. J. Irazoqui. 2019. Biosynthesis of O-N-acetylgalactosamine glycans in the human cell nucleus. J. Biol. Chem. 294:2997–3011. doi:10.1074/jbc.RA118.005524. Available from: http://www.ncbi.nlm.nih.gov/pubmed/30591584

Chauhan, M., A. Betancourt, M. Balakrishnan, U. Yallampalli, Y. Dong, K. Fox, M. Belfort, and C. Yallampalli. 2016. Impaired Vasodilatory Responses of Omental Arteries to CGRP Family Peptides in Pregnancies Complicated by Fetal Growth Restriction. J. Clin. Endocrinol. Metab. 101:2984–2993. doi:10.1210/jc.2016-1798.

Cheema, I. R., C. Hermann, S. Postell, and P. Barnes. 2000. Effect of chronic excess of tumour necrosis factor-alpha on contractile proteins in rat skeletal muscle. Cytobios. 103:169–76. Available from: http://www.ncbi.nlm.nih.gov/pubmed/11086712

Chen, X., A. C. Kelly, D. T. Yates, A. R. Macko, R. M. Lynch, and S. W. Limesand. 2017. Islet adaptations in fetal sheep persist following chronic exposure to high norepinephrine. J. Endocrinol. 232:285–295. doi:10.1530/JOE-16-0445. Available from: https://pubmed.ncbi.nlm.nih.gov/27888197

Cheriyath, V., K. B. Glaser, J. F. Waring, R. Baz, M. A. Hussein, and E. C. Borden.

2007. G1P3, an IFN-induced survival factor, antagonizes TRAIL-induced apoptosis in human myeloma cells. J. Clin. Invest. 117:3107–3117. doi:10.1172/JCI31122.

Chisaka, T., M. Mogi, H. Nakaoka, H. Kan-No, K. Tsukuda, X.-L. Wang, H.-Y. Bai, B.-S. Shan, M. Kukida, J. Iwanami, T. Higaki, E.-I. Ishii, and M. Horiuchi. 2016. Low-Protein Diet-Induced Fetal Growth Restriction Leads to Exaggerated Proliferative Response to Vascular Injury in Postnatal Life. Am. J. Hypertens. 29:54–62. doi:10.1093/ajh/hpv072. Available from: http://www.ncbi.nlm.nih.gov/pubmed/26002925

Chu, A., Y. Dhindsa, M. S. Sim, M. Altendahl, and I. Tsui. 2020. Prenatal intrauterine growth restriction and risk of retinopathy of prematurity. Sci. Rep. 10:17591. doi:10.1038/s41598-020-74600-0. Available from: https://doi.org/10.1038/s41598-020-74600-0

Cotechini, T., and C. H. Graham. 2015. Aberrant maternal inflammation as a cause of pregnancy complications: A potential therapeutic target? Placenta. 36:960–966. doi:10.1016/j.placenta.2015.05.016. Available from: https://linkinghub.elsevier.com/retrieve/pii/S0143400415009480

D'Cunha, J., E. J. Knight, A. L. Haas, R. L. Truitt, and E. C. Borden. 1996. Immunoregulatory properties of ISG15, an interferon-induced cytokine. Proc. Natl. Acad. Sci. U. S. A. 93:211–215. doi:10.1073/pnas.93.1.211.

Dai, C., C.-G. Huh, S. S. Thorgeirsson, and Y. Liu. 2005. β-Cell-Specific Ablation of the Hepatocyte Growth Factor Receptor Results in Reduced Islet Size, Impaired Insulin Secretion, and Glucose Intolerance. Am. J. Pathol. 167:429–436. doi:10.1016/S0002-9440(10)62987-2. Available from: https://linkinghub.elsevier.com/retrieve/pii/S0002944010629872

Darendeliler, F. 2019. IUGR: Genetic influences, metabolic problems, environmental associations/triggers, current and future management. Best Pract. Res. Clin. Endocrinol. Metab. 33:101260. doi:10.1016/j.beem.2019.01.001. Available from: https://linkinghub.elsevier.com/retrieve/pii/S1521690X1930003X

Dashty, M. 2013. A quick look at biochemistry: Carbohydrate metabolism. Clin. Biochem. 46:1339–1352. doi:10.1016/j.clinbiochem.2013.04.027. Available from: http://dx.doi.org/10.1016/j.clinbiochem.2013.04.027

Davis, M. A., L. E. Camacho, M. J. Anderson, N. R. Steffens, A. L. Pendleton, A. C. Kelly, and S. W. Limesand. 2020. Chronically elevated norepinephrine concentrations lower glucose uptake in fetal sheep. Am. J. Physiol. Integr. Comp. Physiol. 319:R255–R263. doi:10.1152/ajpregu.00365.2019. Available from: https://journals.physiology.org/doi/10.1152/ajpregu.00365.2019

Davis, M. A., L. E. Camacho, A. L. Pendleton, A. T. Antolic, R. I. Luna-Ramirez, A. C. Kelly, N. R. Steffens, M. J. Anderson, and S. W. Limesand. 2021. Augmented glucose production is not contingent on high catecholamines in fetal sheep with IUGR. J. Endocrinol. 249:195–207. doi:10.1530/JOE-21-0071. Available from: https://joe.bioscientifica.com/view/journals/joe/249/3/JOE-21-0071.xml

Davis, T. A., and M. L. Fiorotto. 2009. Regulation of muscle growth in neonates. Curr. Opin. Clin. Nutr. Metab. Care. 12:78–85. doi:10.1097/MCO.0b013e32831cef9f. Available from: https://pubmed.ncbi.nlm.nih.gov/19057192

Defronzo, R. A., E. Jacot, E. Jequier, E. Mader, J. Wahren, and J. P. Felber. 1981. The Effect of Insulin on the Disposal of INtravenous Glucose Results from Indirect Calorimetry and Hepatic and Femoral Venous Catheterization. Diabetes. 30:1000–1007.

Desai, M., D. A. Gayle, E. Casillas, J. Boles, and M. G. Ross. 2009. Early undernutrition attenuates the inflammatory response in adult rat offspring. J. Matern. Fetal. Neonatal Med. 22:571–5. doi:10.1080/14767050902874105. Available from: http://www.ncbi.nlm.nih.gov/pubmed/19488945

Deshmukh, A. S. 2016. Insulin-stimulated glucose uptake in healthy and insulin-resistant skeletal muscle. Horm. Mol. Biol. Clin. Investig. 26:13–24. doi:10.1515/hmbci-2015-0041. Available from: https://www.degruyter.com/document/doi/10.1515/hmbci-2015-0041/html

Dickson, M. J., S. K. Kvidera, E. A. Horst, C. E. Wiley, E. J. Mayorga, J. Ydstie, G. A. Perry, L. H. Baumgard, and A. F. Keating. 2019. Impacts of chronic and increasing lipopolysaccharide exposure on production and reproductive parameters in lactating Holstein dairy cows. J. Dairy Sci. 102:3569–3583. doi:10.3168/jds.2018-15631. Available from: https://linkinghub.elsevier.com/retrieve/pii/S0022030219301316

Dinarello, C. A. 2000. Interleukin-18, a proinflammatory cytokine. Eur. Cytokine Netw. 11:483–486. Available from: http://europepmc.org/abstract/MED/11203186

Dixon, R., A. Hyman, E. Gurpide, I. Dyrenfurth, H. Cohen, E. Bowe, T. Engel, S. Daniel, S. James, and R. Vande Wiele. 1970. Feto-maternal transfer and production of cortisol in the sheep. Steroids. 16:771–789. doi:https://doi.org/10.1016/S0039-128X(70)80154-4. Available from: https://www.sciencedirect.com/science/article/pii/S0039128X70801544

Dobin, A., C. A. Davis, F. Schlesinger, J. Drenkow, C. Zaleski, S. Jha, P. Batut, M. Chaisson, and T. R. Gingeras. 2013. STAR: ultrafast universal RNA-seq aligner. Bioinformatics. 29:15–21. doi:10.1093/bioinformatics/bts635.

Dong, Y., W. Hou, J. Wei, and C. P. Weiner. 2009. Chronic Hypoxemia Absent Bacterial Infection Is One Cause of the Fetal Inflammatory Response Syndrome (FIRS). Reprod. Sci. 16:650–656. doi:10.1177/1933719109333662. Available from: https://link.springer.com/10.1177/1933719109333662

Dwyer, C. M., J. Conington, F. Corbiere, I. H. Holmøy, K. Muri, R. Nowak, J. Rooke, J. Vipond, and J.-M. Gautier. 2016. Invited review: Improving neonatal survival in small ruminants: science into practice. animal. 10:449–459. doi:DOI: 10.1017/S1751731115001974. Available from: https://www.cambridge.org/core/article/invited-review-improving-neonatal-survival-in-small-ruminants-science-into-practice/421D97546DA3DEDF22348876399051C7

Dyck, D. J., G. J. F. Heigenhauser, and C. R. Bruce. 2006. The role of adipokines as regulators of skeletal muscle fatty acid metabolism and insulin sensitivity. Acta Physiol. 186:5–16. doi:10.1111/j.1748-1716.2005.01502.x. Available from: https://doi.org/10.1111/j.1748-1716.2005.01502.x

Dzierzak, E., and A. Bigas. 2018. Blood Development: Hematopoietic Stem Cell Dependence and Independence. Cell Stem Cell. 22:639–651. doi:10.1016/j.stem.2018.04.015.

Edwards, A. K., S. M. McKnight, K. Askelson, J. R. McKnight, K. A. Dunlap, and M. C. Satterfield. 2020. Adaptive responses to maternal nutrient restriction alter placental transport in ewes. Placenta. 96:1–9. doi:https://doi.org/10.1016/j.placenta.2020.05.002. Available from: https://www.sciencedirect.com/science/article/pii/S0143400420301326

Eifert, A. W., M. E. Wilson, K. A. Vonnahme, L. E. Camacho, P. P. Borowicz, D. A. Redmer, S. Romero, S. Dorsam, J. Haring, and C. O. Lemley. 2015. Effect of melatonin or maternal nutrient restriction on vascularity and cell proliferation in the ovine placenta. Anim. Reprod. Sci. 153:13–21.

Eltzschig, H. K., and P. Carmeliet. 2011. Hypoxia and inflammation. N. Engl. J. Med. 364:656–65. doi:10.1056/NEJMra0910283. Available from: http://www.ncbi.nlm.nih.gov/pubmed/21323543

Flinn, T., D. O. Kleemann, A. M. Swinbourne, J. M. Kelly, A. C. Weaver, S. K. Walker, K. L. Gatford, K. L. Kind, and W. H. E. J. van Wettere. 2020. Neonatal lamb mortality: major risk factors and the potential ameliorative role of melatonin. J. Anim. Sci. Biotechnol. 11:107. doi:10.1186/s40104-020-00510-w. Available from: https://doi.org/10.1186/s40104-020-00510-w

Fricke, E. M., T. G. Elgin, H. Gong, J. Reese, K. N. Gibson-Corley, R. M. Weiss, K.

Zimmerman, N. C. Bowdler, K. M. Kalantera, D. A. Mills, M. A. Underwood, and S. J. McElroy. 2018. Lipopolysaccharide-induced maternal inflammation induces direct placental injury without alteration in placental blood flow and induces a secondary fetal intestinal injury that persists into adulthood. Am. J. Reprod. Immunol. 79:e12816. doi:https://doi.org/10.1111/aji.12816. Available from: https://doi.org/10.1111/aji.12816

Gagnon, R. 2003. Placental insufficiency and its consequences. Eur. J. Obstet. Gynecol. Reprod. Biol. 110:S99–S107. doi:https://doi.org/10.1016/S0301-2115(03)00179-9. Available from: https://www.sciencedirect.com/science/article/pii/S0301211503001799

Gamalinda, M., J. Jakovljevic, R. Babiano, J. Talkish, J. de la Cruz, and J. L. Woolford. 2013. Yeast polypeptide exit tunnel ribosomal proteins L17, L35 and L37 are necessary to recruit late-assembling factors required for 27SB pre-rRNA processing. Nucleic Acids Res. 41:1965–83. doi:10.1093/nar/gks1272. Available from: http://www.ncbi.nlm.nih.gov/pubmed/23268442

Ganassi, M., and P. S. Zammit. 2022. Involvement of muscle satellite cell dysfunction in neuromuscular disorders: Expanding the portfolio of satellite cell-opathies. Eur. J. Transl. Myol. 32. doi:10.4081/ejtm.2022.10064.

Gao, F., Y. Ni, Z. Luo, Y. Liang, Z. Yan, X. Xu, D. Liu, J. Wang, S. Zhu, and Z. Zhu. 2012. Atorvastatin Attenuates TNF-α–induced Increase of Glucose Oxidation Through PGC-1α Upregulation in Cardiomyocytes. J. Cardiovasc. Pharmacol. 59:500–506. doi:10.1097/FJC.0b013e31824c853c. Available from: http://journals.lww.com/00005344-201206000-00002

Gardner, D. S., D. A. Giussani, and A. L. Fowden. 2003. Hindlimb glucose and lactate metabolism during umbilical cord compression and acute hypoxemia in the late-gestation ovine fetus. Am. J. Physiol. - Regul. Integr. Comp. Physiol. 284:954–964. doi:10.1152/ajpregu.00438.2002.

Gastaldelli, A., M. Gaggini, and R. A. DeFronzo. 2017. Role of Adipose Tissue Insulin Resistance in the Natural History of Type 2 Diabetes: Results From the San Antonio Metabolism Study. Diabetes. 66:815–822. doi:10.2337/db16-1167. Available from: https://doi.org/10.2337/db16-1167

Gatford, K. L., R. A. Simmons, M. J. De Blasio, J. S. Robinson, and J. A. Owens. 2010. Review: Placental programming of postnatal diabetes and impaired insulin action after IUGR. Placenta. 31 Suppl:S60-5. doi:10.1016/j.placenta.2009.12.015. Available from: http://www.ncbi.nlm.nih.gov/pubmed/20096455

Gibbs, R. L. 2023. Adaptive Programming of IUGR Skeletal Muscle Growth and Metabolism. University of Nebraksa.

Gibbs, R. L., R. M. Swanson, J. K. Beard, T. B. Schmidt, J. L. Petersen, and D. T. Yates. 2020. Deficits in growth, muscle mass, and body composition following placental insufficiency-induced intrauterine growth restriction persisted in lambs at 60 d of age but were improved by daily clenbuterol supplementation. Transl. Anim. Sci. 4:S53–S57. doi:10.1093/tas/txaa097. Available from: https://doi.org/10.1093/tas/txaa097

Gibbs, R. L., R. M. Swanson, J. K. Beard, T. B. Schmidt, J. L. Petersen, and D. T. Yates. 2021. Deficits in skeletal muscle glucose metabolism and whole-body oxidative metabolism in the IUGR juvenile lamb are improved by daily treatment with clenbuterol. Transl. Anim. Sci. 5.

Gomez-Lopez, N., R. Romero, M. Arenas-Hernandez, B. Panaitescu, V. Garcia-Flores, T. N. Mial, A. Sahi, and S. S. Hassan. 2018. Intra-amniotic administration of lipopolysaccharide induces spontaneous preterm labor and birth in the absence of a body temperature change. J. Matern. neonatal Med. Off. J. Eur. Assoc. Perinat. Med. Fed. Asia Ocean. Perinat. Soc. Int. Soc. Perinat. Obstet. 31:439–446. doi:10.1080/14767058.2017.1287894.

Gondret, F., C. Larzul, S. Combes, and H. de Rochambeau. 2005. Carcass composition, bone mechanical properties, and meat quality traits in relation to growth rate in rabbits. J. Anim. Sci. 83:1526–1535. doi:10.2527/2005.8371526x.

Gould, S. J. 2013. Peroxisomal Metabolism. In: W. J. Lennarz and M. D. B. T.-E. of B. C. (Second E. Lane, editors. Academic Press, Waltham. p. 413–417. Available from: https://www.sciencedirect.com/science/article/pii/B9780123786302001043

Greenwood, P. L., and A. W. Bell. 2003. Consequences of intra-uterine growth retardation for postnatal growth, metabolism and pathophysiology. Reprod. Suppl. 61:195–206. doi:10.1530/biosciprocs.5.015.

Greenwood, P. L., and A. W. Bell. 2019. Developmental Programming and Growth of Livestock Tissues for Meat Production. Vet. Clin. North Am. Food Anim. Pract. 35:303–319. doi:10.1016/j.cvfa.2019.02.008. Available from: https://doi.org/10.1016/j.cvfa.2019.02.008

Greenwood, P. L., and L. M. Cafe. 2007. Prenatal and pre-weaning growth and nutrition of cattle: long-term consequences for beef production. Animal. 1:1283–1296. doi:https://doi.org/10.1017/S175173110700050X. Available from: https://www.sciencedirect.com/science/article/pii/S175173110700050X

Greenwood, P. L., L. M. Cafe, H. Hearnshaw, and D. W. Hennessy. 2005. Consequences of nutrition and growth retardation early in life for growth and composition of cattle and eating quality of beef. Recent Adv. Anim. Nutr. Aust. 15:183–195.

Greenwood, P. L., A. S. Hunt, J. W. Hermanson, and A. W. Bell. 2000. Effects of birth weight and postnatal nutrition on neonatal sheep: II. Skeletal muscle growth and development. J. Anim. Sci. 78:50. doi:10.2527/2000.78150x. Available from: https://doi.org/10.2527/2000.78150x

Haddad, F., F. Zaldivar, D. M. Cooper, and G. R. Adams. 2005. IL-6-induced skeletal muscle atrophy. J. Appl. Physiol. 98:911–917. doi:10.1152/japplphysiol.01026.2004. Available from: https://doi.org/10.1152/japplphysiol.01026.2004

Hales, C. N., and D. J. Barker. 1992. Type 2 (non-insulin-dependent) diabetes mellitus: the thrifty phenotype hypothesis*. Diabetologia. 35:595–601.

Hales, C. N., D. J. Barker, P. M. Clark, L. J. Cox, C. Fall, C. Osmond, and P. D. Winter. 1991. Fetal and infant growth and impaired glucose tolerance at age 64. BMJ. 303:1019–1022. doi:10.1136/bmj.303.6809.1019. Available from: http://www.bmj.com/

Hamernik, D. L. 2019. Farm animals are important biomedical models. Anim. Front. 9:3–5. doi:10.1093/af/vfz026.

Harms, R. Z., D. N. Yarde, Z. Guinn, K. M. Lorenzo-Arteaga, K. P. Corley, M. S. Cabrera, and N. E. Sarvetnick. 2015. Increased expression of IL-18 in the serum and islets of type 1 diabetics. Mol. Immunol. 64:306–312. doi:10.1016/j.molimm.2014.12.012. Available from: https://www.sciencedirect.com/science/article/pii/S016158901400354X

Hartmann, G., M. Tschöp, R. Fischer, C. Bidlingmaier, R. Riepl, K. Tschöp, H. Hautmann, S. Endres, and M. Toepfer. 2000. High altitude increases circulating interleukin-6, interleukin-1 receptor antagonist and C-reactive protein. Cytokine. 12:246–252. doi:10.1006/cyto.1999.0533.

Hicks, Z. M., H. N. Beer, N. J. Herrera, R. L. Gibbs, T. A. Lacey, P. C. Grijalva, M. A. Most, and D. T. Yates. 2021. Hindlimb tissue composition shifts between the fetal and juvenile stages in the lamb. Transl. Anim. Sci. 5:S38–S40. doi:10.1093/tas/txab164. Available from: https://doi.org/10.1093/tas/txab164

Hicks, Z. M., and D. T. Yates. 2021. Going Up Inflame: Reviewing the Underexplored Role of Inflammatory Programming in Stress-Induced Intrauterine Growth Restricted Livestock. Front. Anim. Sci. 2. doi:10.3389/fanim.2021.761421. Available from: https://www.frontiersin.org/articles/10.3389/fanim.2021.761421/full

Huang, D. W., B. T. Sherman, and R. A. Lempicki. 2009a. Bioinformatics enrichment

tools: paths toward the comprehensive functional analysis of large gene lists. Nucleic Acids Res. 37:1–13. doi:10.1093/nar/gkn923.

Huang, D. W., B. T. Sherman, and R. A. Lempicki. 2009b. Systematic and integrative analysis of large gene lists using DAVID bioinformatics resources. Nat. Protoc. 4:44–57. doi:10.1038/nprot.2008.211.

Hudalla, H., K. Karenberg, R.-J. Kuon, J. Pöschl, R. Tschada, and D. Frommhold. 2018. LPS-induced maternal inflammation promotes fetal leukocyte recruitment and prenatal organ infiltration in mice. Pediatr. Res. 84:757–764. doi:10.1038/s41390-018-0030-z. Available from: https://doi.org/10.1038/s41390-018-0030-z

Hume, D. A., and K. P. A. MacDonald. 2012. Therapeutic applications of macrophage colony-stimulating factor-1 (CSF-1) and antagonists of CSF-1 receptor (CSF-1R) signaling. Blood. 119:1810–1820. doi:10.1182/blood-2011-09-379214.

Inoue, T., Y. Ito, N. Nishizawa, K. Eshima, K. Kojo, F. Otaka, T. Betto, S. Yamane, K. Tsujikawa, W. Koizumi, and M. Majima. 2018. RAMP1 in Kupffer cells is a critical regulator in immune-mediated hepatitis. PLoS One. 13:e0200432. doi:10.1371/journal.pone.0200432. Available from: http://www.ncbi.nlm.nih.gov/pubmed/30462657

Jensen, C. B., H. Storgaard, F. Dela, J. J. Holst, S. Madsbad, and A. A. Vaag. 2002. Early Differential Defects of Insulin Secretion and Action in 19-Year-Old Caucasian Men Who Had Low Birth Weight. Diabetes. 51:1271–1280. doi:10.2337/diabetes.51.4.1271. Available from: http://diabetes.diabetesjournals.org/cgi/doi/10.2337/diabetes.51.4.1271

Ji, Y., Z. Wu, Z. Dai, X. Wang, J. Li, B. Wang, and G. Wu. 2017. Fetal and neonatal programming of postnatal growth and feed efficiency in swine. J. Anim. Sci. Biotechnol. 8:42. doi:10.1186/s40104-017-0173-5. Available from: https://doi.org/10.1186/s40104-017-0173-5

Johansson, Å., J. Lau, M. Sandberg, L. A. H. Borg, P. U. Magnusson, and P.-O. Carlsson. 2009. Endothelial cell signalling supports pancreatic beta cell function in the rat. Diabetologia. 52:2385–2394. doi:10.1007/s00125-009-1485-6. Available from: http://link.springer.com/10.1007/s00125-009-1485-6

Johnson, D. E., R. A. O'Keefe, and J. R. Grandis. 2018. Targeting the IL-6/JAK/STAT3 signalling axis in cancer. Nat. Rev. Clin. Oncol. 15:234–248. doi:10.1038/nrclinonc.2018.8. Available from: https://doi.org/10.1038/nrclinonc.2018.8

Jones, A. K., L. D. Brown, P. J. Rozance, N. J. Serkova, W. W. Hay, J. E. Friedman, and S. R. Wesolowski. 2019. Differential effects of intrauterine growth restriction and

a hypersinsulinemic-isoglycemic clamp on metabolic pathways and insulin action in the fetal liver. Am. J. Physiol. Regul. Integr. Comp. Physiol. 316:R427–R440. doi:10.1152/ajpregu.00359.2018. Available from: http://www.ncbi.nlm.nih.gov/pubmed/30758974

Jung, M., J. Choi, S.-A. Lee, H. Kim, J. Hwang, and E. H. Choi. 2014. Pyrrolidone carboxylic acid levels or caspase-14 expression in the corneocytes of lesional skin correlates with clinical severity, skin barrier function and lesional inflammation in atopic dermatitis. J. Dermatol. Sci. 76:231–239. doi:10.1016/j.jdermsci.2014.09.004.

Katsu, Y., and M. E. Baker. 2021. Subchapter 123D - Cortisol. In: H. Ando, K. Ukena, and S. B. T.-H. of H. (Second E. Nagata, editors. Academic Press, San Diego. p. 947–949. Available from: https://www.sciencedirect.com/science/article/pii/B9780128206492002618

Kelly, A. C., C. A. Bidwell, F. M. McCarthy, D. J. Taska, M. J. Anderson, L. E. Camacho, and S. W. Limesand. 2017. RNA Sequencing Exposes Adaptive and Immune Responses to Intrauterine Growth Restriction in Fetal Sheep Islets. Endocrinology. 158:743–755. doi:10.1210/en.2016-1901. Available from: https://doi.org/10.1210/en.2016-1901

Kemp, M. W. 2014. Preterm Birth, Intrauterine Infection, and Fetal Inflammation. Front. Immunol. 5. doi:10.3389/fimmu.2014.00574. Available from: http://journal.frontiersin.org/article/10.3389/fimmu.2014.00574/abstract

Kesavan, K., and S. U. Devaskar. 2019. Intrauterine Growth Restriction. Pediatr. Clin. North Am. 66:403–423. doi:10.1016/j.pcl.2018.12.009. Available from: https://doi.org/10.1016/j.pcl.2018.12.009

Kirchofer, K. S., C. R. Calkins, and B. L. Gwartney. 2002. Fiber-type composition of muscles of the beef chuck and round. J. Anim. Sci. 80:2872–2878. doi:10.2527/2002.80112872x. Available from: https://doi.org/10.2527/2002.80112872x

Knudsen, J. G., A. Gudiksen, L. Bertholdt, P. Overby, I. Villesen, C. L. Schwartz, and H. Pilegaard. 2017. Skeletal muscle IL-6 regulates muscle substrate utilization and adipose tissue metabolism during recovery from an acute bout of exercise. A. Philp, editor. PLoS One. 12:e0189301. doi:10.1371/journal.pone.0189301. Available from: https://doi.org/10.1371/journal.pone.0189301

Krajewski, P., P. Sieroszewski, A. Karowicz-Bilinska, M. Kmiecik, A. Chudzik, B. Strzalko-Gloskowska, M. Kwiatkowska, M. Pokrzywnicka, K. Wyka, J. Chlapinski, M. Kaminski, and K. Wieckowska. 2014. Assessment of interleukin-6, interleukin-8 and interleukin-18 count in the serum of IUGR newborns. J.

Matern. Neonatal Med. 27:1142–1145. doi:10.3109/14767058.2013.851186. Available from: https://doi.org/10.3109/14767058.2013.851186

Kubota, T., N. Kubota, H. Kumagai, S. Yamaguchi, H. Kozono, T. Takahashi, M. Inoue, S. Itoh, I. Takamoto, T. Sasako, K. Kumagai, T. Kawai, S. Hashimoto, T. Kobayashi, M. Sato, K. Tokuyama, S. Nishimura, M. Tsunoda, T. Ide, K. Murakami, T. Yamazaki, O. Ezaki, K. Kawamura, H. Masuda, M. Moroi, K. Sugi, Y. Oike, H. Shimokawa, N. Yanagihara, M. Tsutsui, Y. Terauchi, K. Tobe, R. Nagai, K. Kamata, K. Inoue, T. Kodama, K. Ueki, and T. Kadowaki. 2011. Impaired Insulin Signaling in Endothelial Cells Reduces Insulin-Induced Glucose Uptake by Skeletal Muscle. Cell Metab. 13:294–307. doi:10.1016/j.cmet.2011.01.018. Available from: https://www.sciencedirect.com/science/article/pii/S155041311100043X

Lacey, T. A., R. L. Gibbs, M. S. Most, H. N. Beer, Z. H. Hicks, P. C. Grijalva, J. . Petersen, and D. T. Yates. 2021. Decreased fetal biometrics and impaired β cell function in IUGR fetal sheep are improved by daily ω-3 PUFA infusion. Transl. Anim. Sci. 5:S41–S45.

Lackman, F., V. Capewell, R. Gagnon, and B. Richardson. 2001. Fetal umbilical cord oxygen values and birth to placental weight ratio in relation to size at birth. Am. J. Obstet. Gynecol. 185:674–682. doi:https://doi.org/10.1067/mob.2001.116686. Available from: https://www.sciencedirect.com/science/article/pii/S0002937801293387

Lang, C. H., R. A. Frost, A. C. Nairn, D. A. MacLean, and T. C. Vary. 2002. TNF-α impairs heart and skeletal muscle protein synthesis by altering translation initiation. Am. J. Physiol. Metab. 282:E336–E347. doi:10.1152/ajpendo.00366.2001. Available from: https://doi.org/10.1152/ajpendo.00366.2001

Lemley, C. O., A. M. Meyer, L. E. Camacho, T. L. Neville, D. J. Newman, J. S. Caton, and K. A. Vonnahme. 2012. Melatonin supplementation alters uteroplacental hemodynamics and fetal development in an ovine model of intrauterine growth restriction. Am. J. Physiol. Integr. Comp. Physiol. 302:R454--R467.

Li, C., Q. Chen, Y. Zhou, Y. Niu, X. Wang, X. Li, H. Zheng, T. Wei, L. Zhao, and H. Gao. 2020. S100A2 promotes glycolysis and proliferation via GLUT1 regulation in colorectal cancer. FASEB J. Off. Publ. Fed. Am. Soc. Exp. Biol. 34:13333–13344. doi:10.1096/fj.202000555R.

Li, N., and X. Liu. 2020. Phosphoglycerate Mutase 1: Its Glycolytic and Non-Glycolytic Roles in Tumor Malignant Behaviors and Potential Therapeutic Significance. Onco. Targets. Ther. 13:1787–1795. doi:10.2147/OTT.S238920. Available from: http://www.ncbi.nlm.nih.gov/pubmed/32161473

Li, W., J. S. Moylan, M. A. Chambers, J. Smith, and M. B. Reid. 2009. Interleukin-1 stimulates catabolism in C2C12 myotubes. Am. J. Physiol. Cell Physiol. 297:C706–C714. doi:10.1152/ajpcell.00626.2008. Available from: https://pubmed.ncbi.nlm.nih.gov/19625606

Li, X., L. Zhu, X. Chen, and M. Fan. 2007. Effects of hypoxia on proliferation and differentiation of myoblasts. Med. Hypotheses. 69:629–636. doi:https://doi.org/10.1016/j.mehy.2006.12.050. Available from: https://www.sciencedirect.com/science/article/pii/S0306987707000576

Li, Y.-P., and M. B. Reid. 2001. Effect of tumor necrosis factor-α on skeletal muscle metabolism. Curr. Opin. Rheumatol. 13. Available from: https://journals.lww.com/co-rheumatology/Fulltext/2001/11000/Effect_of_tumor_necrosis_factor___on_skeletal.5.aspx

Limesand, S. W., J. Jensen, J. C. Hutton, and W. W. Hay. 2005. Diminished β-cell replication contributes to reduced β-cell mass in fetal sheep with intrauterine growth restriction. Am. J. Physiol. Integr. Comp. Physiol. 288:R1297–R1305. doi:10.1152/ajpregu.00494.2004. Available from: https://doi.org/10.1152/ajpregu.00494.2004

Limesand, S. W., and P. J. Rozance. 2017. Fetal adaptations in insulin secretion result from high catecholamines during placental insufficiency. J. Physiol. 595:5103–5113. doi:10.1113/JP273324. Available from: https://pubmed.ncbi.nlm.nih.gov/28194805

Limesand, S. W., P. J. Rozance, A. R. Macko, M. J. Anderson, A. C. Kelly, and W. W. J. Hay. 2013. Reductions in insulin concentrations and β-cell mass precede growth restriction in sheep fetuses with placental insufficiency. Am. J. Physiol. Endocrinol. Metab. 304:E516-23. doi:10.1152/ajpendo.00435.2012.

Limesand, S. W., P. J. Rozance, D. Smith, and W. W. Hay. 2007. Increased insulin sensitivity and maintenance of glucose utilization rates in fetal sheep with placental insufficiency and intrauterine growth restriction. Am. J. Physiol. Metab. 293:E1716–E1725. doi:10.1152/ajpendo.00459.2007. Available from: https://doi.org/10.1152/ajpendo.00459.2007

Limesand, S. W., P. J. Rozance, G. O. Zerbe, J. C. Hutton, and W. W. Hay. 2006. Attenuated Insulin Release and Storage in Fetal Sheep Pancreatic Islets with Intrauterine Growth Restriction. Endocrinology. 147:1488–1497. doi:10.1210/en.2005-0900. Available from: https://academic.oup.com/endo/article/147/3/1488/2501395

Liu, J. B., and J. He. 2014. Effects of birth weight and postnatal high-fat diet on growth performance, carcass and meat quality in pigs. J. Anim. Plant Sci. 24:1606–1612.

Liu, L., H. Cui, R. Fu, M. Zheng, R. Liu, G. Zhao, and J. Wen. 2017. The regulation of IMF deposition in pectoralis major of fast- and slow- growing chickens at hatching. J. Anim. Sci. Biotechnol. 8:77. doi:10.1186/s40104-017-0207-z.

Lo, J., L. E. Bernstein, B. Canavan, M. Torriani, M. B. Jackson, R. S. Ahima, and S. K. Grinspoon. 2007. Effects of TNF-α neutralization on adipocytokines and skeletal muscle adiposity in the metabolic syndrome. Am. J. Physiol. Metab. 293:E102–E109. doi:10.1152/ajpendo.00089.2007. Available from: https://doi.org/10.1152/ajpendo.00089.2007

Love, M. I., W. Huber, and S. Anders. 2014. Moderated estimation of fold change and dispersion for RNA-seq data with DESeq2. Genome Biol. 15:550. doi:10.1186/s13059-014-0550-8.

Luan, Y., N. Tang, J. Yang, S. Liu, C. Cheng, Y. Wang, C. Chen, Y.-N. Guo, H. Wang, W. Zhao, Q. Zhao, W. Li, M. Xiang, R. Ju, and Z. Xie. 2022. Deficiency of ribosomal proteins reshapes the transcriptional and translational landscape in human cells. Nucleic Acids Res. 50:6601–6617. doi:10.1093/nar/gkac053.

Macko, A. R., D. T. Yates, X. Chen, L. A. Shelton, A. C. Kelly, M. A. Davis, L. E. Camacho, M. J. Anderson, and S. W. Limesand. 2016. Adrenal Demedullation and Oxygen Supplementation Independently Increase Glucose-Stimulated Insulin Concentrations in Fetal Sheep With Intrauterine Growth Restriction. Endocrinology. 157:2104–2115. doi:10.1210/en.2015-1850. Available from: https://doi.org/10.1210/en.2015-1850

Magister, S., and J. Kos. 2013. Cystatins in immune system. J. Cancer. 4:45–56. doi:10.7150/jca.5044. Available from: http://www.ncbi.nlm.nih.gov/pubmed/23386904

Maier, A., J. C. McEwan, K. G. Dodds, D. A. Fischman, R. B. Fitzsimons, and A. J. Harris. 1992. Myosin heavy chain composition of single fibres and their origins and distribution in developing fascicles of sheep tibialis cranialis muscles. J. Muscle Res. Cell Motil. 13:551–572. doi:10.1007/BF01737997. Available from: http://link.springer.com/10.1007/BF01737997

Mäkikallio, K., T. Kaukola, J. Tuimala, S. F. Kingsmore, M. Hallman, and M. Ojaniemi. 2012. Umbilical artery chemokine CCL16 is associated with preterm preeclampsia and fetal growth restriction. Cytokine. 60:377–384. doi:https://doi.org/10.1016/j.cyto.2012.07.008. Available from: https://www.sciencedirect.com/science/article/pii/S1043466612005704

Maltby, S., N. G. Hansbro, H. L. Tay, J. Stewart, M. Plank, B. Donges, H. F. Rosenberg, and P. S. Foster. 2014. Production and differentiation of myeloid cells driven by proinflammatory cytokines in response to acute pneumovirus infection in mice. J. Immunol. 193:4072–4082. doi:10.4049/jimmunol.1400669.

Marcondes Machado Nardozza, L., A. Carolina Rabachini Caetano, A. Cristina Perez Zamarian, J. Brandão Mazzola, C. Pacheco Silva, V. Macedo Gomes Marçal, T. Frutuoso Lobo, A. Borges Peixoto, and E. Araujo Júnior. 2017. Fetal growth restriction: current knowledge. Arch. Gynecol. Obstet. 295:1061–1077. doi:10.1007/s00404-017-4341-9.

Markiewicz, A., D. Sigorski, M. Markiewicz, A. Owczarczyk-Saczonek, and W. Placek. 2021. Caspase-14-From Biomolecular Basics to Clinical Approach. A Review of Available Data. Int. J. Mol. Sci. 22. doi:10.3390/ijms22115575. Available from: http://www.ncbi.nlm.nih.gov/pubmed/34070382

Matyba, P., T. Florowski, K. Dasiewicz, K. Ferenc, J. Olszewski, M. Trela, G. Galemba, M. Słowiński, M. Sady, D. Domańska, Z. Gajewski, and R. Zabielski. 2021. Performance and Meat Quality of Intrauterine Growth Restricted Pigs. Animals. 11:254. doi:10.3390/ani11020254. Available from: https://doi.org/10.3390/ani11020254

McGlory, C., and S. M. Phillips. 2015. Exercise and the Regulation of Skeletal Muscle Hypertrophy. 1st ed. Elsevier Inc. Available from: http://dx.doi.org/10.1016/bs.pmbts.2015.06.018

Mericq, V., K. K. Ong, R. Bazaes, V. Peña, A. Avila, T. Salazar, N. Soto, G. Iñiguez, and D. B. Dunger. 2005. Longitudinal changes in insulin sensitivity and secretion from birth to age three years in small- and appropriate-for-gestational-age children. Diabetologia. 48:2609–2614. doi:10.1007/s00125-005-0036-z.

Merz, K. E., and D. C. Thurmond. 2020. Role of Skeletal Muscle in Insulin Resistance and Glucose Uptake. Compr. Physiol. 10:785–809. doi:10.1002/cphy.c190029. Available from: http://www.ncbi.nlm.nih.gov/pubmed/32940941

Mikolajczyk, J., F. L. Scott, S. Krajewski, D. P. Sutherlin, and G. S. Salvesen. 2004. Activation and substrate specificity of caspase-14. Biochemistry. 43:10560–10569. doi:10.1021/bi0498048.

Morrison, J. L. 2008. Sheep Models Of Intrauterine Growth Restriction: Fetal Adaptations And Consequences. Clin. Exp. Pharmacol. Physiol. 35:730–743. doi:10.1111/j.1440-1681.2008.04975.x. Available from: https://doi.org/10.1111/j.1440-1681.2008.04975.x

Munnur, D., A. Banducci-Karp, and S. Sanyal. 2022. ISG15 driven cellular responses to

virus infection. Biochem. Soc. Trans. 50:1837–1846. doi:10.1042/BST20220839. Available from: https://doi.org/10.1042/BST20220839

Nawabi, M. D., K. P. Block, M. C. Chakrabarti, and M. G. Buse. 1990. Administration of endotoxin, tumor necrosis factor, or interleukin 1 to rats activates skeletal muscle branched-chain alpha-keto acid dehydrogenase. J. Clin. Invest. 85:256–263. doi:10.1172/JCI114421. Available from: https://doi.org/10.1172/JCI114421

Neel, J. V. 1962. Diabetes mellitus: a "thrifty" genotype rendered detrimental by "progress"? Am. J. Hum. Genet. 14:353–62. Available from: https://www.ncbi.nlm.nih.gov/pmc/articles/PMC1932342/

Nenci, A., M. Huth, A. Funteh, M. Schmidt-Supprian, W. Bloch, D. Metzger, P. Chambon, K. Rajewsky, T. Krieg, I. Haase, and M. Pasparakis. 2006. Skin lesion development in a mouse model of incontinentia pigmenti is triggered by NEMO deficiency in epidermal keratinocytes and requires TNF signaling. Hum. Mol. Genet. 15:531–542. doi:10.1093/hmg/ddi470.

Nicotera, P., and G. Melino. 2007. Caspase-14 and epidermis maturation. Nat. Cell Biol. 9:621–622. doi:10.1038/ncb0607-621.

Niu, Y., J. He, H. Ahmad, M. Shen, Y. Zhao, Z. Gan, L. Zhang, X. Zhong, C. Wang, and T. Wang. 2019a. Dietary Curcumin Supplementation Increases Antioxidant Capacity, Upregulates Nrf2 and Hmox1 Levels in the Liver of Piglet Model with Intrauterine Growth Retardation. Nutrients. 11. doi:10.3390/nu11122978.

Niu, Y., J. He, H. Ahmad, C. Wang, X. Zhong, L. Zhang, T. Cui, J. Zhang, and T. Wang. 2019b. Curcumin attenuates insulin resistance and hepatic lipid accumulation in a rat model of intra-uterine growth restriction through insulin signalling pathway and sterol regulatory element binding proteins. Br. J. Nutr. 122:616–624. doi:10.1017/S0007114519001508.

Niu, Y., J. He, Y. Zhao, M. Shen, L. Zhang, X. Zhong, C. Wang, and T. Wang. 2019c. Effect of Curcumin on Growth Performance, Inflammation, Insulin level, and Lipid Metabolism in Weaned Piglets with IUGR. Anim. an open access J. from MDPI. 9. doi:10.3390/ani9121098.

Oh, J.-W., C.-W. Park, K. C. Moon, J. S. Park, and J. K. Jun. 2019. The relationship among the progression of inflammation in umbilical cord, fetal inflammatory response, early-onset neonatal sepsis, and chorioamnionitis. L. Reyes, editor. PLoS One. 14:e0225328. doi:10.1371/journal.pone.0225328. Available from: https://pubmed.ncbi.nlm.nih.gov/31743377

Oleson, B. J., J. A. McGraw, K. A. Broniowska, M. Annamalai, J. Chen, J. R. Bushkofsky, D. B. Davis, J. A. Corbett, and C. E. Mathews. 2015. Distinct

differences in the responses of the human pancreatic β-cell line EndoC-βH1 and human islets to proinflammatory cytokines. Am. J. Physiol. Integr. Comp. Physiol. 309:R525–R534. doi:10.1152/ajpregu.00544.2014. Available from: https://doi.org/10.1152/ajpregu.00544.2014

Oliveira, V., S. D. Silva Junior, M. H. C. de Carvalho, E. H. Akamine, L. C. Michelini, and M. C. Franco. 2017. Intrauterine growth restriction increases circulating mitochondrial DNA and Toll-like receptor 9 expression in adult offspring: could aerobic training counteract these adaptations? J. Dev. Orig. Health Dis. 8:236–243. doi:10.1017/S2040174416000714. Available from: http://www.ncbi.nlm.nih.gov/pubmed/28004624

Ong, K. K., C. J. Petry, P. M. Emmett, M. S. Sandhu, W. Kiess, C. N. Hales, A. R. Ness, and D. B. Dunger. 2004. Insulin sensitivity and secretion in normal children related to size at birth, postnatal growth, and plasma insulin-like growth factor-I levels. Diabetologia. 47. doi:10.1007/s00125-004-1405-8. Available from: http://link.springer.com/10.1007/s00125-004-1405-8

Otis, J. S., S. Niccoli, N. Hawdon, J. L. Sarvas, M. A. Frye, A. J. Chicco, and S. J. Lees. 2014. Pro-Inflammatory Mediation of Myoblast Proliferation. G. L. Lluch, editor. PLoS One. 9:e92363. doi:10.1371/journal.pone.0092363. Available from: https://dx.plos.org/10.1371/journal.pone.0092363

Owhashi, M., Y. Taoka, K. Ishii, S. Nakazawa, H. Uemura, and H. Kambara. 2003. Identification of a ubiquitin family protein as a novel neutrophil chemotactic factor. Biochem. Biophys. Res. Commun. 309:533–539. doi:10.1016/j.bbrc.2003.08.038.
Padovan, E., L. Terracciano, U. Certa, B. Jacobs, A. Reschner, M. Bolli, G. C. Spagnoli, E. C. Borden, and M. Heberer. 2002. Interferon stimulated gene 15 constitutively produced by melanoma cells induces e-cadherin expression on human dendritic cells. Cancer Res. 62:3453–3458.

Pantham, P., F. J. Rosario, S. T. Weintraub, P. W. Nathanielsz, T. L. Powell, C. Li, and T. Jansson. 2016. Down-Regulation of Placental Transport of Amino Acids Precedes the Development of Intrauterine Growth Restriction in Maternal Nutrient Restricted Baboons1. Biol. Reprod. 95. doi:10.1095/biolreprod.116.141085. Available from: https://doi.org/10.1095/biolreprod.116.141085

Pendleton, A. L., A. T. Antolic, A. C. Kelly, M. A. Davis, L. E. Camacho, K. Doubleday, M. J. Anderson, P. R. Langlais, R. M. Lynch, and S. W. Limesand. 2020. Lower oxygen consumption and Complex I activity in mitochondria isolated from skeletal muscle of fetal sheep with intrauterine growth restriction. Am. J. Physiol. Metab. 319:E67–E80. doi:10.1152/ajpendo.00057.2020. Available from: https://journals.physiology.org/doi/10.1152/ajpendo.00057.2020

Pendleton, A. L., L. R. Humphreys, M. A. Davis, L. E. Camacho, M. J. Anderson, and S. W. Limesand. 2019. Increased pyruvate dehydrogenase activity in skeletal muscle of growth-restricted ovine fetuses. Am. J. Physiol. Integr. Comp. Physiol. 317:R513–R520. doi:10.1152/ajpregu.00106.2019. Available from: https://www.physiology.org/doi/10.1152/ajpregu.00106.2019

Pendleton, A. L., S. R. Wesolowski, T. R. H. Regnault, R. M. Lynch, and S. W. Limesand. 2021. Dimming the Powerhouse: Mitochondrial Dysfunction in the Liver and Skeletal Muscle of Intrauterine Growth Restricted Fetuses. Front. Endocrinol. (Lausanne). 12:515. doi:10.3389/fendo.2021.612888. Available from: https://www.frontiersin.org/article/10.3389/fendo.2021.612888

Perng, Y.-C., and D. J. Lenschow. 2018. ISG15 in antiviral immunity and beyond. Nat. Rev. Microbiol. 16:423–439. doi:10.1038/s41579-018-0020-5. Available from: https://doi.org/10.1038/s41579-018-0020-5

Pink, R. C., K. Wicks, D. P. Caley, E. K. Punch, L. Jacobs, and D. R. F. Carter. 2011. Pseudogenes: pseudo-functional or key regulators in health and disease? RNA. 17:792–8. doi:10.1261/rna.2658311. Available from: http://www.ncbi.nlm.nih.gov/pubmed/21398401

Plomgaard, P., M. Penkowa, and B. K. Pedersen. 2005. Fiber type specific expression of TNF-alpha, IL-6 and IL-18 in human skeletal muscles. Exerc. Immunol. Rev. 11:53–63. Available from: http://www.ncbi.nlm.nih.gov/pubmed/16385844

Popa, C., M. G. Netea, P. L. C. M. van Riel, J. W. M. van der Meer, and A. F. H. Stalenhoef. 2007. The role of TNF-α in chronic inflammatory conditions, intermediary metabolism, and cardiovascular risk. J. Lipid Res. 48:751–762. doi:10.1194/jlr.R600021-JLR200. Available from: https://doi.org/10.1194/jlr.R600021-JLR200

Posont, R., C. Cadaret, T. Barnes, and D. Yates. 2017. A potential role for mTORC1/2 in β2 adrenergic regulation of skeletal muscle glucose oxidation in models of intrauterine growth restriction. Diabesity. 3:9. doi:10.15562/diabesity.2017.40. Available from: http://diabesity.ejournals.ca/index.php/diabesity/article/view/40

Posont, R. J., K. A. Beede, S. W. Limesand, and D. T. Yates. 2018. Changes in myoblast responsiveness to TNFα and IL-6 contribute to decreased skeletal muscle mass in intrauterine growth restricted fetal sheep1. Transl. Anim. Sci. 2:S44–S47. doi:10.1093/tas/txy038. Available from: https://doi.org/10.1093/tas/txy038

Posont, R. J., C. N. Cadaret, J. K. Beard, R. M. Swanson, R. L. Gibbs, E. S. Marks-Nelson, J. L. Petersen, and D. T. Yates. 2021. Maternofetal inflammation induced for 2 wk in late gestation reduced birth weight and impaired neonatal growth and

skeletal muscle glucose metabolism in lambs. J. Anim. Sci. 99. doi:10.1093/jas/skab102. Available from: https://doi.org/10.1093/jas/skab102

Posont, R. J., M. S. Most, C. N. Cadaret, E. S. Marks-Nelson, K. A. Beede, S. W. Limesand, T. B. Schmidt, J. L. Petersen, and D. T. Yates. 2022. Primary myoblasts from intrauterine growth-restricted fetal sheep exhibit intrinsic dysfunction of proliferation and differentiation that coincides with enrichment of inflammatory cytokine signaling pathways. J. Anim. Sci. 100. doi:10.1093/jas/skac145.

Posont, R. J., and D. T. Yates. 2019. Postnatal Nutrient Repartitioning due to Adaptive Developmental Programming. Vet. Clin. North Am. Food Anim. Pract. 35:277–288. doi:10.1016/j.cvfa.2019.02.001. Available from: https://doi.org/10.1016/j.cvfa.2019.02.001

Poudel, R., I. C. McMillen, S. L. Dunn, S. Zhang, and J. L. Morrison. 2014. Impact of chronic hypoxemia on blood flow to the brain, heart, and adrenal gland in the late-gestation IUGR sheep fetus. Am. J. Physiol. Integr. Comp. Physiol. 308:R151–R162. doi:10.1152/ajpregu.00036.2014. Available from: https://doi.org/10.1152/ajpregu.00036.2014

Powell, S. E., and E. D. Aberle. 1980. Effects of birth weight on growth and carcass composition of swine. J. Anim. Sci. 50:860–868. doi:10.2527/jas1980.505860x.
Raclot, T., and R. Groscolas. 1993. Differential mobilization of white adipose tissue fatty acids according to chain length, unsaturation, and positional isomerism. J. Lipid Res. 34:1515–1526. doi:https://doi.org/10.1016/S0022-2275(20)36944-3. Available from: https://www.sciencedirect.com/science/article/pii/S0022227520369443

Raychaudhuri, N., S. Raychaudhuri, M. Thamotharan, and S. U. Devaskar. 2008. Histone Code Modifications Repress Glucose Transporter 4 Expression in the Intrauterine Growth-restricted Offspring. J. Biol. Chem. 283:13611–13626. doi:10.1074/jbc.M800128200. Available from: https://linkinghub.elsevier.com/retrieve/pii/S0021925820715930

RefSeq - CSTL1. 2023. Natl. Cent. Biotechnol. Inf. Available from: https://www.ncbi.nlm.nih.gov/gene/128817

RefSeq - ENO3. 2022. Natl. Cent. Biotechnol. Inf. Available from: https://www.ncbi.nlm.nih.gov/gene/443086

RefSeq - GCNT1. 2023. Natl. Cent. Biotechnol. Inf. Available from: https://www.ncbi.nlm.nih.gov/gene/2650

RefSeq - IFI6. 2023. Natl. Cent. Biotechnol. Inf. Available from:

https://www.ncbi.nlm.nih.gov/gene/?term=IFI6+ovis+aries

RefSeq - ISG15. 2023. Natl. Cent. Biotechnol. Inf. Available from: https://www.ncbi.nlm.nih.gov/gene/443057

RefSeq - LOC101120797. 2021. Natl. Cent. Biotechnol. Inf. Available from: https://www.ncbi.nlm.nih.gov/gene/?term=LOC101120797

RefSeq - LOC101121371. 2021. Natl. Cent. Biotechnol. Inf. Available from: www.ncbi.nlm.nih.gov/nuccore/XM_004016143.5

RefSeq - LOC105607887. 2021. Natl. Cent. Biotechnol. Inf. Available from: https://www.ncbi.nlm.nih.gov/gene/?term=LOC105607887

RefSeq - LOC114108604. 2022. Natl. Cent. Biotechnol. Inf. Available from: https://www.ncbi.nlm.nih.gov/gene/?term=LOC114108604

RefSeq - LOC114109685. 2021. Natl. Cent. Biotechnol. Inf. Available from: https://www.ncbi.nlm.nih.gov/gene/?term=LOC11410968

RefSeq - LOC121816987. 2021. Available from: https://www.ncbi.nlm.nih.gov/gene/?term=LOC121816987

RefSeq - MT-ND5. 2023. Natl. Cent. Biotechnol. Inf. Available from: https://www.ncbi.nlm.nih.gov/gene/4540#summary

RefSeq - PGAM1. 2023. Natl. Cent. Biotechnol. Inf.

RefSeq - RAMP1. 2023. Natl. Cent. Biotechnol. Inf. Available from: https://www.ncbi.nlm.nih.gov/gene/?term=ramp1+ovis+aries

RefSeq - S100A2. 2023. Natl. Cent. Biotechnol. Inf. Available from: https://www.ncbi.nlm.nih.gov/gene/6273

Regnault, T. R. H., J. E. Friedman, R. B. Wilkening, R. V Anthony, and W. W. J. Hay. 2005. Fetoplacental transport and utilization of amino acids in IUGR--a review. Placenta. 26 Suppl A:S52-62. doi:10.1016/j.placenta.2005.01.003.

Regnault, T. R. H., B. de Vrijer, H. L. Galan, M. L. Davidsen, K. A. Trembler, F. C. Battaglia, R. B. Wilkening, and R. V Anthony. 2003. The relationship between transplacental O2 diffusion and placental expression of PlGF, VEGF and their receptors in a placental insufficiency model of fetal growth restriction. J. Physiol. 550:641–656. doi:10.1113/jphysiol.2003.039511. Available from: https://pubmed.ncbi.nlm.nih.gov/12740423

Reid, M. B., and Y.-P. Li. 2001. Cytokines and oxidative signalling in skeletal muscle. Acta Physiol. Scand. 171:225–232. doi:10.1046/j.1365-201x.2001.00824.x. Available from: http://doi.wiley.com/10.1046/j.1365-201x.2001.00824.x

Remels, A. H. V, H. R. Gosker, K. J. P. Verhees, R. C. J. Langen, and A. M. W. J. Schols. 2015. TNF-α-Induced NF-κB Activation Stimulates Skeletal Muscle Glycolytic Metabolism Through Activation of HIF-1α. Endocrinology. 156:1770–1781. doi:10.1210/en.2014-1591. Available from: https://doi.org/10.1210/en.2014-1591

Reynolds, L. P., P. P. Borowicz, J. S. Caton, M. S. Crouse, C. R. Dahlen, and A. K. Ward. 2019. Developmental Programming of Fetal Growth and Development. Vet. Clin. North Am. Food Anim. Pract. 35:229–247. doi:10.1016/j.cvfa.2019.02.006. Available from: https://www.sciencedirect.com/science/article/pii/S0749072019300064

Reynolds, L. P., P. P. Borowicz, J. S. Caton, K. A. Vonnahme, J. S. Luther, C. J. Hammer, K. R. Maddock Carlin, A. T. Grazul-Bilska, and D. A. Redmer. 2010. Developmental programming: The concept, large animal models, and the key role of uteroplacental vascular development. J. Anim. Sci. 88:E61–E72. doi:10.2527/jas.2009-2359. Available from: https://doi.org/10.2527/jas.2009-2359

Rhoades, R. D., D. A. King, B. E. Jenschke, J. M. Behrends, T. S. Hively, and S. B. Smith. 2005. Postmortem regulation of glycolysis by 6-phosphofructokinase in bovine M. Sternocephalicus pars mandibularis. Meat Sci. 70:621–626. doi:10.1016/j.meatsci.2005.01.024. Available from: https://www.sciencedirect.com/science/article/pii/S0309174005000847

Riddle, E. S., M. S. Campbell, B. Y. Lang, R. Bierer, Y. Wang, H. N. Bagley, and L. A. Joss-Moore. 2014. Intrauterine growth restriction increases TNF α and activates the unfolded protein response in male rat pups. J. Obes. 2014:829862. doi:10.1155/2014/829862. Available from: http://www.ncbi.nlm.nih.gov/pubmed/24804087

Roberge, S., K. Nicolaides, S. Demers, J. Hyett, N. Chaillet, and E. Bujold. 2017. The role of aspirin dose on the prevention of preeclampsia and fetal growth restriction: systematic review and meta-analysis. Am. J. Obstet. Gynecol. 216:110-120.e6. doi:10.1016/j.ajog.2016.09.076. Available from: https://linkinghub.elsevier.com/retrieve/pii/S0002937816307839

Robinson, D. L., L. M. Cafe, and P. L. Greenwood. 2013. Meat science and muscle biology symposium: developmental programming in cattle: consequences for growth, efficiency, carcass, muscle, and beef quality characteristics. J. Anim. Sci. 91:1428–1442.

Rogatzki, M. J., B. S. Ferguson, M. L. Goodwin, and L. B. Gladden. 2015. Lactate is always the end product of glycolysis. Front. Neurosci. 9:1–7. doi:10.3389/fnins.2015.00022.

Romero, R., F. Gotsch, B. Pineles, and J. P. Kusanovic. 2008. Inflammation in Pregnancy: Its Roles in Reproductive Physiology, Obstetrical Complications, and Fetal Injury. Nutr. Rev. 65:S194–S202. doi:10.1111/j.1753-4887.2007.tb00362.x. Available from: https://academic.oup.com/nutritionreviews/article-lookup/doi/10.1111/j.1753-4887.2007.tb00362.x

Rong Guo, Weijian Hou, Yafeng Dong, Zhiyong Yu, J. Stites, and C. P. Weiner. 2010. Brain Injury Caused by Chronic Fetal Hypoxemia Is Mediated by Inflammatory Cascade Activation. Reprod. Sci. 17:540–548. doi:10.1177/1933719110364061. Available from: https://doi.org/10.1177/1933719110364061

Rozance, P. J., M. Anderson, M. Martinez, A. Fahy, A. R. Macko, J. Kailey, G. J. Seedorf, S. H. Abman, W. W. Hay, and S. W. Limesand. 2015. Placental Insufficiency Decreases Pancreatic Vascularity and Disrupts Hepatocyte Growth Factor Signaling in the Pancreatic Islet Endothelial Cell in Fetal Sheep. Diabetes. 64:555–564. doi:10.2337/db14-0462. Available from: http://diabetes.diabetesjournals.org/lookup/doi/10.2337/db14-0462

Rozance, P. J., L. Zastoupil, S. R. Wesolowski, D. A. Goldstrohm, B. Strahan, M. Cree-Green, M. Sheffield-Moore, G. Meschia, W. W. Hay, R. B. Wilkening, and L. D. Brown. 2018a. Skeletal muscle protein accretion rates and hindlimb growth are reduced in late gestation intrauterine growth-restricted fetal sheep. J. Physiol. 596:67–82. doi:10.1113/JP275230.

Rozance, P. J., L. Zastoupil, S. R. Wesolowski, D. A. Goldstrohm, B. Strahan, M. Cree-Green, M. Sheffield-Moore, G. Meschia, W. W. Hay, R. B. Wilkening, L. D. Brown, W. W. Hay Jr, R. B. Wilkening, and L. D. Brown. 2018b. Skeletal muscle protein accretion rates and hindlimb growth are reduced in late gestation intrauterine growth-restricted fetal sheep. J. Physiol. 596:67–82. doi:https://doi.org/10.1113/JP275230. Available from: https://doi.org/10.1113/JP275230

Saghizadeh, M., J. M. Ong, W. T. Garvey, R. R. Henry, and P. A. Kern. 1996. The expression of TNF alpha by human muscle. Relationship to insulin resistance. J. Clin. Invest. 97:1111–1116. doi:10.1172/JCI118504. Available from: https://doi.org/10.1172/JCI118504

Saleem, T., N. Sajjad, S. Fatima, N. Habib, S. R. Ali, and M. Qadir. 2011. Intrauterine growth retardation - small events, big consequences. Ital. J. Pediatr. 37:41. doi:10.1186/1824-7288-37-41. Available from: https://doi.org/10.1186/1824-

7288-37-41

Sandovici, I., K. Hoelle, E. Angiolini, and M. Constância. 2012. Placental adaptations to the maternal–fetal environment: implications for fetal growth and developmental programming. Reprod. Biomed. Online. 25:68–89. doi:10.1016/j.rbmo.2012.03.017. Available from: https://linkinghub.elsevier.com/retrieve/pii/S1472648312002052

Sarr, O., K. Yang, and T. R. H. Regnault. 2012. In utero programming of later adiposity: the role of fetal growth restriction. J. Pregnancy. 2012:134758. doi:10.1155/2012/134758.

Schiaffino, S., and C. Reggiani. 2011. Fiber Types in Mammalian Skeletal Muscles. Physiol. Rev. 91:1447–1531. doi:10.1152/physrev.00031.2010. Available from: https://doi.org/10.1152/physrev.00031.2010

Sedgh, G., S. Singh, and R. Hussain. 2014. Intended and Unintended Pregnancies Worldwide in 2012 and Recent Trends. Stud. Fam. Plann. 45:301–314. doi:https://doi.org/10.1111/j.1728-4465.2014.00393.x. Available from: https://doi.org/10.1111/j.1728-4465.2014.00393.x

Sharma, D., N. Farahbakhsh, S. Shastri, and P. Sharma. 2016a. Intrauterine growth restriction – part 2. J. Matern. Neonatal Med. 29:4037–4048. doi:10.3109/14767058.2016.1154525. Available from: https://www.tandfonline.com/action/journalInformation?journalCode=ijmf20http://informahealthcare.com/

Sharma, D., P. Sharma, and S. Shastri. 2017. Genetic, metabolic and endocrine aspect of intrauterine growth restriction: an update. J. Matern. Neonatal Med. 30:2263–2275. doi:10.1080/14767058.2016.1245285. Available from: https://www.tandfonline.com/action/journalInformation?journalCode=ijmf20http://informahealthcare.com/

Sharma, D., S. Shastri, N. Farahbakhsh, and P. Sharma. 2016b. Intrauterine growth restriction-part 1. J. Matern. Neonatal Med. 29:3977–3987. doi:10.3109/14767058.2016.1152249. Available from: https://www.tandfonline.com/action/journalInformation?journalCode=ijmf20http://informahealthcare.com/

Sijts, E. J. A. M., and P. M. Kloetzel. 2011. The role of the proteasome in the generation of MHC class I ligands and immune responses. Cell. Mol. Life Sci. 68:1491–502. doi:10.1007/s00018-011-0657-y. Available from: http://www.ncbi.nlm.nih.gov/pubmed/21387144

Soto, N., R. A. Bazaes, V. Peña, T. Salazar, A. Avila, G. Iñiguez, K. K. Ong, D. B.

Dunger, and M. V. Mericq. 2003. Insulin sensitivity and secretion are related to catch-up growth in small-for-gestational-age infants at age 1 year: results from a prospective cohort. J. Clin. Endocrinol. Metab. 88:3645–3650. doi:10.1210/jc.2002-030031.

Soto, S. M., A. C. Blake, S. R. Wesolowski, P. J. Rozance, K. B. Barthel, B. Gao, B. Hetrick, C. E. McCurdy, N. G. Garza, W. W. Hay, L. A. Leinwand, J. E. Friedman, and L. D. Brown. 2017. Myoblast replication is reduced in the IUGR fetus despite maintained proliferative capacity in vitro. J. Endocrinol. 232:475–491. doi:10.1530/JOE-16-0123. Available from: https://joe.bioscientifica.com/view/journals/joe/232/3/475.xml

Stanirowski, P. J., D. Szukiewicz, M. Pazura-Turowska, W. Sawicki, and K. Cendrowski. 2018. Placental Expression of Glucose Transporter Proteins in Pregnancies Complicated by Gestational and Pregestational Diabetes Mellitus. Can. J. diabetes. 42:209–217. doi:10.1016/j.jcjd.2017.04.008.

Steyn, P. J., K. Dzobo, R. I. Smith, and K. H. Myburgh. 2019. Interleukin-6 Induces Myogenic Differentiation via JAK2-STAT3 Signaling in Mouse C2C12 Myoblast Cell Line and Primary Human Myoblasts. Int. J. Mol. Sci. 20. doi:10.3390/ijms20215273.

Stremming, J., T. Jansson, T. L. Powell, P. J. Rozance, and L. D. Brown. 2020. Reduced Na + K + -ATPase activity may reduce amino acid uptake in intrauterine growth restricted fetal sheep muscle despite unchanged ex vivo amino acid transporter activity. J. Physiol. 598:1625–1639. doi:10.1113/JP278933. Available from: https://onlinelibrary.wiley.com/doi/10.1113/JP278933

Su, Y.-L., X. Wang, M. Mann, T. P. Adamus, D. Wang, D. F. Moreira, Z. Zhang, C. Ouyang, X. He, B. Zhang, P. M. Swiderski, S. J. Forman, D. Baltimore, L. Li, G. Marcucci, M. P. Boldin, and M. Kortylewski. 2020. Myeloid cell-targeted miR-146a mimic inhibits NF-κB-driven inflammation and leukemia progression in vivo. Blood. 135:167–180. doi:10.1182/blood.2019002045.

Sugino, H., and Y. Sawada. 2022. Influence of S100A2 in Human Diseases. Diagnostics. 12:1756. doi:10.3390/diagnostics12071756. Available from: https://www.mdpi.com/2075-4418/12/7/1756

Sumitani, S., K. Goya, J. R. Testa, H. Kouhara, and S. Kasayama. 2002. Akt1 and Akt2 Differently Regulate Muscle Creatine Kinase and Myogenin Gene Transcription in Insulin-Induced Differentiation of C2C12 Myoblasts. Endocrinology. 143:820–828. doi:10.1210/endo.143.3.8687. Available from: https://doi.org/10.1210/endo.143.3.8687

Sutton, G. M., A. V Centanni, and A. A. Butler. 2010. Protein malnutrition during

pregnancy in C57BL/6J mice results in offspring with altered circadian physiology before obesity. Endocrinology. 151:1570–80. doi:10.1210/en.2009-1133. Available from: http://www.ncbi.nlm.nih.gov/pubmed/20160133

Swanson, R. M., R. G. Tait, B. M. Galles, E. M. Duffy, T. B. Schmidt, J. L. Petersen, and D. T. Yates. 2020. Heat stress-induced deficits in growth, metabolic efficiency, and cardiovascular function coincided with chronic systemic inflammation and hypercatecholaminemia in ractopamine-supplemented feedlot lambs. J. Anim. Sci. 98. doi:10.1093/jas/skaa168. Available from: https://academic.oup.com/jas/article/doi/10.1093/jas/skaa168/5840746

Tarnopolsky, M. A. 2018. Myopathies Related to Glycogen Metabolism Disorders. Neurotherapeutics. 15:915–927. doi:10.1007/s13311-018-00684-2. Available from: https://doi.org/10.1007/s13311-018-00684-2

Tarrant, J. 2017. 4.15 - Emerging Translatable Safety Biomarkers. In: S. Chackalamannil, D. Rotella, and S. E. B. T.-C. M. C. I. I. I. Ward, editors. Elsevier, Oxford. p. 255–284. Available from: https://www.sciencedirect.com/science/article/pii/B978012409547212387X

Tarry-Adkins, J. L., D. S. Fernandez-Twinn, I. P. Hargreaves, V. Neergheen, C. E. Aiken, M. S. Martin-Gronert, J. M. McConnell, and S. E. Ozanne. 2016. Coenzyme Q10 prevents hepatic fibrosis, inflammation, and oxidative stress in a male rat model of poor maternal nutrition and accelerated postnatal growth. Am. J. Clin. Nutr. 103:579–88. doi:10.3945/ajcn.115.119834. Available from: http://www.ncbi.nlm.nih.gov/pubmed/26718412

Taylor, B. C., and J. M. Balko. 2022. Mechanisms of MHC-I Downregulation and Role in Immunotherapy Response. Front. Immunol. 13. doi:10.3389/fimmu.2022.844866. Available from: https://www.frontiersin.org/articles/10.3389/fimmu.2022.844866

Thorn, S. R., T. R. H. Regnault, L. D. Brown, P. J. Rozance, J. Keng, M. Roper, R. B. Wilkening, W. W. Hay, and J. E. Friedman. 2009. Intrauterine Growth Restriction Increases Fetal Hepatic Gluconeogenic Capacity and Reduces Messenger Ribonucleic Acid Translation Initiation and Nutrient Sensing in Fetal Liver and Skeletal Muscle. Endocrinology. 150:3021–3030. doi:10.1210/en.2008-1789. Available from: https://doi.org/10.1210/en.2008-1789

Todorov, V., and P. Filzmoser. 2009. An Object-Oriented Framework for Robust Multivariate Analysis. J. Stat. Softw. 32. doi:10.18637/jss.v032.i03. Available from: http://www.jstatsoft.org/v32/i03/

Tracey, K. J., and A. Cerami. 1993. Tumor Necrosis Factor, Other Cytokines and Disease. Annu. Rev. Cell Biol. 9:317–343.

doi:10.1146/annurev.cb.09.110193.001533. Available from: http://www.annualreviews.org/doi/10.1146/annurev.cb.09.110193.001533

Tsujikawa, K., K. Yayama, T. Hayashi, H. Matsushita, T. Yamaguchi, T. Shigeno, Y. Ogitani, M. Hirayama, T. Kato, S. Fukada, S. Takatori, H. Kawasaki, H. Okamoto, M. Ikawa, M. Okabe, and H. Yamamoto. 2007. Hypertension and dysregulated proinflammatory cytokine production in receptor activity-modifying protein 1-deficient mice. Proc. Natl. Acad. Sci. U. S. A. 104:16702–16707. doi:10.1073/pnas.0705974104.

Tsuru, S., Y. Ito, H. Matsuda, K. Hosono, T. Inoue, S. Nakamoto, C. Kurashige, T. Mishima, K. Tsujikawa, H. Okamoto, and M. Majima. 2020. RAMP1 signaling in immune cells regulates inflammation-associated lymphangiogenesis. Lab. Investig. 100:738–750. doi:10.1038/s41374-019-0364-0. Available from: https://doi.org/10.1038/s41374-019-0364-0

Villamayor, L., V. Rivero, D. López-García, D. J. Topham, L. Martínez-Sobrido, A. Nogales, and M. L. DeDiego. 2023. Interferon alpha inducible protein 6 is a negative regulator of innate immune responses by modulating RIG-I activation. Front. Immunol. 14:1105309. doi:10.3389/fimmu.2023.1105309. Available from: http://www.ncbi.nlm.nih.gov/pubmed/36793726

Visentin, S., A. Lapolla, A. Pietro Londero, C. Cosma, M. Dalfrà, M. Camerin, D. Faggian, M. Plebani, and E. Cosmi. 2014. Adiponectin Levels Are Reduced While Markers of Systemic Inflammation and Aortic Remodelling Are Increased in Intrauterine Growth Restricted Mother-Child Couple. G. Drummond, editor. Biomed Res. Int. 2014:1–10. doi:10.1155/2014/401595. Available from: https://doi.org/10.1155/2014/401595

Wai, S. G., P. J. Rozance, S. R. Wesolowski, W. W. Hay, and L. D. Brown. 2018. Prolonged amino acid infusion into intrauterine growth-restricted fetal sheep increases leucine oxidation rates. Am. J. Physiol. Metab. 315:E1143–E1153. doi:10.1152/ajpendo.00128.2018. Available from: https://www.physiology.org/doi/10.1152/ajpendo.00128.2018

Wang, J., M. Cao, M. Yang, Y. Lin, L. Che, Z. Fang, S. Xu, B. Feng, J. Li, and D. Wu. 2016. Intra-uterine undernutrition amplifies age-associated glucose intolerance in pigs via altered DNA methylation at muscle GLUT4 promoter. Br. J. Nutr. 116:390–401. doi:10.1017/S0007114516002166. Available from: https://www.cambridge.org/core/product/identifier/S0007114516002166/type/journal_article

Wang, J., A. Platt, R. Upmanyu, S. Germer, G. Lei, C. Rabe, R. Benayed, A. Kenwright, A. Hemmings, M. Martin, and O. Harari. 2013. IL-6 pathway-driven investigation of response to IL-6 receptor inhibition in rheumatoid arthritis. BMJ Open.

3:e003199. doi:10.1136/bmjopen-2013-003199. Available from: https://bmjopen.bmj.com/lookup/doi/10.1136/bmjopen-2013-003199

Watts, E. R., and S. R. Walmsley. 2019. Inflammation and Hypoxia: HIF and PHD Isoform Selectivity. Trends Mol. Med. 25:33–46. doi:10.1016/j.molmed.2018.10.006. Available from: https://linkinghub.elsevier.com/retrieve/pii/S1471491418302028

Wei, Y., K. Chen, A. T. Whaley-Connell, C. S. Stump, J. A. Ibdah, and J. R. Sowers. 2008. Skeletal muscle insulin resistance: role of inflammatory cytokines and reactive oxygen species. Am. J. Physiol. Regul. Integr. Comp. Physiol. 294:R673-80. doi:10.1152/ajpregu.00561.2007.

Wilson, S. J., J. C. McEwan, P. W. Sheard, and A. J. Harris. 1992. Early stages of myogenesis in a large mammal: Formation of successive generations of myotubes in sheep tibialis cranialis muscle. J. Muscle Res. Cell Motil. 13:534–550. doi:10.1007/BF01737996. Available from: http://link.springer.com/10.1007/BF01737996

Wolsk, E., H. Mygind, T. S. Grøndahl, B. K. Pedersen, and G. van Hall. 2010. IL-6 selectively stimulates fat metabolism in human skeletal muscle. Am. J. Physiol. Metab. 299:E832–E840. doi:10.1152/ajpendo.00328.2010. Available from: https://doi.org/10.1152/ajpendo.00328.2010

Wu, G., F. W. Bazer, J. M. Wallace, and T. E. Spencer. 2006. Intrauterine growth retardation: Implications for the animal sciences. J. Anim. Sci. 84:2316–2337. doi:10.2527/jas.2006-156. Available from: https://doi.org/10.2527/jas.2006-156

Wu, Yueheng, S. Chen, P. Wen, M. Wu, Yijing Wu, M. Mai, and J. Huang. 2021. PGAM1 deficiency ameliorates myocardial infarction remodeling by targeting TGF-β via the suppression of inflammation, apoptosis and fibrosis. Biochem. Biophys. Res. Commun. 534:933–940. doi:10.1016/j.bbrc.2020.10.070.

Xing, Y., H. Wei, X. Xiao, Z. Chen, H. Liu, X. Tong, and W. Zhou. 2020. Methylated Vnn1 at promoter regions induces asthma occurrence via the PI3K/Akt/NFκB-mediated inflammation in the IUGR mice. Biol. Open. 9. doi:10.1242/bio.049106. Available from: https://journals.biologists.com/bio/article/doi/10.1242/bio.049106/266319/Methylated-Vnn1-at-promoter-regions-induces-asthma

Yates, D. T., C. N. Cadaret, K. A. Beede, H. E. Riley, A. R. Macko, M. J. Anderson, L. E. Camacho, and S. W. Limesand. 2016. Intrauterine growth-restricted sheep fetuses exhibit smaller hindlimb muscle fibers and lower proportions of insulin-sensitive Type I fibers near term. Am. J. Physiol. Integr. Comp. Physiol. 310:R1020–R1029. doi:10.1152/ajpregu.00528.2015. Available from:

https://doi.org/10.1152/ajpregu.00528.2015

Yates, D. T., L. E. Camacho, A. C. Kelly, L. V. Steyn, M. A. Davis, A. T. Antolic, M. J. Anderson, R. Goyal, R. E. Allen, K. K. Papas, W. W. Hay, and S. W. Limesand. 2019. Postnatal β2 adrenergic treatment improves insulin sensitivity in lambs with IUGR but not persistent defects in pancreatic islets or skeletal muscle. J. Physiol. 597:5835–5858. doi:10.1113/JP278726.

Yates, D. T., D. S. Clarke, A. R. Macko, M. J. Anderson, L. A. Shelton, M. Nearing, R. E. Allen, R. P. Rhoads, and S. W. Limesand. 2014a. Myoblasts from intrauterine growth-restricted sheep fetuses exhibit intrinsic deficiencies in proliferation that contribute to smaller semitendinosus myofibres. J. Physiol. 592:3113–3125. doi:10.1113/jphysiol.2014.272591. Available from: https://doi.org/10.1113/jphysiol.2014.272591

Yates, D. T., D. S. Clarke, A. R. Macko, M. J. Anderson, L. A. Shelton, M. Nearing, R. E. Allen, R. P. Rhoads, and S. W. Limesand. 2014b. Myoblasts from intrauterine growth-restricted sheep fetuses exhibit intrinsic deficiencies in proliferation that contribute to smaller semitendinosus myofibres. J. Physiol. 592:3113–3125. doi:10.1113/jphysiol.2014.272591.

Yates, D. T., C. A. Löest, T. T. Ross, D. M. Hallford, B. H. Carter, and S. W. Limesand. 2011. Effects of bacterial lipopolysaccharide injection on white blood cell counts, hematological variables, and serum glucose, insulin, and cortisol concentrations in ewes fed low- or high-protein diets1. J. Anim. Sci. 89:4286–4293. doi:10.2527/jas.2011-3969. Available from: http://academic.oup.com/jas/article/89/12/4286/4772103

Yates, D. T., A. R. Macko, X. Chen, A. S. Green, A. C. Kelly, M. J. Anderson, A. L. Fowden, and S. W. Limesand. 2012. Hypoxaemia-induced catecholamine secretion from adrenal chromaffin cells inhibits glucose-stimulated hyperinsulinaemia in fetal sheep. J. Physiol. 590:5439–5447. doi:10.1113/jphysiol.2012.237347.

Yates, D T, A. R. Macko, M. Nearing, X. Chen, R. P. Rhoads, and S. W. Limesand. 2012. Developmental Programming in Response to Intrauterine Growth Restriction Impairs Myoblast Function and Skeletal Muscle Metabolism. T. Regnault, editor. J. Pregnancy. 2012:1–10. doi:10.1155/2012/631038. Available from: https://doi.org/10.1155/2012/631038

Yates, D. T., A. R. Macko, M. Nearing, X. Chen, R. P. Rhoads, and S. W. Limesand. 2012. Developmental Programming in Response to Intrauterine Growth Restriction Impairs Myoblast Function and Skeletal Muscle Metabolism. J. Pregnancy. 2012:1–10. doi:10.1155/2012/631038. Available from: http://www.hindawi.com/journals/jp/2012/631038/

Yates, D. T., J. L. Petersen, T. B. Schmidt, C. N. Cadaret, T. L. Barnes, R. J. Posont, and K. A. Beede. 2018. ASAS-SSR Triennnial Reproduction Symposium: Looking Back and Moving Forward—How Reproductive Physiology has Evolved: Fetal origins of impaired muscle growth and metabolic dysfunction: Lessons from the heat-stressed pregnant ewe1. J. Anim. Sci. 96:2987–3002. doi:10.1093/jas/sky164. Available from: https://academic.oup.com/jas/article/96/7/2987/4986415

Yin, H., F. Price, and M. A. Rudnicki. 2013. Satellite Cells and the Muscle Stem Cell Niche. Physiol. Rev. 93:23–67. doi:10.1152/physrev.00043.2011. Available from: https://pubmed.ncbi.nlm.nih.gov/23303905

Youd, J. M., S. Rattigan, and M. G. Clark. 2000. Acute impairment of insulin-mediated capillary recruitment and glucose uptake in rat skeletal muscle in vivo by TNF-alpha. Diabetes. 49:1904–1909. doi:10.2337/diabetes.49.11.1904. Available from: http://diabetes.diabetesjournals.org/cgi/doi/10.2337/diabetes.49.11.1904

Zaretsky, M. V., J. M. Alexander, W. Byrd, and R. E. Bawdon. 2004. Transfer of Inflammatory Cytokines Across the Placenta. Obstet. Gynecol. 103:546–550. doi:10.1097/01.AOG.0000114980.40445.83. Available from: http://journals.lww.com/00006250-200403000-00023

Zhang, X., D. Bogunovic, B. Payelle-Brogard, V. Francois-Newton, S. D. Speer, C. Yuan, S. Volpi, Z. Li, O. Sanal, D. Mansouri, I. Tezcan, G. I. Rice, C. Chen, N. Mansouri, S. A. Mahdaviani, Y. Itan, B. Boisson, S. Okada, L. Zeng, X. Wang, H. Jiang, W. Liu, T. Han, D. Liu, T. Ma, B. Wang, M. Liu, J.-Y. Liu, Q. K. Wang, D. Yalnizoglu, L. Radoshevich, G. Uzé, P. Gros, F. Rozenberg, S.-Y. Zhang, E. Jouanguy, J. Bustamante, A. García-Sastre, L. Abel, P. Lebon, L. D. Notarangelo, Y. J. Crow, S. Boisson-Dupuis, J.-L. Casanova, and S. Pellegrini. 2015. Human intracellular ISG15 prevents interferon-α/β over-amplification and auto-inflammation. Nature. 517:89–93. doi:10.1038/nature13801.

Zhao, M., Y.-H. Chen, X.-T. Dong, J. Zhou, X. Chen, H. Wang, S.-X. Wu, M.-Z. Xia, C. Zhang, and D.-X. Xu. 2013. Folic acid protects against lipopolysaccharide-induced preterm delivery and intrauterine growth restriction through its anti-inflammatory effect in mice. PLoS One. 8:e82713. doi:10.1371/journal.pone.0082713.